

การเปลี่ยนกลีเซอรอลเป็นกรดอะคริลิกบนตัวเร่งปฏิกิริยาพอลิออกโซเมทาเลต



นางสาวศราวลี ธนศิลป์

จุฬาลงกรณ์มหาวิทยาลัย

CHULALONGKORN UNIVERSITY

บทคัดย่อและแฟ้มข้อมูลฉบับเต็มของวิทยานิพนธ์ตั้งแต่ปีการศึกษา 2554 ที่ให้บริการในคลังปัญญาจุฬาฯ (CUIR)

เป็นแฟ้มข้อมูลของนิสิตเจ้าของวิทยานิพนธ์ ที่ส่งผ่านทางบัณฑิตวิทยาลัย

The abstract and full text of theses from the academic year 2011 in Chulalongkorn University Intellectual Repository (CUIR) are the thesis authors' files submitted through the University Graduate School.

วิทยานิพนธ์นี้เป็นส่วนหนึ่งของการศึกษาตามหลักสูตรปริญญาวิทยาศาสตรดุษฎีบัณฑิต

สาขาวิชาเคมีเทคนิค ภาควิชาเคมีเทคนิค

คณะวิทยาศาสตร์ จุฬาลงกรณ์มหาวิทยาลัย

ปีการศึกษา 2557

ลิขสิทธิ์ของจุฬาลงกรณ์มหาวิทยาลัย

CONVERSION OF GLYCEROL TO ACRYLIC ACID OVER POLYOXOMETALATE CATALYSTS

Miss Sarawalee Thanasilp



A Dissertation Submitted in Partial Fulfillment of the Requirements
for the Degree of Doctor of Philosophy Program in Chemical Technology

Department of Chemical Technology

Faculty of Science

Chulalongkorn University

Academic Year 2014

Copyright of Chulalongkorn University

Thesis Title	CONVERSION OF GLYCEROL TO ACRYLIC ACID OVER POLYOXOMETALATE CATALYSTS
By	Miss Sarawalee Thanasilp
Field of Study	Chemical Technology
Thesis Advisor	Associate Professor Mali Hunsom, Ph.D., Dr. de L'INPT
Thesis Co-Advisor	Assistant Professor Sitthipong Pengpanich, Ph.D. Professor Johannes W. Schwank, Ph.D.

Accepted by the Faculty of Science, Chulalongkorn University in Partial
Fulfillment of the Requirements for the Doctoral Degree

.....Dean of the Faculty of Science
(Professor Supot Hannongbua, Dr. rer. nat.)

THESIS COMMITTEE

.....Chairman
(Associate Professor Kejvalee Pruksathorn, Dr. de L'INPT)

.....Thesis Advisor
(Associate Professor Mali Hunsom, Ph.D., Dr. de L'INPT)

.....Thesis Co-Advisor
(Assistant Professor Sitthipong Pengpanich, Ph.D.)

.....Thesis Co-Advisor
(Professor Johannes W. Schwank, Ph.D.)

.....Examiner
(Assistant Professor Prapan Kuchonthara, Ph.D.)

.....Examiner
(Assistant Professor Siriporn Jongpatiwut, Ph.D.)

.....External Examiner
(Mr. Siriphong Rojluechai, Ph.D.)

ศราวลี ธนศิลป์ : การเปลี่ยนกลีเซอรอลเป็นกรดอะคริลิกบนตัวเร่งปฏิกิริยาพอลิออกโซเมทาเลต (CONVERSION OF GLYCEROL TO ACRYLIC ACID OVER POLYOXOMETALATE CATALYSTS) อ.ที่ปรึกษาวิทยานิพนธ์หลัก: รศ. ดร. มะลิ หุ่นสม, อ.ที่ปรึกษาวิทยานิพนธ์ร่วม: ผศ. ดร. สิทธิพงษ์ เพ็งพานิช, ศ. ดร. โจฮานเนส ชวางค์, 189 หน้า.

งานวิจัยนี้ศึกษาการเปลี่ยนกลีเซอรอลเป็นกรดอะคริลิกในวัฏภาคของเหลวด้วยตัวเร่งปฏิกิริยาพอลิออกโซเมทาเลตบนตัวรองรับ ตัวแปรที่ศึกษา ได้แก่ ความเข้มข้นของไฮโดรเจนเปอร์ออกไซด์ (2.74-6.85 โมลต่อลิตร) อุณหภูมิ (70-90 องศาเซลเซียส) ชนิดของตัวเร่งปฏิกิริยาพอลิออกโซเมทาเลต (PW, PMo, SiW) ชนิดของตัวรองรับ (Al_2O_3 , SiO_2 , HZSM-5) และสัดส่วนของตัวเร่งปฏิกิริยาพอลิออกโซเมทาเลตต่อสารตั้งต้นกลีเซอรอล (2-8 โดยน้ำหนัก) พบว่าตัวเร่งปฏิกิริยา SiW/HZSM-5 สามารถเปลี่ยนกลีเซอรอลได้ร้อยละ 85.54 ที่ความเข้มข้นของไฮโดรเจนเปอร์ออกไซด์เท่ากับ 2.74 โมลต่อลิตร อุณหภูมิเท่ากับ 90 องศาเซลเซียส สัดส่วนตัวเร่งปฏิกิริยาต่อกลีเซอรอลร้อยละ 4 โดยน้ำหนัก และให้ร้อยละผลได้ของกรดอะคริลิกเท่ากับ 30.57 การเติมวาเนเดียมร้อยละ 6 โดยน้ำหนักบนพื้นผิวของตัวเร่งปฏิกิริยา SiW/HZSM-5 (V6-SiW/HZSM-5) ให้ร้อยละการเปลี่ยนกลีเซอรอล 99.67 และผลได้ของกรดไกลโคลิก กรดฟอร์มิก กรดแอสติก อะโครลีน กรดอะคริลิก และกรดโพรพิโอนิก ร้อยละ 19.45, 12.03, 23.62, 0.25 36.23 และ 7.06 ตามลำดับ โดยอัตราการเปลี่ยนของกลีเซอรอลบนตัวเร่งปฏิกิริยา V6-SiW/HZSM-5 เป็นปฏิกิริยาอันดับหนึ่งเทียมขึ้นกับความเข้มข้นของกลีเซอรอล มีค่าพลังงานกระตุ้นเท่ากับ 26.63 กิโลจูลต่อโมล จลนพลศาสตร์การดูดซับสารตั้งต้นบนพื้นผิวของตัวเร่งปฏิกิริยาดังกล่าวสามารถอธิบายได้โดยแบบจำลอง Eley-Rideal ซึ่งเป็นการเกิดปฏิกิริยาระหว่างโมเลกุลของออกซิเจนที่เกิดจากการแตกตัวของไฮโดรเจนเปอร์ออกไซด์บนตัวเร่งปฏิกิริยาและโมเลกุลกลีเซอรอล

ภาควิชา เคมีเทคนิค

สาขาวิชา เคมีเทคนิค

ปี ๒๕๕๖

ลายมือชื่อ นิสิต

ลายมือชื่อ อ.ที่ปรึกษาหลัก

.....

5373910823 : MAJOR CHEMICAL TECHNOLOGY

KEYWORDS: : GLYCEROL/ POLYOXOMETALATES/ ACRYLIC ACID

SARAWALEE THANASILP: CONVERSION OF GLYCEROL TO ACRYLIC ACID OVER POLYOXOMETALATE CATALYSTS. ADVISOR: ASSOC. PROF. MALI HUNSOM, Ph.D., Dr. de L'INPT, CO-ADVISOR: ASST. PROF. SITTHIPONG PENG PANICH, Ph.D., PROF. JOHANNES W. SCHWANK, Ph.D., 189 pp.

This work was carried out to convert glycerol to acrylic acid in liquid phase over supported polyoxometalate (POM) catalysts. The investigated parameters were H_2O_2 concentration (2.74-6.85 mol/L), reaction temperatures (70-90 °C), POM types (PW, PMo, SiW), support types (Al_2O_3 , SiO_2 , HZSM-5) and the catalyst to glycerol ratio (2-8 wt%). It was found that the SiW/HZSM-5 catalyst can enhance the conversion of glycerol of around 85.54% at H_2O_2 concentration of 2.74 mol/L, temperature of 90 °C, the catalyst to glycerol of 4 wt%. The doping of vanadium (V) at 6 wt.% on the surface of SiW/HZSM-5 (V6-SiW/HZSM-5) catalyst can promote the conversion of glycerol up to 99.67% and provide the yield of glycolic acid, formic acid, acetic acid, acrolein, acrylic acid and propionic acid of 19.45%, 12.03%, 23.62%, 0.25%, 36.23% and 7.06%, respectively. The rate of glycerol conversion was fit with a pseudo-first order reaction with respect to glycerol concentration, with the activation energy of 26.63 kJ/mol. The Eley-Rideal model, assuming a reaction between adsorbed oxygen molecule, obtained from H_2O_2 dissociation, and glycerol molecule provided the best fit with the experimental results.

Department: Chemical Technology Student's Signature

Field of Study: Chemical Technology Advisor's Signature

ACKNOWLEDGEMENTS

The author would like to express sincere appreciation and thankfulness to my dissertation advisor, Assoc. Prof. Dr. Mali Hunsom and co-advisor, Asst. Prof. Dr. Sitthiphong Pengpanich, and Prof. Dr. Johannes W. Schwank for the helpful suggestions, encouraging guidance, supervision and support throughout my research. Moreover, I especially extend my appreciation to Asst. Prof. Dr. Prapan Kuchontara, Asst. Prof. Dr. Siriporn Jongpatiwut, and Dr. Siriphong Rojluechai for their participation on the dissertation chairman and members of thesis committee and for their worthy comments and suggestions.

The author gratefully also extends to the Thailand Research Fund (the Royal Golden Jubilee (RGJ) Ph.D. Program) for their financial support throughout this dissertation research.

Many thanks are going to the Department of Chemical Technology, Faculty of Science, Chulalongkorn University and the Department of Chemical Engineering, Mahanakorn University of Technology, and the Department of Chemical Engineering, University of Michigan.

Finally, I would like to thank my family for their love, support and encouragement throughout graduate study. Also, special thanks are extended to my friend for friendship, encouragements and cheerful moral support.

CONTENTS

	Page
THAI ABSTRACT	iv
ENGLISH ABSTRACT	v
ACKNOWLEDGEMENTS	vi
CONTENTS	vii
LIST OF TABLES	xi
LIST OF FIGURES	xiv
CHAPTER I INTRODUCTION.....	1
1.1 Background and rationale	1
1.2 Objectives of dissertation.....	2
1.3 Experimental procedure.....	2
CHAPTER II THEORY AND LITERATURE REVIEW	4
2.1 Renewable energy resource	4
2.2 Biodiesel production	4
2.2.1 Global biodiesel market.....	4
2.2.2 Process flow chart	7
2.2.3 By-product from biodiesel production.....	7
2.3 Glycerol.....	9
2.3.1 Properties	9
2.3.2 Application	10
2.4 Acrylic acid	19
2.4.1 Properties	19
2.4.2 Application.....	20

	Page
2.4.3 Acrylic acid production processes	23
2.5 Polyoxometalate (POM)	29
2.6 Oxidizing agent (Hudlicky, 1990)	32
2.7 Literature reviews	34
CHAPTER III METHODOLOGY	40
3.1 Chemical substances	40
3.2 Catalyst preparation	41
3.2.1 Supported POM catalysts	41
3.2.2 Metal-doped supported POM catalysts	41
3.3 Catalyst characterization	42
3.3.1 Brunauer–Emmett–Teller method (BET method)	42
3.3.2 X-ray Diffraction (XRD)	42
3.3.3 Fourier Transform Infrared Spectroscopy (FT-IR)	43
3.3.4 Scanning Electron Microscopy/Energy Dispersive X-Ray Spectroscopy (SEM/EDX)	43
3.3.5 X-ray fluorescence (XRF)	44
3.3.6 Phosphorus-31 and Silicon-29 Magic Angle Spinning Nuclear Magnetic Resonance spectroscopy (^{31}P and ^{29}Si MAS NMR)	44
3.3.7 Temperature Programmed Desorption of ammonia (NH_3 -TPD)	44
3.3.8 Temperature Programmed Desorption of oxygen (O_2 -TPD)	45
3.3.9 Temperature Programmed Reduction of hydrogen (H_2 -TPR)	45
3.4 Activity test	45
3.4.1 Gas Chromatograph and Mass Spectrometry (GC-MS)	47
3.4.2 High Performance Liquid Chromatography (HPLC)	47

	Page
3.5 Kinetic studies.....	48
CHAPTER IV CONVERSION OF GLYCEROL TO ACRYLIC ACID VIA Al_2O_3 -SUPPORTED POM CATALYSTS	49
4.1 Characterization of Al_2O_3 -supported POM catalysts.....	49
4.2 Catalytic activity test of Al_2O_3 -supported POM catalysts	58
4.2.1 Effect of oxidizing agent and reaction temperature	58
4.2.2 Effect of catalyst types and loading.....	61
4.3 Reaction mechanism of conversion of glycerol	69
CHAPTER V CONVERSION OF GLYCEROL TO ACRYLIC ACID VIA SUPPORTED SiW CATALYSTS.....	72
5.1 Effect of supports	72
5.2 Effect of oxidizing agent and reaction temperature.....	78
5.3 Effect of SiW loading.....	82
5.4 Kinetic studies of glycerol conversion.....	90
CHAPTER VI CONVERSION OF GLYCEROL TO ACRYLIC ACID VIA METAL-DOPED SiW/HZSM-5 CATALYSTS	96
6.1 Effect of transition metal types.....	96
6.2 Effect of transition metal loadings.....	112
6.3 Kinetic studies of V-SiW/HZSM-5 catalyst.....	122
6.3.1 Power law model	126
6.3.2 Surface reaction kinetic models (Richard, 1996).....	129
6.3.2.1 Langmuir-Hinshelwood model (Model LH1)	129
6.3.2.2 Langmuir-Hinshelwood model (Model LH2)	130
6.3.2.3 Langmuir-Hinshelwood model (Model LH3)	131

	Page
6.3.2.4 Langmuir-Hinshelwood model (Model LH4)	132
6.3.2.5 Eley-Rideal model (Model ER1).....	133
6.3.2.6 Eley-Rideal model (Model ER2).....	134
6.3.2.7 Eley-Rideal model (Model ER3).....	134
6.3.2.8 Eley-Rideal model (Model ER4).....	135
6.4 Reusability test.....	146
CHAPTER VII CONCLUSIONS AND RECOMMENDATIONS	149
REFERENCES	151
APPENDICES.....	162
APPENDIX A.....	163
APPENDIX B	165
APPENDIX C	182
APPENDIX D.....	185
VITA.....	189

LIST OF TABLES

Table	Page
2.1 Physical properties of acrylic acid.....	21
2.2 Standard electrode potentials in aqueous solution at 25°C.....	33
4.1 Textural properties of Al ₂ O ₃ and Al ₂ O ₃ -supported POM catalysts.....	50
4.2 NH ₃ -TPD results for Al ₂ O ₃ , POM and Al ₂ O ₃ -supported POM catalysts.....	56
4.3 O ₂ -TPD results for Al ₂ O ₃ , POM and Al ₂ O ₃ -supported POM catalysts.....	58
4.4 Effect of H ₂ O ₂ content and reaction temperature on the performance of glycerol conversion over SiW/Al ₂ O ₃ catalyst with 4 wt.% catalyst loading at 240 min.....	60
4.5 Effect of catalyst types and catalyst loading on the performance of glycerol conversion over Al ₂ O ₃ -supported POM catalyst at 90 °C and 240 min.....	68
5.1 Textural properties and surface chemistry of supported SiW catalysts and the corresponding supports.....	74
5.2 Effect of supports on the performance of glycerol conversion over supported SiW catalysts at SiW loading of 30 wt.%, temperature of 90 °C at 240 min.....	79
5.3 Effect of H ₂ O ₂ concentration and reaction temperature on glycerol conversion over 30 wt.% SiW/HZSM-5 catalyst with 4 wt.% catalyst loading at 240 min.....	81
5.4 Textural properties and surface chemistry of supported SiW catalysts in the presence of different SiW loading.....	84
5.5 Effect of SiW loading on the performance of glycerol conversion over SiW/HZSM-5 catalysts with different SiW loadings at reaction temperature of 90 °C at 240 min.....	87
5.6 Estimated parameters of the rate expression of conversion by power law model.....	94

Table	Page
6.1 Textural properties of HZSM-5, SiW , 30 wt.% SiW/HZSM-5 and transition metals-doped SiW/HZSM-5 catalysts with 4 wt.% transition metals doping.....	97
6.2 NH ₃ -TPD results for HZSM-5, SiW, 30 wt.% SiW/HZSM-5 and metals-doped SiW/HZSM-5 catalysts with 4 wt.% metals doping.....	105
6.3 O ₂ -TPD results for 30 wt.% SiW/HZSM-5 and metals-doped SiW/HZSM-5 catalysts with 4 wt.% metals doping.....	107
6.4 Effect of metals on the performance of glycerol conversion over 30 wt.% SiW/HZSM-5 catalyst, temperature of 90 °C at 240 min.....	111
6.5 Textural properties and surface chemistry of V-SiW/HZSM-5 catalysts at different V loadings.....	116
6.6 O ₂ -TPD results for SiW/HZSM-5 and V-SiW/HZSM-5 catalysts at different V loadings.....	117
6.7 Effect of V loading over SiW/HZSM-5 catalysts on the performance of glycerol conversion at SiW loading of 30 wt.%, temperature of 90 °C at 240 min.....	121
6.8 Estimated parameters of the rate expression of glycerol conversion by power Law Model.....	127
6.9 Surface reaction kinetic models used to fit the glycerol conversion reaction.....	136
6.9 (Cont.) Surface reaction kinetic models used to fit the glycerol conversion reaction.....	137
6.9 (Cont.) Surface reaction kinetic models used to fit the glycerol conversion reaction.....	138
6.9 (Cont.) Surface reaction kinetic models used to fit the glycerol conversion reaction.....	139
6.10 Rate parameters on kinetic rate expression from surface reaction kinetic models tested in fitting the glycerol conversion reaction at 60 °C.....	140

Table	Page
6.11 Rate parameters on kinetic rate expression from surface reaction kinetic models tested in fitting the glycerol conversion reaction at 70 °C.....	141
6.12 Rate parameters on kinetic rate expression from surface reaction kinetic models tested in fitting the glycerol conversion reaction at 80 °C.....	142
6.13 Rate parameters on kinetic rate expression from surface reaction kinetic models tested in fitting the glycerol conversion reaction at 90 °C.....	143
6.14 Textural properties and surface chemistry of V6-SiW/HZSM-5 catalyst and after use in glycerol conversion for 6 catalytic cycles.....	148



LIST OF FIGURES

Figure	Page
2.1 Global biodiesel productions	5
2.2 Global biodiesel (bars) and crude glycerol (lines) production between 2005 and 2010.....	6
2.3 Top ten biodiesel producing countries in 2010.....	6
2.4 Simplified process flow chart of alkali-catalyzed biodiesel production.....	8
2.5 Yield of transesterification of triglyceride with methanol.....	9
2.6 Chemical structure of glycerol.....	10
2.7 Market for refined glycerol.....	11
2.8 Glycerol dehydration routes involving the reaction mechanisms.....	14
2.9 Glycerol as a primary biorefinery platform chemical.....	18
2.10 Chemical structure of acrylic acid.....	20
2.11 USA acrylic acid consumption by end-use.....	22
2.12 Global acrylic acid production in 2012.....	23
2.13 Reaction route for dehydration and oxidation of glycerol to acrylic acid..	27
2.14 Lindqvist structure.....	29
2.15 Anderson-Evans structure.....	30
2.16 Wells-Dawson structure.....	30
2.17 Keggin structure of the phosphotungstic acid.....	31
3.1 Schematic diagram of the preparation of modified supported POM catalysts by sequential incipient wetness impregnation method.....	42
3.2 Fourier transform infrared spectroscopy (FTIR).....	43
3.3 Schematic diagram of experiment set up: (1) cooling water outlet, (2) condenser, (3) cooling water inlet, (4) syringe, (5) three-necked flask, (6) magnetic bar, (7) magnetic stirrer and (8) thermometer.....	46
3.4 Gas chromatograph and mass spectrometry (GC-MS).....	47
3.5 High Performance Liquid Chromatography (HPLC).....	48
4.1 XRD patterns of Al ₂ O ₃ , POM and Al ₂ O ₃ -supported POM catalysts at 30 wt.% POM loading.....	50

Figure	Page
4.2 FT-IR spectra of Al ₂ O ₃ and Al ₂ O ₃ -supported POM catalysts at 30 wt.% POM loading.....	52
4.3 ³¹ P MAS NMR spectra of unsupported PW and PW/Al ₂ O ₃ catalysts spectra at 30 wt.% POM loading.....	54
4.4 ³¹ P MAS NMR spectra of unsupported PMo and PMo/Al ₂ O ₃ catalysts spectra at 30 wt.% POM loading.....	54
4.5 ²⁹ Si MAS NMR spectra of unsupported SiW and SiW/Al ₂ O ₃ catalysts spectra at 30 wt.% POM loading.....	55
4.6 NH ₃ -TPD profiles for utilized POM, Al ₂ O ₃ and Al ₂ O ₃ -supported POM catalysts at 30 wt.% POM loading.....	55
4.7 O ₂ -TPD profiles for utilized POM, Al ₂ O ₃ and Al ₂ O ₃ -supported POM catalysts at 30 wt.% POM loading.....	57
4.8 Variation of (●) glycerol conversion and yields of (□) glycolic acid, (Δ) formic acid, (X) acetic acid, (+) acrolein and (◇) acrylic acid as a function of time of glycerol conversion over Al ₂ O ₃ catalyst (a) 2 wt.%, (b) 4 wt.% and (c) 8 wt.% catalyst loading at 90 °C.....	64
4.9 Variation of (●) glycerol conversion and yields of (□) glycolic acid, (Δ) formic acid, (X) acetic acid, (+) acrolein and (◇) acrylic acid as a function of time of glycerol conversion over PW/Al ₂ O ₃ catalyst (a) 2 wt.%, (b) 4 wt.% and (c) 8 wt.% catalyst loading at 90 °C.....	65
4.10 Variation of (●) glycerol conversion and yields of (□) glycolic acid, (Δ) formic acid, (X) acetic acid, (+) acrolein and (◇) acrylic acid as a function of time of glycerol conversion over PMo/Al ₂ O ₃ catalyst (a) 2 wt.%, (b) 4 wt.% and (c) 8 wt.% catalyst loading at 90 °C.....	66
4.11 Variation of (●) glycerol conversion and yields of (□) glycolic acid, (Δ) formic acid, (X) acetic acid, (+) acrolein and (◇) acrylic acid as a function of time of glycerol conversion over SiW/Al ₂ O ₃ catalyst (a) 2 wt.%, (b) 4 wt.% and (c) 8 wt.% catalyst loading at 90 °C.....	67

Figure	Page
4.12 GC-MS chromatogram of solutions obtained from glycerol conversion over 30 wt.% SiW/Al ₂ O ₃ catalyst at 90 °C.....	70
4.13 Proposed reaction pathways of glycerol conversion. The products detected by GC-MS are indicated by dashed line.....	71
5.1 XRD patterns of SiW and supported SiW catalyst at 30 wt.% SiW loading..	73
5.2 NH ₃ -TPD profiles of supported SiW catalysts and their supports at 30 wt.% SiW loading.....	76
5.3 Variation of (●) glycerol conversion and yields of (□) glycolic acid, (△) formic acid, (×) acetic acid, (+) acrolein and (◇) acrylic acid as a function of time over (a) SiW/Al ₂ O ₃ , (b) SiW/SiO ₂ and (c) SiW/HZSM-5 with 30 wt.% SiW loading at 90 °C.....	77
5.3 (Cont.) Variation of (●) glycerol conversion and yields of (□) glycolic acid, (△) formic acid, (×) acetic acid, (+) acrolein and (◇) acrylic acid as a function of time over (a) SiW/Al ₂ O ₃ , (b) SiW/SiO ₂ and (c) SiW/HZSM-5 with 30 wt.% SiW loading at 90 °C.....	78
5.4 XRD patterns of unsupported SiW, HZSM-5 and SiW/HZSM-5 catalysts with different SiW loading.....	82
5.5 NH ₃ -TPD profiles of unsupported SiW, HZSM-5 and SiW/HZSM-5 catalysts with different SiW loading.....	85
5.6 Variation of (●) glycerol conversion and yields of (□) glycolic acid, (△) formic acid, (x) acetic acid, (+) acrolein and (◇) acrylic acid as a function of time over (a) HZSM-5, (b) 20, (c) 30, (d) 40, (e) 50 and (f) 60 wt.% SiW/HZSM-5 catalyst.....	88
5.6 (Cont.) Variation of (●) glycerol conversion and yields of (□) glycolic acid, (△) formic acid, (x) acetic acid, (+) acrolein and (◇) acrylic acid as a function of time over (a) HZSM-5, (b) 20, (c) 30, (d) 40, (e) 50 and (f) 60 wt.% SiW/HZSM-5 catalyst.....	89

Figure	Page	
5.7	Variation of glycerol conversion rate as a function of time at catalyst loading of 4 wt.% in the presence of 2.74 mol/L H ₂ O ₂ with glycerol concentrations of 2.75 mol/L at (■) 70 °C, (▲) 80 °C and (●) 90 °C.....	90
5.8	Variation of rate of glycerol conversion as a function of glycerol concentrations in the presence of H ₂ O ₂ at 70 °C.....	91
5.9	Variation of rate of glycerol conversion as a function of glycerol concentrations in the presence of H ₂ O ₂ at 80 °C.....	91
5.10	Variation of rate of glycerol conversion as a function of glycerol concentrations in the presence of H ₂ O ₂ at 90 °C.....	92
5.11	Variation of rate of glycerol conversion as a function of H ₂ O ₂ concentrations in the presence of glycerol concentration at 70 °C.....	92
5.12	Variation of rate of glycerol conversion as a function of H ₂ O ₂ concentrations in the presence of glycerol concentration at 80 °C.....	93
5.13	Variation of rate of glycerol conversion as a function of H ₂ O ₂ concentrations in the presence of glycerol concentration at 90 °C.....	93
5.14	The rate of glycerol conversion from the experiments compared with the rate of glycerol conversion from power law model at 90 °C.....	95
5.15	Arrhenius plot of <i>k</i> constants for liquid phase conversion of glycerol over SiW/HZSM-5 catalyst with 30 wt.% SiW loading.....	95
6.1	XRD patterns of HZSM-5, SiW, 30 wt.% SiW/HZSM-5 and metals-doped SiW/HZSM-5 catalysts with 4 wt.% metals doping.....	98
6.2	EDX analysis of SiW/HZSM-5 and metal-doped SiW/HZSM-5 at constant metal loading of 4 wt.%.....	99
6.3	FT-IR spectra of HZSM-5, SiW, 30 wt.% SiW/HZSM-5 and metals-doped SiW/HZSM-5 catalysts with 4 wt.% metals doping.....	100
6.4	H ₂ -TPR profiles for utilized SiW/HZSM-5 (physical mixing), SiW/HZSM-5 and metal-doped SiW/HZSM-5 catalysts with 4 wt.% metal doping.....	102
6.5	NH ₃ -TPD profiles for utilized HZSM-5, SiW, 30 wt.% SiW/HZSM-5 and metals-doped SiW/HZSM-5 catalysts with 4 wt.% metals doping.....	104

Figure	Page
6.6 O ₂ -TPD profiles for utilized HZSM-5, SiW, 30 wt.% SiW/HZSM-5 and metals-doped SiW/HZSM-5 catalysts with 4 wt.% metals doping.....	106
6.7 Variation of (●) glycerol conversion and yields of (□) glycolic acid, (△) formic acid, (×) acetic acid, (+) acrolein, (◇) acrylic acid and (■) propionic acid as a function of time over (a) SiW/HZSM-5, (b) Ce-SiW/HZSM-5, (c) Co-SiW/HZSM-5, (d) Ni-SiW/HZSM-5 and (e) V-SiW/HZSM-5 with 4 wt.% metal loading at 90 °C.....	109
6.7 (Cont.) Variation of (●) glycerol conversion and yields of (□) glycolic acid, (△) formic acid, (×) acetic acid, (+) acrolein, (◇) acrylic acid and (■) propionic acid as a function of time over (a) SiW/HZSM-5, (b) Ce-SiW/HZSM-5, (c) Co-SiW/HZSM-5, (d) Ni-SiW/HZSM-5 and (e) V-SiW/HZSM-5 with 4 wt.% metal loading at 90 °C.....	110
6.8 XRD patterns of HZSM-5, SiW and V-SiW/HZSM-5 catalysts at different V loadings.....	112
6.9 EDX analysis of V-SiW/HZSM-5 catalysts at different V loadings.....	113
6.10 FT-IR spectra of HZSM-5, SiW and V-SiW/HZSM-5 catalysts at different V loadings.....	114
6.11 H ₂ -TPR profiles for utilized SiW/HZSM-5 and V-SiW/HZSM-5 catalysts at different V loadings.....	115
6.12 Variation of (●) glycerol conversion and yields of (□) glycolic acid, (△) formic acid, (×) acetic acid, (+) acrolein, (◇) acrylic acid and (■) propionic acid as a function of time over (a) V2-SiW/HZSM-5, (b) V4-SiW/HZSM-5, (c) V6-SiW/HZSM-5 and (d) V8-SiW/HZSM-5 catalysts at 90 °C.....	119
6.12 (Cont.) Variation of (●) glycerol conversion and yields of (□) glycolic acid, (△) formic acid, (×) acetic acid, (+) acrolein, (◇) acrylic acid and (■) propionic acid as a function of time over (a) V2-SiW/HZSM-5, (b) V4-SiW/HZSM-5, (c) V6-SiW/HZSM-5 and (d) V8-SiW/HZSM-5 catalysts at 90 °C.....	120

Figure	Page
6.13 Variation of glycerol conversion rate as a function of time at catalyst loading of 4 wt.% in the presence of 2.74 mol/L H ₂ O ₂ with glycerol concentrations of 2.75 mol/L at (◆) 60 °C, (■) 70 °C, (▲) 80 °C and (●) 90 °C.....	122
6.14 Variation of rate of glycerol conversion as a function of glycerol concentrations in the presence of H ₂ O ₂ at 60 °C.....	123
6.15 Variation of rate of glycerol conversion as a function of glycerol concentrations in the presence of H ₂ O ₂ at 70 °C.....	123
6.16 Variation of rate of glycerol conversion as a function of glycerol concentrations in the presence of H ₂ O ₂ at 80 °C.....	124
6.17 Variation of rate of glycerol conversion as a function of glycerol concentrations in the presence of H ₂ O ₂ at 90 °C.....	124
6.18 Variation of rate of glycerol conversion as a function of H ₂ O ₂ concentrations in the presence of glycerol concentration at 60 °C.....	125
6.19 Variation of rate of glycerol conversion as a function of H ₂ O ₂ concentrations in the presence of glycerol concentration at 70 °C.....	125
6.20 Variation of rate of glycerol conversion as a function of H ₂ O ₂ concentrations in the presence of glycerol concentration at 80 °C.....	126
6.21 Variation of rate of glycerol conversion as a function of H ₂ O ₂ concentrations in the presence of glycerol concentration at 90 °C.....	126
6.22 The rate of glycerol conversion from the experiments compared with the rate of glycerol conversion from power law model at 90 °C.....	128
6.23 Arrhenius plot of <i>k</i> constants for liquid phase conversion of glycerol over V-SiW/HZSM-5 catalyst with 6 wt.% V loading.....	128
6.24 Relation of ln(<i>k</i> ₂) vs. 1/ <i>T</i> (Arrhenius Plot) from the surface reaction kinetic Eley-Rideal model (model ER2).....	145
6.25 Relation of ln(<i>K</i> ₁) vs. 1/ <i>T</i> (Arrhenius Plot) from the surface reaction kinetic Eley-Rideal model (model ER2).....	146
6.26 Catalytic performance of V6-SiW/HZSM-5 catalyst used in consecutive one-pot conversion of glycerol to acrylic acid.....	147

Figure	Page
6.27 NH ₃ -TPD profiles of fresh V6-SiW/HZSM-5 catalyst and after used in glycerol conversion for 6 catalytic cycles.....	148



CHAPTER I

INTRODUCTION

1.1 Background and rationale

Due to the significant global energy crisis, alternative fuels such as biodiesel have been widely used for partial replacing fossil fuel. Biodiesel is an alternative fuel produced from renewable resources such as palm, canola, soya bean, vegetable oils and animal fats by using the reaction known as “Transesterification” in the presence of acidic or alkaline catalysts. The rapidly rising production of biodiesel from vegetable oils has led to a drastic surplus of by-product glycerol in the chemical markets. Approximately 100 kg of glycerol is generated when a ton of biodiesel is produced. Any further increase in biodiesel production rates will significantly raise the quantity of glycerol above the demands and so decrease its economic value. Therefore, using the growing supply of glycerol is a logical step in moving toward a more sustainable economy. In order to find new uses of glycerol, various previous research efforts have focused on transforming glycerol into more valuable chemicals such as 1,2-propanediol, 1,3-propanediol, propionic acid, glycolic acid, acetic acid, formic acid, acrolein, acrylic acid, dihydroxyacetone, etc.

Acrylic acid is one of the most interesting and important chemicals that is widely used in adhesive, paint, plastic, and rubber synthesis. Typically, acrylic acid can be produced from glycerol by sequential dehydration and oxidation reactions in the presence of catalyst. Initially, glycerol is dehydrated to the intermediate species; acrolein. This species is very reactive. It can be further oxidized to acrylic acid in the presence of oxygen donating-catalyst. Previously, the conversion of glycerol to acrylic acid was carried out in separated bed systems including a dehydration bed containing an acid catalyst and an oxidation bed containing a mixed oxide catalyst (Witsuthammakul & Sooknoi, 2012). Although high glycerol conversion and product selectively were obtained, this work was carried in the gas phase and at high temperature (275-400 °C), leading to high cost and complexity of the system.

To avoid the previous drawbacks, the conversion of glycerol to acrylic acid in one-step process is more interesting because it can reduce the engineering investment cost, making operation and control easier. This work attempts to convert glycerol to acrylic acid in a one-step process at low temperature in liquid phase by using an oxygen donating catalyst on acid support. The advantages of this catalyst are the possibility to control solid acid strength and the enhancement of active surface area (Moffat, 2001). Among the oxygen donated-catalysts, the polyoxometalate (POM) is a promising candidate because it has high acid strength with high redox catalysis activity and high thermal stability, and high solubility in polar solvents such as water and alcohol (Marchal-Rochand & Millet, 2001). In addition, it is considered as a green catalyst because most POM catalysts are environment friendly (Xiaoli et al., 2013).

1.2 Objectives of dissertation

1. Investigate the effect of parameters on conversion of glycerol to acrylic acid in the presence of POM catalysts
2. Study the kinetics and mechanism of acrylic acid from glycerol in the presence of POM catalysts

1.3 Experimental procedure

1. Literature review of relevant publications from both national and international journals.
2. Prepare all tools, equipment and chemical reagents required for the experiments.
3. Feasibility and activity tests for glycerol conversion to acrylic acid in liquid phase by using commercial POM catalysts on supports.
 - 3.1 Prepare various types of POM including $\text{H}_3\text{PW}_{12}\text{O}_{40}$ (PW), $\text{H}_3\text{PMo}_{12}\text{O}_{40}$ (PMo) and $\text{H}_4\text{SiW}_{12}\text{O}_{40}$ (SiW) on various supports including Al_2O_3 , HZSM-5, and SiO_2 by impregnation method at constant catalyst loading of 30 wt.%.

- 3.2 Characterize the identity and morphology of as-prepared supported POM catalysts by BET, XRD, FT-IR, ^{31}P MAS NMR, ^{29}Si MAS NMR, NH_3 -TPD and O_2 -TPD
- 3.3 Study glycerol conversion and product yield and selectivity by using as-prepared supported POM catalysts. The investigated parameters are
 - Reaction temperature (70 and 90 °C)
 - Oxidizing agent, H_2O_2 (1.37-6.85 mol/L)
 - Catalyst loading (2-8 wt.%)
4. Activity tests for conversion of glycerol to acrylic acid in liquid phase by using transition metal-doped supported POM catalysts.
 - 4.1 Study the addition of transition metals on supported POM catalysts. The investigated parameters are
 - Types of transition metals (Ce, Co, Ni and V)
 - Loadings of transition metals (2-8 wt.%)
 - 4.2 Characterize the identity and morphology of as-prepared supported POM catalysts by BET, XRD, FT-IR, ^{31}P MAS NMR, ^{29}Si MAS NMR, XRF, SEM/EDX, NH_3 -TPD, O_2 -TPD and H_2 -TPR.
 - 4.3 Study glycerol conversion and product yield by using as-prepared supported POM catalysts at optimum condition obtained from 3.3.
5. Study the kinetics and mechanisms of conversion of glycerol to acrylic acid over supported POM catalysts.
6. Summarize the experiments, discuss the results and write up a thesis.

CHAPTER II

THEORY AND LITERATURE REVIEW

2.1 Renewable energy resource

In this decade, 80-85% of global energy consumption comes from the combustion of fossil fuels such as oil, coal, and natural gas. However, these fossil fuels are limited and fast depleted because of constant use. In addition, the consumption of fossil fuels has increased carbon dioxide (CO₂) in the atmosphere, resulting concerns about global warming. According to the environmental effect and the increasing fossil fuels consumption, the development of renewable energy resources has been increased. Nowadays, an attempt to replace the non-renewable energy resources by various alternative fuels such as biomass and biofuels (ethanol and biodiesel) is an alternative issue to address those problems. Biodiesel is gaining significance as one of the most important substitutes for the depleting fossil fuels. The combustion properties of biodiesel are also very close to those of petroleum diesel (Subramanian, Singal, Saxena, & Singhal, 2005). In addition, it is highly biodegradable (Ma & Hanna, 1999), non-toxic as well as renewable and environmentally friendly.

2.2 Biodiesel production

2.2.1 Global biodiesel market

Biodiesel industry is a strong industry with a fast global market growth. Over the past decade, the biodiesel production was directorially driven aiming to the development of large scale industries. Furthermore, the global biodiesel production in 2008 reached more than 11.1×10^6 ton (Figure 2.1).

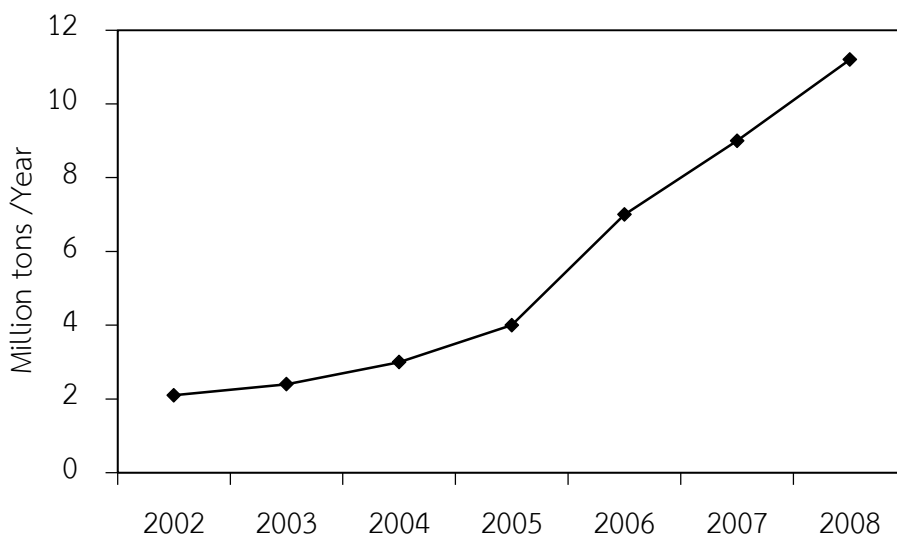


Figure 2.1 Global biodiesel productions (EMO, 2014).

As demonstrated in Figure 2.2, biodiesel production increased considerably in the past few years. Europe took the lead with more than 3.8×10^6 ton of biodiesel production in 2005, while in the United States of America (USA) including North, Central and South USA, approximate 0.3×10^6 tons were produced. The biodiesel production of Asia had tendency increasing production around $18.2 \times 10^6 \text{ m}^3$ in 2010. Eurasia had the lowest growth in biodiesel production compared with other countries. Although Europe represents 80% of global biodiesel production, the USA increased its production at a faster rate than Europe in between 2006-2010. However, Brazil had the highest growth in production rate in the last years compared with USA and Europe and is expected to surpass the USA and European biodiesel production by the year 2015 (Dharmadi, Murarka, & Gonzalez, 2006), i.e. from $736 \times 10^6 \text{ m}^3$ in 2005 to $2.4 \times 10^6 \text{ m}^3$ in 2010. In 2010 (Figure 2.3), there are top ten countries that produce biodiesel. Their production corresponds to approximately 71.3% of the total $19.2 \times 10^6 \text{ m}^3$ of biodiesel. The production of crude glycerol was estimated assuming 0.106 liter per liter of biodiesel. Specifically, the five countries with the biggest biodiesel production are Germany, Brazil, France, Argentina, and USA contributing to more than 50% of global biodiesel production. Thailand is still a small biodiesel producer compared with other countries.

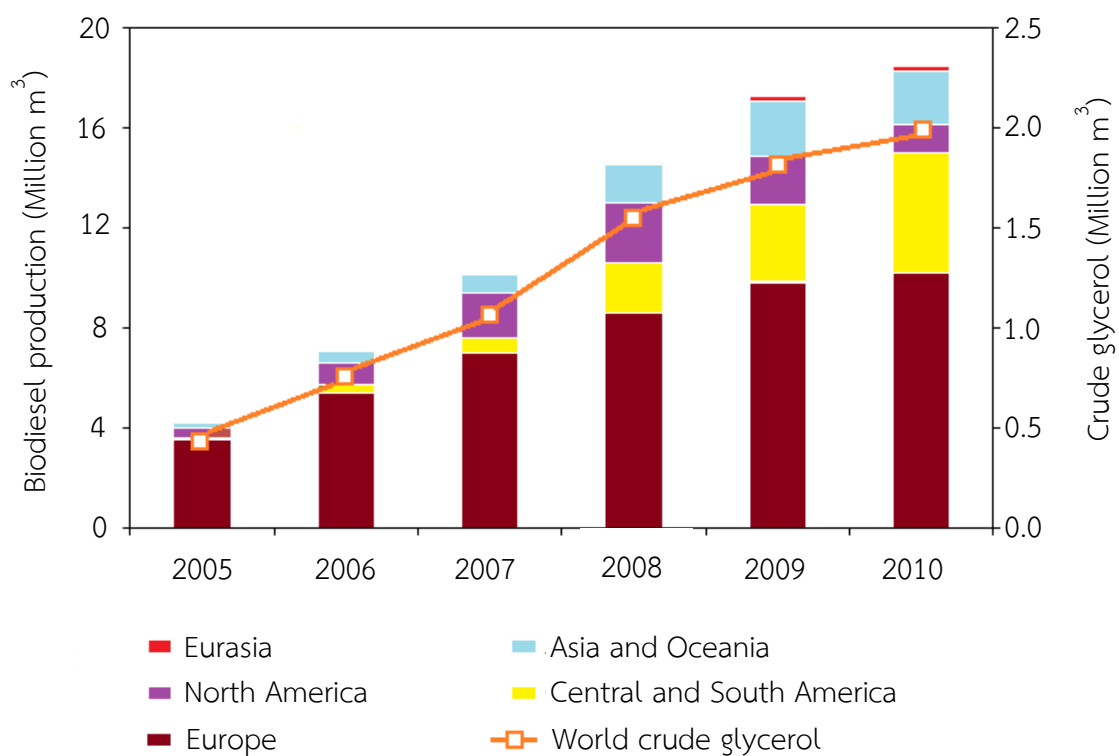


Figure 2.2 Global biodiesel (bars) and crude glycerol (lines) production between 2005 and 2010 (João, Fávoro, & Quirino, 2012).

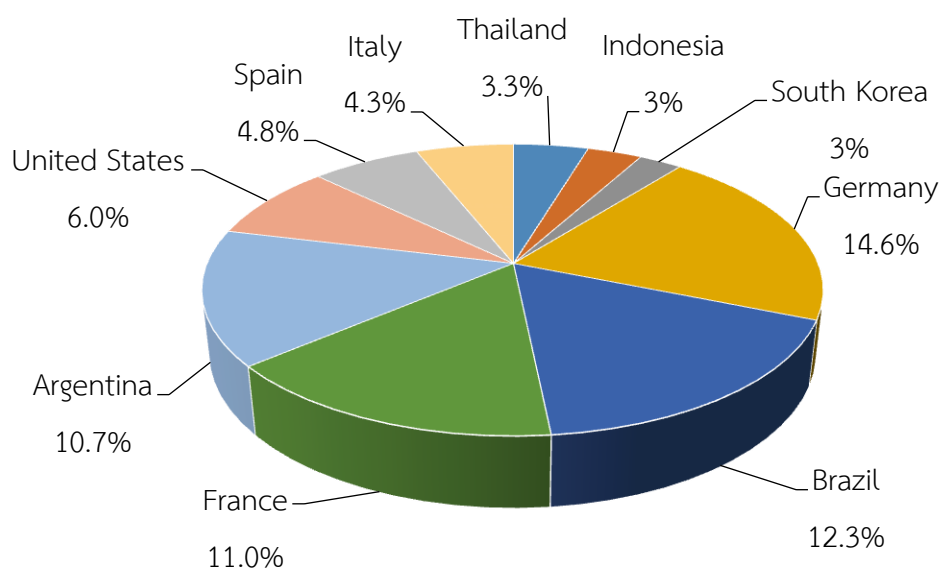


Figure 2.3 Top ten biodiesel producing countries in 2010 (João et al., 2012).

2.2.2 Process flow chart

At the present time, most of the biodiesel is produced by the alkali-catalyzed process as shown in Figure 2.4. The amount of free fatty acids in an alkali-catalyzed process should be lower than 2.5 wt.%. If the oil or fat raw materials have a free fatty acid content over 2.5 wt.%, a pretreatment step is necessary before the transesterification process (ISTC, 2006). Pretreatment methods for reducing the high free fatty acid content in the raw materials are using strong acids such as sulfuric acid (H_2SO_4) or phosphoric acid (H_3PO_4). For the biodiesel production process, raw materials with high free fatty acid will react undesirably with the alkali catalyst thereby forming soap (saponification reaction), providing a lower yield of biodiesel production and inhibiting the separation of fatty acid methyl esters from crude glycerol.

2.2.3 By-product from biodiesel production

Crude glycerol is a main by-product coming from biodiesel production via the transesterification reaction of vegetable oil or animal fat with alcohol. In this process, 1,000 kg of biodiesel usually generates about 100 kg of crude glycerol or 10% production (ASAIM, 2014). With continuous increasing biodiesel production, glycerol capacity quickly increases (Figure 2.2). The rapid increase in glycerol capacity caused a decrease of the market price of glycerol from \$0.43/kg in 2003 to \$0.18/kg in 2010 for pure glycerol, and to only \$0.02/kg for crude glycerol (Maglinao & He, 2011). Crude glycerol with 70-80% purity is often concentrated and purified prior to commercial sale to 95.5-99.0% purity. Sometime, crude glycerol is considered as a waste instead of by product because it contains methanol, salts, soaps and water as the main contaminants. Concentration and the presence of each contaminant will vary drastically from one industry to another, due to a variety of raw material.

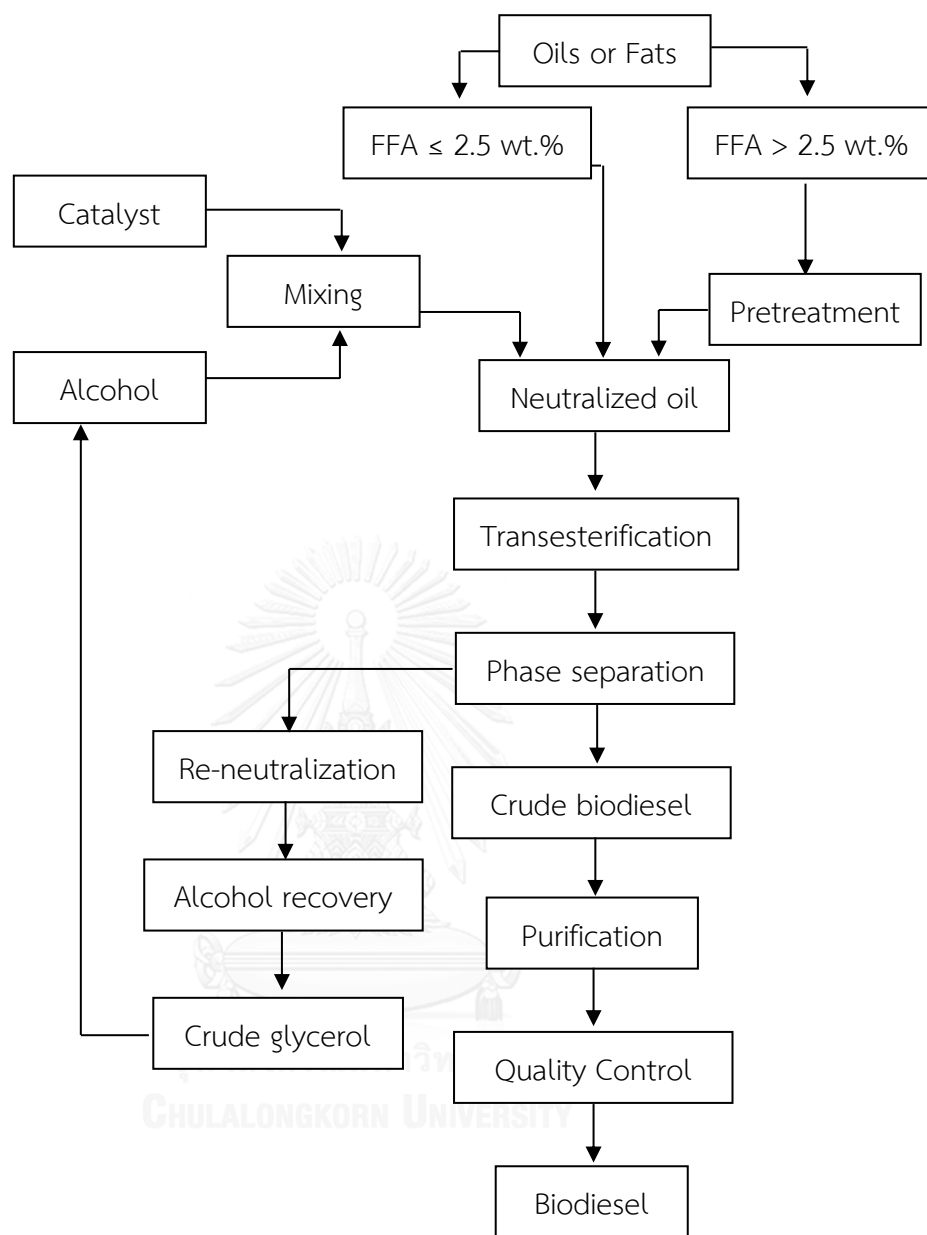


Figure 2.4 Simplified process flow chart of alkali-catalyzed biodiesel production (Leung, Wu, & Leung, 2010).

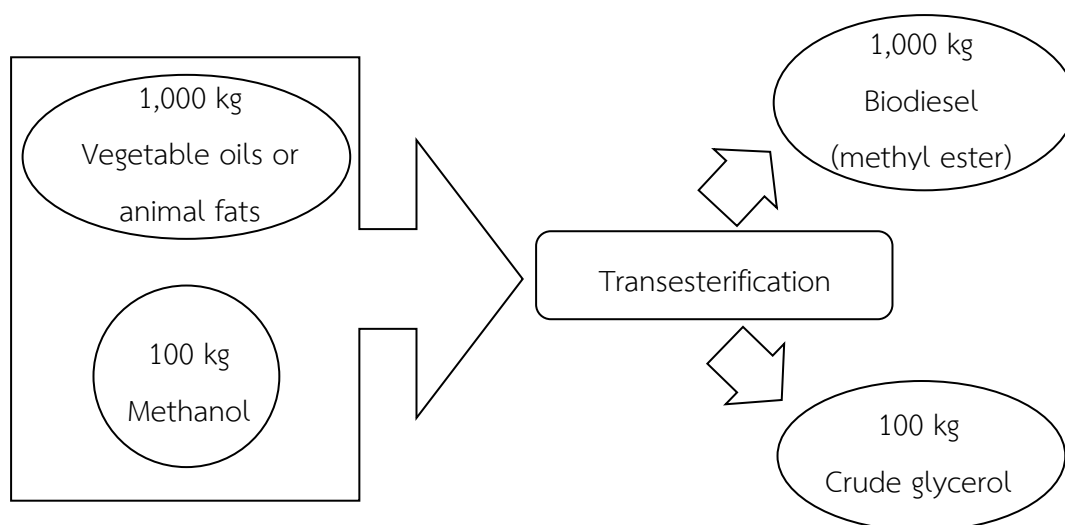


Figure 2.5 Yield of transesterification of triglyceride with methanol (ASAIM, 2014).

2.3 Glycerol

2.3.1 Properties

Glycerol (1,2,3-propanetriol, Figure 2.6), which was called “sweet oil” was discovered more than two centuries ago in 1779 by Swedish chemist named Carl W. Scheele, who obtained a novel transparent, syrupy liquid by heating olive oil with a mixture of lead oxide (PbO, used in lead glazes for ceramics). It is completely soluble in alcohol and water, slightly soluble in many common solvents such as ether and dioxane, but it is insoluble in hydrocarbons. In 1786, the French chemist, Michel E. Chevreul, found the structure of fats as contains tri-esters made up three moles of mixed fatty acid and one mole of “sweet oil”, which is called “glycerin”. The name of glycerol originates from the Greek word for “sweet”, *glykys*, and terms glycerol. On the other hand, the expression of glycerol generally refers to a commercial solution of glycerol in water, of which the principal component is glycerol.

Glycerol contains three hydrophilic alcoholic hydroxyl groups (–OH), which are responsible for its solubility in water and its hygroscopic nature. It is a highly flexible molecule, forming both intra- and intermolecular hydrogen bonds. In its pure anhydrous condition, glycerol has a specific gravity of 1.261 g/cm^3 , molecular weight of 92.09 g/mol , a melting point of $18.2 \text{ }^\circ\text{C}$ and a boiling point of $290 \text{ }^\circ\text{C}$ under normal atmospheric pressure. At low temperature, glycerol may form crystals which melt at

17.9 °C. Glycerol is a colorless, odorless, viscous liquid with a sweet taste. Moreover, it is non-toxic and biodegradable. It has a pleasant taste and odor, which makes it an ideal ingredient in food and cosmetic applications.

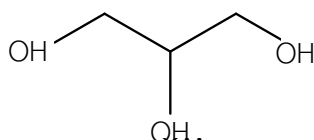


Figure 2.6 Chemical structure of glycerol.

2.3.2 Application

Glycerol has high relative energy, because all three -OH groups are involved in intramolecular hydrogen bonding with the backbone structure of glycerol. Currently, many industries have started to utilize glycerol as a raw material in their product processes. Besides, the research community as well as the biodiesel industry utilizes glycerol as additive material and for value-added applications.

(a) Application of glycerol as additive material

Key glycerol applications are the use without modification, or very basic structural modifications, as an additive to materials. The glycerol is widely used in the manufacture of food and beverages, tobacco, pharmaceuticals, personal care products, urethane foams and synthetic resins. The top use for glycerol is food, personal care and oral care products. These three uses account for 64% of refined glycerol consumption. Figure 2.7 represents a complete breakdown of glycerol consumption by end use.

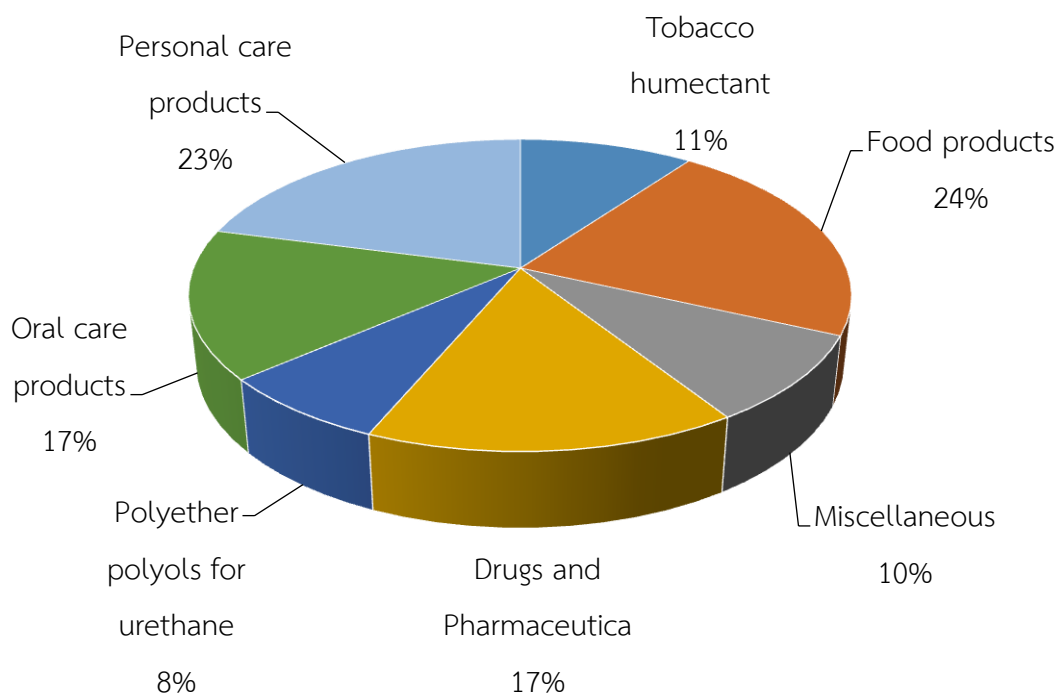


Figure 2.7 Market for refined glycerol (ASAIM, 2014).

For example, in food and beverages industries, glycerol and glycerol esters are approved as food additives in several countries. They improve the quality of food products by preventing desiccation, improving texture and extending shelf life. Glycerol is a humectants, solvent and sweetener and preservative. It acts as a solvent for flavors and food colors in beverages and softening agent in candy, cheese and cakes. It is also used as filter in commercially prepared low-fat foods. Glycerol is added to ice-cream to improve the texture, and its sweet taste decreases the amount of sugar needed. The monoglyceride, the glycerol esters of fatty acids are emulsifiers and stabilizers for many products. They are used in salad dressing, frozen desserts, candy, fondant, gums, wine, bread and food coating. Monoglyceride also helps to maintain moisture balance in a product and permits richer formulations with longer shelf life.

The personal and oral care products account for 23% and 17% of the usage of refined glycerol demand, respectively. The properties of glycerol are ideal ingredients in many personal care products, mostly helping to prevent the moisture loss. Thus, glycerol is used as an emollient in skin creams, lotions, shaving creams, makeup and deodorant. For oral care products, glycerol is commonly found in toothpastes, mouthwashes and sugar-free gum, giving these products a sweet taste without contributing to tooth decay. Gel toothpastes generally contain more glycerol than traditional toothpastes because glycerin helps to provide a smooth appearance.

Glycerol is used as humectants and sweetener in the manufacture of tobacco, accounting for 11% of refined glycerin consumption. Glycerin is often sprayed on leaves before processing to prevent crumbling and dehydration. It is used as a plasticizer in cigarette papers as well as a sweetener in chewing tobacco. Polyether polyols for urethanes, glycerol provides one of the major raw materials for the construction of less rigid polyurethane foams and flexible foams. Moreover, glycerol is the initiator which propylene oxide/ethylene oxide is added. The usage in this category accounts for 8% of glycerol consumption.

For drugs and pharmaceuticals industries, glycerol can function as a plasticizer, moisturizer, solvent, laxative, elixir and for the adjustment of viscosity and osmotic pressure. Glycerol is a component of many pharmaceutical formulations including gelatin capsules, creams, syrups, suppositories, ointments and parenteral solutions. Glycerol trinitrate is well known for the treatment of angina pectoris.

(b) Derivatives of glycerol

The glycerol molecule has two primary and one secondary hydroxyl group (-OH) on adjacent carbons. Because of the multiple -OH groups and their positions on the carbon chain, glycerol has the potential to form more derivatives than an ordinary alcohol. Utilizing the reactivity of the -OH groups, several derivatives can be prepared, including mono-, di- and triesters and ether. Oxidation can lead to many derivatives, such as glyceraldehyde, glyceric aldehyde, and dihydroxyl acetone. Reaction involving -OH groups at adjacent carbon atoms can result in breakage of the carbon-carbon bonds, as in the well-known analytical procedure with periodic

acid (H_5IO_6), or by the condensation of two $-\text{OH}$ groups with another reagent, such as ketone to form heterocyclic derivatives. Many of these reactions find applications in the production of industrially important materials.

(1) Dehydration of glycerol

Catalytic and thermal dehydration of glycerol produces several chemical derivatives (Figure 2.8). Depending upon conditions, dehydration occurs via the loss of a primary $-\text{OH}$ group to form hydroxypropionaldehyde (3-HPA) and acrolein, or at the secondary $-\text{OH}$ group to form hydroxyacetone. Acrolein has received the most attention, primarily due to its use as a precursor to acrylic acid, a high volume industrial chemical with annual production of 2.6×10^9 lb. Acrolein is produced with 86% selectivity and 70% conversion by treating glycerol with hot compressed water at 400°C and 30 MPa (supercritical conditions) in the presence of H_2SO_4 (Watanabe, Iida, Aizawa, Aida, & Inomata, 2007), or at 75% selectivity and 50% glycerol conversion using zinc sulfate promoters (Ott, Bicker, & Vogel, 2006). Glycerol dehydration in the gas phase over a family of supported acid catalysts (15wt% WO_3/ZrO_2) produces acrolein with 65% selectivity at 100% conversion (Chai, Wang, Liang, & Xu, 2007). The mesoporous SiW gave 85% selectivity to acrolein with nearly 100% conversion at 275°C (Tsukuda, Sato, Takahashi, & Sodesawa, 2007). Older processes for converting glycerol to acrolein were not commercialized due to high cost and low catalyst stability. Acrolein can be formed in trace quantities when glycerol is stored in inadequately protected metal containers and exposed to elevated temperature, resulting in very noticeable, strong pungent off-odors. The aqueous acrolein solution may be directly used, for example, in the production of acrylic acid by oxidation reaction or in the production of 1,3-propanediol by catalytic hydrogenation to 3-hydroxypropionaldehyde with subsequent catalytic hydrogenation reaction.

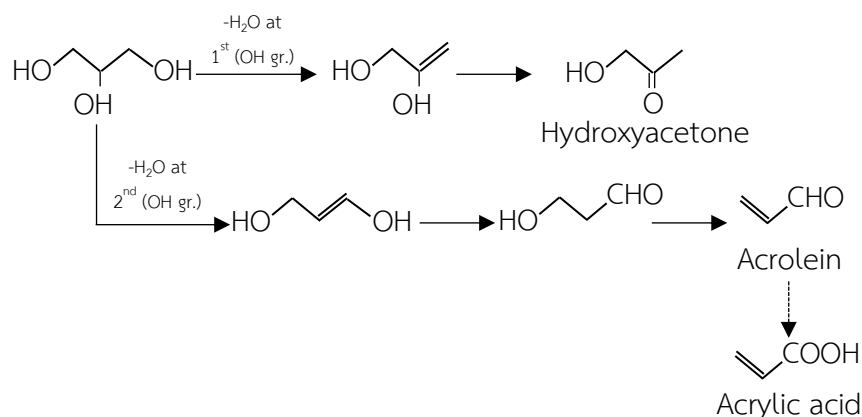
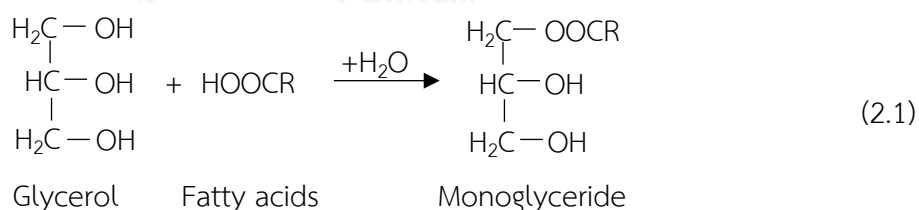


Figure 2.8 Glycerol dehydration routes involving the reaction mechanisms (Tsukuda et al., 2007).

(2) Esterification of glycerol

Esterification of glycerol gives a variety of valuable products and, in recent years, it has been an active area of research. The monoesters and diesters of glycerol occur naturally in fats that have become partially hydrolyzed. The triglycerides are primary components of occurring fats and oils. Monoglyceride and diglycerides are prepared by the direct condensation of a fatty acid or a fat (triglyceride) with glycerol resulting in mixtures containing 40-60% monoglyceride, 30-45% diglycerides and free glycerol. The example of monoglyceride is shown in Eq.(2.1).

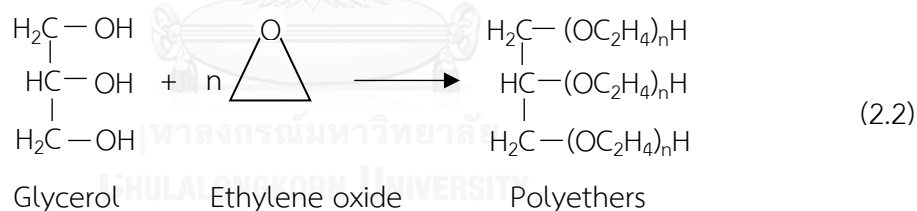


A mixture of monoglyceride, diglycerides and triglycerides is manufactured in huge quantities for use in superglycerinated shortenings. Monoglyceride and diglycerides are important modifying agents in the manufacture of detergents, alkyd resins and other surface-active agents (Knothe, Gerpen, & Krahl, 2005).

(3) Etherification of glycerol

Etherification of glycerol gives various products with isobutylene or *tert*-butanol, including polyglycerols and glycosyl glycerol (Ancillotti & Fattore, 1998). In general, the addition of ethers has a positive effect on the performance of diesel fuels and reduces the quantity of fumes and particulates, oxide of carbon and carbonyl compounds present in engine exhausts. Ethers of glycerol and fatty alcohols occur in natural products. Some typical examples of occurring fatty ethers of glycerol are the alpha glycerol monoethers of stearyl, oleyl and acetyl alcohol.

Glycerol reacts with ethylene oxide or propylene oxide to form polyether. By adding, the hydrophobic propoxy chain followed by the addition of the hydrophilic ethoxyl chain or vice versa, “block copolymer” can be prepared. When the ethoxyl and propoxy chain are properly balanced, these block copolymers have surface-active properties. They also have been used as intermediates in the manufacture of some polymers. Reaction of polyethers production is shown in Eq.(2.2).



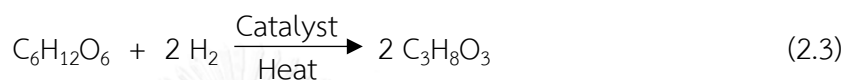
Sunder et al., (1999) studied the restricted synthesis of hyperbranched polyglycerols by ring-opening multi-branching polymerization. In this case, they used glycidol as a monomer and used 1,1,1-tri(hydroxymethyl)propane (TMP) as initiator for the anionic polymerization without initiator as well as cyclization. The major advantage of this preparation is the narrow molecular weight distribution.

(4) Hydrogenolysis of glycerol

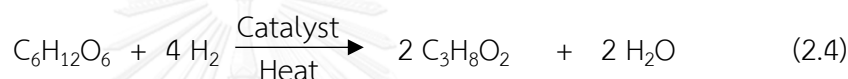
Hydrogenolysis is a term describing the chemical reaction, in which hydrogen (H_2) is used to break molecular bonds in large organic molecules in

order to provide smaller molecules. Hydrogenolysis reaction is usually controlled over a catalyst at high temperature and high H₂ pressure.

Theoretically, the primary reaction is H₂ splitting of the alditol molecule at the center carbon-carbon bond to produce glycerol, or propylene glycol and water. However, there seems to be no evidence that these reactions occur completely, since it is almost always the case that both glycerol and propylene glycol are produced in alditol hydrocracking. Eq.(2.3)-(2.4) are the simple chemical equations for formation of glycerol and propylene glycol from sorbitol.

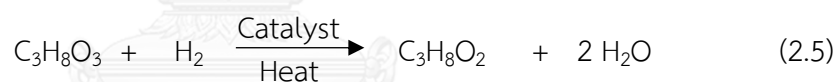


Sorbitol Glycerol



Sorbitol Propylene glycol

It was found that glycerol will be hydrocracked to propylene glycol, as in Eq. (2.5).

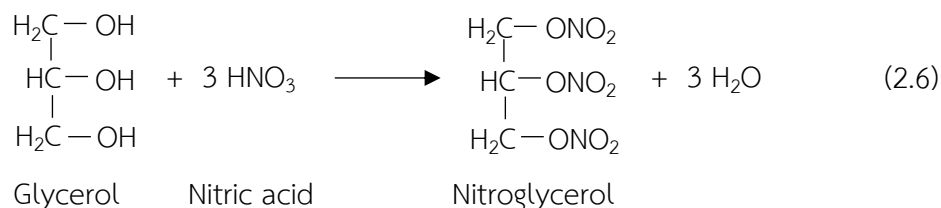


Glycerol Propylene glycol

A screening study of catalysts has shown that good selectivity for propylene glycol and high conversion is readily achieved using a copper chromite catalyst (Suppes, Chiu, Sutterlin, & Ramos, 2006). Practically, pure propylene glycol is obtained from the autoclave. At temperatures above 200 °C, the selectivity to propylene glycol decreases, due to excessive hydrogenolysis of the 1,2-propanediol.

(5) Nitration of glycerol

Nitration of glycerol is used to produce nitroglycerol, which is a common biological molecule from which triglycerides fats and oil are made. All the -OH groups have been replaced by -NO₂ as is shown in Eq.(2.6).



When glycerol is treated with nitrating agents, it forms a solution containing dinitroglycerol. Then, the solution is treated with a cyclizing agent. The dinitroglycerol is then converted into glycidyl nitrate, which can be further polymerized to poly(glycidyl nitrate) (PGN).

(6) Oxidation of glycerol

Oxidation of glycerol is of particular interest due to the commercial importance of oxygenated glycerol derivatives. During the last decade, an electrochemical and biological oxidation method has been explored for creating a market outlet for the large surplus of biodiesel glycerol. Glycerol is quite stable in the presence of oxygen under common conditions but it is oxidized in the presence of certain catalysts such as iron and copper. Moreover, glycerol is readily oxidized by a variety of chemical and microbiological oxidants, as well as electrolysis.

Theoretically, glycerol can be oxidized to many oxidation products such as glyceraldehyde, dihydroxyl acetone as shown in Eq.(2.7), glyceric acid, mesoxalic acid, and etc. Partial oxidation is usually hard to control. The oxidation products have been isolated through more often they are prepared by indirect methods rather than the controlled oxidation of glycerol.

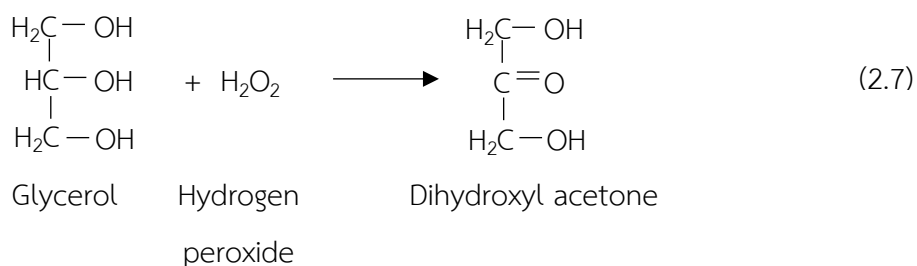
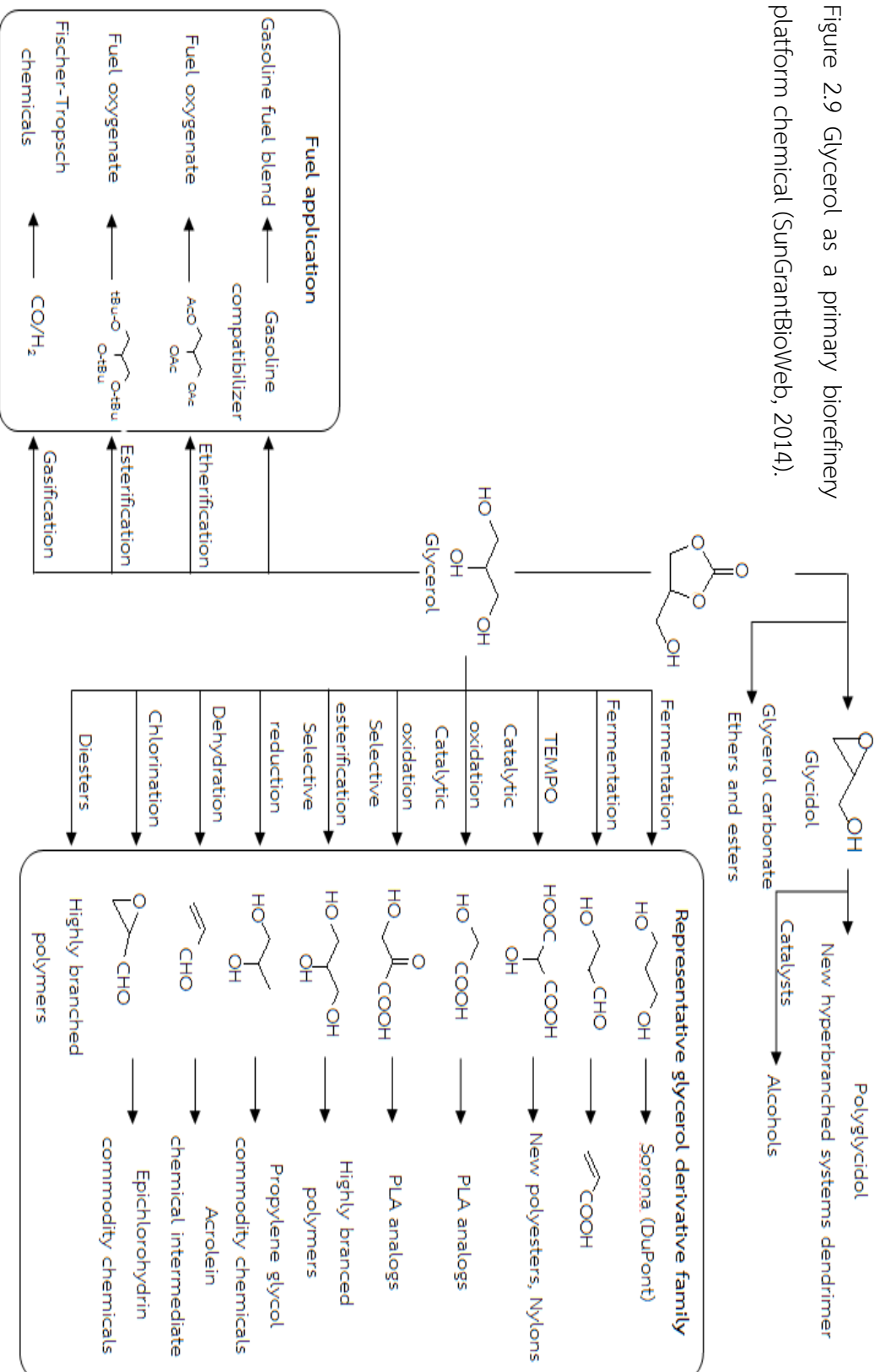


Figure 2.9 summarizes the products of glycerol conversion via various processes.

Figure 2.9 Glycerol as a primary biorefinery platform chemical (SunGrantBioWeb, 2014).



2.4 Acrylic acid

2.4.1 Properties

Acrylic acid (2-propenoic acid, Figure 2.10) is an unsaturated carboxylic acid having the chemical formula of $\text{CH}_2=\text{CHCOOH}$. Purified (glacial) acrylic acid is a colorless liquid with an irritating acid odor at room temperature and pressure. Its odor threshold is low (0.20-3.14 mg/m^3). It is miscible in water and most organic solvents. Acrylic acid is commercially available in two grades: technical grade (94% for esterification, and glacial grade (98-99.5% by weight and a maximum of 0.3% water by weight) for production of water-soluble resins. Acrylic acid can polymerize easily when it is exposed to heat, light or metals. So, a polymerization inhibitor is added to commercial acrylic acid to prevent the strong exothermic polymerization.

Acrylic acid reacts readily with free radicals and electrophilic or nucleophilic agents. It may polymerize in the presence of acids (sulfuric acid (H_2SO_4), chlorosulfonic acid (ClSO_3H)), alkalis (ammonium hydroxide (NH_4OH)), amines (ethylenediamine, ethyleneimine, 2- aminoethanol), iron salts, elevated temperature, light, peroxides, and other compounds that form peroxides or free radicals. In the absence of inhibitor, peroxides are formed when oxygen is sparing into acrylic acid. The presence of oxygen is required for the stabilizer to function effectively. Acrylic acid must never be handled under an inert atmosphere. Freezing of acrylic acid occurs at 13°C . Acrylic acid is a strong corrosive agent to many metals, such as unalloyed steel, copper and brass. Physical properties of acrylic acid are listed in Table 2.1.

Acrylic acid undergoes the reaction characteristics of both unsaturated acids and aliphatic carboxylic acids or esters. The high reactivity of these compounds emanates from the two unsaturated centers situated in the conjugated position. The β -carbon atom, polarized by carbonyl group, behaves as an electrophile. This favors the addition of a large variety of nucleophiles and active hydrogen compounds to the vinyl group. Moreover, the carbon-carbon double bond undergoes the radical-initiated addition reactions, Diels-Alder reactions with dienes, and polymerization reactions. The carboxyl function is subject to the displacement reactions typical of aliphatic acids and esters, such as esterification and transesterification. Joint reactions

of the vinyl and carboxyl functions, especially with bifunctional reagents, often constitute a convenient route to polycyclic and heterocyclic substances. Acrylic acids polymerize very easily. The polymerization is catalyzed by light, heat and peroxides and inhibited by stabilizers. The highly exothermic, spontaneous polymerization of acrylic acid is extremely violent.

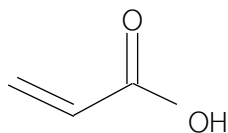


Figure 2.10 Chemical structure of acrylic acid.

2.4.2 Application

In 1994, the worldwide acrylic acid production was anticipated to be around 2 million tones. Acrylic acid is used mainly as a starting material in the production of acrylic esters; as a monomer for polyacrylic acid and salts, as a comonomer with acrylamide for polymers used as flocculants, with ethylene for ion exchange resin polymers, with methyl ester for polymers. Acrylic acid is used in the field of

- Plastics, paper manufacture and coating
- Exterior house paints for wood and masonry
- Coatings for compressed board and related building materials
- Flocculation of mineral ore fines and waste water and treatment of sewage
- Printing inks
- Floor polishes
- Floor and wall coverings
- Industrial primers
- Textile sizing, treatment and finishing
- Leather impregnation and finishing
- Masonry sealers
- Lubricating and fuel oil additives
- Lacquers for automotive, appliance and furniture finishes
- Pharmaceutical binders
- Hot metal coatings

Table 2.1 Physical properties of acrylic acid. (Digitallibrary, 2014).

Physical property	
Molecular weight	72
Melting point (°C)	13.5
Density at 25 °C (g/cm ³)	1.045
Boiling point (°C/mm Hg)	141/760
Refractive index at 25 °C	1.4185
Flash Point (°C)	68
Kinematic viscosity at 25 °C (cSt)	1.1
Dissociation constant at 25 °C	5.50×10^{-5}
pK _a	4.26
Solubility at 25 °C in water	infinity
Critical temperature (°C)	380
Critical pressure (MPa)	5.06
Heat of vaporization at 101.3 kPa (kJ/mol)	45.6
Heat of combustion (kJ/mol)	1376
Heat of melting at 13 °C (kJ/mol)	11.1
Heat of neutralization (kJ/mol)	58.2
Heat of polymerization (kJ/mol)	77.5
Autoignition temperature (°C)	390-446
Henry's law constant (atm.m ³ /mol)	3.2×10^{-7}
Solubility in organic solvents	
• Alcohol	Miscible
• Chloroform	Miscible
• Benzene	Miscible
• Acetone	Soluble (>10%)

From the acrylic acid market analysis, the acrylic acid industry is mature in the United States of America (Figure 2.11), but still developing rapidly in some parts of Asia and the Middle East. End-use demand for acrylic acid in a mature market is exemplified below (Nexant'sGlobal, 2014).

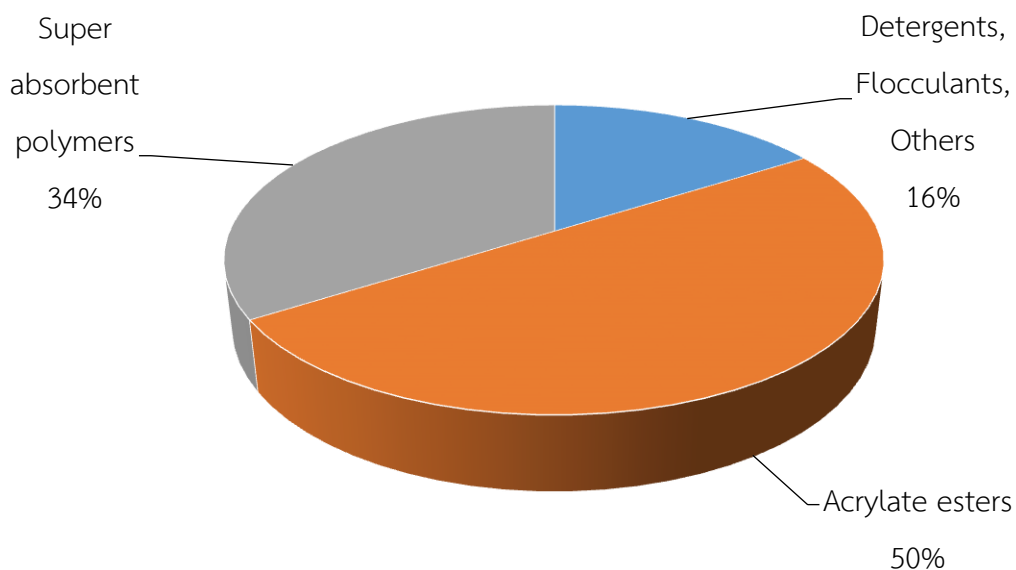


Figure 2.11 USA acrylic acid consumption by end-use (Nexant'sGlobal, 2014).

Acrylic acid, as well as its derivatives, has received much popularity in the global market (Figure 2.12). It can be explained by the growth of super absorbent polymers usage, which is one of the main applications of acrylic acid. System application product market is expected to grow 5% per year in the future. These market conditions contribute to introduction of new acrylic acid. Asia such as China, South Korea and Japan are on track to become the world largest acrylic acid manufacturer with approximately 47% share (MRC, 2014).

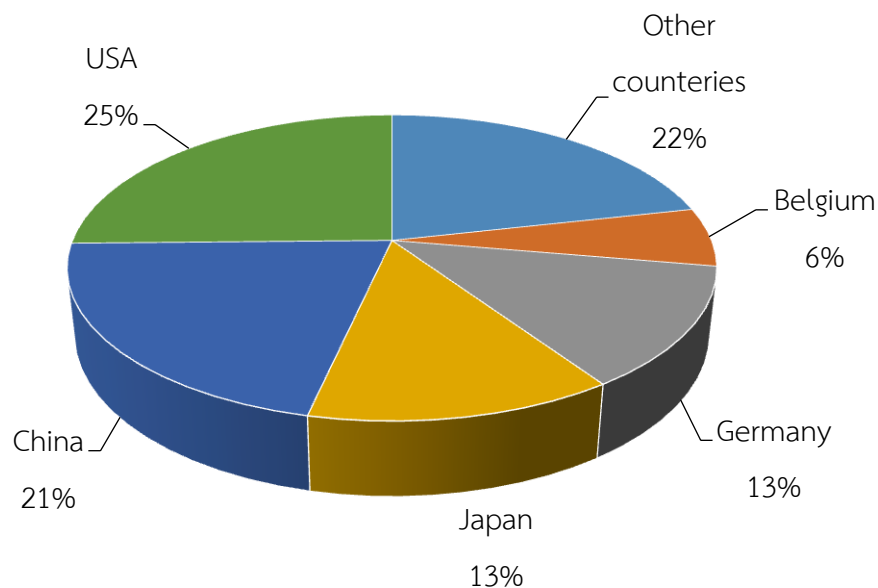


Figure 2.12 Global acrylic acid production in 2012 (MRC, 2014).

2.4.3 Acrylic acid production processes (Sbioinformatics.com, 2014)

(1) Acrylonitrile process

Acrylonitrile is used as a reactant in the production of acrylic acid by using acidic hydrolysis reaction as shown in Eq.(2.8). The remaining acrylonitrile in the reaction will inhibit the occurrence of acrylic acid. As a result of the increasing molecular weight on hydrolysis, it provides a definite yield improvement.



(2) Acrylic ester process

The acrylic ester process is impeded by the ready polymerisability of the acrylic ester. Generally, the products of this process are acrylic acid and alcohols when using acid hydrolysis as shown in Eq.(2.9).



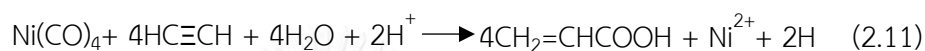
It is normally preferable to use saponification of the ester to generate the salt as shown in Eq.(2.10).



(3) Carbonyl reaction process

Basic raw materials in the preparation of acrylic acid by the carbonyl reaction are acetylene, carbon monoxide (in the form of nickel carbonyl), and water. This process is the hydrocarboxylation of acetylene ("Reppe chemistry"). Three different processes are known.

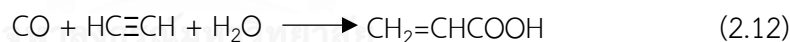
- Stoichiometric carbonyl reaction



This reaction is very fast at atmospheric pressure and at low temperature. According to Eq.(2.11), consumed by side reaction, the hydrogen in gaseous form does not appear.

- Catalytic carbonyl reaction

The catalytic reaction requires elevated temperature and high pressures as shown in Eq.(2.12). Nickel salts or complexes are used as catalysts.

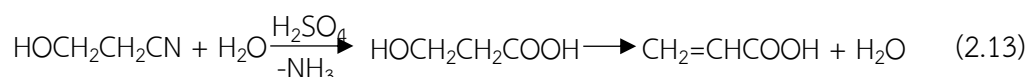


- Semicatalytic carbonyl reaction

The catalytic reaction of acetylene, carbon monoxide and water imposed upon the stoichiometric reaction of nickel carbonyl, acetylene, water and acid. The characteristic of stoichiometric reaction can use in the mild conditions, with a large quantity of the total carbon monoxide (CO) being supplied as carbon monoxide gas, the nickel carbonyl ($\text{Ni}(\text{CO})_4$) is used as catalyst.

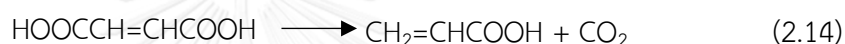
(4) Ethylene cyanohydrin process

This process involves the acidic hydrolysis and dehydration of ethylene cyanohydrins as shown in Eq.(2.13). The products from the reaction mixture are separated by distillation. The product, like all other polymerizable monomers, should be carefully separated from the reaction mixture and appropriately cooled before uncontrolled polymerization can ensue.



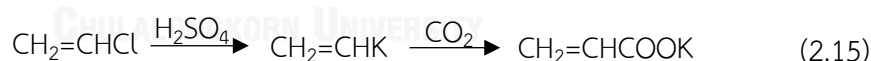
(5) Maleic acid process

The maleic acid process is a patented method that involves the decarboxylation of maleic acid to form the acrylic acid as shown below:



(6) Potassium vinyl process

The low temperature conversion of vinyl chloride with potassium metal and a subsequent treatment of the cold vinyl potassium with dry ice are reported to give potassium acrylate ($\text{C}_3\text{H}_3\text{KO}_2$) in 70% conversion. Customary process produces acrylic acid as shown in Eq.(2.15).

(7) β -Propiolactone process

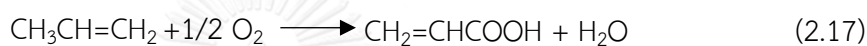
This commercial process is based on the polymerization of β -propiolactone and the destructive distillation of this polymer to form acrylic acid as shown in Eq.(2.16).



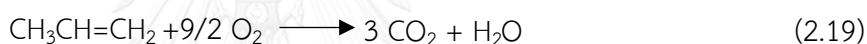
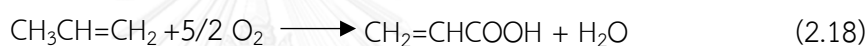
(8) Propylene process

The most widely accepted process for making acrylic acid is the vapor phase oxidation of propylene. This is normally done as a standard process

involving two reactors in series, utilizing two separate catalysts. In this process, the first reactor converts the propylene to acrolein while the second reactor completes the conversion from acrolein to acrylic acid. Instead of utilizing this common process for production, this design project specifies a one-reactor system using a molten salt heat transfer medium in order to relieve the system of the heat of reaction produced. When implemented properly, the temperature distribution should result in approximately 90% conversion of propylene. Under production conditions, the reaction to optimize is the conversion of propylene to acrylic acid over the use of a catalyzed reaction, given by Eq. (2.17) to (2.19):



However, a couple of competing reactions are involved:



An alternative route is the catalytic oxidation to acrolein and to acrylic acid with oxygen over certain metallic catalysts such as molybdenum (Mo), cobalt (Co) or cerium (Ce).

(9) Vinyl “Grignard reagent” process

This interesting process involves the use of the well-known carboxylation of a Grignard reagent to form the acid as shown below.



(X: Halogen elements such as F, Cl, Br, I and At)

For a route to be commercially attractive, the raw material costs and utilization must be low, plant investment and operating cost should not be excessive, and waste disposal charges should be minimal. A lead time of several years for development and plant construction is important in a period where the availability of hydrocarbon raw materials is changing rapidly and significantly. Natural gas costs are expected to rise steadily while the supply is decreasing. Acetylene should be in short supply with increasing costs in the next decade unless new technology based

on coal is developed. Hence, acrylic acid manufacture by acetylene routes will be increasingly uneconomical. Ethylene cost, depend on crude oil is expected to increase, but not sharply. Propylene may be considered as by-product from the large volume manufacture of ethylene from heavy petroleum feed stocks. New ethylene facilities, based on naphtha and other heavy feed stocks, will ensure a large supply of co-products including propylene. Propylene requirements for acrylic acid will be small, compared to other chemical uses such as polypropylene, acrylonitrile, propylene oxide, isopropanol and cumene for acetone and phenol. For this reason, the cost of propylene is expected to rise; this should be at a slower rate than the increase of the other raw materials. The favorable supply and cost projection for propylene suggest that all new acrylic acid plants will employ propylene oxidation technology for at least the next two decades. The most economical process for the manufacture of acrylic acid is based on the two-stage vapor phase oxidation of propylene to acrylic acid. Processes based on acetylene at high pressure, "Repp process (BASF)" or the modified "Repp process (Rohm Haas)" based on acrylonitrile is still being used for the production of acrylic acid. A ketone and an ethylene cyanohydrin process were once commercially important, but are no longer used. The propylene oxidation process is attractive because of the availability of highly active and selective catalysts and the relatively low cost of propylene (Sbioinformatics.com, 2014).

Besides, acrylic acid can also be produced from glycerol via a two-step reaction process in the presence of catalyst as demonstrated in Figure 2.13. Initially, glycerol is dehydrated to the acrolein or acrylaldehyde that is very reactive species. It can further oxidize to acrylic acid by either using a single bifunctional catalyst via the one-pot approach or by using a process that involves two separate steps (Chiericato et al., 2012).

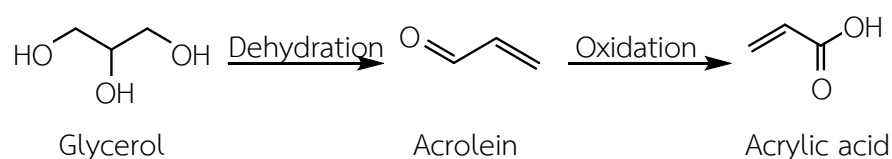


Figure 2.13 Reaction route for dehydration and oxidation of glycerol to acrylic acid.

For the one-pot approach, the iron oxide (FeO_x) domains on the surface of an iron orthovanadate (FeVO_4) phase exhibited a better catalytic activity for the oxidative dehydration than FeO_x catalyst prepared by impregnation method and a mixture of FeVO_4 and iron (III) oxide (Fe_2O_3) (Xu, Dubois, & Ueda, 2010). High acrylic acid yields up to 14% were obtained in a fixed-bed reactor at $300\text{ }^\circ\text{C}$ with a feed composition $\text{N}_2:\text{O}_2:\text{H}_2\text{O}:\text{glycerol} = 66.6:1.7:30.3:1.5$. The hemihydrate $\text{VOHPO}_{40}\cdot 5\text{H}_2\text{O}$ oxide emerged as the best catalyst for complete dehydration of glycerol at $300\text{ }^\circ\text{C}$ in a gas-phase fixed-bed reactor (Wang, Dubois, & Ueda, 2009). The addition of oxygen helped to maintain an oxidized state of the catalyst and eliminate the coke formation (Wang, Dubois, & Ueda, 2009). However, this catalyst was less active toward the one-step conversion of glycerol to acrylic acid due to its low oxidation ability. In the gas phase reaction at $300\text{ }^\circ\text{C}$ over MoVTenbO catalysts, almost complete conversion of glycerol (99.6%) was achieved with a high yield of acrylic acid (28.4%) (Deleplanque, Dubois, Devaux, & Ueda, 2010). However, this was accompanied by a high yield (up to 23%) of undesired acetic acid byproduct. W-V-O bronze catalysts with hexagonal tungsten bronze (HBT) structure and a V/(W+V) ratio in the range of 0.12-0.21 allowed the consecutive one-pot oxidation of acrolein into acrylic acid with up to 25% yield (Soriano et al., 2011). High acrylic acid yield up to 34% was obtained at $290\text{ }^\circ\text{C}$ by incorporation of Nb^{5+} into the tri-component bronze structure (W-V-Nb) with atomic ratios $\text{V}/(\text{W}+\text{V}+\text{Nb}) = 0.13$ and $\text{Nb}/(\text{W}+\text{V}+\text{Nb}) = 0.13$ (Chiericato et al., 2012). To increase acrylic acid yield, a two-bed system was used to convert glycerol to acrolein over a zeolite catalyst followed by selective oxidation of acrolein to acrylic acid over a V-Mo oxide catalyst (Witsuthammakul & Sooknoi, 2012). Although high glycerol conversion and product selectivity were obtained, this work was carried out in gas phase and high temperature ($275\text{-}400\text{ }^\circ\text{C}$), which leads to high cost and complex system.

To avoid previous these, the synthesis of acrylic acid from glycerol in one-step process is more interesting because it can reduce the engineering investment cost, simplify the operation and control, and is environmentally friendly. In the present work, supported POM catalysts are used in a one-pot process for the liquid phase conversion of glycerol to acrylic acid, with the goal to simplify the process and

reduce the capital cost of the process. The supported POM catalysts must be oxygen donating-catalysts on acid support. The advantage of these catalysts is the possibility to control solid acid strength and the enhancement of active surface area (Moffat, 2001). The influence of catalyst types, catalyst loadings, and reaction time on glycerol conversion and product yields is investigated.

2.5 Polyoxometalate (POM)

Among oxygen donating-catalysts, POM is a promising candidate because it has high acid strength with high redox catalysis and thermal stability and high solubility in polar solvents such as water and alcohol (Marchal-Rochand & Millet, 2001). Generally, POM is a polyatomic ion, usually an anion, which consists of three or more transition metal oxyanions linked together by shared oxygen atoms to form a large, closed 3-dimensional framework. The metal atoms are usually group V or group VI transition metals (M) such as V, Nb, Mo and W. In their high oxidation states, their electron configuration is d^0 or d^1 , which is very reactive to form the reaction. The framework of transition metal oxyanions may enclose one or more heteroatoms (X) such as phosphorus (P) or silicon (Si), themselves sharing neighboring oxygen atoms with the framework (Kozhevnikov, 1998). Generally, POMs are found in four different types including:

- Lindqvist structure

It is an iso-polyoxometalate having the general formula of $[M_6O_{19}]^{n-}$, where the value of n is depending upon the metal substitutions. The advantages of this structure are acid strength and high symmetry (Figure 2.14).

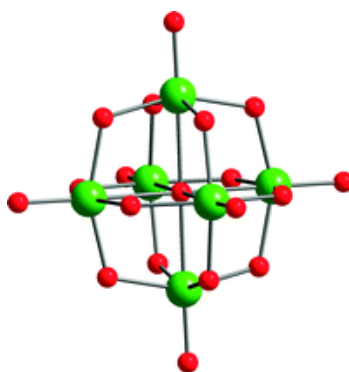


Figure 2.14 Lindqvist structure (May & Peter, 2012).

- Anderson-Evans structure

It is an hetro-polyoxometalate having the general formula of $[XM_6O_{24}]^{n-}$, where the value of n is depending upon the metal substitutions. The advantages of this structure are attractive planar structures and each addenda atom has two terminal oxygen atoms with high reactivity (Figure 2.15).

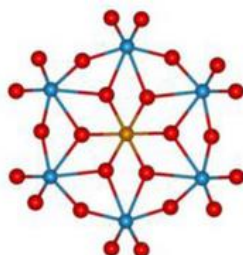


Figure 2.15 Anderson-Evans structure (Mauro & Silvia, 2014).

- Dawson structure

It is an hetro-polyoxometalate, having the general formula of $[X_2M_{18}O_{62}]^{n-}$, where the value of n is depending upon the metal substitutions. The advantages of this structure are that it is easily recoverable and reusable (Figure 2.16).

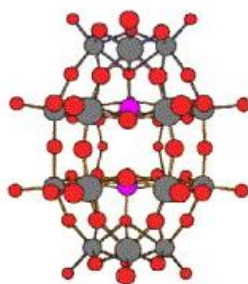


Figure 2.16 Wells-Dawson structure (Li, Ding, Wang, Wang, & Suo, 2007).

- Keggin structures

It is an hetro-polyoxometalate composed of a central tetrahedral (XO_4^-) surrounded by 12 linked octahedral containing the addenda atom ($M_{12}O_{36}$) (Figure 2.17) with the general formula of $[XM_{12}O_{40}]^{n-}$. The overall charge of the central tetrahedral is delocalized over the entire structure. Although other metals could be used as central atom, phosphorus leads to the more stable anions and is most of the time present in POM-compounds used as catalysts.

The POM with Keggin structures have been widely employed as oxidation catalysts in various homogeneous and heterogeneous chemical reactions (Hill & Prosser-McCarthy, 1995; Kozhevnikov, 1995; Okuhara, Mizuno, & Misono, 1996) of their good basis for the molecular design, high capabilities in practical uses, controllability in a systematic way of framework polyatom, strong Brønsted acidity, high thermal stability and high solubility in polar solvents (Song & Barteau, 2002).

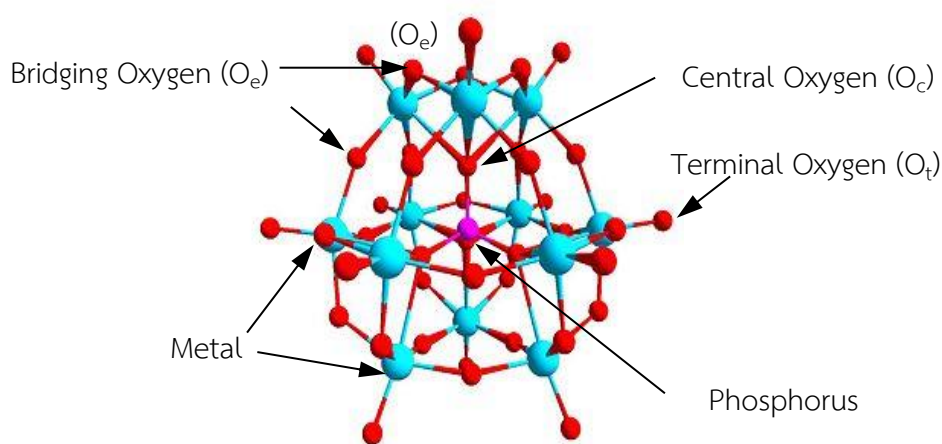


Figure 2.17 Keggin structure of the phosphotungstic acid (Liu, Wang, Zhai, Li, & Wang, 2004).

The catalytic function of the Keggin structure, the types of metal substituted POM structures, has attracted much attention particularly because these compounds provide a good basis for the molecular design and high capabilities in practical uses. There are several large-scale industrial processes that use POMs as oxidation and acid catalysts since most of them are environment friendly. Wang et al. (2005) studied the oxidation of alcohols with oxidizing agent in biphasic system. Mono-substituted Keggin-POM complex $\text{Na}_6[\text{SiW}_{11}\text{ZnH}_2\text{O}_{40}]\cdot 12\text{H}_2\text{O}$ was demonstrated to be an effective catalyst for the selective oxidation of alcohols in the presence of oxidizing agent such as hydrogen peroxide (H_2O_2). This indicates that the oxidizing agent might play an important role in the oxidation reaction.

2.6 Oxidizing agent (Hudlicky, 1990)

An oxidizing agent (also called an oxidizer or oxidant) is a chemical compound that voluntarily transfers oxygen atoms or a substance that gains electrons in an oxidation. There are several types of oxidizing agents such as air, oxygen (O_2), ozone (O_3), and hydrogen peroxide (H_2O_2). The relative strengths of oxidizing agents can be obtained from the value of their standard potential.

- Air

Air is the cheapest oxidant. It is used only rarely without irradiation and without catalysts. Examples of oxidation by pure air are the conversion of aldehydes into carboxylic acid (auto-oxidation). Generally, exposure to light, irradiation with ultraviolet light or catalysts is needed.

- Oxygen (O_2)

It exists in two states including stable ground-state and excited-state. The stable ground-state oxygen (triplet oxygen) has two odd electrons with parallel spins. It behaves like a di-radical and is paramagnetic. In excited-state oxygen (singlet oxygen), the two odd electrons possess anti-parallel spins. Such molecule are unstable, with a half-life of 10^{-6} s, and are diamagnetic. Each form reacts differently with organic molecules.

- Ozone (O_3)

A blue gas and a dark blue liquid (bp. -106°C , -116°C or -125°C ; depending on the data source) are used in a mixture with oxygen. Ozonizations are carried out by passing ozone-containing oxygen through solution of organic compounds in solvents that do not react with ozone and liquids at low temperature. Cooling with dry ice acetone bath (-78°C) is frequently needed to prevent the decomposition of ozone, which is unstable at room temperature. The most common solvents are pentane, dichloromethane, chloroform, cyclohexane, methanol, ethyl acetate and acetic acid.

- Hydrogen peroxide (H_2O_2)

Hydrogen peroxide is an effective oxidant that could be used in many industrial processes. Because the by-product of oxidation using hydrogen

peroxide is only water, it could become the ultimate green chemical for the manufacture of many oxygenated petrochemicals. However, the current method for producing is inefficient and too costly. It is commercially available in aqueous solution of 30 wt.% or 90 wt.% concentration. The 30 wt.% H_2O_2 is a colorless liquid (density at 20 °C: 1.350 g/cm^3) and it is stabilized against decomposition, which occurs in the presence of traces of aluminum (Al), platinum (Pt), iron (Fe), copper (Cu) and other transition metals. The 30 wt.% H_2O_2 does not mix with non-polar organic compounds.

The relative strengths of oxidizing agents can be inferred from their standard electrode potentials as demonstrated in Table 2.2.

Table 2.2 Standard electrode potentials in aqueous solution at 25°C (HyperPhysics, 2014).

Cathode (Reduction) Half-Reaction	Standard Potential E° (volts)
$2\text{H}_2\text{O}(\text{l}) + 2\text{e}^- \longrightarrow \text{H}_2(\text{g}) + 2\text{OH}^-(\text{aq})$	-0.83
$\text{ClO}_4^-(\text{aq}) + \text{H}_2\text{O}(\text{l}) + 2\text{e}^- \longrightarrow \text{ClO}_3^-(\text{aq}) + 2\text{OH}^-(\text{aq})$	0.17
$\text{ClO}_3^-(\text{aq}) + \text{H}_2\text{O}(\text{l}) + 2\text{e}^- \longrightarrow \text{ClO}_2^-(\text{aq}) + 2\text{OH}^-(\text{aq})$	0.35
$\text{IO}^-(\text{aq}) + \text{H}_2\text{O}(\text{l}) + 2\text{e}^- \longrightarrow \text{I}^-(\text{aq}) + 2\text{OH}^-(\text{aq})$	0.49
$\text{ClO}_2^-(\text{aq}) + \text{H}_2\text{O}(\text{l}) + 2\text{e}^- \longrightarrow \text{ClO}^-(\text{aq}) + 2\text{OH}^-(\text{aq})$	0.59
$\text{ClO}^-(\text{aq}) + \text{H}_2\text{O}(\text{l}) + 2\text{e}^- \longrightarrow \text{Cl}^-(\text{aq}) + 2\text{OH}^-(\text{aq})$	0.90
$\text{NO}_3^-(\text{aq}) + 4\text{H}^+(\text{aq}) + 3\text{e}^- \longrightarrow \text{NO}(\text{g}) + 2\text{H}_2\text{O}(\text{l})$	0.96
$\text{O}_2(\text{g}) + 4\text{H}^+(\text{aq}) + 4\text{e}^- \longrightarrow 2\text{H}_2\text{O}(\text{l})$	1.23
$\text{Cr}_2\text{O}_7^{2-}(\text{aq}) + 14\text{H}^+(\text{aq}) + 6\text{e}^- \longrightarrow 2\text{Cr}^{3+}(\text{aq}) + 7\text{H}_2\text{O}(\text{l})$	1.33
$\text{Cl}_2(\text{g}) + 2\text{e}^- \longrightarrow 2\text{Cl}^-(\text{aq})$	1.36
$\text{MnO}_4^-(\text{aq}) + 8\text{H}^+(\text{aq}) + 5\text{e}^- \longrightarrow \text{Mn}^{2+}(\text{aq}) + 4\text{H}_2\text{O}(\text{l})$	1.49
$\text{H}_2\text{O}_2(\text{aq}) + 2\text{H}^+(\text{aq}) + 2\text{e}^- \longrightarrow 2\text{H}_2\text{O}(\text{l})$	1.78
$\text{S}_2\text{O}_8^{2-}(\text{aq}) + 2\text{e}^- \longrightarrow 2\text{SO}_4^{2-}(\text{aq})$	2.01
$\text{O}_3(\text{g}) + 2\text{H}^+(\text{aq}) + 2\text{e}^- \longrightarrow \text{O}_2(\text{g}) + \text{H}_2\text{O}(\text{l})$	2.07
$\text{F}_2(\text{g}) + 2\text{e}^- \longrightarrow 2\text{F}^-(\text{aq})$	2.87

2.7 Literature reviews

In the preceding few decades, the use of polyoxometalate (POM) and POM-based compounds as catalysts has become a very important both in commercial scale and in research area. The vapor-phase oxidation of methacrolein into methacrylic acid is a typical commercialized process utilizing the Keggin structure POM as a heterogeneous oxidation catalyst (Ai, 1981; Mori, Mizuno, & Misono, 1991). In the research field, various research works focused on effective catalysts for oxidation.

Shen et al., (2012) studied the catalytic performance of silicotungstic ($H_4SiW_{12}O_{40}$, SiW), phosphotungstic ($H_3PW_{12}O_{40}$, PW), and phosphomolybdic acids ($H_3PMo_{12}O_{40}$, PMo) in the liquid phase dehydration of glycerol to acrolein in a semi-batch reactor. The SiW exhibited high catalytic activity in the dehydration of glycerol to acrolein. The maximum acrolein yield of 78.6% was achieved when glycerol was completely converted at the reaction temperature of 300 °C with the mole ratio of SiW to glycerol of 0.0001:1. The catalytic activities of the POM toward the formation of acrolein were in an order of SiW > PW > PMo, revealing that the dehydration of glycerol to acrolein was affected by the acidity and the stability of the POM. Hydroxyacetone and acetic acid were also detected with yields of less than 10%, respectively.

The effect of surface area and acidity of nanoparticles of supported POM catalysts on catalytic activity was studied by Kim et al., (2011) using a microemulsion technique to prevent the dissolution of POM in polar solvents including water. The particle size was controlled within the range from 100 to 500 nm. As the particle size of POM/SiO₂ decreased, the exposure of POM increased and thus the amount of the acid site was also increased. The catalytic activity of ethanol oxidation was enhanced with the reduction of the particle size of POM/SiO₂. The catalytic properties of POM in the silica nano phase might be different from those in the bulk phase due to the physico-chemical differences of nano phase.

The POM catalysts were used by Kanjina and Trakarnpruk, (2009) who studied the use of H₂O₂ as an oxidant for the oxidation of cyclohexanol and benzyl alcohol under green condition using POM catalysts. The results showed that catalytic activity

depended on types of counter cation and metal of the catalysts. For transition metal-substituted phosphotungstic acid the $[(n-C_4H_9)_4N]_4H[PW_{11}M(H_2O)O_{39}]$, the catalytic order was $Ni > Co > Mn$. For a series of vanadium (V)-substituted phosphotungstic acid, the catalytic activity decreased with increasing numbers of vanadium atoms in the catalyst. These results indicated that using $[(n-C_4H_9)_4N]_4H[PW_{11}Ni(H_2O)O_{39}]$ as a catalyst, cyclohexanol was oxidized to cyclohexanone with 98% yield and 100% selectivity at 90°C in 5 h whereas benzyl alcohol was oxidized to benzaldehyde with 96% yield and 37% selectivity to benzaldehyde and 63% selectivity to benzoic acid at 90°C in 12 h.

Wang et al., (2005) studied the oxidation of alcohols in the presence of POM to produce aldehyde, ketone and carboxylic acid. The results indicated that POM catalyst $Na_6[SiW_{11}ZnH_2O_{40}].12H_2O$ was an effective catalyst for the oxidation of alcohols in the presence of H_2O_2 as oxidant. The reaction was carried out in an aqueous/oil biphasic system, which allowed easy recovery of catalyst, under relatively mild conditions. The catalyst could be reused five times without appreciable loss of activity.

Tsukuda et al., (2007) studied the dehydration of glycerol to produce acrolein over several solid acids. Supported POM catalysts were effective as a catalyst for the dehydration of glycerol. The catalytic activity depended on the types of POM and on the size of the mesopores in the silica (SiO_2) support. The SiW supported on silica with mesopores of 10 nm showed stable catalytic activity with the highest acrolein selectivity of >85 mol% at an ambient pressure and 275 °C. The size of the mesopores in the SiO_2 support affected the catalytic activity. SiO_2 support with small mesopores of 3 nm induced steep deactivation.

Lili et al., (2008) studied the production of acrolein from glycerol dehydration by using SiW supported on activated carbon (AC) catalysts. The results indicated that catalysts with 10% SiW loading exhibited the highest activity and selectivity. The space time yield (STY) of acrolein reached 68.5 mmol/(g.h). The properties of the catalysts were closely related to the SiW dispersion and the relative quantities of strong acid sites. However, acrolein was easily overoxidized to acrylic acid. Deleplanque et al., (2010) studied the one-step process to acrylic acid directly from

glycerol by oxydehydration. In this work, dehydration of and further oxidation of glycerol solution have been investigated with mixed oxide catalysts ($H_3PW_{12}O_{40}$, $FePO_4$, Mo_3VO , $MoVTenbO$, W_3VO catalysts) in gas phase reaction. Among all, iron phosphates ($FePO_4$) were found highly active and selective toward acrolein. Glycerol conversion was nearly complete and acrolein yields reached 80-90% after 5 h of the test. Introducing some oxygen in the feed allowed decreasing the amount of those by-products. Using appropriate mixed oxide catalysts showed satisfactory performances on obtaining acrylic acid directly from glycerol.

The effect of support of supported SiW catalysts on catalytic activity were studied by Kim et al., (2010) using a gas-phase dehydration of glycerol to acrolein. The reaction was carried out over 10 wt.% SiW catalysts supported on different supports; $\gamma-Al_2O_3$, $SiO_2-Al_2O_3$, TiO_2 , ZrO_2 , SiO_2 , AC, CeO_2 and MgO . The same reaction was also conducted over each support without SiW for comparison. The glycerol conversion generally increased with increasing amount of acid sites. The CeO_2 showed the highest 1-hydroxyacetone selectivity of 23.4 % at 315 °C among the various metal oxides. The supported SiW catalysts showed better catalytic activity than the corresponding support itself. Among the supported SiW catalysts, SiW/ ZrO_2 and SiW/ $SiO_2-Al_2O_3$ showed the highest acrolein selectivity of 58.1% and 58%, respectively. The glycerol conversion increased with increasing amount of acid sites. In the case of SiW/ ZrO_2 , comparable catalytic activity to that of the fresh catalyst was obtained over the used catalyst after the regeneration step, in which the coke deposit was burnt off in an air stream at 550 °C.

Witsuthammakul and Sooknoi, (2012) used a single reactor to subsequent oxidation of the dehydrated glycerol, for successfully producing acrylic acid. Selective dehydration of glycerol to acrolein was studied at 275-400 °C over HZSM-5, HBeta, HMordenite and HY. The V-Mo oxides (15-70 mol% V) on silicic acid support (20-100 wt.% mixed oxides loading) were then included as a second bed for subsequent oxidation of the dehydrated products. Over the acid zeolites, acrolein and acetol were mainly generated, together with acetaldehyde, propionaldehyde, pyruvaldehyde and other oxygenates as secondary products. A complete conversion of glycerol with high selectivity to acrolein (up to 81 mol %) can be obtained when

medium pore zeolites (HZSM-5) and low glycerol concentration (10-30 wt.%) was used at 300 °C. A separated-sequential bed system provides high selectivity for acrylic acid with small amounts of acetic acid and acetaldehyde (~15 mol%). The catalyst with high vanadium content promotes total oxidation of the dehydrated products to CO while that with highly dispersed V-Mo-O phases affords 98% selectivity to acrylic acid with 48% acrolein conversion.

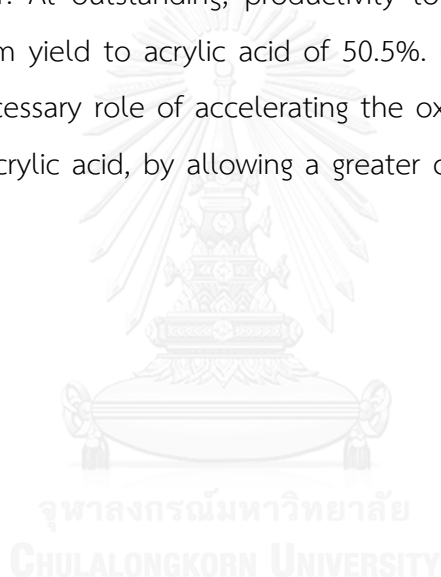
The improvements of catalytic activity of supported POM catalysts were studied by Atia et al., (2011) using a continuous flow set-up for dehydration of glycerol to acrolein over supported POM catalysts. In general, the catalysts are discussed in terms of nature of the POM compound and its acidity and porosity of supports. In this work, addition of alkaline metals Li, K and Cs has proved to adjust the properties of SiW supported on both SiO₂ and SiO₂/Al₂O₃ and to improve its performance in particular acrolein selectivity of the glycerol dehydration. The added alkaline metals decreased activity, but increased acrolein selectivity. Acidic properties did not depend on the nature of alkaline metal. The catalysts were evaluated at standardized reaction conditions (10 wt.% of glycerol in water, 225-300 °C, modified contact time 0.15 kg.h/mol). Among the supported catalysts, Li enhanced SiW showed the highest activity and highest acrolein selectivity of 70% at complete conversion. Acrolein selectivity increased in the order Li > K > Cs with temperature, independent from the chosen support. Besides, the nature of the alkaline metal, the preparation sequence played a significant role for catalyst performance. The highest acrolein selectivity reached 78% at 75% conversion using the SiW/Cs/S11 catalyst that was synthesized in an inverted preparation sequence compared to all other catalysts.

Muhammad et al., (2012) studied the dehydration of glycerol using rubidium- and caesium-doped SiW catalysts. Initially, catalysts were screened at various temperatures and with different glycerol feed concentrations. The catalysts were prepared by varying the concentration of the rubidium (Rb) and caesium (Cs) and keeping the constant concentration of POM. Rb- and Cs-doped SiW catalysts have been found that both catalysts showed high acrolein selective for formation. High acrolein selectivity (94-96%) was observed with unsupported Rb- and Cs-doped SiW

with a 0.5 wt.% in water of glycerol feed. These catalysts were then supported on Al_2O_3 -1 (alpha) and Al_2O_3 -2 (mixture of theta and delta phases). For 10 wt.% glycerol in water, Cs-doped SiW supported on Al_2O_3 -2 gave the highest selectivity of ca. 90% at 100% glycerol conversion at 90 h reaction time, with a space time yield of 105 $\text{g}_{(\text{acrolein})}/\text{kg}_{(\text{cat})}\cdot\text{h}$. When the glycerol feed concentration was increased to 20 wt.% glycerol, a space time yield of 210 $\text{g}_{(\text{acrolein})}/\text{kg}_{(\text{cat})}\cdot\text{h}$ was attained, although it was stable for a shorter time-on-stream. The catalyst was investigated further to determine the origin of the long-term stability. The binding strength of the partially doped SiW on the Al_2O_3 was found to be crucial to sustain the supported Keggin structure and hence the acidity of the active sites resulting in a high acrolein yield. These catalysts appear to be the most stable SiW-derived catalysts and do not require oxygen in the feed gas to attain stable operation. Finally, doping with Cs maintains the Keggin structure of the POM and hence the acidity of the active sites resulting in a high acrolein yield.

Shen et al., (2014) studied the gas phase oxydehydration of glycerol to acrylic acid over Mo/V and W/V oxide catalysts in a fixed bed reactor by one-step reactor method. The Mo/V and W/V oxide catalysts were prepared with a direct drying and subsequent calcination method. The reaction with V in the oxide catalysts led to high acrylic acid yield at 300 °C. For Mo/V oxide catalysts, $\text{Mo}_1\text{V}_{0.25}$ oxide catalyst gave the highest acrylic acid yield of 20.1% and Mo_1V_4 oxide catalyst gave acrolein yield of 28.8%. For W/V oxide catalysts, the $\text{W}_1\text{V}_{0.25}$ oxide catalyst gave the highest acrylic acid yield of 25.7%. However, pure WO_3 catalyst gave acrolein yield of 50.3%. The presence of V content in Mo/V and W/V oxide catalysts was analyzed by XPS technique. It was found that the presence of low concentrations of V in $\text{Mo}_1\text{V}_{0.25}$ and $\text{W}_1\text{V}_{0.25}$ catalysts gave high acrylic acid yield while pure MoO_3 , WO_3 , and V_2O_5 oxides had no catalytic activity for the formation of acrylic acid because the presence of increasing V content in Mo/V and W/V oxide catalysts likely increased their acidities as compared to pure MoO_3 , WO_3 , and V_2O_5 catalysts, respectively. With high V content, Mo/V and W/V oxide catalysts gave low yields of acrylic acid but high yields of CO and CO_2 . The formation of V_2O_5 phase at high V content gave high catalytic oxidation activity for the oxidation of resultant acrylic acid to CO and CO_2 .

Chiericato et al., (2014) reported the reaction parameters in oxydehydration of glycerol to acrylic acid over W-V-Nb mixed oxides with hexagonal tungsten bronze. The two step process demonstrated that glycerol dehydrated to acrolein and oxidized to acrylic acid over acid catalysts. The side reaction of acrolein conversion to ketals and oligomers was achieved by using oxygen partial pressures above that needed for the stoichiometric oxydehydration of glycerol to acrylic acid. The best-performing W-V-Nb catalyst depended on strongly oxidizing conditions. The high surface area and high concentration of stronger acid sites were highly important for an efficient dehydration of glycerol to acrolein, but the formation of undesired by-products might occur. At outstanding, productivity to desired products of 1.6 h^{-1} showed the maximum yield to acrylic acid of 50.5%. Certainly, oxygen as oxidizing agent played the necessary role of accelerating the oxidation of the intermediately formed acrolein to acrylic acid, by allowing a greater concentration of the oxidizing V^{5+} sites.



CHAPTER III

METHODOLOGY

This chapter describes the detail about the experimental set up for studying the conversion of glycerol to acrylic acid with supported POM catalysts.

3.1 Chemical substances

The reagents and solvents used in this experiment are analytical grade listed as following

1. Glycerol ($C_3H_8O_3$), 99.5% purity, Fisher Scientific Inc., USA
2. Hydrogen peroxide (H_2O_2), 30% purity, Merck, Germany
3. Phosphomolybdic acid ($H_3PMo_{12}O_{40} \cdot xH_2O$, PMo), Sigma-Aldrich[®] Inc., USA
4. Phosphotungstic acid ($H_3PW_{12}O_{40} \cdot xH_2O$, PW), Sigma-Aldrich[®] Inc., USA
5. Silicotungstic acid ($H_4SiW_{12}O_{40} \cdot xH_2O$, SiW), Sigma-Aldrich[®] Inc., USA
6. Gamma-Aluminiumoxide ($\gamma-Al_2O_3$), pore diameter of 5.8 nm, Sigma-Aldrich[®] Inc., USA
7. Silica (SiO_2 , CARIACT_{Q30}), pore diameter of 30 nm, Fuji Silycia Chemical Ltd., Japan
8. HZSM-5 ($SiO_2/Al_2O_3=25$), Zibo Xinhong Chem. Ltd., China
9. Ammonia (NH_4OH), 99.9% purity, Merck, Germany
10. Methanol (CH_3OH), 99.9% purity, Merck, Germany
11. 2-propanol (C_3H_8O), $\geq 99.8\%$ (GC), Sigma-Aldrich[®] Inc., USA
12. Sulfuric acid (H_2SO_4), 98% purity, RCI Labscan Limited, Thailand
13. Distilled water (H_2O), HPLC, RCI Labscan Limited, Thailand
14. Acetic acid ($C_2H_4O_2$), $\geq 99\%$ purity, Sigma-Aldrich[®] Inc., USA
15. Formic acid (CH_2O_2), $\geq 95\%$ purity, Sigma-Aldrich[®] Inc., USA
16. Glycolic acid ($C_2H_4O_3$), 70% w/w solution, Ajax Finechem Ltd., Australia
17. Acrylic acid ($C_3H_4O_2$), $\geq 99\%$, Merck, Germany
18. Acrolein (C_3H_4O), Restek Corporation, USA
19. Propionic acid ($C_3H_6O_2$), $\geq 99.5\%$ purity, Sigma-Aldrich[®] Inc., USA

20. Cerium(III) nitrate hexahydrate ($\text{Ce}(\text{NO}_3)_3 \cdot 6\text{H}_2\text{O}$), Sigma-Aldrich[®] Inc., USA
21. Cobalt(II) nitrate hexahydrate ($\text{Co}(\text{NO}_3)_2 \cdot 6\text{H}_2\text{O}$), Sigma-Aldrich[®] Inc., USA
22. Nickel(II) nitrate hexahydrate ($\text{Ni}(\text{NO}_3)_2 \cdot 6\text{H}_2\text{O}$), Sigma-Aldrich[®] Inc., USA
23. Sodium metavanadate (NaVO_3), Sigma-Aldrich[®] Inc., USA

3.2 Catalyst preparation

3.2.1 Supported POM catalysts

Three types of commercial POM including phosphomolybdic acid ($\text{H}_3\text{PMo}_{12}\text{O}_{40} \cdot x\text{H}_2\text{O}$, PMo), phosphotungstic acid ($\text{H}_3\text{PW}_{12}\text{O}_{40} \cdot x\text{H}_2\text{O}$, PW) and silicotungstic acid ($\text{H}_4\text{SiW}_{12}\text{O}_{40} \cdot x\text{H}_2\text{O}$) were impregnated on commercial alumina (Al_2O_3), HZSM-5 ($\text{SiO}_2/\text{Al}_2\text{O}_3 = 25$) and silica (SiO_2) by the incipient wetness impregnation method at POM loading of 20-60 wt.%. Initially, 2.14 g of POM was dissolved thoroughly in 5 ml distilled water at room temperature. Then, approximately 5 g of supports were added slowly into this solution. The obtained slurry was stirred at constant rate of 200 rpm at room temperature for 1 h. The ready-to-use supported POM catalysts were obtained after drying at 110 °C and calcination at 400 °C for 20 and 4 h, respectively. The investigated parameters were

- Types of POM: $\text{H}_3\text{PMo}_{12}\text{O}_{40}$, $\text{H}_3\text{PW}_{12}\text{O}_{40}$ and $\text{H}_4\text{SiW}_{12}\text{O}_{40}$
- Types of support: Al_2O_3 , SiO_2 and HZSM-5
- Loadings of POM on support: 20-60 wt.%

3.2.2 Metal-doped supported POM catalysts

In this part, four types of transition metals including Cerium (Ce), Cobalt (Co), Nickel (Ni) and Vanadium (V) were impregnated on the best supported POM catalysts obtained from 3.2.1 by incipient wetness impregnation method. Initially, 5 g of each transition metal precursors (cerium(III) nitrate hexahydrate ($\text{Ce}(\text{NO}_3)_3 \cdot 6\text{H}_2\text{O}$), cobalt(II) nitrate hexahydrate ($\text{Co}(\text{NO}_3)_2 \cdot 6\text{H}_2\text{O}$), nickel(II) nitrate hexahydrate ($\text{Ni}(\text{NO}_3)_2 \cdot 6\text{H}_2\text{O}$) and sodium metavanadate (NaVO_3)) were dissolved thoroughly in 50 ml distilled water at room temperature. To obtain the Ce, Co, Ni, and V on supported POM catalysts at identical loading of 4 wt.%, 5.16, 8.23, 8.25 and 3.99 ml of these solutions were mixed thoroughly with 4 g of supported POM catalysts at room temperature. Then,

transition metal-doped supported POM catalysts were added slowly into this solution. The slurry was stirred at constant rate of 200 rpm at room temperature for 1 h. The ready-to-use transition metal-doped supported POM catalysts were obtained after drying at 110 °C for 20 h and calcination at 400 °C 4 h. The preparation of transition metal-doped supported POM catalysts by sequential incipient wetness impregnation method was demonstrated in Figure 3.1. The investigated parameters were

- Types of transition metal: Ce, Co, Ni and V
- Loadings of transition metal: 2-8 wt.%

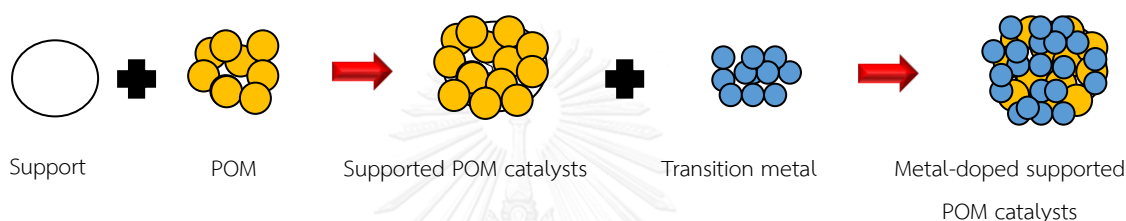


Figure 3.1 Schematic diagram of the preparation of transition metal-doped supported POM catalysts by sequential incipient wetness impregnation method.

3.3 Catalyst characterization

3.3.1 Brunauer–Emmett–Teller method (BET method)

The BET surface area, pore volume, and average pore diameter for the supports and supported POM catalysts were derived from nitrogen (N₂) adsorption isotherms measured at -196 °C (Micromeritics ASAP 2020). Prior the measurement, each sample was degassed at 200 °C for 20-24 h. The BJH method was used as calculating average pore diameters.

3.3.2 X-ray Diffraction (XRD)

The phase structures of the catalysts were determined based on powder X-ray diffraction (XRD) patterns on a Siemens PE-2004 X-ray diffractometer using CuK α radiation (wavelength λ = 0.15406 nm). The tube voltage and the current were 40 kV and 20 mA, respectively. The samples were dried at 110 °C for 24 h before the XRD

measurement. The data were collected in the range of $2\theta = 5^\circ$ - 80° with a step size of 0.02° and step time 0.6 s at 25°C .

3.3.3 Fourier Transform Infrared Spectroscopy (FT-IR)

The structural integrity of the Keggin units in supported POM catalysts were monitored by the FTIR analysis (Figure 3.2) between 400 - $2,500\text{ cm}^{-1}$ with resolution of 0.5 cm^{-1} at room temperature by Perkin Elmer, model Spectrum One instrument, FTIR spectrometer equipped with a temperature-stabilized fast recovery deuterated triglycine sulfate (FR-DTGS). A liquid nitrogen cooled mercury cadmium telluride (MCT) detector is used as a second detector. All recorded spectra were corrected for IR penetration depth using the attenuated total reflectance (ATR) correction procedure implemented in the OMNIC[®] (Thermo Nicolet Corp.) software. Consequently, the ATR-corrected spectrum was evaluated using OMNIC[®] and MicroCal[®] Origin software.



Figure 3.2 Fourier transform infrared spectroscopy (FTIR).

3.3.4 Scanning Electron Microscopy/Energy Dispersive X-Ray Spectroscopy (SEM/EDX)

EDX analyses were attachments to Electron Microscopy instruments SEM instruments where the imaging capability of the microscope identifies the specimen of interest. The composition of the catalysts was determined by SEM/EDX spectroscopy on Jeol JSM-5800 LV and Link ISIS Series 300 at magnifications 20,000x and with an accelerating voltage of 0.3 to 30 kV. It can also operate in a high-vacuum mode.

3.3.5 X-ray fluorescence (XRF)

The elemental analyses of catalysts were determined by X-ray fluorescence (XRF) patterns on Bruker AXS, Germany Model: S4 Pioneer Wavelength dispersive X-Ray Fluorescence (WDXRF) Spectrometry. The tube voltage and the current were 60 kV and 50 mA, respectively. The data were collected in the range of 0.2-20 Å (60-0.6 keV) with total resolution 3-100 eV and typical measurement time 2-10 s per element. The program was used SPECTRA^{Plus} software of the Bruker with the Standardless Analysis.

3.3.6 Phosphorus-31 and Silicon-29 Magic Angle Spinning Nuclear Magnetic Resonance spectroscopy (³¹P and ²⁹Si MAS NMR)

The local interactions in PW and PMo on the support were determined by ³¹P MAS NMR spectra on a Varian INOVA-500 MHz spectrometer with CP/MAS solid-probe and nano-probe with the Larmor frequencies of ¹H and ³¹P at 500.16 MHz and 202.46 MHz, respectively. The local interaction in SiW on the support was probed by ²⁹Si MAS NMR spectra on a Varian INOVA-500 MHz spectrometer with CP/MAS solid-probe and nano-probe with the Larmor frequencies of ¹H and ²⁹Si at 500.15 MHz and 99.36 MHz, respectively.

3.3.7 Temperature Programmed Desorption of ammonia (NH₃-TPD)

The acidities of all supported POM catalysts were determined by temperature-programmed desorption of ammonia in a fixed-bed continuous flow microreactor at atmospheric pressure equipped with thermal conductivity detector (TCD). 50 mg of catalysts were pretreated at 200 °C for 60 min under helium (He) flow. After cooling down to room temperature under He flow, ammonia chemisorption was carried out by passing He at a flow rate of 30 mL/min first through a saturator containing ammonium hydroxide solution (NH₄OH) at room temperature, then through a moisture trap. The NH₃-saturated He stream was then passed through the catalyst bed for 30 min at room temperature. Finally, the reactor was purged with pure He flow at room temperature for 30 min. The catalysts were then heated under He flow (30 mL/min) up to 900 °C with a linear heating rate of 10 °C/min, and the

temperature-programmed desorption of NH_3 was measured using a thermal conductivity detector.

3.3.8 Temperature Programmed Desorption of oxygen (O_2 -TPD)

To determine the amount of O_2 adsorbed/desorbed on the surface of the supported POM catalysts, the temperature-programmed desorption of oxygen was carried out in a fixed-bed continuous flow micro reactor at atmospheric pressure equipped with thermal conductivity detector, using 5% O_2 in He at various adsorption temperatures. Prior to desorption, the 5% O_2 in He flow was passed with a flow rate 30 ml/min through the catalyst bed at 200 °C for 60 min. The prepared catalysts were then heated under He flow (30 ml/min) up to 1,000 °C with a linear heating rate of 10 °C/min.

3.3.9 Temperature Programmed Reduction of hydrogen (H_2 -TPR)

The redox properties of all supported POM catalysts were determined by temperature-programmed reduction of hydrogen in a fixed-bed continuous flow microreactor at atmospheric pressure equipped with thermal conductivity detector (TCD). About 50 mg of catalysts were placed in a quartz tube and pretreated in a 10 ml/min He flow at 400 °C for 60 min. After cooling down to room temperature under He flow, H_2 was carried out by passing He at a flow rate of 30 ml/min was used as reducing gas. Finally, the reactor was purged with pure He flow at room temperature for 30 min. The catalysts were then heated under He flow (30 ml/min) up to 900 °C with a linear heating rate of 10 °C/min, and the temperature-programmed reduction of hydrogen was measured using a thermal conductivity detector.

3.4 Activity test

Catalytic conversion of glycerol to acrylic acid was carried out in liquid phase system at 70 °C and 90 °C and ambient pressure. The concentration of H_2O_2 was varied from 1.37-6.85 mol/L. From previous literature, Shen et al., (2012) recommended that an appropriate glycerol concentration for catalytic activity test was 20 wt.% in water of glycerol. Thus, this glycerol concentration was used for our study. Initially, 30 ml of 20 wt.% (2.75 mol/L) aqueous glycerol solution (99.5% (v/v),

Fisher) was mixed with a desired quantity of supported POM catalyst (0.15 g, 0.30 g and 0.60 g for 2 wt.%, 4 wt.% and 8 wt.%, respectively) in a 500 ml three-neck flask equipped with a condenser, a thermometer and a sampling port. A heating mantle fit with the three-necked flask was used for heating up and the temperature was monitored with a thermometer. A magnetic stirrer was used to agitate the solution. The experimental set-up is shown in Figure 3.3. Consequently, the temperature of the system was raised to 70 °C or 90 °C by an external electrical heater. When the required temperature was arrived, 2.74 mol/L H₂O₂ was slowly added at rate of 1.27 ml/min. The reaction was monitored by taking the liquid sample of around 1.0 ml at regular time intervals during a 4 h period. To terminate the reaction, all detected liquid products were collected in an ice-water trap at temperature of 0-5 °C and then centrifuged on a Hermle Z206A Digital Laboratory Centrifuge to separate the solid catalyst from the liquid product. The investigated parameters were

- Reaction temperature: 70 °C and 90 °C
- Concentration of H₂O₂: 1.37-6.85 mol/L
- Concentration of glycerol: 1.37-5.50 mol/L
- Amount of catalyst loading: 2-8 wt.%

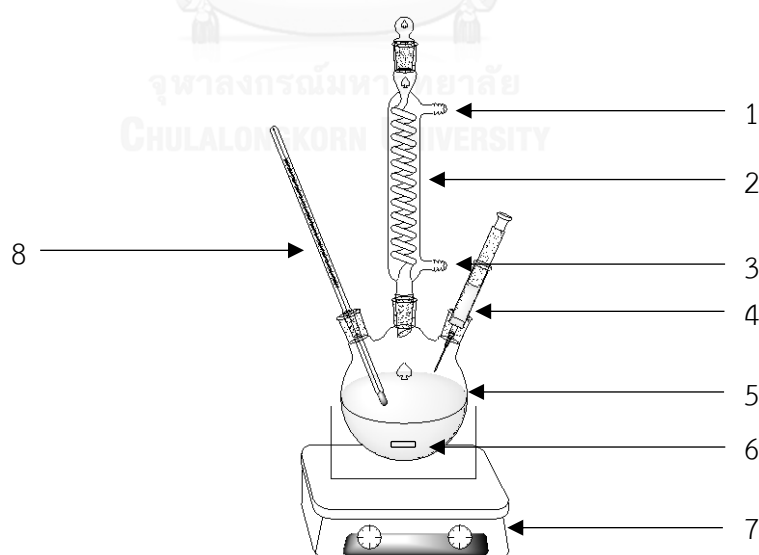


Figure 3.3 Schematic diagram of experiment set up: (1) cooling water outlet, (2) condenser, (3) cooling water inlet, (4) syringe, (5) three-necked flask, (6) magnetic bar, (7) magnetic stirrer and (8) thermometer.

3.4.1 Gas Chromatograph and Mass Spectrometry (GC-MS)

The generated products from the conversion of glycerol were characterized by gas chromatograph and mass spectrometry (GC 7890A/MS 5975C, Agilent technologies) equipped with flame ionization detector as shown in Figure 3.4. A DB-wax capillary column (30m × 250mm × 0.25mm) was used as separating column. The data was collected by Hewlett-Packard Chemstation software. 2-propanol was used as solvent.



Figure 3.4 Gas chromatograph and mass spectrometry (GC-MS).

3.4.2 High Performance Liquid Chromatography (HPLC)

The quantities of the desired products including glycolic acid, formic acid, acetic acid, acrolein, acrylic acid and propionic acid were quantitatively analyzed by high performance liquid chromatography (HPLC, Waters 410 HPLC controller) equipped with a refractive index detector (Figure 3.5) in series. The stationary phase was a Phenomenex Luna 5 μm C18 (2) 100 (250mm × 4.6mm) and the mobile phase was a 98.0: 2.0 (volume/volume) ratio of 0.05 mM H_2SO_4 with HPLC water at flow rate of 1.0 ml/min. The column temperature was controlled at ambient temperature (27 °C). The pump pressure was operated in the range of 2,500-3,000 psi. The products were diluted with water and the injection volume was 20 μl .



Figure 3.5 High performance liquid chromatography (HPLC).

The glycerol conversion, the product yield of selected products as well as the carbon selectivity were calculated on the basis of Eq.(3.1) to (3.3), respectively:

$$\text{Glycerol conversion (\%)} = \frac{\text{C mole of glycerol converted}}{\text{C mole of glycerol initially added}} \times 100 \quad (3.1)$$

$$\text{Product yield (\%)} = \frac{\text{C mole of glycerol converted to each product}}{\text{C mole of glycerol initially added}} \times 100 \quad (3.2)$$

$$\text{Carbon selectivity (\%)} = \frac{\text{C mole of glycerol converted to all desired product}}{\text{C mole of glycerol converted}} \times 100 \quad (3.3)$$

3.5 Kinetic studies

The kinetics of glycerol conversion was carried out via the best catalyst under the same condition as mentioned earlier at reaction temperatures of 60 °C, 70 °C, 80 °C and 90 °C. The concentrations of the glycerol and oxidizing agent (H₂O₂) were varied between 1.37-5.50 mol/L and 1.37-6.85 mol/L, respectively. The kinetic data were obtained using the initial rate method from the linear section of glycerol conversion. Surface reaction mechanisms, classical Langmuir Hinshelwood (LH) models and Eley-Rideal (ER) models, were propose for the glycerol conversion over the best catalyst in this study.

CHAPTER IV

CONVERSION OF GLYCEROL TO ACRYLIC ACID VIA Al_2O_3 -SUPPORTED POM CATALYSTS

In the present chapter, alumina-supported polyoxometalate (Al_2O_3 -supported POM) catalysts were used in a one-pot process for the liquid phase conversion of glycerol to acrylic acid, in order to simplify the process and reduce the capital cost of the process. The influences of concentration of oxidizing agent (H_2O_2), reaction temperature ($70\text{ }^\circ\text{C}$ and $90\text{ }^\circ\text{C}$), POM catalyst types (PW, PMo and SiW) and catalyst loadings (2-8 wt.% based on glycerol), on the glycerol conversion and product yields were investigated. Finally, a reaction pathway of glycerol conversion in the presence of Al_2O_3 -supported POM catalysts was proposed.

4.1 Characterization of Al_2O_3 -supported POM catalysts

Textural properties for supported POM catalyst immobilized on Al_2O_3 support derived from nitrogen physisorption isotherms are summarized in Table 4.1. The Brunauer–Emmett–Teller (BET) surface area, pore volume and average pore diameter of all Al_2O_3 -supported POM catalysts decreased significantly compared to the original POM-free supports. The decrease in BET surface may be attributed to the support pores blocking by active POM. This is because the pores of Al_2O_3 are 5.46 \AA and the Keggin unit diameter is 12 \AA (Popa et al., 2005). Thus, it is reasonable to conclude that the pores are blocked by the active phase.

The identities and characteristics of as-prepared catalysts were characterized as shown in Figure 4.1. The XRD pattern of Al_2O_3 was amorphous and showed no crystalline phase. For non-supported POM catalysts, the PW catalyst demonstrated the sharp peaks of Keggin-type PW phase at 2θ of 10.3° and 25.3° (PDF 75-2125). The PMo revealed the characteristic peaks at 2θ of 27.3° and 23.3° , indicating the presence of MoO_3 phase (PDF89-7112). For SiW, the XRD pattern showed the peaks at 2θ of 27.3° assigned to the SiW hexahydrate (Pope, 1983). However, for Al_2O_3 -supported POMs, the XRD patterns resembled those of Al_2O_3 and no characteristic

peaks assigned to the utilized POM catalysts were observed, suggesting that the POM catalysts were highly dispersed on the Al_2O_3 surface.

Table 4.1 Textural properties of Al_2O_3 and Al_2O_3 -supported POM catalysts.

Catalysts	BET surface area (m^2/g)	Pore volume (cm^3/g)	Average pore diameter (\AA)
Al_2O_3	267.8	0.229	5.46
$\text{PW}/\text{Al}_2\text{O}_3$	227.4	0.156	4.53
$\text{PMo}/\text{Al}_2\text{O}_3$	221.5	0.143	4.26
$\text{SiW}/\text{Al}_2\text{O}_3$	214.6	0.128	4.11

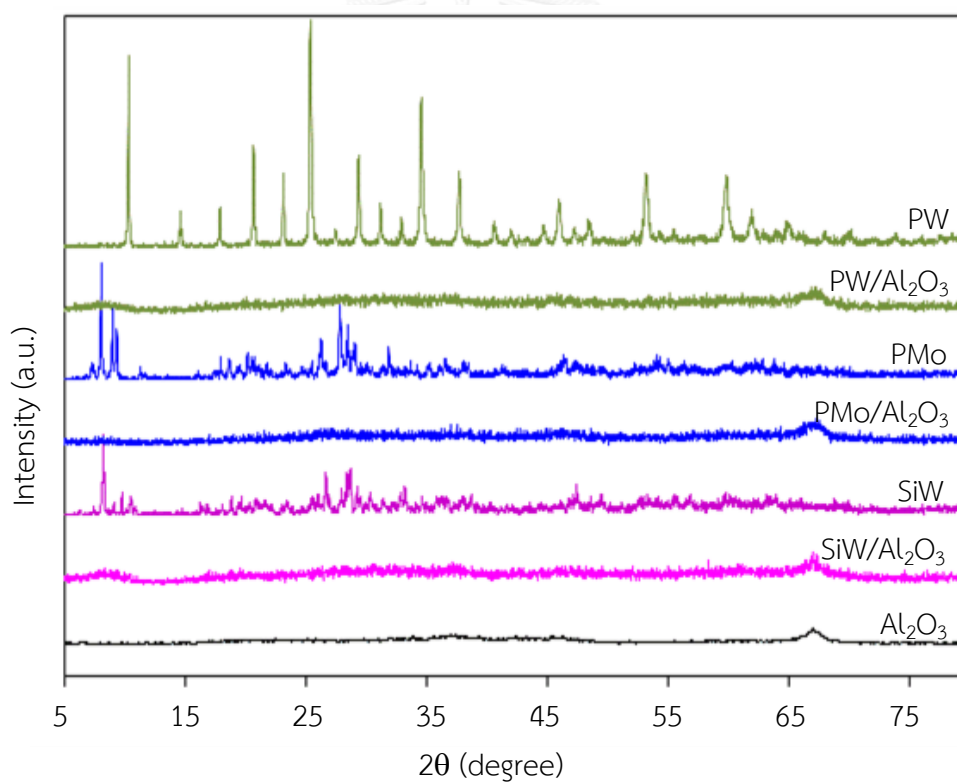


Figure 4.1 XRD patterns of Al_2O_3 , POM and Al_2O_3 -supported POM catalysts at 30 wt.% POM loading.

To confirm the presence of the Keggin anions on the Al_2O_3 surface, FT-IR spectra were recorded (Figure 4.2). The blank Al_2O_3 displayed the broad absorption bands at $3,300\text{--}3,700\text{ cm}^{-1}$ and at around $1,650\text{ cm}^{-1}$, assigned to hydroxyl group O–H vibration. The broad overlapping peaks in the lower frequency range ($500\text{--}1,000\text{ cm}^{-1}$) were due to the presence of Al–O (780 cm^{-1} and 690 cm^{-1}) vibrations. For supported POM catalysts, besides the main characteristic peaks of Al_2O_3 , additional peaks were observed. The polyanions ($\text{PW}_{12}\text{O}_{40}^{3-}$) consisted of a PO_4 tetrahedron surrounded by four W_3O_{13} groups formed by edge-sharing octahedral. These groups were connected to each other by corner-sharing oxygen (Tsukuda et al., 2007), and this arrangement gives rise to four types of bands between $1,200\text{ cm}^{-1}$ and 700 cm^{-1} . The bands observed at $1,079\text{ cm}^{-1}$, 983 cm^{-1} and 878 cm^{-1} were related to the asymmetric stretching of P–O, asymmetric stretching of terminal oxygen ($\text{W}=\text{O}_t$) and asymmetric stretching of center oxygen ($\text{W}-\text{O}_c-\text{W}$), respectively. Also, a shoulder peak at wave number of 797 cm^{-1} can be assigned to the asymmetric stretching of edge oxygen ($\text{W}-\text{O}_e-\text{W}$) (Staiti, Freni, & Hocevar, 1999; Padiyan, Ethilton, & Paulraj, 2000). For $\text{PMo}/\text{Al}_2\text{O}_3$ catalyst, the main characteristic bands of the Keggin unit at $1,078\text{ cm}^{-1}$ and 963 cm^{-1} were assigned to the asymmetric stretching of P–O and center oxygen ($\text{Mo}-\text{O}_c-\text{Mo}$), respectively. The weak shoulders at 876 cm^{-1} and 785 cm^{-1} were related to the symmetric stretching of terminal oxygen ($\text{Mo}-\text{O}_t$) and edge oxygen ($\text{Mo}-\text{O}_e-\text{Mo}$), respectively (Babou, Coudurier, & Vadrine, 1995; Tatibouët, Montalescot, & Brückman, 1996). For $\text{SiW}/\text{Al}_2\text{O}_3$ catalyst, the parent ($\text{SiW}_{12}\text{O}_{40}^{4-}$) Keggin structure displayed the characteristic bands due to W–O–W vibrations of edge- and corner-sharing WO_6 octahedral linked to the central SiO_4 tetrahedral (Deltcheff, Fournier, Franck, & Thouvenot, 1983; Stangar, Grosej, Orel, & Colomban, 2000). As demonstrated in Figure 4.2, the stretching modes of edge-sharing ($\text{W}-\text{O}_e-\text{W}$) and center-sharing ($\text{W}-\text{O}_c-\text{W}$) units emerged as shoulders at 793 cm^{-1} and 872 cm^{-1} , respectively, whereas the Si–O stretching modes appeared at 931 cm^{-1} and 974 cm^{-1} . According to the obtained FT-IR results, it could be confirmed that the POMs supported on Al_2O_3 retained their Keggin structures under our preparation procedure.

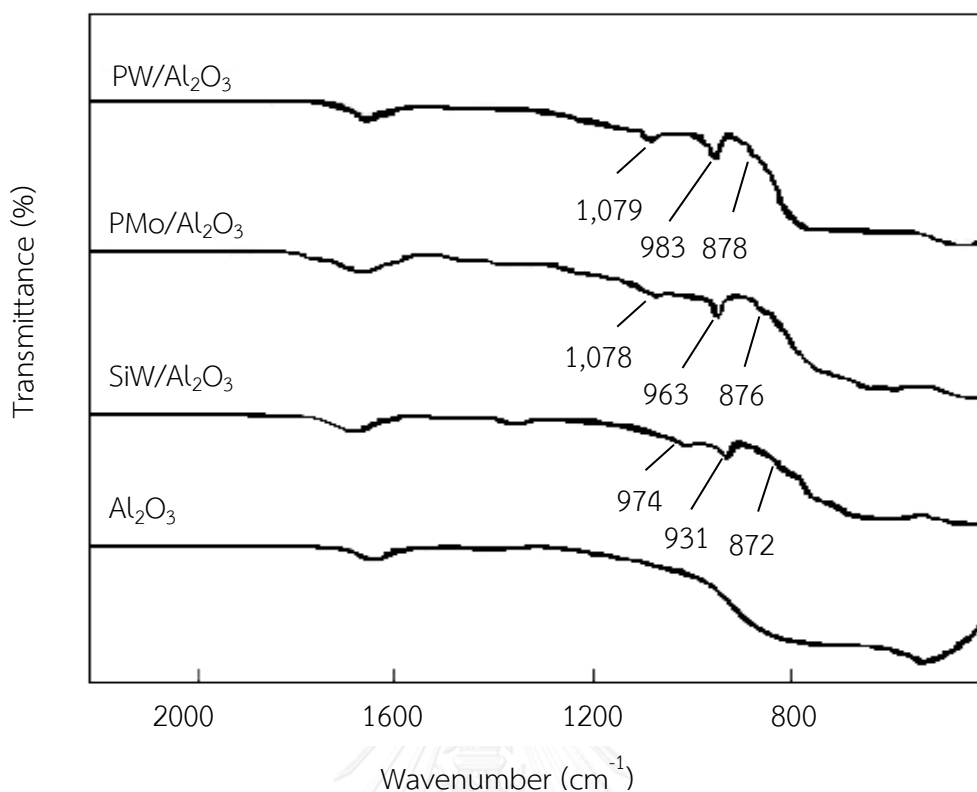


Figure 4.2 FT-IR spectra of Al_2O_3 and Al_2O_3 -supported POM catalysts at 30 wt.% POM loading.

In order to examine the local interactions and structural changes in catalyst and its support, ^{31}P MAS NMR spectroscopy was utilized. For unsupported PW, a single symmetry narrow peak was observed at -16.1 ppm (Figure 4.3), indicating the presence of PW in hexahydrated form. The $\text{PW}_{12}\text{O}_{40}^{3-}$ anions in the hexahydrate are packed in a cubic structure and all acidic protons are presented in the form of H_5O_2^+ cations (Kim, Shul, & Han, 2006). A down field shift of the peak to -14.2 ppm was observed for $\text{PW}/\text{Al}_2\text{O}_3$ catalyst. This might be attributed to the partial loss of some water molecules from the PW crystallites during the immobilization of PW onto the Al_2O_3 support during impregnation (Uchida, Inumaru, & Misono, 2000). In addition, the down field chemical shift of the peak in ^{31}P MAS NMR spectrum indicated the interaction of PW with the Al_2O_3 support. This shift behavior was also observed during the immobilization of PW onto another support such as SiO_2 (Kim et al., 2006; Kozhevnikov, 1998; Damyanova, Fierro, Sobrados, & Sanz, 1999). A single peak was

observed in the NMR spectra for both PW and PW/Al₂O₃ catalysts, suggesting the uniformity and high symmetry of the crystal structure in which all polyanions are equally hydrogen bonded by H₅O₂⁺. In the case of unsupported PMo, the fresh PMo exhibited an almost symmetric resonance peak at a chemical shift of -5.1 ppm (Figure 4.4), indicating the presence of phosphorous in the tetrahedral position of the Keggin structure (Rao, Rao, Nagaraju, Prasad, & Lingaiah, 2009) or a uniform phosphorus environment in the highly hydrated structure of PMo (Thouvenot, Rocchiccioli-Deltcheff, & Fournier, 1991). A smaller shoulder peak close to the main peak at a chemical shift of -4.6 ppm was attributed to a non-uniform hydration of the sample (Pawelec et al., 2004). The ³¹P MAS NMR spectrum of PMo/Al₂O₃ catalyst shifted considerably toward lower field at a chemical shift of -4.6 ppm, caused by loss of water as well as the interaction between the Keggin unit and the Al₂O₃ support (Rao et al., 2009). For investigating the local interaction and structural changes in the SiW/Al₂O₃ catalyst, ²⁹Si MAS NMR spectroscopy was utilized (Figure 4.5). No peaks assigned to the main characteristics of SiW in the ²⁹Si MAS NMR of either unsupported SiW or SiW/Al₂O₃ catalysts were observed. This is because ²⁹Si MAS NMR signal is limited both by low isotopic natural abundance and by a small, negative magnetogyric ratio (Delak, Farrar, & Sahai, 2005).

The surface acidity of the utilized POMs and all supported POM catalysts was determined by NH₃-TPD analysis as shown in Figure 4.6. Theoretically, acid sites can be classified as weak- (150-300 °C), medium- (300-500 °C) and strong- (500-650 °C) strength (Atia, Armbruster, & Martin, 2008). For PW, two broad NH₃-TPD peaks appearing at the temperature of 280 °C and 610 °C indicated the presence of medium- and strong- strength acid sites. For PW/Al₂O₃ catalyst, both peaks shifted to lower temperatures and lost some intensity, indicating a weakening of the acid sites due to interactions with the alumina support. For PMo, peaks assigned to weak- and medium-strength acid sites appeared at 189 °C and 352 °C. For PMo/Al₂O₃ catalyst, the peaks shifted to slightly lower temperatures and lost considerable intensity, again indicating loss of acid strength due to interactions with the support. SiW gave peak at 203 °C and 388 °C. For SiW/Al₂O₃ catalyst, the medium strength peak lost most of its intensity but appeared to shift toward higher temperature (~475 °C).

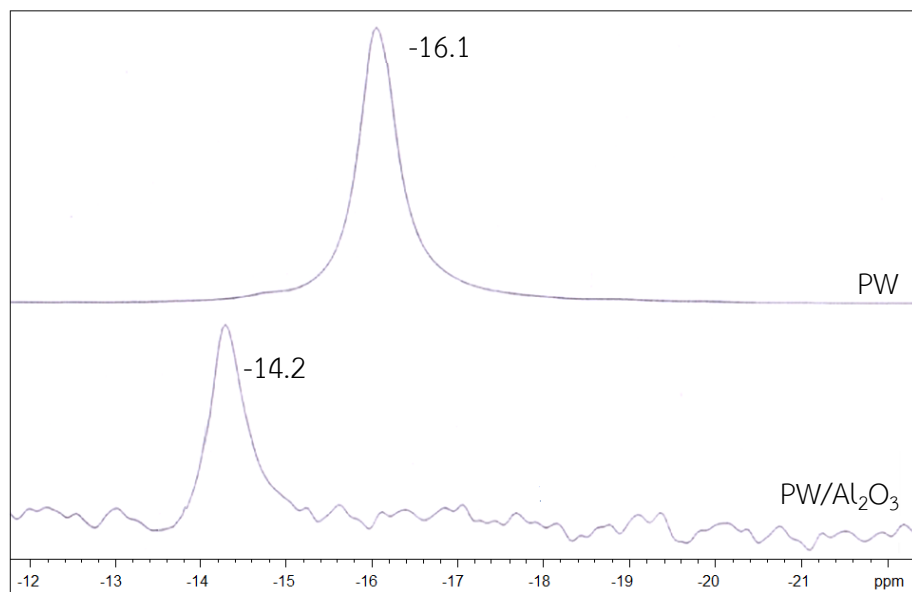


Figure 4.3 ^{31}P MAS NMR spectra of unsupported PW and PW/Al₂O₃ catalysts spectra at 30 wt.% POM loading.

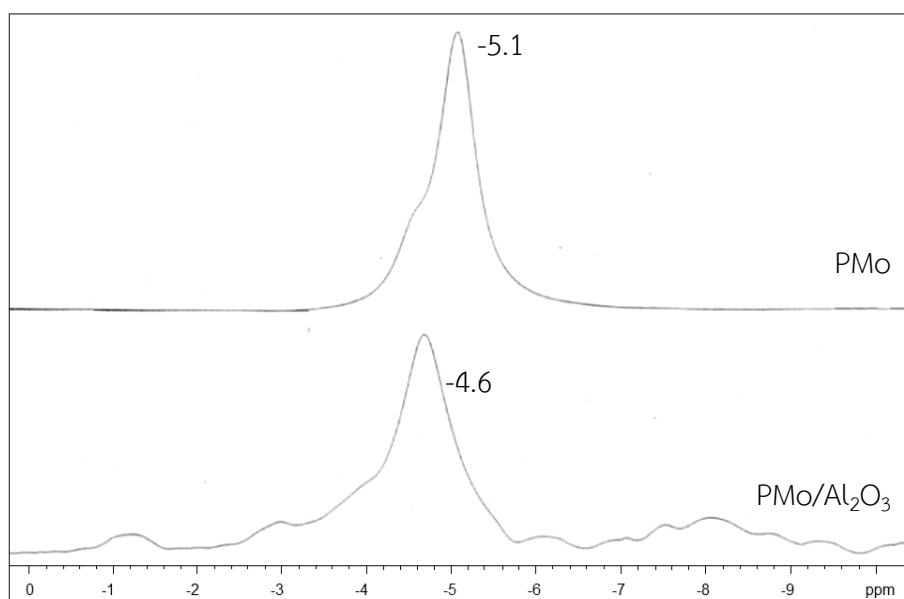


Figure 4.4 ^{31}P MAS NMR spectra of unsupported PMo and PMo/Al₂O₃ catalysts spectra at 30 wt.% POM loading.

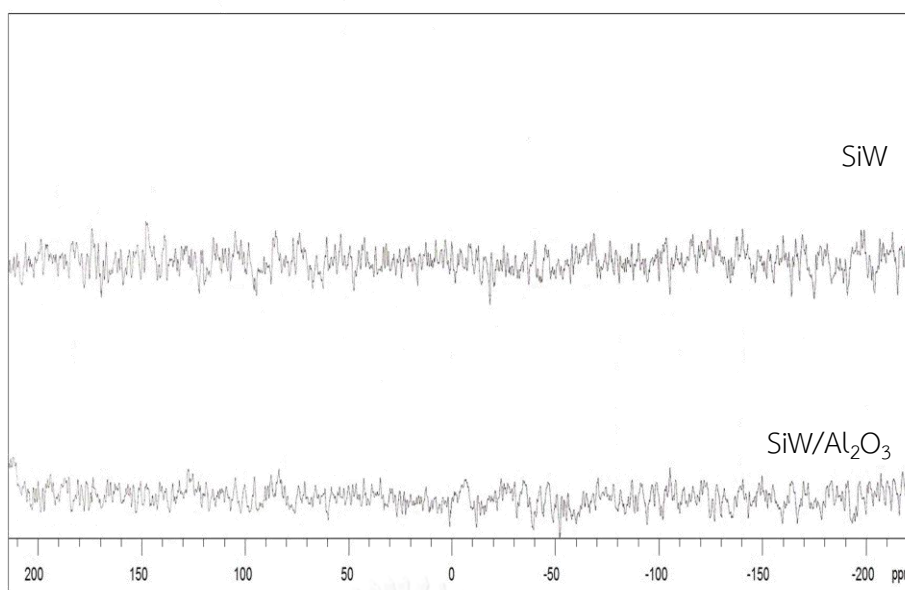


Figure 4.5 ^{29}Si MAS NMR spectra of unsupported SiW and SiW/ Al_2O_3 catalysts spectra at 30 wt.% POM loading.

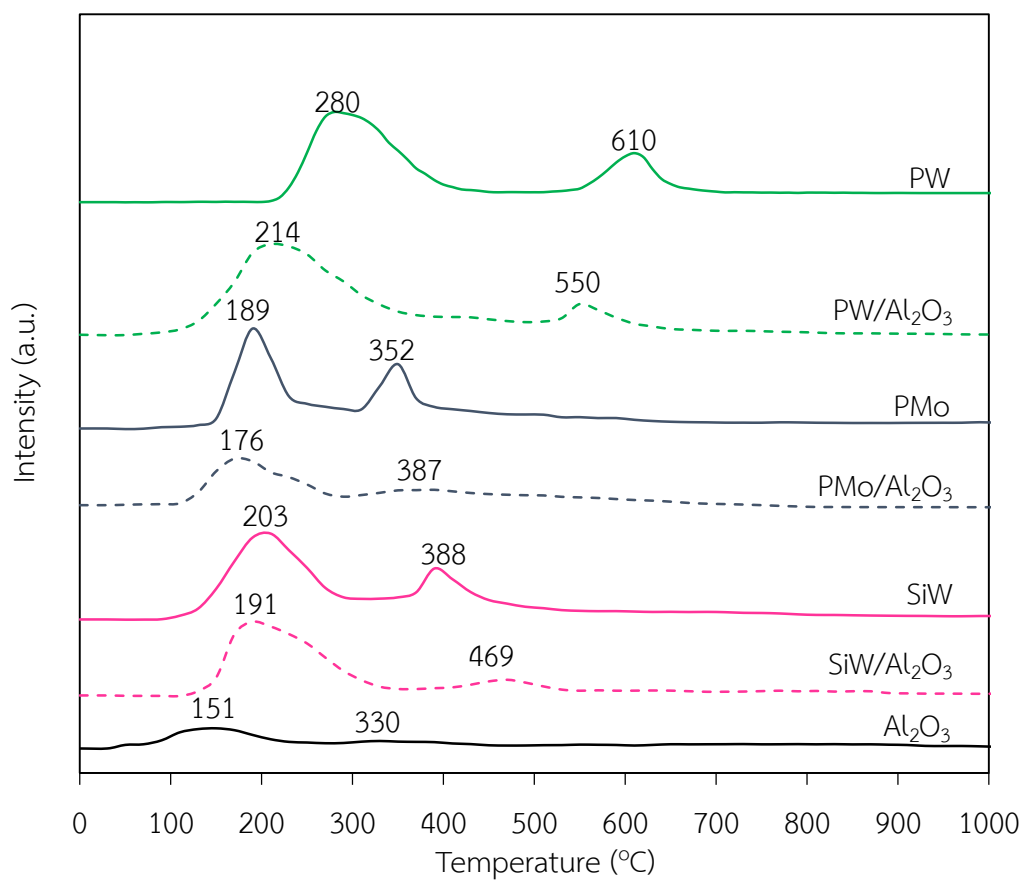


Figure 4.6 NH_3 -TPD profiles for utilized POM, Al_2O_3 and Al_2O_3 -supported POM catalysts at 30 wt.% POM loading.

As summarized in Table 4.2, the total acidity of the POM catalysts was in an order of PW > SiW > PMo, consistent with that reported by Shen et al., (2012). When POMs were impregnated on the surface of Al₂O₃, the intensity of NH₃-TPD peaks was reduced and shifted to low temperature indicating the decrease in acid concentration and acidity strength of Al₂O₃-supported POM catalysts. However, the acidities of the POM catalysts were still greater than that of pure Al₂O₃. Atia et al., (2008) suggested that the addition of POM did not introduce any new acid sites on support surface, but led to a replacement by other acidic sites. The weak interaction of Al₂O₃ with the POM kept its Brønsted acid character and led to an increased proportion of medium- and strong-strength acid sites. In this case, a portion of the POM would loosen its acidity due to the distortion of the Keggin structure.

Table 4.2 NH₃-TPD results for Al₂O₃, POM and Al₂O₃-supported POM catalysts.

Catalysts	NH ₃ -TPD peak position (°C)	Acid amount (mmol NH ₃ /g Cat.)	Total acidity (mmol NH ₃ /g Cat.)
PW	280	3.73 (204-445 °C)	4.92
	610	1.19 (540-664 °C)	
PMo	189	2.28 (151-257 °C)	3.14
	352	0.88 (311-410 °C)	
SiW	203	2.88 (108-303 °C)	3.81
	388	0.93 (351-439 °C)	
PW/Al ₂ O ₃	214	1.24 (62-370 °C)	1.51
	550	0.27 (510-641 °C)	
PMo/Al ₂ O ₃	176	0.66 (101-290 °C)	0.86
	387	0.20 (297-501 °C)	
SiW/Al ₂ O ₃	191	1.19 (110-356 °C)	1.42
	469	0.23 (390-543 °C)	
Al ₂ O ₃	151	0.50 (46-275 °C)	0.68
	330	0.18(275-453 °C)	

The O₂-TPD spectra of the unsupported POM catalysts and Al₂O₃-supported POM catalysts after O₂ adsorption at different temperatures are shown in Figure 4.7 and Table 4.3. The results show that both POM and Al₂O₃-supported POM catalysts have the ability to adsorb and desorb O₂. The total O₂ desorption of the POM catalysts was in an order of SiW > PW > PMo, suggesting that the SiW demonstrated the highest reducibility or oxidative ability. When POMs were impregnated on the surface of Al₂O₃, a similar trend of oxidative ability was still observed. That is, the total O₂ desorption was in the order of SiW/Al₂O₃ > PW/Al₂O₃ > PMo/Al₂O₃. Nevertheless, the quantities of the total O₂ desorption were reduced, indicating the decrease in adsorption/desorption strength of Al₂O₃-supported POM catalysts.

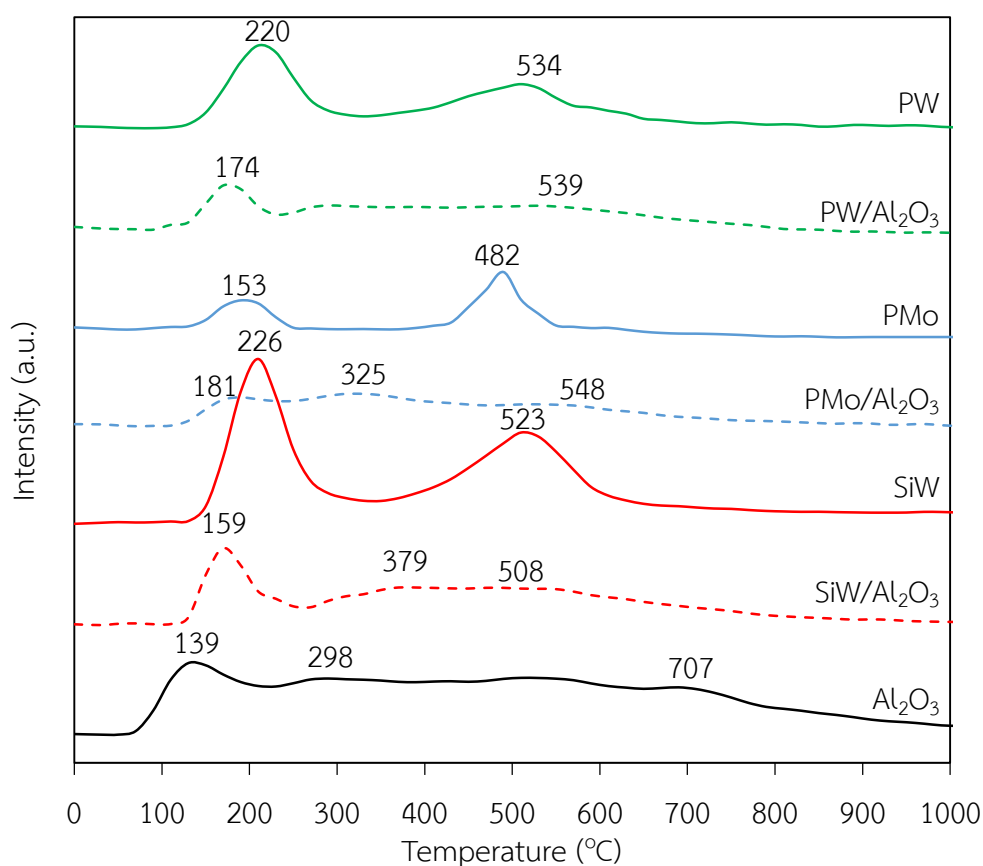


Figure 4.7 O₂-TPD profiles for utilized POM, Al₂O₃ and Al₂O₃-supported POM catalysts at 30 wt.% POM loading.

Table 4.3 O₂-TPD results for Al₂O₃, POM and Al₂O₃-supported POM catalysts.

Catalysts	O ₂ -TPD peak position (°C)	O ₂ desorption (mmol O ₂ /g Cat.)	Total O ₂ desorption (mmol O ₂ /g Cat.)
PW	220	0.084 (104-319 °C)	0.123
	534	0.039 (386-650 °C)	
PMo	153	0.031 (145-256 °C)	0.090
	482	0.059 (397-549 °C)	
SiW	226	0.096 (124-313 °C)	0.185
	523	0.090 (365-669 °C)	
PW/Al ₂ O ₃	174	0.039 (101-147 °C)	0.075
	539	0.037 (404-678 °C)	
PMo/Al ₂ O ₃	181	0.024 (119-148 °C)	0.047
	325	0.015 (158-401 °C)	
	548	0.007 (454-667 °C)	
SiW/Al ₂ O ₃	159	0.066 (119-275 °C)	0.102
	379	0.023 (281-479 °C)	
	508	0.013 (488-525 °C)	
Al ₂ O ₃	139	0.063 (68-221 °C)	0.079
	298	0.006 (213-398 °C)	
	707	0.009 (649-851 °C)	

4.2 Catalytic activity test of Al₂O₃-supported POM catalysts

4.2.1 Effect of oxidizing agent and reaction temperature

The effect of the oxidizing agent was examined at the H₂O₂ concentration of 2.74 mol/L and 6.85 mol/L over 30 wt.% SiW/Al₂O₃ catalyst with 4 wt.% catalyst loading at reaction temperature of 70 °C and 90 °C. The glycerol conversion and yield of all desired products at 240 min were summarized in Table 4.4. The H₂O₂ concentration had a significant effect on the variations of the glycerol conversion. In the absence of H₂O₂, glycerol conversion was obviously low. The presence of 2.74 mol/L H₂O₂ led to an increasing glycerol conversion from 9.07% to 64.30% and

17.84% to 83.78% at 70 °C and 90 °C, respectively. Further raising the H₂O₂ concentration from 2.74 mol/L to 6.85 mol/L resulted in the raise of glycerol conversion from 83.78% to 93.87%, approximately 1.12-fold increasing at 90 °C (Table 4.4). This suggests that high concentration of H₂O₂ affected positively on the glycerol conversion. Consider the acrylic acid yield, further raising the H₂O₂ concentration from 2.74 mol/L to 6.85 mol/L resulted in a slight decrease of acrylic acid yield, approximately 0.71-fold decreasing. This suggests that oxidation of the dehydrated products of glycerol can be promoted when glycerol is in contact with the oxidative catalyst in the presence of high amount of oxidizing agent. The glycerol conversion should be slowly oxidized to acid products. This is because acid products are obtained from the dehydrated products in the system. In addition, the presence of H₂O₂ at 2.74 mol/L can reduce the production of other products observing from the carbon selectivity of around 13.67-fold and 9.17-fold at 70 °C and 90 °C, respectively. That is, the carbon selectivity increased from 3.86% to 52.76% and 7.92% to 72.62% when H₂O₂ was added into the reaction, indicating the decrease of glycerol conversion to undesired products from 96.14% to 47.24% and 92.08% to 27.38% at 70 °C and 90 °C, respectively. This can be explained by the fact that H₂O₂ is the reactive oxygen donor providing the ideal conditions for oxidation of glycerol to glycerol aldehyde, an intermediate for glyceric acid in liquid phase (Atia et al., 2008). However, the presence of only H₂O₂ in the absence catalyst (Blank test 1 and 2) cannot promote the progress of the glycerol conversion reaction. The glycerol conversions were proceeded only 6.91% and 9.27% at the reaction temperature of 70 °C and 90 °C, respectively (Table 4.4). Less than 1% of each of measurable detected products was generated at such condition. This indicates that the presence of H₂O₂ and SiW catalysts had the positive synergetic effect on glycerol conversion and product yields. Further raising the H₂O₂ concentration of 6.85 mol/L at the reaction temperature of 90 °C can enhance a more glycerol conversion up to 93.87%. However, the presence of such high concentrations could lead to dangerous reaction conditions. Therefore, for safety reasons, the reaction was carried out with H₂O₂ concentration of 2.74 mol/L.

Table 4.4 Effect of H₂O₂ content and reaction temperature on the performance of glycerol conversion over SiW/Al₂O₃ catalyst with 4 wt.% catalyst loading at 240 min.

Types of catalysts	Concentration of H ₂ O ₂ (mol/L)	Temperature (°C)	Glycerol conversion (%)	Product yield (%)				Carbon selectivity (%) ^f	
				Glycolic acid	Formic acid	Acetic acid	Acrolein		Acrylic acid
Blank 1 ^a	2.74	70	6.91±0.06	0.22±0.09	0.40±0.06	0.44±0.01	0.08±0.05	0.39±0.05	1.54±0.58
Blank 2 ^b	2.74	90	9.27±0.09	0.29±0.03	0.52±0.09	0.55±0.02	0.16±0.00	0.67±0.02	2.19±0.01
Al ₂ O ₃	2.74	70	43.24±0.32	3.31±0.12	1.47±0.01	6.77±0.11	1.31±0.06	3.08±0.09	15.94±0.29
Al ₂ O ₃	2.74	90	63.51±0.14	6.64±0.10	3.40±0.07	7.29±0.12	2.08±0.01	7.59±0.08	26.98±0.34
30wt.% SiW/Al ₂ O ₃	0	70	9.07±0.27	0.64±0.02	0.34±0.01	0.77±0.02	1.46±0.09	0.65±0.03	3.86±0.11
30wt.% SiW/Al ₂ O ₃	0	90	17.84±0.27	1.11±0.10	0.93±0.09	1.37±0.09	3.35±0.08	1.17±0.03	7.92±0.32
30wt.% SiW/Al ₂ O ₃	2.74	70	64.30±0.79	10.01±0.11	6.11±0.08	16.20±0.21	5.16±0.20	15.28±0.16	52.76±0.44
30wt.% SiW/Al ₂ O ₃	2.74	90	83.78±0.13	15.34±0.23	7.90±0.18	18.83±0.42	5.44±0.24	25.11±0.28	72.62±0.81
30wt.% SiW/Al ₂ O ₃	6.85	90	93.87±0.21	11.22±0.58	10.31±0.35	23.43±0.75	2.79±0.11	17.86±0.50	65.62±0.25

^aReaction at 70 °C for 240 min in the presence of only 2.74 mol/L H₂O₂

^bReaction at 90 °C for 240 min in the presence of only 2.74 mol/L H₂O₂

^cPercent of carbon accounted for after 240 min of reaction

The effect of the reaction temperature was examined at the H_2O_2 concentration of 2.74 mol/L over 30 wt.% SiW/ Al_2O_3 catalyst with 4 wt.% catalyst loading at reaction temperature of 70 °C and 90 °C. As demonstrated in Table 4.4, raising the reaction temperature from 70 °C to 90 °C in the absence of H_2O_2 concentration resulted to the raise of glycerol conversion from 9.07% to 17.84%, approximately 1.97-fold increasing. A similar positive effect of temperature on glycerol conversion was also observed in the presence of H_2O_2 . That is, the glycerol conversion increased from 64.30% to 83.78%, approximately 1.30-fold increasing, when H_2O_2 concentration of 2.74 mol/L was introduced. The yield of all desired products from glycerol conversion in the presence of 2.74 mol/L increased significantly, particularly the yield of acrylic acid. It increased from 15.28% to 25.11%, approximately 1.64-fold increasing. It could be confirmed that the generation of undesired products, diagnosing from carbon selectivity, decreased significantly from 72.62% to less than 52.76%. Obviously, increasing the reaction temperature had a positive effect of glycerol conversion and yield of desired product. The increase in the glycerol conversion and product yield at high reaction temperature was due to high dehydration rate of glycerol in the presence of POM catalysts, consistent with the previous report (Shen et al., 2012). The acrylic acid yield was due to high kinetics of acrolein oxidation to acrylic acid (Tichý, 1997), resulting to the low generation of undesired products. However, the reaction temperature higher than 90 °C was not used as it would have a control system that would have been impractical in operation.

4.2.2 Effect of catalyst types and loading

The variation of the glycerol conversion and yield of desired product as a function of time over Al_2O_3 -supported POM catalysts were investigated with different catalyst loadings in the range of 2-8 wt.%, at 90 °C and ambient pressure in the presence of 2.74 mol/L H_2O_2 . A similar trend of glycerol conversion and yield of desired products were observed at all conditions (Figure 4.8-4.11). Glycerol conversion increased initially with increasing reaction time and then leveled off at reaction times longer than 120 min. With regards to the variation of product yield,

the yields of acetic acid, glycolic acid and formic acid increased with increasing reaction time. The acrylic acid yield was low during the first 90-120 min of reaction time, while a high acrolein yield was obtained during the same period. However, at longer reaction times, the acrolein yield decreased, whilst the acrylic acid yield increased. This implies that acrolein was oxidized to acrylic acid in the presence of pure Al_2O_3 support as well as Al_2O_3 -supported POM catalysts (Kampe et al., 2007; Kunert, Dochner, Ott, Vogel, & Fueß, 2004). Table 4.5 summarizes the glycerol conversion and yield of all desired products at 240 min by the glycerol conversion. In the presence of all Al_2O_3 -supported POM catalysts, the glycerol conversion was greater than that in the presence of solely Al_2O_3 for all catalyst types and catalyst loadings. At the same catalyst loading, the glycerol conversion and yield of acrylic acid were ranked in the order of $\text{SiW}/\text{Al}_2\text{O}_3 > \text{PW}/\text{Al}_2\text{O}_3 > \text{PMo}/\text{Al}_2\text{O}_3$, inconsistent with the total acidity as listed in Table 4.2. It seemed to be that catalytic activity of Al_2O_3 -supported POM catalysts for glycerol conversion was depending on the types and quantity of acidity strength. The $\text{SiW}/\text{Al}_2\text{O}_3$ catalyst provided the highest catalytic activity for glycerol conversion and also the highest quantity of low-strength acid sites compared with $\text{PW}/\text{Al}_2\text{O}_3$ and $\text{PMo}/\text{Al}_2\text{O}_3$ catalysts. This suggests that the catalytic activity is positively correlated to low-strength acid sites of catalyst that can enhance the glycerol conversion to desired products.

Consider the same catalysts types, the glycerol conversion was ranked in the order of 4 wt.% > 8 wt.% > 2 wt.% catalyst loading. Approximately 9.27% of glycerol can be converted in the absence of catalysts (Blank test) with less than 0.7% of each of the measurable detected products. The carbon selectivity in the blank test was approximately 2.19%. In the presence of solely Al_2O_3 , the glycerol conversion increased compared with the blank test. The glycerol conversion increased nearly doubled when the catalyst loading was increased from 2 wt.% to 4 wt.% for all types of POM catalysts. This might be attributed to the presence of sufficient acid sites of catalysts that can enhance the dehydration of glycerol to other substances.

However, further raising the catalyst loading from 4 wt.% to 8 wt.% resulted in only a slight increase of glycerol conversion, probably due to the mass transfer effect or the limited availability of H_2O_2 in the system.

Regarding the effect of catalyst type and loading on yield of all desired products when 2 wt.% catalyst loading was added, the yields of glycolic acid, acetic acid and acrolein increased significantly compared with that in the absence of catalyst. The yields of all desired products in the presence of Al_2O_3 -supported POM catalysts increased considerably when the catalyst loading was increased from 2 wt.% to 4 wt.% but decreased somewhat when the catalyst loading was further increased to 8 wt.%, similar to the trend of glycerol conversion and product yield observed in the presence of solely Al_2O_3 . One possible explanation is that, at high catalyst loading, the larger number of acidic sites or oxidative ability accelerated the conversion of glycerol to other undesired products, resulting in the decrease of desired product yields. Another possible reason might be due to the lack of sufficient oxidizing agent and the onset of mass transfer limitations in the presence high catalyst loading.

Among the utilized Al_2O_3 -supported POM catalysts, the SiW/ Al_2O_3 catalyst had lower acid strength than PW/ Al_2O_3 catalyst, and it gave higher glycerol conversion under the same operating conditions. This could be due to the fact that SiW has better stability than PW under high reaction temperatures in aqueous media (Tsukuda et al., 2007), resulting in a better chance to supply strong acid protons for the dehydration reaction of glycerol. PMo/ Al_2O_3 catalyst had the lowest glycerol conversion compared with utilized catalysts due to its low acid strength and thermal stability (Bardin, Bordawekar, Neurock, & Davis, 1998).

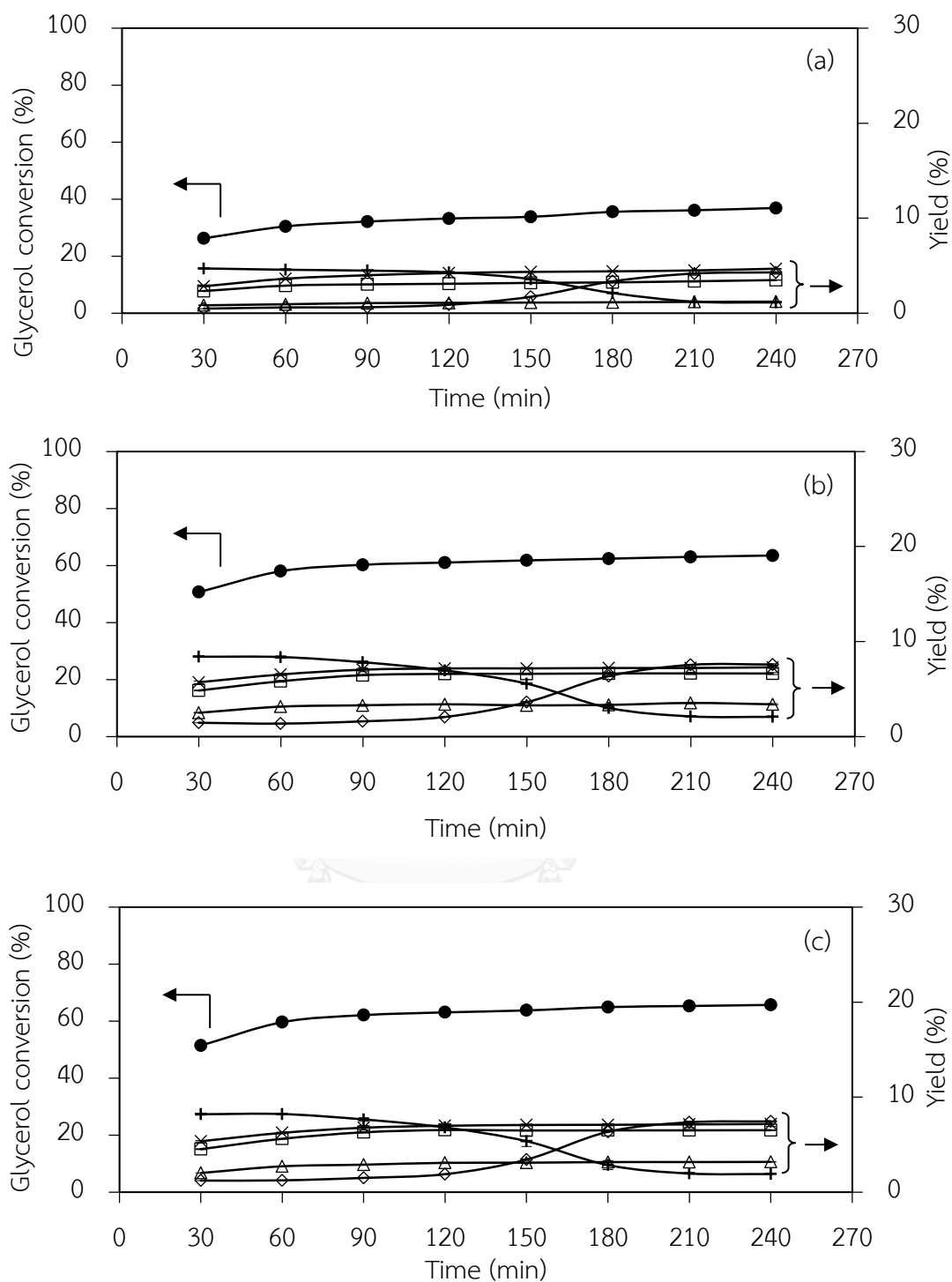


Figure 4.8 Variation of (●) glycerol conversion and yields of (□) glycolic acid, (△) formic acid, (×) acetic acid, (+) acrolein and (◇) acrylic acid as a function of time of glycerol conversion over Al_2O_3 catalyst (a) 2 wt.%, (b) 4 wt.% and (c) 8 wt.% catalyst loading at 90°C .

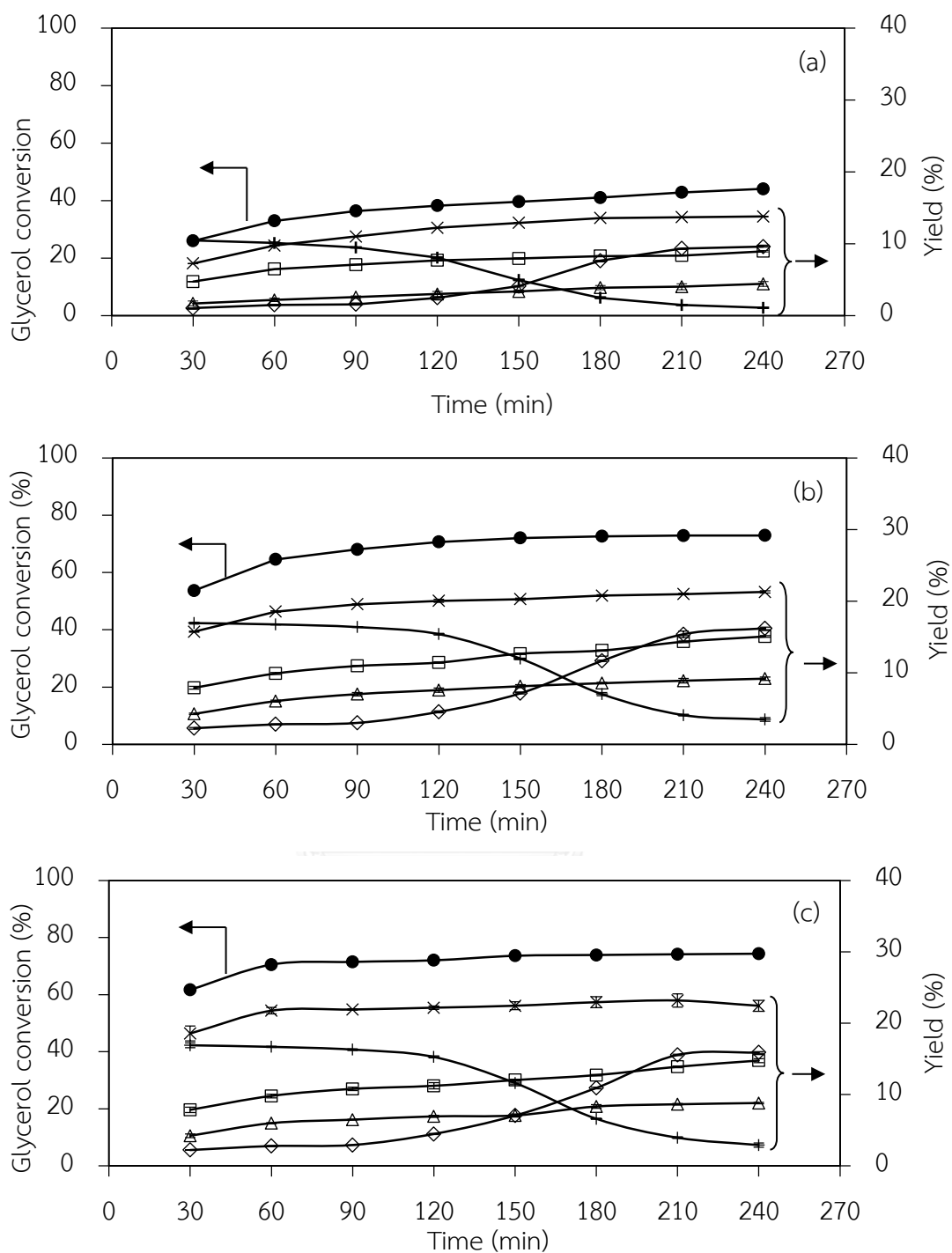


Figure 4.9 Variation of (●) glycerol conversion and yields of (□) glycolic acid, (Δ) formic acid, (X) acetic acid, (+) acrolein and (◇) acrylic acid as a function of time of glycerol conversion over PW/Al_2O_3 catalyst (a) 2 wt.%, (b) 4 wt.% and (c) 8 wt.% catalyst loading at $90^\circ C$.

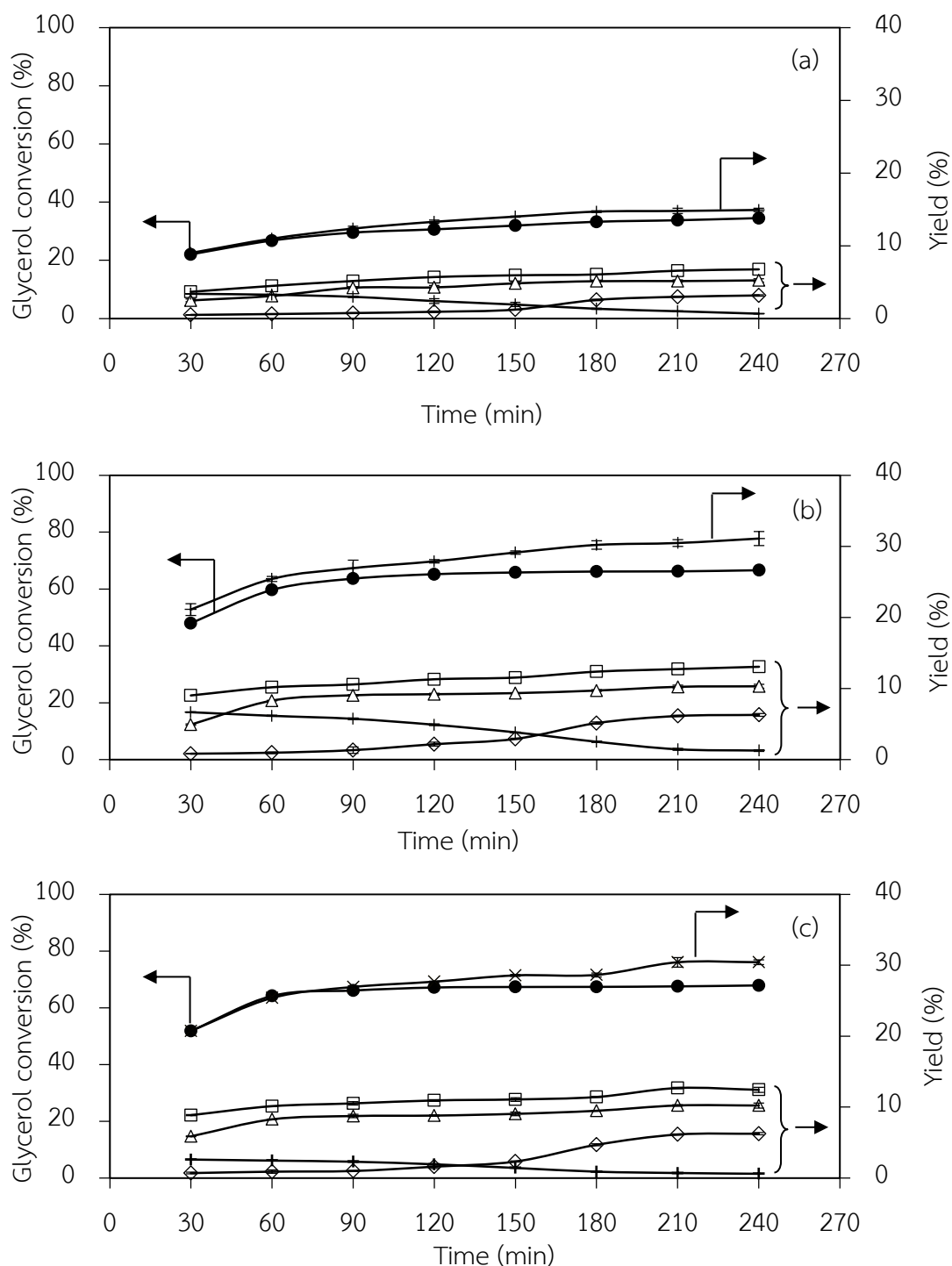


Figure 4.10 Variation of (●) glycerol conversion and yields of (□) glycolic acid, (△) formic acid, (×) acetic acid, (+) acrolein and (◇) acrylic acid as a function of time of glycerol conversion over $\text{PMo}/\text{Al}_2\text{O}_3$ catalyst (a) 2 wt.%, (b) 4 wt.% and (c) 8 wt.% catalyst loading at 90 °C.

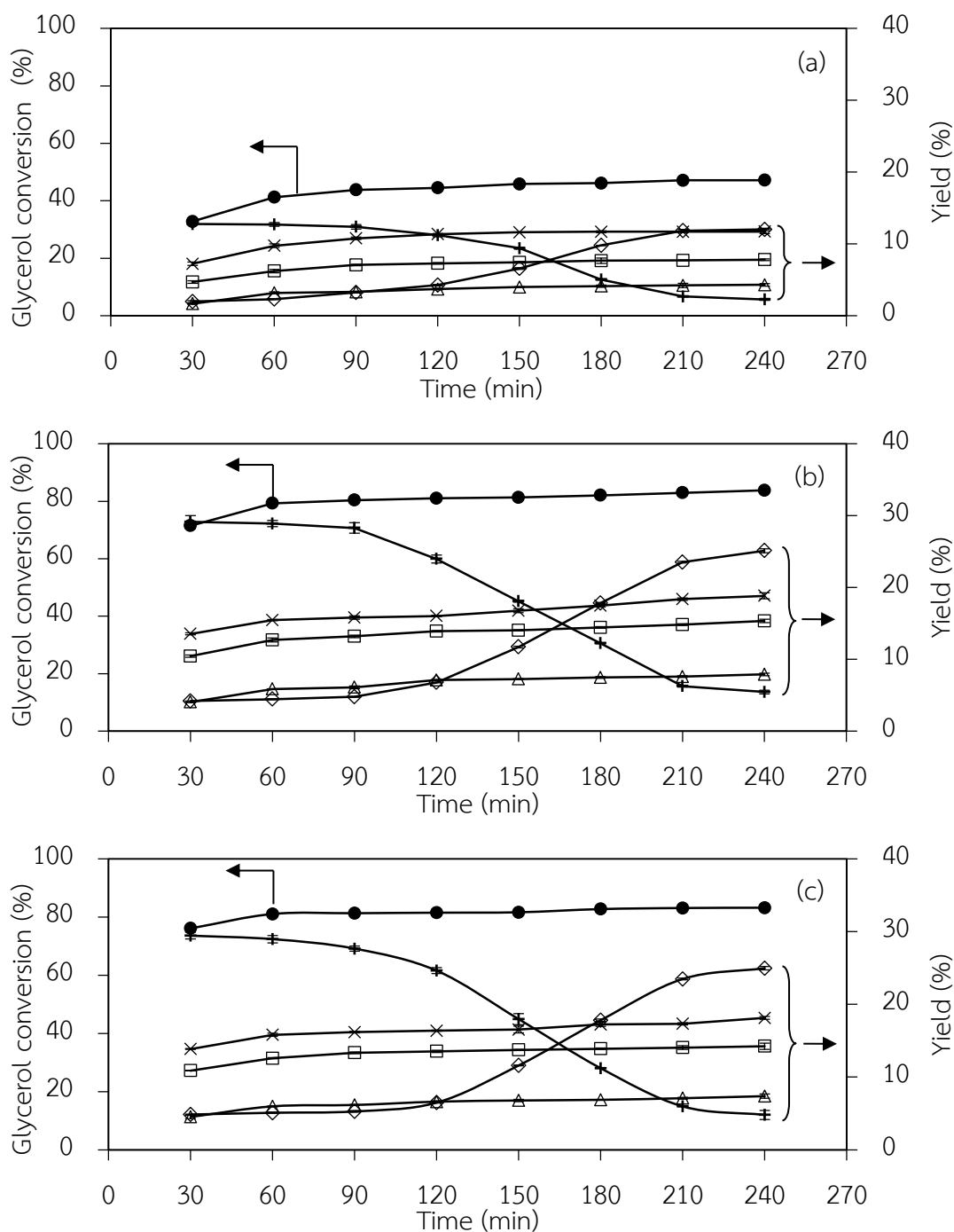


Figure 4.11 Variation of (●) glycerol conversion and yields of (□) glycolic acid, (△) formic acid, (×) acetic acid, (+) acrolein and (◇) acrylic acid as a function of time of glycerol conversion over $\text{SiW}/\text{Al}_2\text{O}_3$ catalyst (a) 2 wt.%, (b) 4 wt.% and (c) 8 wt.% catalyst loading at 90°C .

Table 4.5 Effect of catalyst types and catalyst loading on the performance of glycerol conversion over Al₂O₃-supported POM catalyst at 90 °C and 240 min.

Types of catalysts	Catalyst loading (wt.%)	Glycerol conversion (%)	Product yield (%)							Carbon selectivity (%)
			Glycolic acid	Formic acid	Acetic acid	Acrolein	Acrylic acid			
Blank ^a	-	9.27±0.09	0.29±0.03	0.52±0.09	0.55±0.02	0.16±0.00	0.67±0.02			2.19±0.01
Al ₂ O ₃	2	36.94±0.17	3.50±0.02	1.23±0.03	4.69±0.01	1.15±0.02	4.31±0.07			14.88±0.11
	4	63.51±0.14	6.64±0.10	3.40±0.07	7.29±0.12	2.08±0.01	7.59±0.08			26.98±0.34
	8	65.69±0.19	6.53±0.05	3.20±0.01	7.18±0.27	1.92±0.01	7.46±0.07			26.28±0.26
PW/Al ₂ O ₃	2	44.10±0.11	8.95±0.07	4.42±0.10	13.79±0.33	1.09±0.11	9.60±0.05			37.85±0.17
	4	72.93±0.28	15.07±0.12	9.17±0.23	23.19±0.16	3.48±0.25	16.20±0.18			65.20±0.35
	8	74.34±0.14	14.77±0.28	8.82±0.10	22.44±0.77	2.92±0.31	15.90±0.11			64.84±0.69
PMO/Al ₂ O ₃	2	34.52±0.44	6.76±0.25	5.24±0.23	14.93±0.22	0.66±0.02	3.17±0.10			30.76±0.26
	4	66.62±0.32	13.07±0.23	10.32±0.27	31.10±0.99	1.28±0.12	6.30±0.19			62.08±0.18
	8	67.88±0.36	12.43±0.35	10.22±0.12	30.43±0.34	1.49±0.02	6.25±0.15			60.81±0.43
SiW/Al ₂ O ₃	2	47.19±0.15	7.80±0.12	4.31±0.17	11.72±0.30	2.27±0.15	12.01±0.18			38.11±0.20
	4	83.78±0.13	15.34±0.23	7.90±0.18	18.83±0.42	5.44±0.24	25.11±0.28			72.62±0.81
	8	83.19±0.07	14.23±0.44	7.38±0.30	18.13±0.20	4.80±0.63	24.96±0.22			69.51±0.26

^aReaction at 90 °C for 240 min in the presence of only 2.74 mol/L H₂O₂

4.3 Reaction mechanism of conversion of glycerol

In order to monitor the reaction mechanism of glycerol conversion over the SiW/Al₂O₃ catalyst, the liquid products were analyzed by GC-MS. As clearly demonstrated in Figure 4.12, besides the preferable compound (acrylic acid), several other products were detected in the GC-MS chromatogram such as oxygenated products including acrolein, formic acid, acetic acid, acrylic acid, glycolic acid glyceric acid, hydroxyacetone, propionic acid, 1,3-propanediol, 1,3-ethoxythylidene glycerol and 2-ethoxyethanol as well as higher cyclic molecules including 5-hydroxy-1,3-dioxolane, benzoic acid, 2-ethyl-1,3-dioxolane-4-methanol, and stearic acid were generated. Compared to glycerol, all of these formed compounds have many hydrogen and oxygen substitutions with C₂-C₆ carbon compounds being principally formed. While some of these compounds have known reaction pathways from glycerol, others do not. To optimize or standardize the conversion of glycerol over the SiW/Al₂O₃ catalyst, it is important to know and so to evaluate the mechanisms of synthesis of these compounds from glycerol. However, it is still difficult to deduce the exact synthesis route of each compound from glycerol because some intermediate products cannot be measured. Rather, a hypothetical general scheme (Figure 4.13) can be proposed with some paths more or less possible for each studied system. According to this scheme, in the presence of supported SiW catalysts, the dehydration of glycerol can occur both at the terminal and at the middle (or secondary) -OH groups. If glycerol is dehydrated at the terminal -OH group, 2,3-dihydroxypropene is generated. It can further rearrange to 1-hydroxyl-2-propanone or acetol, the detected product (Suprun, Lutecki, Haber, & Papp, 2009). The acetol is very reactive, it is hydrogenated in the presence of acid catalysts to 1,2-propanediol, a commercially valuable chemical. Besides, acetol can be oxidized and decarboxylated to glycolic acid according to selective oxidation reaction and decarboxylation (Rodrigues, Pereira, Delgado, Chen, & Órfão, 2011). On the contrary, if glycerol was dehydrated at the second -OH group, H₂O and H⁺ are extruded from the dehydrated glycerol to form two species; either 1,3-dihydroxypropene or 3-hydroxypropanal by tautomerism (Tsukuda et al., 2007). However, these species were

not detected in our analysis since they are very reactive. They readily undergo secondary dehydration into acrolein (Suprun et al., 2009; Yan & Suppes, 2009), the observed product. Furthermore, 3-hydroxypropanal can cleave the C₁-C₂ bond leading to the formation of formaldehyde and acetaldehyde, through retro-aldol reaction. In the presence of oxygen, the generated compounds were oxidized. That is, formaldehyde and acetaldehyde were rapidly oxidized to formic acid and acetic acid, respectively, while acrolein was oxidized to acrylic acid.

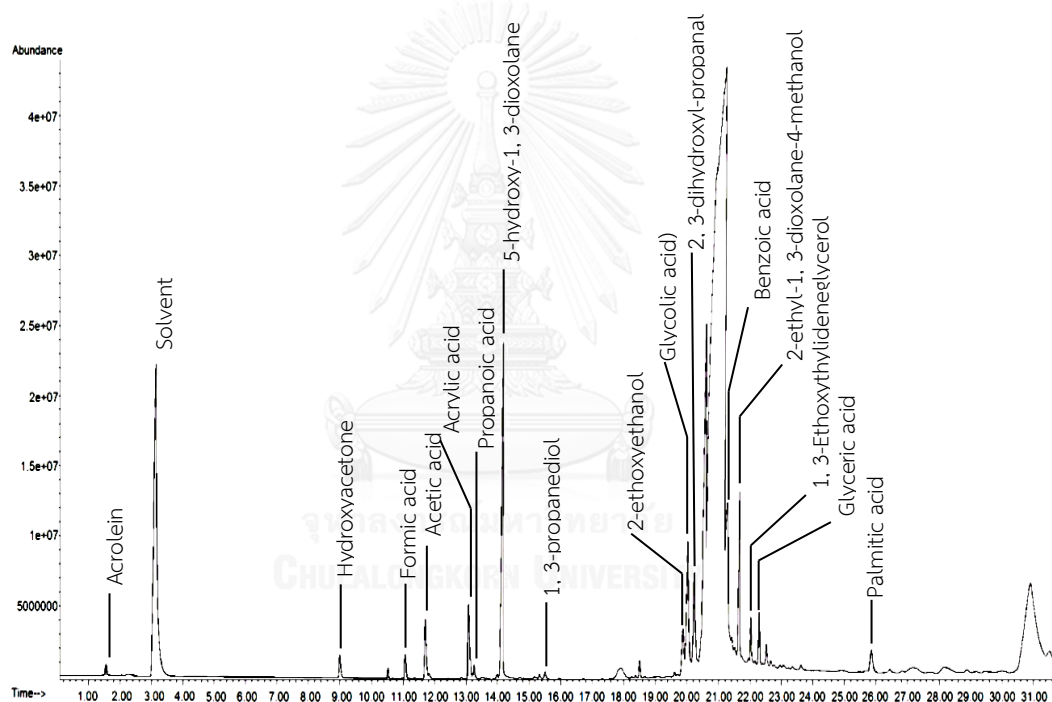


Figure 4.12 GC-MS chromatogram of solutions obtained from glycerol conversion over 30 wt.% SiW/Al₂O₃ catalyst at 90 °C.

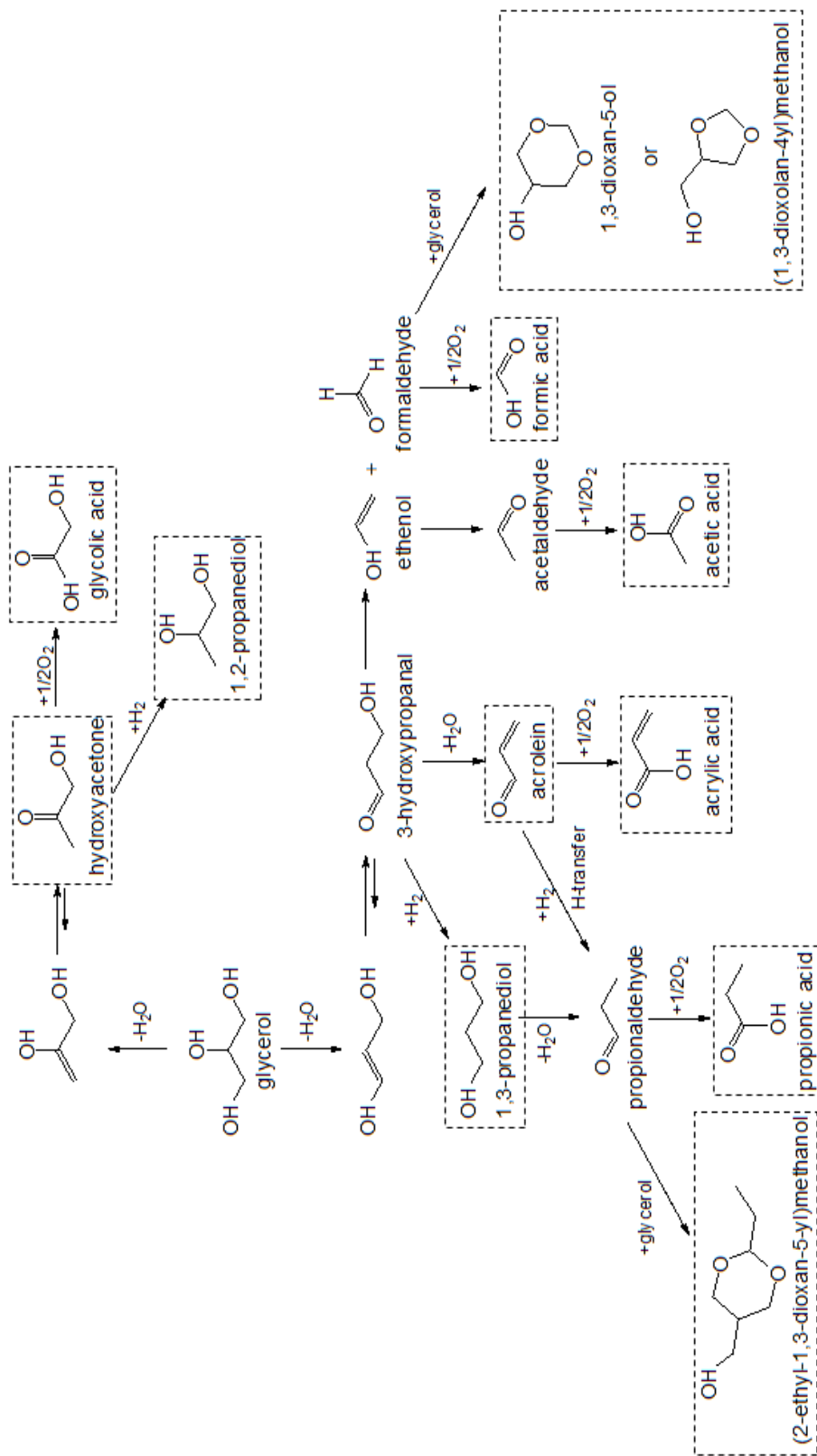


Figure 4.13 Proposed reaction pathways of glycerol conversion. The products detected by GC-MS are indicated by dashed line.

CHAPTER V

CONVERSION OF GLYCEROL TO ACRYLIC ACID VIA SUPPORTED SiW CATALYSTS

In a previous chapter, it was found that various higher market value products were generated in the liquid phase conversion of glycerol via Al_2O_3 -supported POM catalysts at 90°C , such as glycolic acid, 1,2-propanediol, formic acid, acetic acid, and acrolein. The highest glycerol conversion and acrylic acid yield were obtained with $\text{SiW}/\text{Al}_2\text{O}_3$ catalyst (~25%) at 4 wt.% catalyst loading in the presence of 2.74 mol/L H_2O_2 at reaction temperature of 90°C . In the current chapter, in order to achieve a higher glycerol conversion and product yield, we continue our work with SiW catalyst. The influence of support types and SiW loadings was investigated. Finally, the kinetic of glycerol conversion over the best supported SiW catalyst was examined.

5.1 Effect of supports

Three types of support were utilized in this part including Al_2O_3 , SiO_2 and HZSM-5. Figure 5.1 reveals the XRD pattern of unsupported SiW catalyst and all supported SiW catalysts at constant loading of SiW on support of 30 wt.%. The XRD pattern of SiW shows the crystalline phase at 2θ of 27.3° , assigned to the SiW hexahydrate (Tsukuda et al., 2007). For the SiW/SiO_2 and $\text{SiW}/\text{Al}_2\text{O}_3$ catalysts, no characteristic peaks assigned to the utilized SiW were observed, suggesting that SiW catalysts were highly dispersed on the support. In case of $\text{SiW}/\text{HZSM-5}$ catalyst, the detected reflections were like to that of SiW, implying the presence of the cubic SiW hexahydrate phase on its support. Textural properties for supported SiW catalysts immobilized on Al_2O_3 , SiO_2 and HZSM-5 supports derived from N_2 physisorption isotherms are summarized in Table 5.1. The BET surface area of utilized supports was in an order of $\text{HZSM-5} > \text{Al}_2\text{O}_3 > \text{SiO}_2$, while the inverse order was observed in their pore volumes. The pore diameter changed in the order of $\text{Al}_2\text{O}_3 > \text{HZSM-5} > \text{SiO}_2$. When SiW impregnated on the support surface, a similar trend of change of BET surface area, pore volume and average pore diameter was observed. However, the

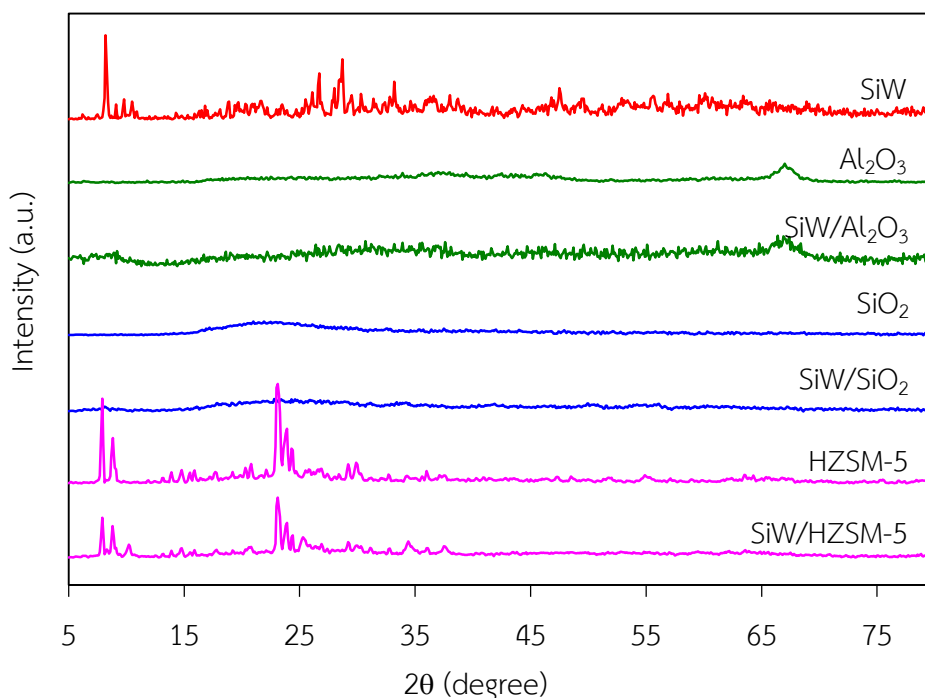


Figure 5.1 XRD patterns of SiW and supported SiW catalyst at 30 wt.% SiW loading.

catalysts were decreased significantly compared to the original SiW-free supports. The decrease in BET surface area may be attributed to the support pores blocking by catalyst particle. This is because the pores of Al_2O_3 , SiO_2 and HZSM-5 are 5.46, 2.89 and 4.32 Å, respectively, and the Keggin unit diameter is ~12 Å (Popa et al., 2005).

The surface acidity of all utilized supports and supported SiW catalysts were determined by NH_3 -TPD analysis as shown in Figure 5.2. Two desorption peaks at 203 °C and 388 °C were observed for unsupported SiW, indicating the presence of weak- and medium-strength acid sites on the surface of the catalysts. No sharp desorption peaks were observed for all utilized supports, they appeared as a board peaks. For supported SiW catalysts, two broad NH_3 -TPD peaks were observed at the temperature of 161 °C and 522 °C and 191 °C and 469 °C for SiW/HZSM-5 and SiW/ Al_2O_3 catalysts, respectively, indicating the presence of weak- and strong-strength acid sites in their structures. Peaks appearing at 154 °C, 491 °C and 735 °C were observed on the NH_3 -TPD profile of SiW/ SiO_2 catalysts, denoting the presence of weak-, medium- and strong-strength acid sites on its structure. Compared with the

Table 5.1 Textural properties and surface chemistry of supported SiW catalysts and corresponding supports

Catalysts	Textural properties			Surface chemistry		
	BET surface area (m ² /g)	Pore volume (cm ³ /g)	Average pore diameter (Å)	Acid amount (mmol NH ₃ /g Cat.)	Acid amount (mmol NH ₃ /g Cat.)	Total acidity (mmol NH ₃ /g Cat.)
SiW	121.5	0.357	3.74	2.88 (108-303 °C) 0.93 (351-439 °C)	2.88 (108-303 °C) 0.93 (351-439 °C)	3.81
Al ₂ O ₃	267.8	0.229	5.46	0.50 (46-275 °C) 0.18(275-453 °C)	0.50 (46-275 °C) 0.18(275-453 °C)	0.68
SiO ₂	223.6	0.835	2.89	0.28 (71-229 °C) 0.57 (248-921 °C)	0.28 (71-229 °C) 0.57 (248-921 °C)	0.85
HZSM-5	289.4	0.173	4.32	0.71 (81-349 °C) 0.25 (362-640 °C)	0.71 (81-349 °C) 0.25 (362-640 °C)	0.96
SiW/Al ₂ O ₃	214.6	0.128	4.11	1.19 (110-356 °C) 0.23 (390-543 °C)	1.19 (110-356 °C) 0.23 (390-543 °C)	1.42
SiW/SiO ₂	201.2	0.644	2.08	0.78 (56-312 °C) 0.42 (375-610 °C) 0.04 (617-906 °C)	0.78 (56-312 °C) 0.42 (375-610 °C) 0.04 (617-906 °C)	1.24
SiW/HZSM-5	233.4	0.153	2.62	0.88 (78-321 °C) 0.43 (355-669 °C)	0.88 (78-321 °C) 0.43 (355-669 °C)	1.31

desorption peaks of the unsupported SiW catalyst, the NH_3 -TPD peaks of all supported SiW catalysts were shifted to lower temperature and lost some intensity, indicating a weakening of the acid site due to interactions with their supports. Upon supporting SiW on all supports, the medium-strength peak lost most of intensity but appeared to shift toward higher temperature ($\sim 480^\circ\text{C}$).

The amounts of acid sites of all supported SiW catalysts calculated from NH_3 -TPD desorption peak areas are also summarized in Table 5.1. The acidity of all supported SiW catalysts was lower than that of unsupported SiW catalyst, but it was still greater than that of fresh Al_2O_3 , SiO_2 and HZSM-5 supports. This is because the addition of SiW did not introduce any new acid sites on the support surface, but led to a replacement by other acidic sites (Atia et al., 2008; Chino & Okubo, 2005). The weak interaction of the support with the SiW kept its Brønsted acid character and led to an increased proportion of medium- and strong-strength acid sites. In this case, a portion of the SiW lost its acidity due to the distortion of the Keggin structure. In summary, the total acidity of the supported SiW catalysts was in an order of $\text{SiW}/\text{Al}_2\text{O}_3 > \text{SiW}/\text{HZSM-5} > \text{SiW}/\text{SiO}_2$.

Figure 5.3 shows the variation of glycerol conversion and product yield as a function of reaction time for glycerol conversion over supported SiW catalysts at identical SiW loading of 30 wt.% with 4 wt.% catalyst loading in the presence of 2.74 mol/L H_2O_2 at reaction temperature of 90°C and ambient pressure. A similar pattern of the glycerol conversion and product yield was apparent in the presence of all supported SiW catalysts. Glycerol conversion increased initially with increasing reaction time and then leveled off at reaction times longer than 120 min. The yields of acetic acid, glycolic acid and formic acid increased slightly with increasing reaction time. The yield of acrylic acid was low during the first 30-120 minutes of reaction time, while a high yield of acrolein was obtained during the same period. However, at longer reaction times, the yield of acrolein decreased, whilst the yield of acrylic acid increased. This implies that acrolein was oxidized to acrylic acid in the presence of supported SiW catalysts.

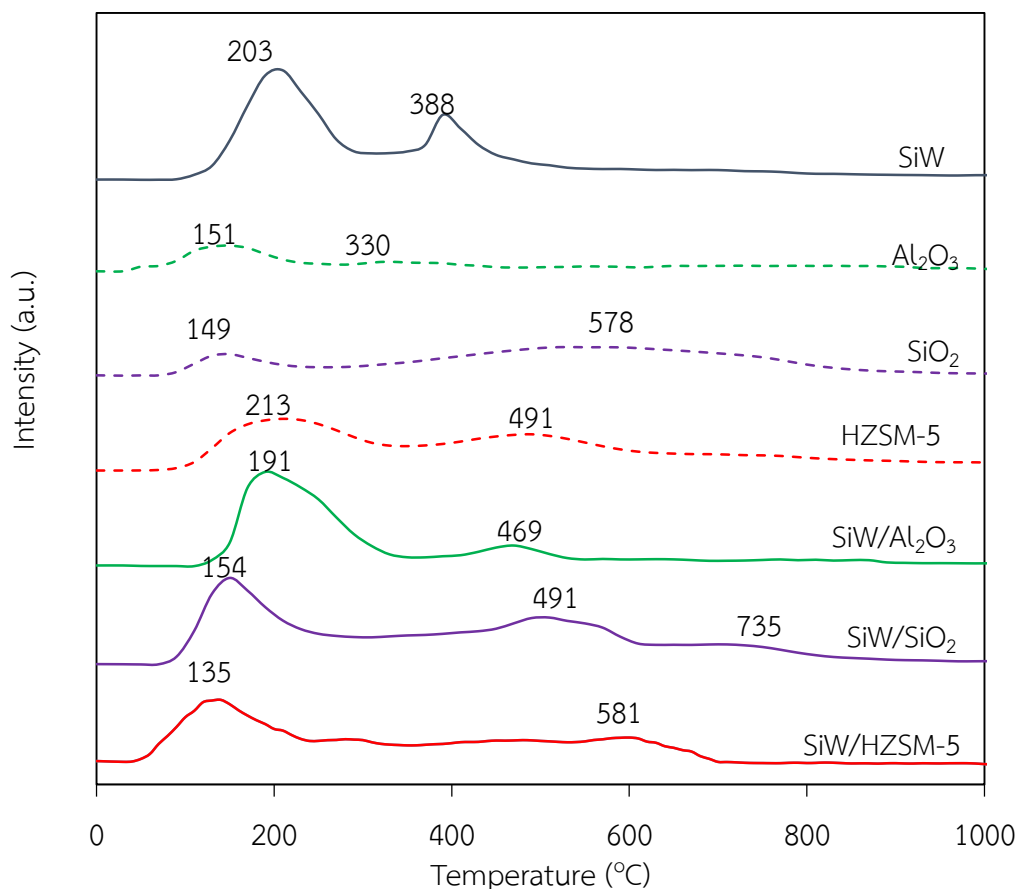


Figure 5.2 NH₃-TPD profiles of supported SiW catalysts and their supports at 30 wt.% SiW loading.

Considering at long reaction time (240 min), as summarized in Table 5.2, the glycerol conversion and yield of desired products were ranked in the order of SiW/HZSM-5 > SiW/Al₂O₃ > SiW/SiO₂. Less than 16% of converted carbons were transformed to the undesired products in the presence of SiW/HZSM-5 catalyst. This suggests that the SiW/HZSM-5 catalyst was more active than the other two types. Although SiW/HZSM-5 catalyst had lower acid strength than SiW/Al₂O₃ catalyst, it gave higher glycerol conversion under the same operating conditions. This might be attributed to the important role of low-strength acid sites of catalysts that can enhance the glycerol conversion to desired products. The trend of catalytic activity of supported SiW catalysts for the conversion of glycerol was a good coincidence with the trends of BET surface area, but not the acidity, pore volume and average

pore diameter of corresponding catalysts (Table 5.1). This suggests that the dehydration of glycerol over supported SiW catalysts required just a certain value of acidity and then low-strength acid sites and BET surface area of catalysts played an important role. The catalyst with high BET surface area and appropriate acidity allowed a more available area for adsorption of glycerol, which can further undergo dehydration to intermediate/product species. This hypothesis is supported by the low BET surface area and high acidity of SiW/SiO₂ catalyst, where glycerol conversion and low product yield were obtained. Thus it can be concluded that the BET surface area played a more important role on the activity for glycerol conversion via supported SiW catalysts than the total acidity.

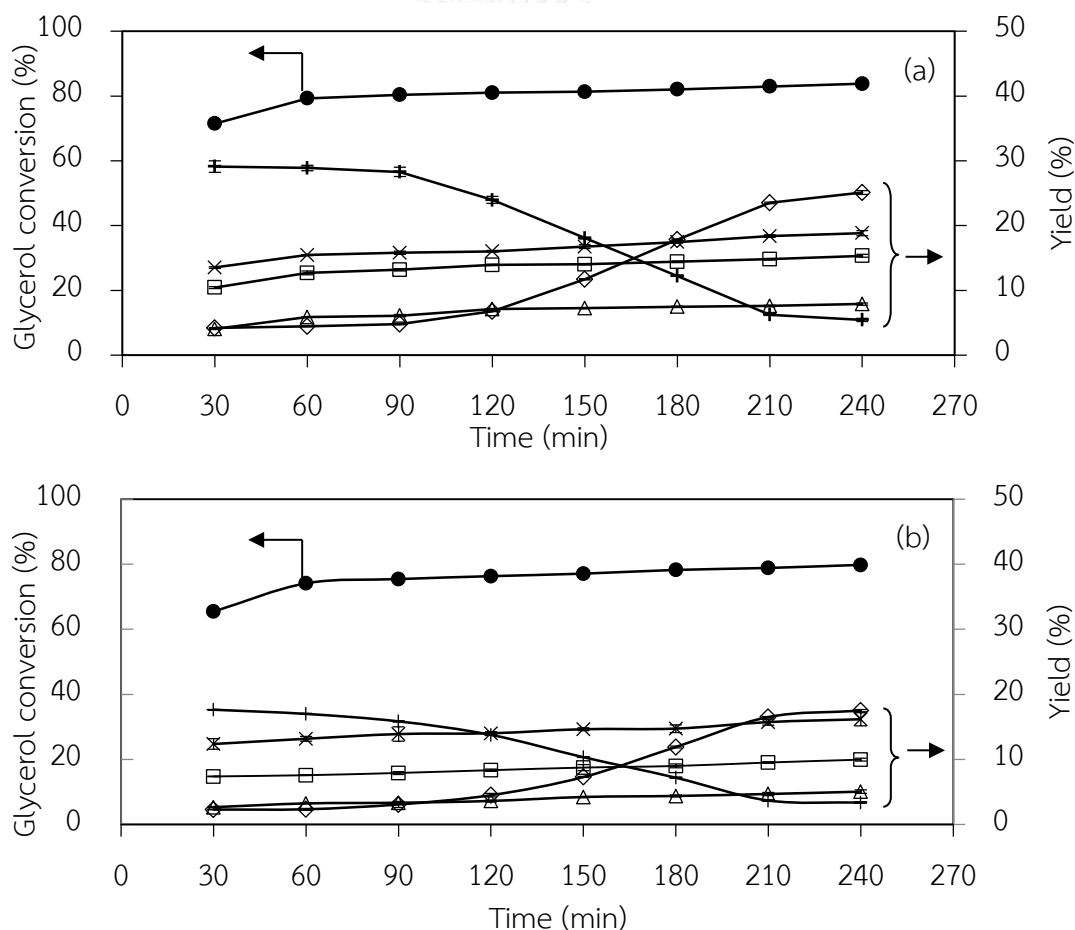


Figure 5.3 Variation of (●) glycerol conversion and yields of (□) glycolic acid, (△) formic acid, (×) acetic acid, (+) acrolein and (◇) acrylic acid as a function of time over (a) SiW/Al₂O₃, (b) SiW/SiO₂ and (c) SiW/HZSM-5 catalysts with 30 wt.% SiW loading at 90 °C.

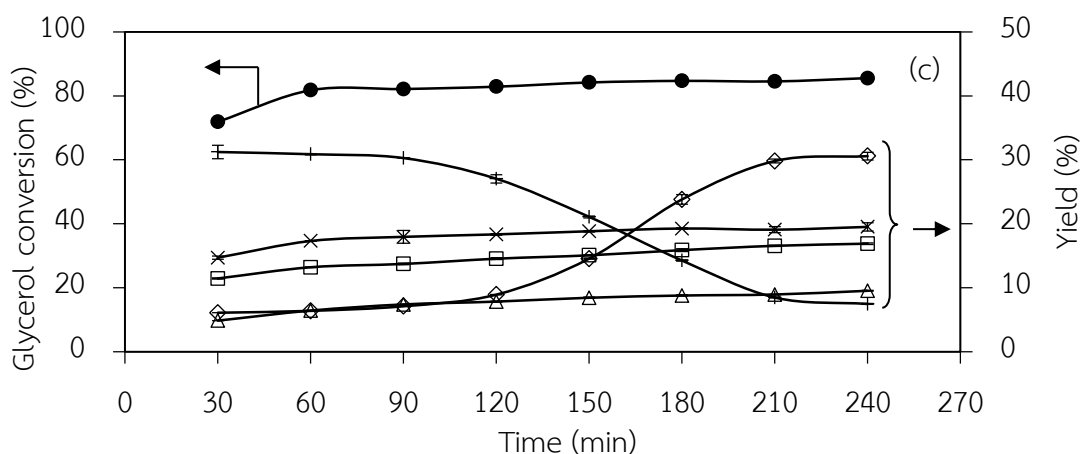


Figure 5.3 (Cont.) Variation of (●) glycerol conversion and yields of (□) glycolic acid, (△) formic acid, (×) acetic acid, (+) acrolein and (◇) acrylic acid as a function of time over (a) SiW/Al₂O₃, (b) SiW/SiO₂ and (c) SiW/HZSM-5 catalysts with 30 wt.% SiW loading at 90 °C.

5.2 Effect of oxidizing agent and reaction temperature

The effect of the oxidizing agent and reaction temperature was then examined over 30 wt.% SiW/HZSM-5 catalyst. As demonstrated in Table 5.3, the presence of H₂O₂ concentration had significant effect on the variations of the glycerol conversion. Glycerol conversion is obviously low in the absence of H₂O₂. The addition of 2.74 mol/L H₂O₂ can enhance the glycerol conversion from 17.04% to 42.69% and 33.75% to 85.54% at temperature of 70 °C and 90 °C, respectively, approximately 2.50-fold and 2.53-fold increasing. For product yield, addition of 2.74 mol/L H₂O₂ resulted in significantly increase of acrylic acid yield of approximately 3.49-fold and 5.81-fold at 70 °C and 90 °C, respectively. This suggests that oxidation of the dehydrated products of glycerol can be promoted when glycerol is in contact with the oxidative catalyst or oxidizing agent. In addition, the presence of 2.74 mol/L H₂O₂ can decrease the production of other products, as observed from the increasing carbon selectivity from 8.21% to 33.65% at reaction temperature of 70 °C when H₂O₂ was added into

Table 5.2 Effect of supports on the performance of glycerol conversion over supported SiW catalysts at SiW loading of 30 wt.%, temperature of 90 °C at 240 min.

Catalysts	Glycerol conversion (%)	Product yield (%)				Carbon selectivity (%)	
		Glycolic acid	Formic acid	Acetic acid	Acrolein		
SiW/Al ₂ O ₃	83.78±0.13	15.34±0.23	7.90±0.18	18.83±0.42	5.44±0.24	25.11±0.28	72.62±0.81
SiW/SiO ₂	79.80±0.40	9.97±0.23	5.05±0.27	16.17±0.99	3.38±0.12	17.50±0.19	52.08±0.65
SiW/HZSM-5	85.54±0.40	16.95±0.47	9.53±0.67	19.51±0.39	7.47±0.22	30.57±0.21	83.98±0.08

the reaction, indicating the decrease of glycerol conversion to undesired products from 91.79% to 66.35%. At the reaction temperature of 90 °C, the carbon selectivity also increased from 23.13% to 83.98%, suggesting the reduction of glycerol conversion to undesired products from 76.87% to 16.02%. This can be explained by the fact that H₂O₂ is the reactive oxygen donor providing the ideal conditions for oxidation of glycerol to glycerol aldehyde, an intermediate for glyceric acid in liquid phase (Atia et al., 2008). Nevertheless, the presence of only H₂O₂ in the absence catalyst (Blank test 1 and 2) cannot promote the progress of the glycerol conversion. The glycerol conversions proceeded only to 6.91% and 9.27% at the reaction temperature of 70 °C and 90 °C, respectively. Less than 1% of each measurable detected product was generated at such condition. This indicates that the presence of H₂O₂ and SiW/HZSM-5 catalysts had the positive synergetic effect on glycerol conversion and product yields. Obviously, the increasing reaction temperature had a positive effect of glycerol conversion and yield of desired product. The increase in the glycerol conversion in the presence of high reaction temperature was due to high dehydration rate of glycerol in the presence of POM catalysts, consistent with the previous report (Shen et al., 2012). The increasing acrylic acid yield was due to high kinetics of acrolein oxidation to acrylic acid (Tichý, 1997), resulting to the low generation of undesired products. However, the reaction temperature higher than 90 °C was not used as it would have required a proper control system, which would be impractical in operation.

Table 5.3 Effect of H₂O₂ concentration and reaction temperature on glycerol conversion over 30 wt.% SiW/HZSM-5 catalyst with 4 wt.% catalyst loading at 240 min.

Types of catalysts	Concentration of H ₂ O ₂ (M)	Temperature (°C)	Glycerol conversion (%)	Product yield (%)				Carbon selectivity (%)	
				Glycolic acid	Formic acid	Acetic acid	Acrolein		Acrylic acid
Blank 1	2.74	70	6.91±0.06	0.22±0.01	0.40±0.13	0.44±0.05	0.08±0.03	0.39±0.04	1.54±0.00
Blank 2	2.74	90	9.27±0.09	0.29±0.03	0.52±0.09	0.55±0.02	0.16±0.00	0.67±0.02	2.19±0.01
HZSM-5	2.74	90	80.11±0.03	5.12±0.14	3.93±0.33	5.94±0.69	13.76±0.88	8.23±0.47	36.98±0.03
SiW/HZSM-5	0	70	17.04±0.23	2.09±0.21	1.01±0.06	3.09±0.26	0.25±0.02	1.76±0.09	8.21±0.00
SiW/HZSM-5	0	90	33.75±0.31	4.97±0.29	2.79±0.38	7.25±0.37	2.87±0.11	5.26±0.22	23.13±0.01
SiW/HZSM-5	2.74	70	42.69±0.02	8.95±0.45	4.59±0.41	12.52±0.01	3.43±0.34	6.15±0.68	33.65±0.10
SiW/HZSM-5	2.74	90	85.54±0.40	16.95±0.47	9.53±0.67	19.51±0.39	7.47±0.22	30.57±0.21	83.98±0.08

5.3 Effect of SiW loading

The XRD patterns of SiW/HZSM-5 catalysts with different SiW loadings in the range of 20-60 wt.% are exhibited in Figure 5.4. The XRD peaks of all SiW/HZSM-5 catalysts were intermediary between that of unsupported SiW and HZSM-5 support. Increasing the SiW loading reduced the intensity of the main characteristic peaks of HZSM-5, emerging at 2θ of 7.8° , 8.7° , 23.1° , 23.3° , 23.6° , 23.8° , and 24.3° . When the SiW loading was below 40 wt.%, the XRD patterns of SiW/HZSM-5 catalysts were still similar to that of HZSM-5, and peaks assignable to HZSM-5 were observed, suggesting that HZSM-5 was higher crystalline phase.

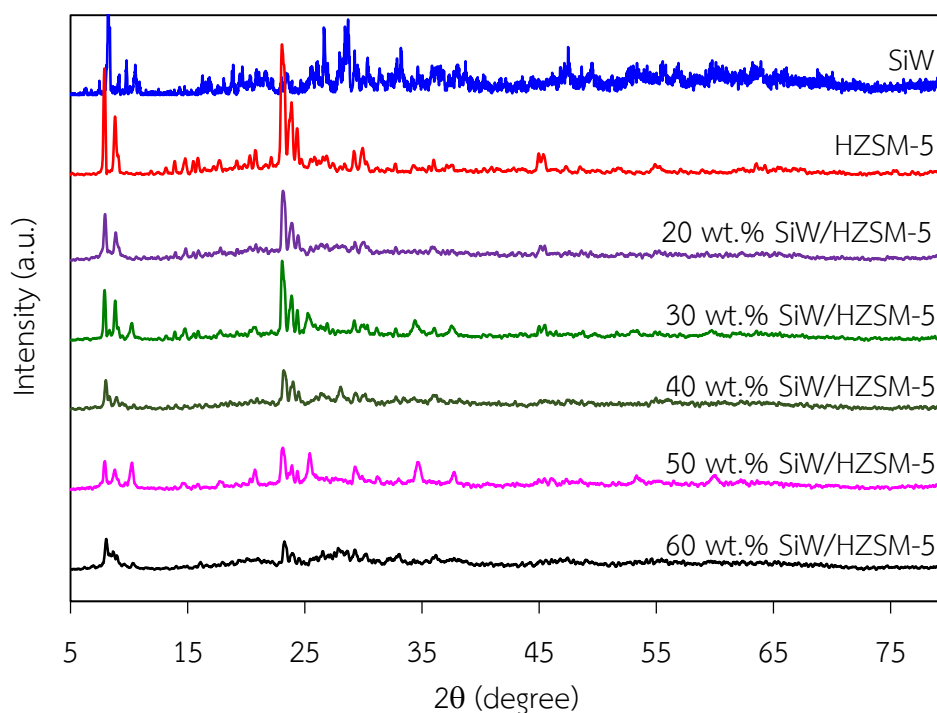


Figure 5.4 XRD patterns of unsupported SiW, HZSM-5 and SiW/HZSM-5 catalysts with different SiW loading.

Regarding the textural properties and surface chemistry of SiW/HZSM-5 catalysts at different SiW loadings, the BET surface area and pore volume diminished with increasing SiW loading (Table 5.4). This might be due to the agglomeration of SiW on the support surface. Namely, the generated agglomerates could not enter the pores of the support because of the presence of diffusion resistance. Thus, they

blocked the pores, resulting in the decrease of pore volume as well as pore diameter, which led to a decline in the BET surface area (Lili et al., 2008). In addition, it also resulted in the decrease of SiW dispersion and the amount of effective acid sites. The NH_3 -TPD profiles of the unsupported SiW, HZSM-5 and SiW/HZSM-5 catalysts with different SiW loadings are illustrated in Figure 5.5. Two desorption peaks at 203 °C and 388 °C were observed for unsupported SiW, indicating the presence weak- and medium-strength acid sites on the surface of catalysts. No sharp desorption peaks were observed for HZSM-5 and all SiW/HZSM-5 catalysts, they appeared as a board peaks. Peaks appeared at 213 °C and 491 °C were observed on the NH_3 -TPD profile of solely HZSM-5, denoting the presence of weak- and medium-strength acid sites on its structure. For SiW/HZSM-5 catalysts, two broad NH_3 -TPD peaks were observed at the temperature of 125 °C and 579 °C, 135 °C and 581 °C, 137 °C and 582 °C, 143 °C and 602 °C and 158 °C and 604 °C for 20 wt.%, 30 wt.%, 40 wt.%, 50 wt.% and 60 wt.% SiW/HZSM-5 catalysts, respectively, indicating the presence of weak- and strong-strength acid sites in their structures. Compared with the desorption peaks of the unsupported SiW catalyst, the NH_3 -TPD peaks of all SiW/HZSM-5 catalysts with different SiW loadings were shifted to lower temperature and lost some intensity, indicating a weakening of the acid site due to interactions with their supports. Upon supporting SiW on HZSM-5 supports, the medium-strength peak lost most of intensity but appeared to shift toward higher temperature (~580°C). However, when the SiW loading exceeded 30 wt.%, the peaks at weak-strength acid sites became strong, implying that the quantity of medium-strength acid sites decreased. The amounts of acid sites of all supported SiW catalysts calculated from NH_3 -TPD desorption peak area are also summarized in Table 5.1. The acidity of all SiW/HZSM-5 catalysts was lower than that of unsupported SiW catalyst. However, it was still greater than that of fresh HZSM-5 supports. This is because the addition of SiW did not introduce any new acid sites on the support surface, but led to a replacement by other acidic sites (Atia et al., 2008; Chino & Okubo, 2005). The total acidity of the supported SiW catalysts increased with SiW loading.

Table 5.4 Textural properties and surface chemistry of SiW/HZSM-5 catalysts in the presence of different SiW loading.

SiW loading (wt.%)	Textural properties			Surface chemistry	
	BET surface area (m ² /g)	Pore volume (cm ³ /g)	Average pore diameter (Å)	Acid amount (mmol NH ₃ /g Cat.)	Total acidity (mmol NH ₃ /g Cat.)
0	289.4 ^a	0.173	4.32	0.71 (81-349 °C) 0.25 (362-640 °C)	0.97
20	250.2	0.164	2.62	0.87 (39-298 °C) 0.15 (542-633 °C)	1.02
30	233.4	0.153	2.62	0.92 (44-236 °C) 0.41 (542-656 °C)	1.33
40	199.13	0.135	2.72	0.90 (25-295 °C) 0.45 (530-662 °C)	1.35
50	157.25	0.110	2.80	0.89 (30-297 °C) 0.65 (527-719 °C)	1.54
60	146.41	0.102	2.79	1.83 (30-389 °C) 0.92 (515-711 °C)	2.75

^a Properties of HZSM-5 support

With regard to the effect of SiW loading on the activity of SiW/HZSM-5 catalysts for the conversion of glycerol, the similar trends of glycerol conversion and product yield along the reaction time were observed as the effect of supports as shown in Figure 5.6-5.7. It shows the glycerol conversion and desired product yields as a function of time over SiW/HZSM-5 catalysts with different SiW loading in the range of 0-60 wt.% in the presence of 2.74 mol/L H₂O₂ at 4 wt.% catalyst loading, at 90 °C and ambient pressure. Glycerol conversion increased considerably during the early period of reaction time and leveled off at reaction times longer than 120 min. The yields of acetic acid, glycolic acid and formic acid increased slightly with increasing

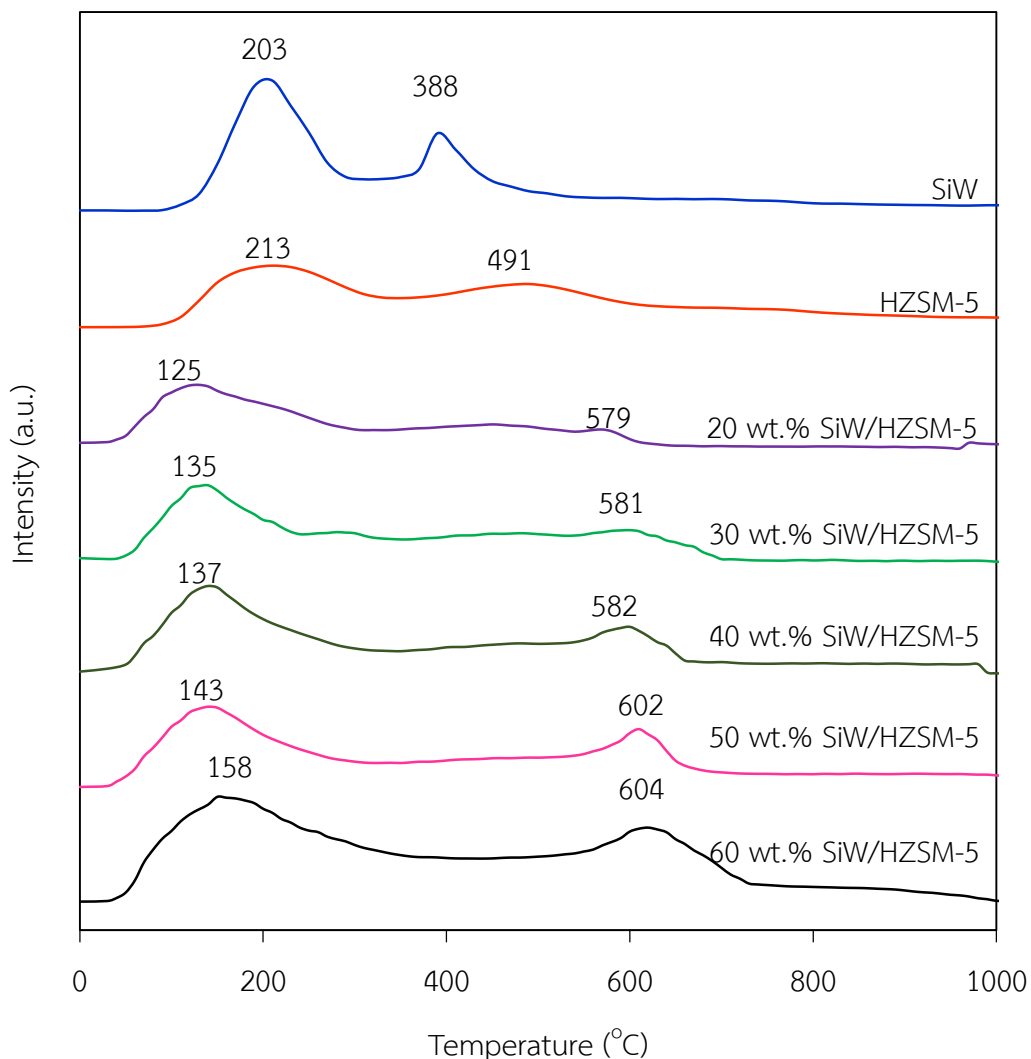


Figure 5.5 NH_3 -TPD profiles of unsupported SiW, HZSM-5 and SiW/HZSM-5 catalysts with different SiW loadings.

reaction time. A high yield of acrolein was obtained during the first 30-120 min and then decreased considerably due to the oxidation to acrylic acid. Table 5.5 summarizes the glycerol conversion as well as yield of various products from glycerol conversion of reaction time at 240 min of reaction time in the presence of different SiW loadings on SiW/HZSM-5 catalysts. The presence of 20% SiW loading can enhance the conversion of glycerol from 74.06% to 87.02%, or around 1.17-fold, and can reduce the transformation of glycerol to undesired products from 63.02% to less

than 26.85%, compared that in the absence of SiW. In addition, it can facilitate a larger generation of glycolic acid, formic acid, acetic acid, acrolein and acrylic acid by 2.69, 2.32, 3.12, 0.39 and 3.19-fold, respectively. The presence of 30 % SiW/HZSM-5 catalyst provided slightly lower glycerol conversion (85.54%) compared with that at 20% SiW loading (87.02%). However, it provided a higher yield of glycolic acid, formic acid, acetic acid, acrolein and acrylic acid of around 1.23, 1.05, 1.05, 1.33 and 1.16-fold, respectively. In addition, it can reduce the glycerol conversion to unwanted species from 26.85% to 16.02%. Further raising the SiW loading to greater than 30% resulted in the decrease of either glycerol conversion or yield of desired products. In addition, it increased the conversion of glycerol to undesired species, as monitored by the decreasing carbon selectivity. This is because the catalysts with too much acidity facilitated the conversion of glycerol to unwanted compounds, which can be observed explicitly by a low carbon selectivity at 60 wt.% SiW loading. Besides, the presence of high SiW loading can block the pores and lowered the available surface area as demonstrated in Table 5.4, leading to a decline in the activity of the catalyst. A similar result was also reported by the dehydration of glycerol to acrolein over activated carbon-supported SiW catalysts (Lili et al., 2008).

Table 5.5 Effect of SiW loading on the performance of glycerol conversion over SiW/HZSM-5 catalysts with different SiW loadings at reaction temperature of 90 °C at 240 min.

SiW loading (wt.%)	Conversion (%)	Yield (%)				Carbon selectivity (%)
		Glycolic acid	Formic acid	Acetic acid	Acrolein Acrylic acid	
0 ^a	74.06±0.24	5.12±0.02	3.93±0.01	5.94±0.02	13.76±0.13	36.98±0.55
20	87.02±0.17	13.79±0.30	9.14±0.16	18.52±0.15	5.41±0.09	73.15±0.73
30	85.54±0.40	16.95±0.47	9.53±0.67	19.51±0.39	7.47±0.22	83.98±0.08
40	73.36±0.28	8.96±0.02	5.39±0.02	13.26±0.03	2.61±0.04	48.54±0.12
50	50.01±0.78	5.72±0.08	3.11±0.24	8.20±0.25	1.41±0.02	30.35±0.27
60	45.91±0.59	3.79±0.01	2.72±0.04	5.22±0.12	0.73±0.05	20.50±0.10

^a Activity of HZSM-5 support

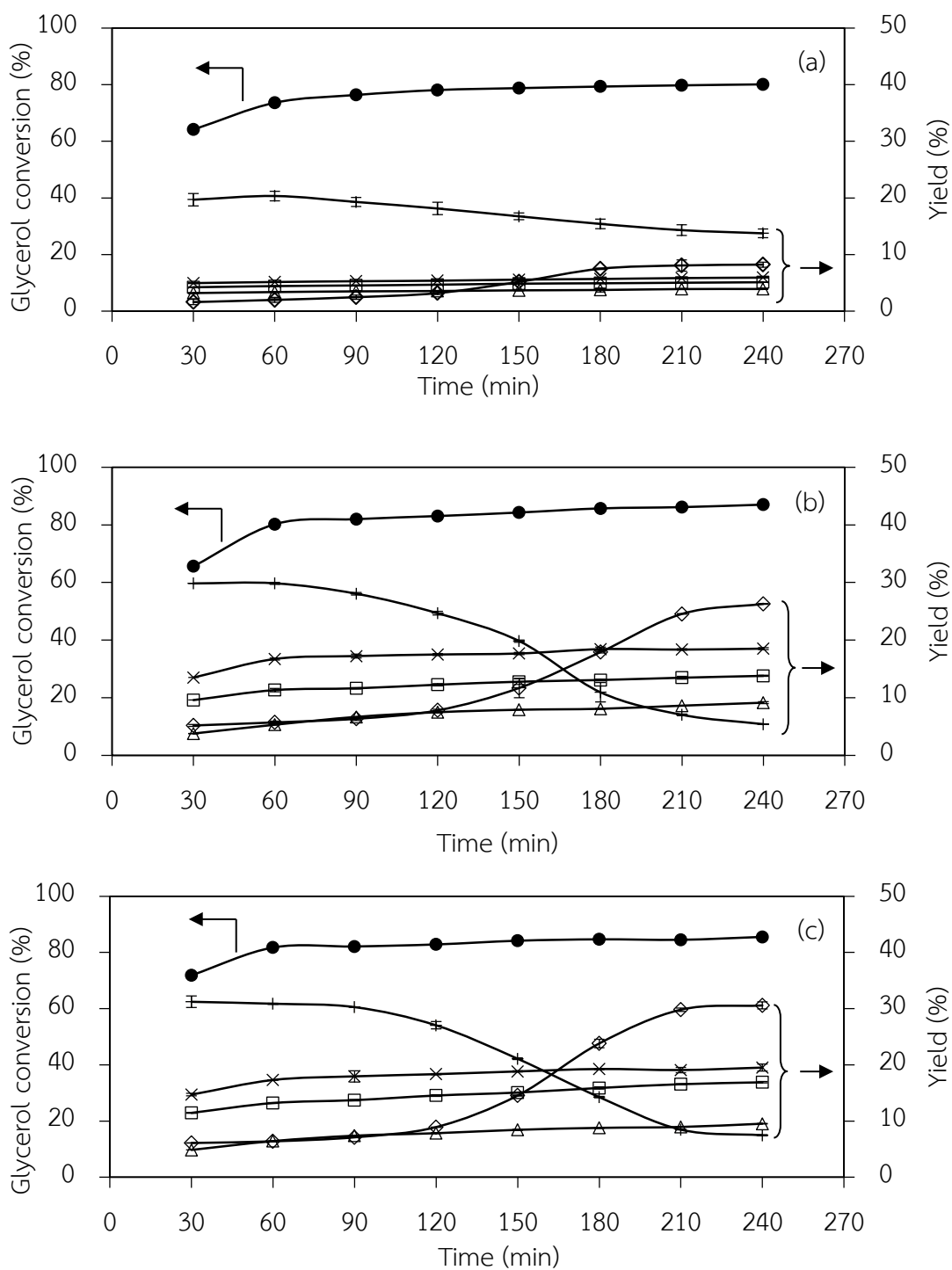


Figure 5.6 Variation of (●) glycerol conversion and yields of (□) glycolic acid, (△) formic acid, (x) acetic acid, (+) acrolein and (◇) acrylic acid as a function of time over (a) HZSM-5, (b) 20, (c) 30, (d) 40, (e) 50 and (f) 60 wt.% SiW/HZSM-5 catalyst.

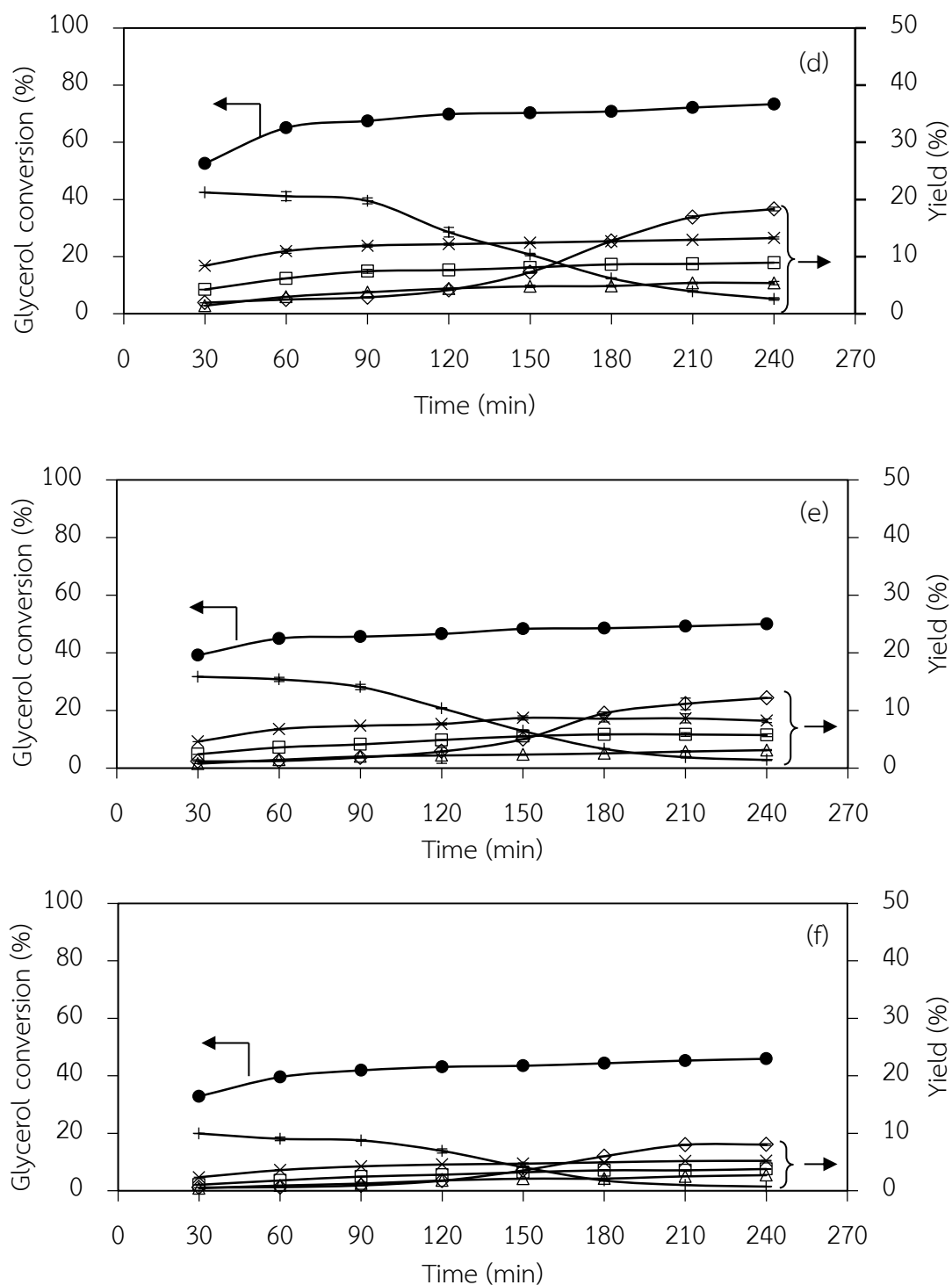


Figure 5.6 (Cont.) Variation of (●) glycerol conversion and yields of (□) glycolic acid, (△) formic acid, (x) acetic acid, (+) acrolein and (◇) acrylic acid as a function of time over (a) HZSM-5, (b) 20, (c) 30, (d) 40, (e) 50 and (f) 60 wt.% SiW/HZSM-5 catalyst.

5.4 Kinetic studies of glycerol conversion

According to results in this part, the 30 wt% SiW/HZSM-5 catalyst showed the highest activity for the conversion of glycerol to acrylic acid. The kinetics study of glycerol conversion was then carried out on the best catalytic activity catalyst, SiW/HZSM-5 catalyst with 30 wt.% SiW loading at different temperatures in the range of 70-90 °C. The kinetic data were obtained using the initial rate method. The data used to determine the kinetics of glycerol conversion was taken from the linear section of glycerol conversion at the conversion less than 40% (Figure 5.7). The glycerol and H₂O₂ concentrations were varied from 1.37-5.50 mol/L and 1.37-6.85 mol/L based on individual volumes, respectively as shown in Table 5.6. As expected, the rate of glycerol conversion increased with increasing reaction temperature.

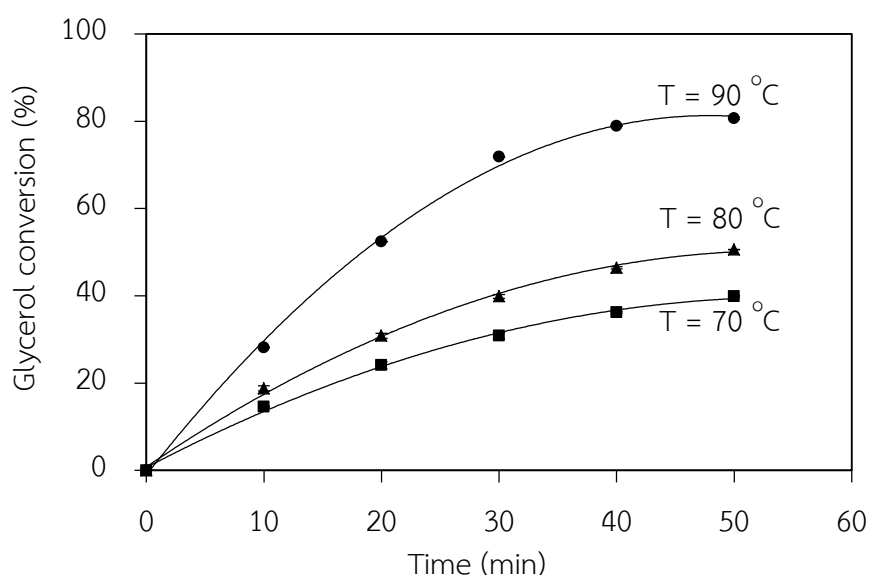


Figure 5.7 Variation of glycerol conversion rate as a function of time at catalyst loading of 4 wt.% in the presence of 2.74 mol/L H₂O₂ with glycerol concentrations of 2.75 mol/L at (■) 70 °C, (▲) 80 °C and (●) 90 °C.

The variation of glycerol conversion rate in the presence of different concentrations of glycerol and H₂O₂ were plotted in Figure 5.8-5.10. It can be seen that the concentration of glycerol affected positively the glycerol conversion rate (Figure 5.8 -5.10), while the concentration of H₂O₂ affected it only very slightly (Figure 5.11-5.13).

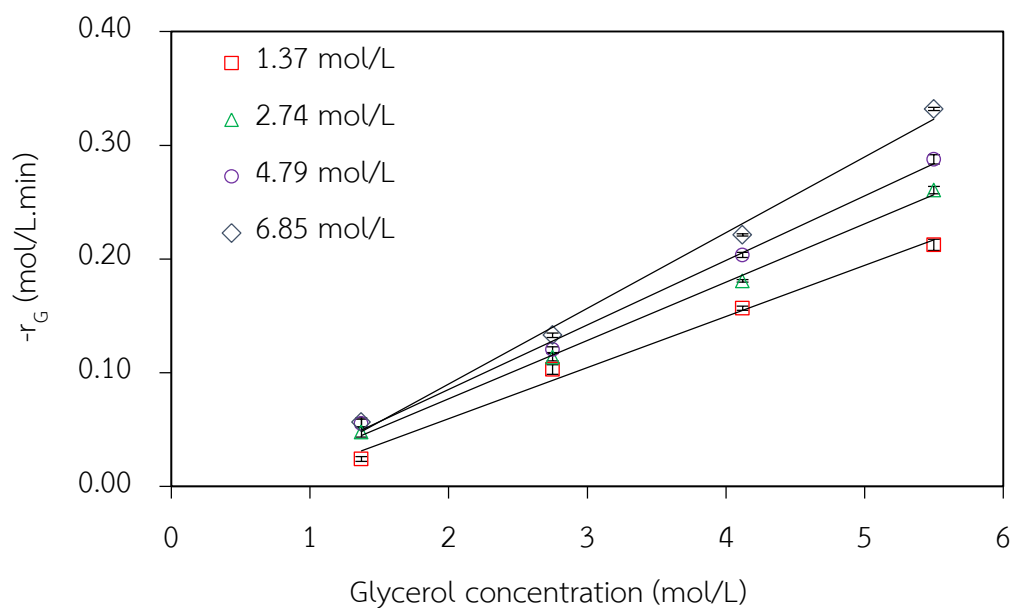


Figure 5.8 Variation of rate of glycerol conversion as a function of glycerol concentrations in the presence of H_2O_2 at 70 °C.

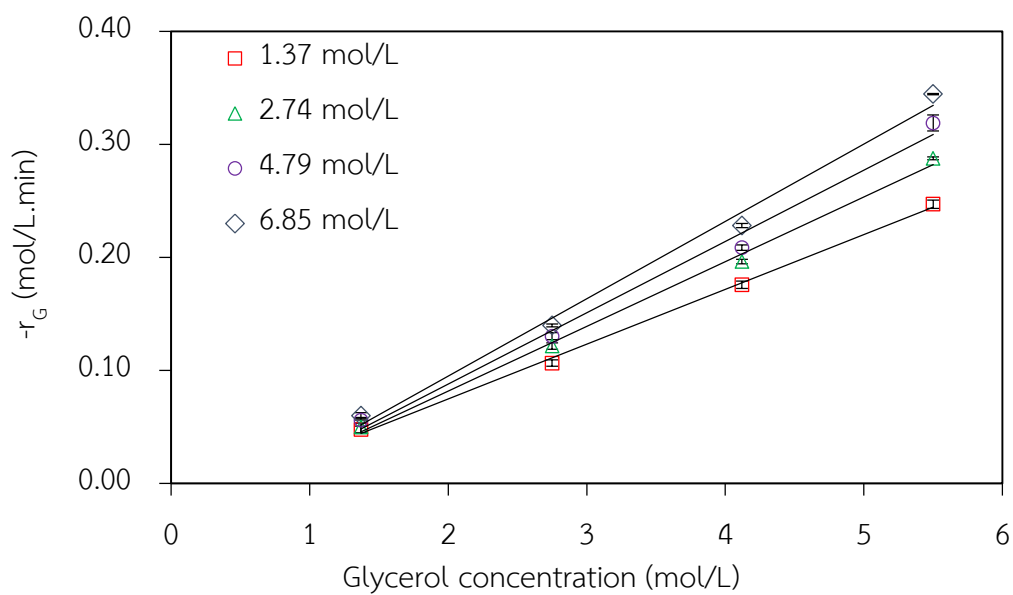


Figure 5.9 Variation of rate of glycerol conversion as a function of glycerol concentrations in the presence of H_2O_2 at 80 °C.

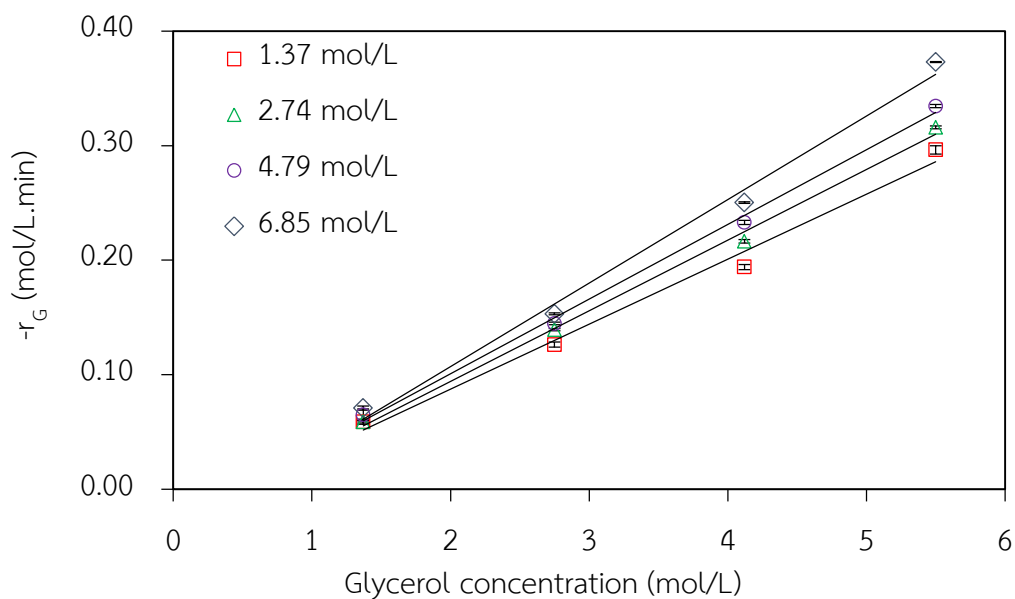


Figure 5.10 Variation of rate of glycerol conversion as a function of glycerol concentrations in the presence of H_2O_2 at $90^\circ C$.

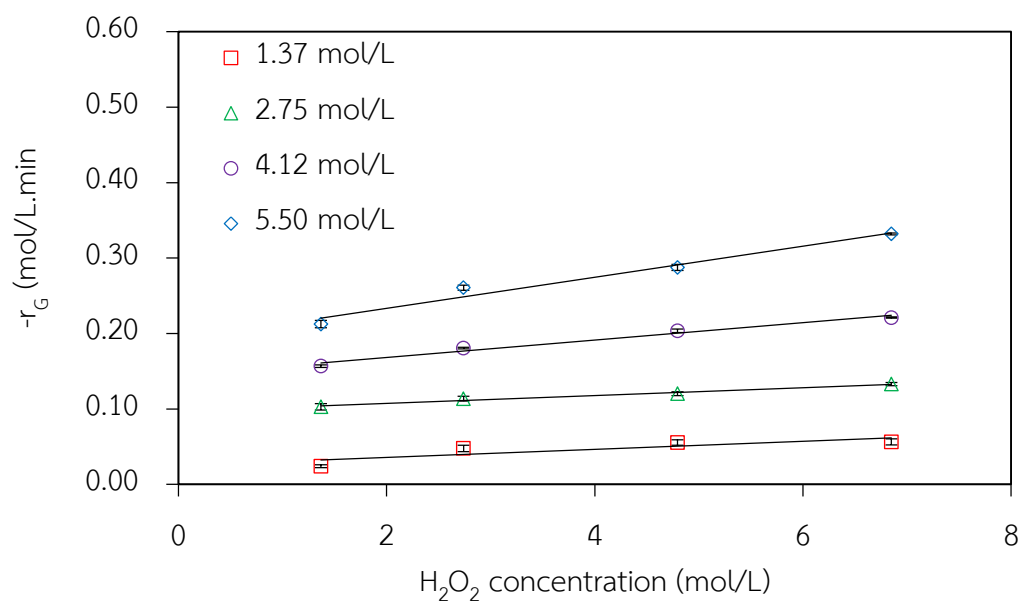


Figure 5.11 Variation of rate of glycerol conversion as a function of H_2O_2 concentrations in the presence of glycerol concentration at $70^\circ C$.

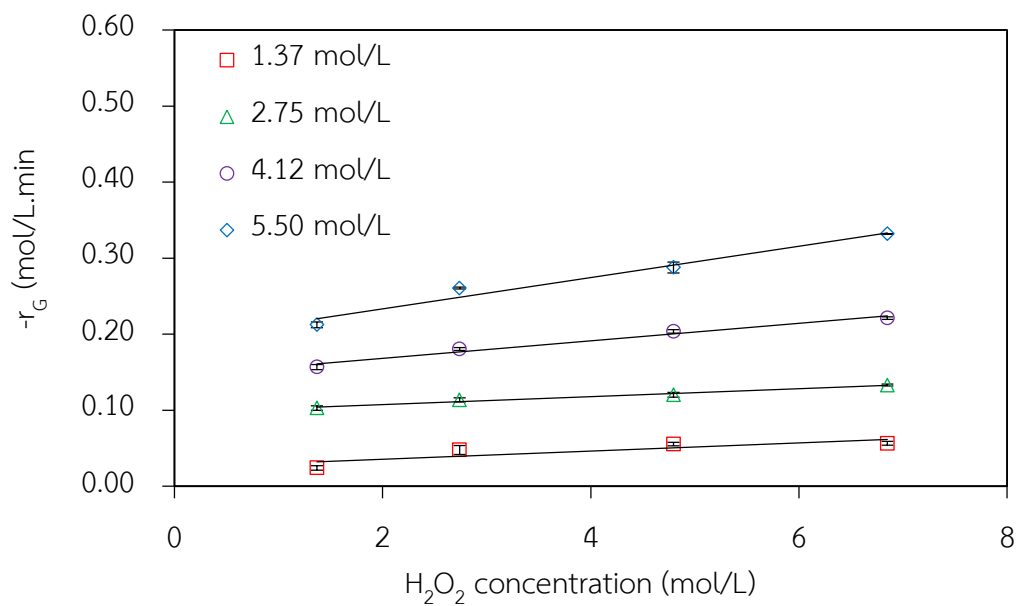


Figure 5.12 Variation of rate of glycerol conversion as a function of H_2O_2 concentrations in the presence of glycerol concentration at 80°C .

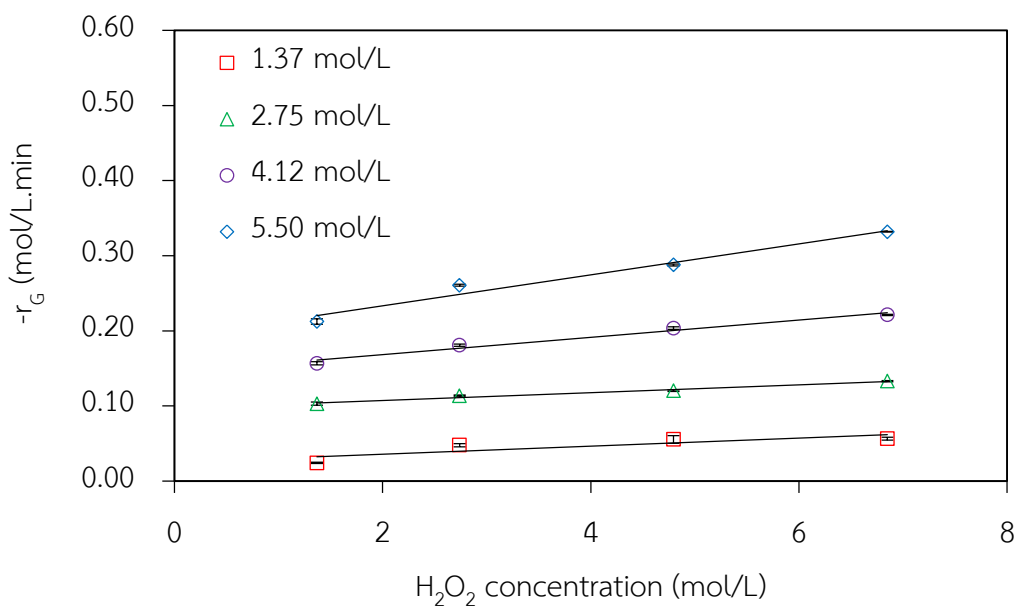


Figure 5.13 Variation of rate of glycerol conversion as a function of H_2O_2 concentrations in the presence of glycerol concentration at 90°C .

The power law model with the rate expression of glycerol conversion as expressed by Eq.(5.1).was used in this study.

$$r_G = -k[G]^a[H_2O_2]^b \quad (5.1)$$

where	r_G	is the rate of glycerol conversion (mol/L.min)
	k	is the rate constant (min^{-1})
	$[G]$	is the glycerol concentration (mol/L)
	$[H_2O_2]$	is the H_2O_2 concentration (mol/L)
	a	is the reaction order of glycerol concentrations
	b	is the reaction order of H_2O_2 concentrations

The linearized form of Eq.(5.1) can be written as:

$$\ln(-r_G) = \ln(k) + a\ln([G]) + b\ln([H_2O_2]) \quad (5.2)$$

Fitting the experimental results, the reaction orders of glycerol (a) and H_2O_2 (b) were listed in Table 5.6. The reaction orders of glycerol (a) and H_2O_2 (b) were 1.2 (ca.1) and 0.2 (ca.0), respectively. This suggests that the rate of glycerol conversion can be explained by a pseudo-first order reaction with respect to glycerol concentration.

Table 5.6 Estimated parameters of the rate expression of glycerol conversion by power law model.

Temperature (°C)	Order of glycerol (a)	Order of H_2O_2 (b)	Rate constant, $k \times 10^{-2}$ (min^{-1})	R^2
70	1.31	0.29	2.09	0.9898
80	1.23	0.17	2.94	0.9811
90	1.18	0.13	3.70	0.9952
Average	1.24 ± 0.07	0.19 ± 0.08		

Figure 5.14 shows the comparison rate of glycerol conversion obtained from the experiments and the power law model. It is worth noting that a good relation between the experimental results and the power law model was observed with $R^2 \geq 0.99$. This demonstrates that the parameters a and b determined from the power

law model were appropriated to predict the rate of glycerol conversion over SiW/HZSM-5 catalyst.

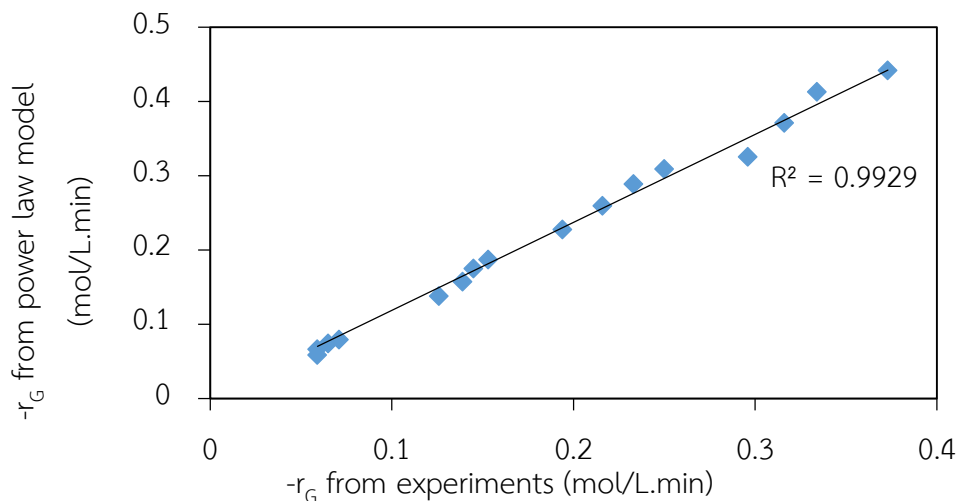


Figure 5.14 The rate of glycerol conversion from the experiments compared with the rate of glycerol conversion from power law model at 90 °C.

According to the Arrhenius's equation, the plot of kinetic rate versus temperature (Figure 5.15) provides the apparent activation energy of 29.58 kJ/mol, which is close to the activation energy reported for the glycerol oxidation over supported gold catalyst at particular oxygen pressures up to 10 bar and at temperatures from 25 °C to 100 °C (Bordoloi, Vinu, & Halligudi, 2007).

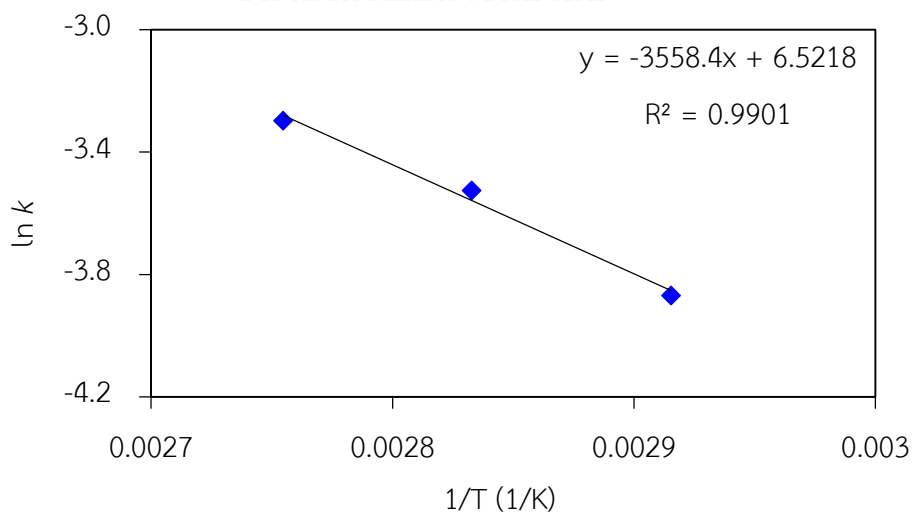


Figure 5.15 Arrhenius plot of k constants for liquid phase conversion of glycerol over SiW/HZSM-5 catalyst with 30 wt.% SiW loading

CHAPTER VI

CONVERSION OF GLYCEROL TO ACRYLIC ACID VIA METAL-DOPED SiW/HZSM-5 CATALYSTS

In the previous chapter, we report that various higher market value products were generated in the liquid phase conversion of glycerol via the best supported POM catalysts at low temperature, such as glycolic acid, formic acid, acetic acid, acrolein and acrylic acid. The highest glycerol conversion (85.54%) and acrylic acid yield (30.57%) was obtained with 30 wt.% HZSM-5-supported SiW (SiW/HZSM-5) catalyst at 4 wt.% catalyst loading in the presence of 2.74 mol/L H₂O₂ at reaction temperature of 90 °C and ambient pressure. In the current chapter, we continue our work by doping transition metal on the 30 wt.% SiW/HZSM-5 catalyst, in order to achieve a higher glycerol conversion and product yield. The influences of transition metal types and transition metal loadings were investigated. The kinetic of the best metal-doped SiW/HZSM-5 catalysts for the conversion of glycerol under optimal condition was examined.

6.1 Effect of transition metal types

Four types of transition metal including Ce, Co, Ni and V were doped on SiW/HZSM-5 catalyst at 4 wt.% metal loading. Textural properties for doped metals immobilized on SiW/HZSM-5 catalysts derived from N₂ physisorption isotherms are summarized in Table 6.1. The BET surface area of HZSM-5 was 289.4 m²/g. When transition metals were doped on the SiW/HZSM-5 catalyst, the surface areas of Ce-SiW/HZSM-5, Co-SiW/HZSM-5, Ni-SiW/HZSM-5 and V-SiW/HZSM-5 catalysts decreased to 209.0 m²/g, 206.2 m²/g, 209.1 m²/g and 225.1 m²/g, respectively. The pore volume of all metal-doped SiW/HZSM-5 catalysts decreased while the average pore diameter of those slightly increased compared to the original SiW/HZSM-5 catalyst. The decrease in BET surface area and pore volume might be attributed to the support pores blocking by the doped metals. This is because the pores of HZSM-5 are 4.32 Å and the Keggin unit diameter is 12 Å (Popa et al., 2005).

Table 6.1 Textural properties of HZSM-5, 30 wt.% SiW/HZSM-5 and metals-doped SiW/HZSM-5 catalysts with 4 wt.% metals doping.

Catalysts	BET surface area (m ² /g)	Pore volume (cm ³ /g)	Average pore diameter (Å)
HZSM-5	289.4	0.173	4.32
SiW/HZSM-5	233.4	0.153	2.62
Ce-SiW/HZSM-5	209.0	0.146	2.79
Co-SiW/HZSM-5	206.2	0.143	2.84
Ni-SiW/HZSM-5	209.1	0.150	2.76
V-SiW/HZSM-5	225.1	0.138	2.65

Figure 6.1 shows the XRD patterns of the metal-doped SiW/HZSM-5 catalysts. That of the SiW/HZSM-5 catalyst exhibits the main characteristic peaks of HZSM-5 at 2θ of 7.8° , 8.7° , 23.1° , 23.3° , 23.6° , 23.8° and 24.3° (JCPDS 00-049-0657) and also the peaks at 2θ of 27.3° , assigned to the SiW hexahydrate (Popa et al., 2005). In the presence of transition metals, the main characteristic peaks of SiW/HZSM-5 catalyst were still observed. The characteristic peaks of doped metals appeared unclear. To confirm the existence of metals in the structure of metal-doped SiW/HZSM-5 catalysts, the EDX analysis was then carried out as demonstrated in Figure 6.2. Quantitatively, the contents of Ce, Co, Ni and V on the SiW/HZSM-5 catalyst were 3.63 wt.%, 3.60 wt.%, 3.45 wt.% and 3.58 wt.%, respectively, which were close to the set quantity of each transition metals (4 wt.%).

To confirm the presence of the SiW in the Keggin anions on the HZSM-5 surface, FT-IR spectra were recorded (Figure 6.3). The blank HZSM-5 displayed the most prominent band in the region of $400\text{-}1,600\text{ cm}^{-1}$, attributed to the stretching and bending modes of the T-O units of the zeolite lattice (T: tetrahedral Si or Al; this band is often called the 'main band') (Barros et al., 2008; Provis & Van Deventer, 2009). The bands at 451 cm^{-1} , 548 cm^{-1} , 797 cm^{-1} , $1,103\text{ cm}^{-1}$ and $1,224\text{ cm}^{-1}$ are

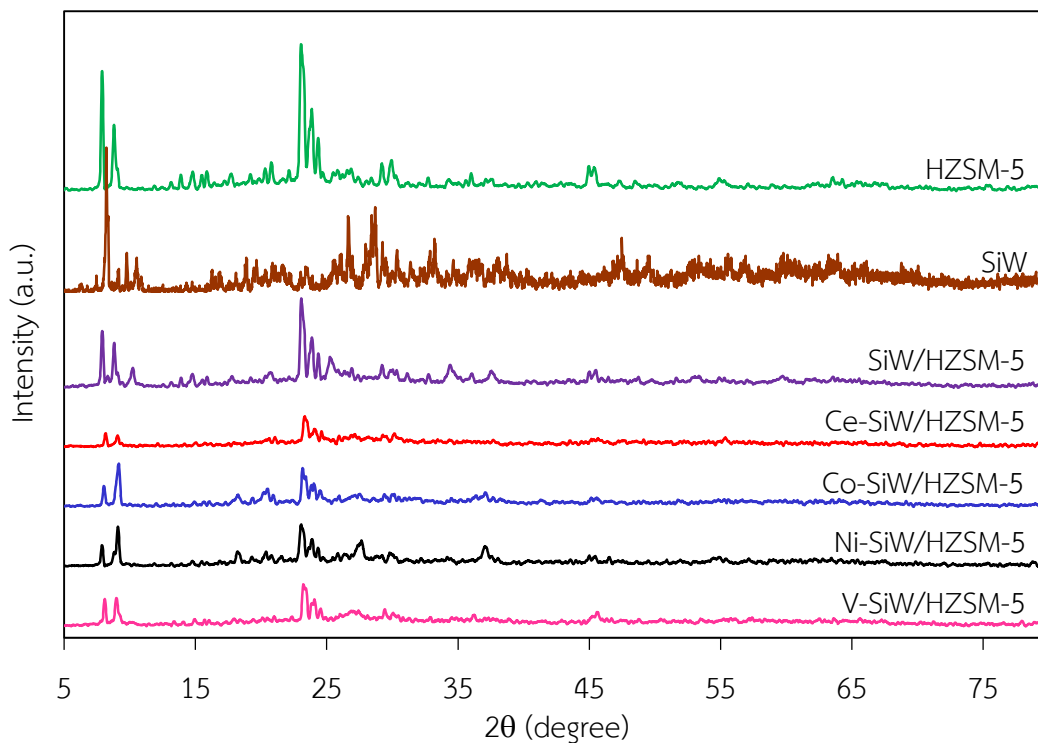


Figure 6.1 XRD patterns of HZSM-5, SiW, 30 wt.% SiW/HZSM-5 and metals-doped SiW/HZSM-5 catalysts with 4 wt.% metals doping.

assigned to different vibrations of tetrahedral and framework atoms in HZSM-5 (Othman, 2007). The strongest absorption peak at $1,103\text{ cm}^{-1}$ of HZSM-5 was assigned to internal asymmetric stretching of Si–O–T bonds (Barros et al., 2008). A band at about 797 cm^{-1} is related to symmetric stretching of external bonds between tetrahedral and, at 548 cm^{-1} , and is a vibration sensitive to the zeolite morphology, caused by external bonds of double five member rings. At last, vibrations of internal bonds (O–T–O) of SiO_4 and AlO_4 tetrahedral are located around 451 cm^{-1} (Ali, Brisdon, & Thomas, 2003; Lercher & Jentys, 2007). The typical infrared adsorption peaks of the pure SiW, the parent $[\text{SiW}_{12}\text{O}_{40}]^{4-}$ Keggin structure displayed the characteristic bands due to W–O–W vibrations of edge- and corner-sharing WO_6 octahedral linked to the central SiO_4 tetrahedral (Deltcheff et al., 1983; Stangar, Groselj, Orel, & Colombar, 2000). As demonstrated in (Figure 6.3), the stretching

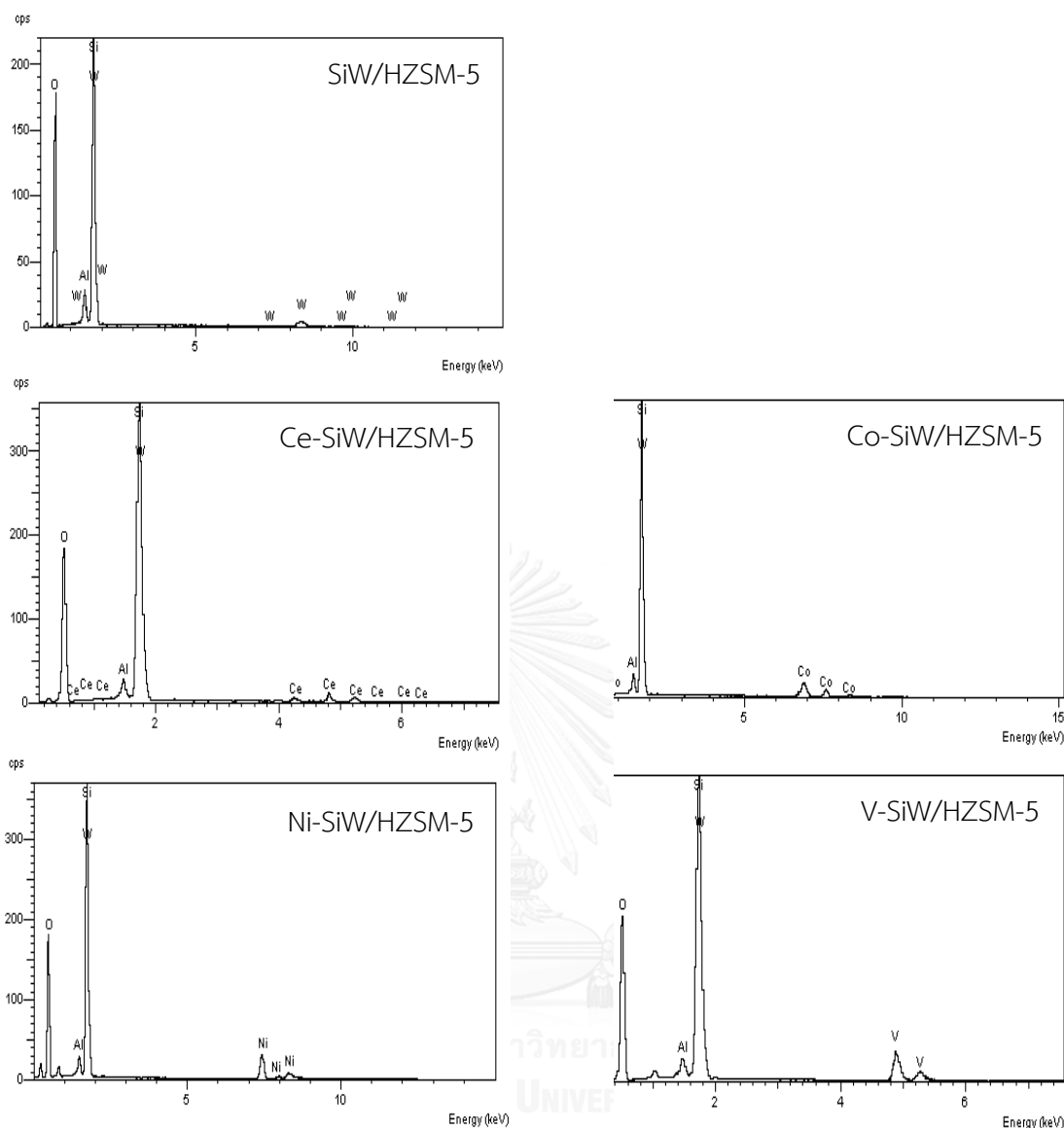


Figure 6.2 EDX analysis of 30 wt.% SiW/HZSM-5 and metal-doped SiW/HZSM-5 catalysts at constant metal loading of 4 wt.%.

modes of edge-sharing ($W-O_e-W$) and center-sharing ($W-O_c-W$) units emerged as shoulders at 797 cm^{-1} and 897 cm^{-1} , respectively, whereas the Si-O stretching modes appeared at 937 cm^{-1} and 990 cm^{-1} . The peaks in the ranges of $3,500-1,400\text{ cm}^{-1}$ have been observed in all the studied catalysts, indicating the presence of water in the SiW structure. The broad absorption band at $3,450\text{ cm}^{-1}$ was attributed to the hydroxyl groups (O-H) vibration and the band at ca. $1,645\text{ cm}^{-1}$ was assigned to the bonding vibration mode of the inter-layer water molecules (Chen, Li, & Li, 2008). The

band at $1,423\text{ cm}^{-1}$ was related to the overtone of the O–H stretching mode (Vafaeian, Haghghi, & Aghamohammadi, 2013). For SiW/HZSM-5 catalyst with 30 wt.% SiW loading, besides the main characteristic peaks of HZSM-5 and SiW, additional peaks were observed.

The FT-IR spectra of all metals-doped SiW/HZSM-5 catalysts showed adsorption peaks ranging from 700 to $1,000\text{ cm}^{-1}$, which were assigned to SiW anions of Keggin structure. The typical infrared adsorption peaks of all metals-doped SiW/HZSM-5 catalysts appeared in the range of $1,000$ to $1,250\text{ cm}^{-1}$ were identified to be the characteristic of HZSM-5. According to the obtained FT-IR results, it can be confirmed that the SiW supported on HZSM-5 retained their Keggin structures under our present doping transition metal on SiW/HZSM-5 catalysts. However, the characteristic peaks of those catalysts were weak. It is suggested that the SiW were well dispersed on the HZSM-5 surfaces.

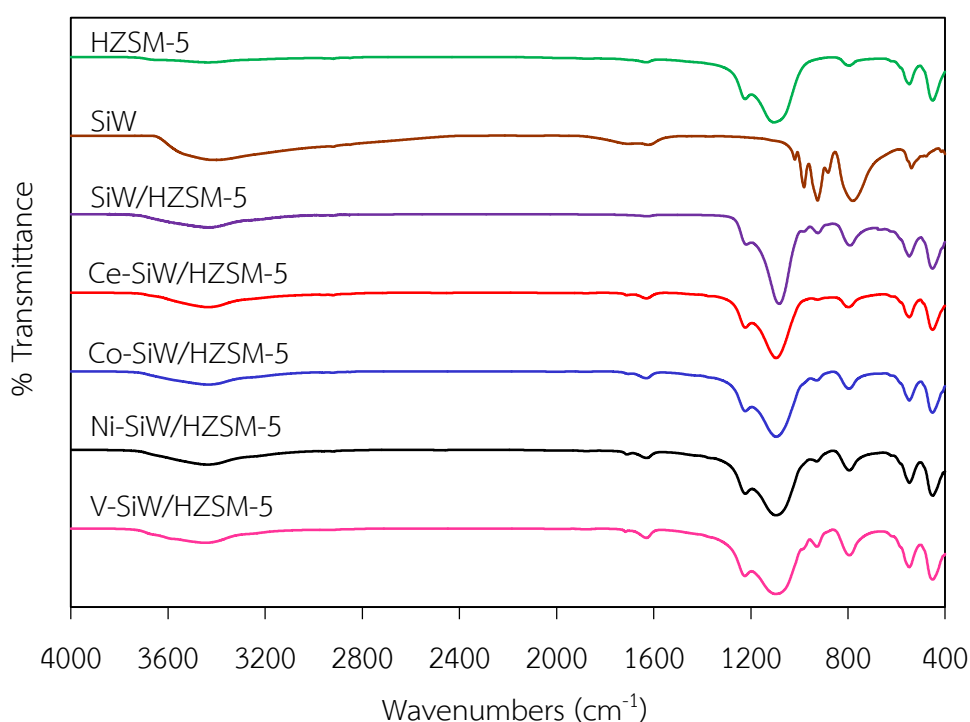


Figure 6.3 FT-IR spectra of HZSM-5, SiW, 30 wt.% SiW/HZSM-5 and metals-doped SiW/HZSM-5 catalysts with 4 wt.% metals doping.

The reducibility of the SiW/HZSM-5 (physical mixing), SiW/HZSM-5 and all metals-doped SiW/HZSM-5 catalysts was determined by H₂-TPR analysis as shown in Figure 6.4. For SiW/HZSM-5 (physical mixing) exhibited two peaks at 619 °C and 790 °C in the H₂-TPR profile. The two peaks corresponded to the reduction of SiW and HZSM-5, respectively. The H₂-TPR profile of SiW/HZSM-5 exhibited at 510 °C, 653 °C and 787 °C, which can be assigned to the interaction between SiW and their support. The H₂-TPR profile of all metals-doped SiW/HZSM-5 catalysts showed the characteristic reduction peaks of SiW, which exhibited that the reduction temperature of SiW slightly changed when doping metal on the SiW/HZSM-5 catalyst. The Ce-SiW/HZSM-5 catalyst had three different reduction peaks at 353 °C, 439 °C and 706 °C. The first reduction peak at 353 °C was attributed to reduction of the surface oxygen stoichiometric Ce (Ce⁴⁺-Ce⁴⁺) (Damyanova, Perez, Schmal, & Bueno, 2002). The second reduction peak at 439 °C was attributed to reduction of the surface oxygen nonstoichiometric Ce (Ce³⁺-Ce⁴⁺) (Murugan & Ramaswamy, 2008), and the peak in the high region at 703 °C was attributed to reduction of bulk oxygen (Otsuka, Wang, & Nakamura, 1999; Fornasiero et al., 1996; Luo & Zheng, 1999). The Co-SiW/HZSM-5 catalyst had two typical steps during the reduction temperature peak, i.e. Co₃O₄ to CoO at the reduction of 290 °C and then CoO to Co at the reduction of 380 °C (Kang et al., 2011). In this work, the reduction peaks of Co-SiW/HZSM-5 catalyst at 281 °C and 387 °C were observed. More interestingly, the first reduction step of Co₃O₄ to CoO clearly shifts to the lower temperature of 281 °C, which facilitates its reducibility. Moreover, it has been widely demonstrated that the interaction of cobalt oxide and its original SiW/HZSM-5 catalyst (Wang, Yin, Guo, Ru, & Zhu, 2013). The incorporation of Ni in the SiW/HZSM-5 catalyst structure exhibited two peaks. The first reduction peak at 317 °C corresponded to the reduction of NiO species, which had weak interaction with original SiW/HZSM-5 catalyst and the second reduction peak at 397 °C corresponded to the reduction of NiO species, which had strong interaction with original SiW/HZSM-5 catalyst (Jin et al., 2010; Fang, Ren, & Sun, 2005). For V-SiW/HZSM-5 catalyst, the first reduction peak was attributed at 322 °C this reduction temperature is lower than that obtained for SiW/HZSM-5

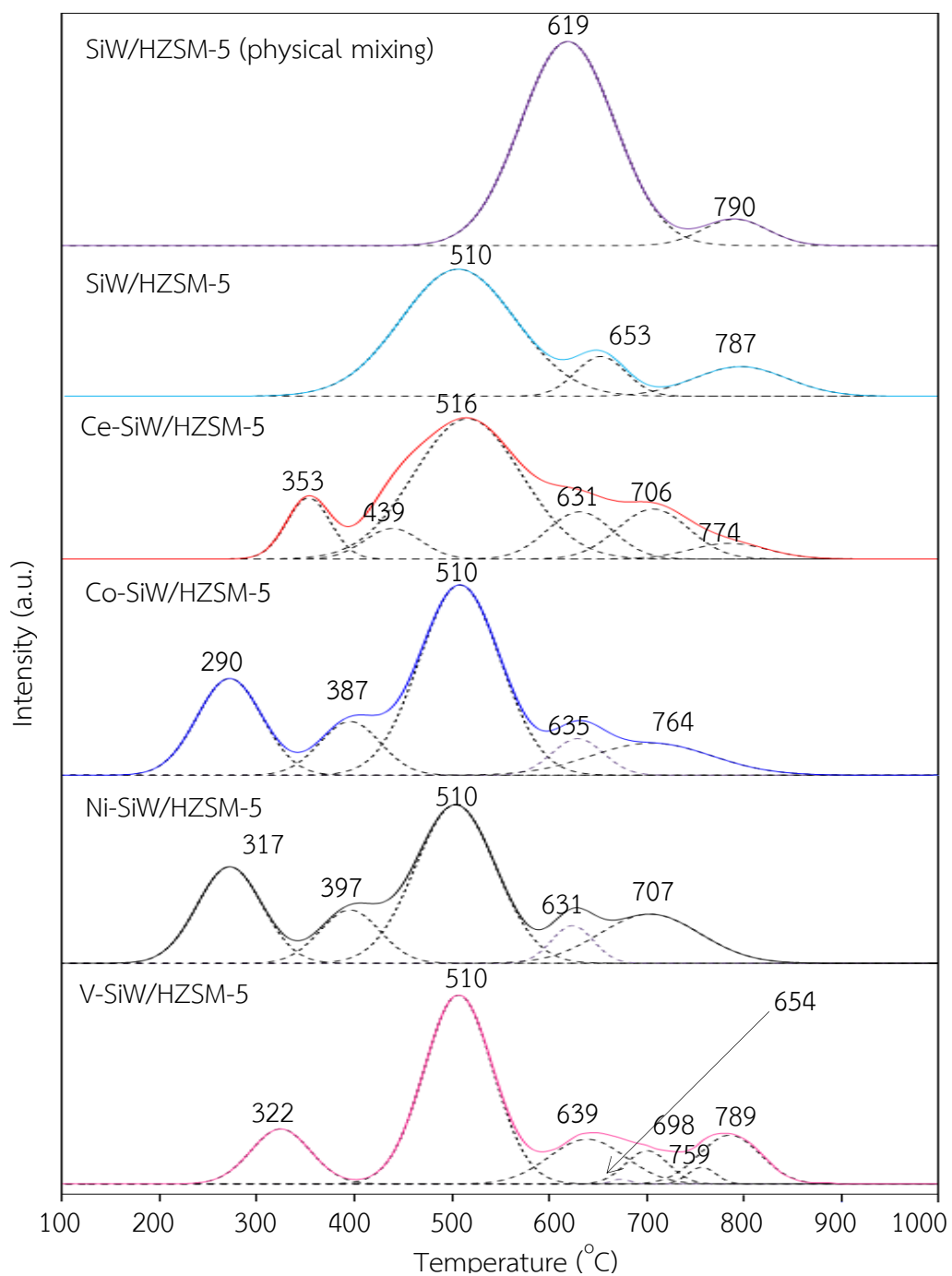


Figure 6.4 H₂-TPR profiles for utilized 30 wt.% SiW/HZSM-5 and metal-doped SiW/HZSM-5 catalysts with 4 wt.% metal doping.

catalyst (Lee, Kim, & Hong, 2012). It is likely to be a V–O–W interaction when the V species are covered with SiW/HZSM-5 catalyst surface. The general the H₂-TPR profile of bulk V₂O₅ exhibited the reduction peak at 655 °C, 686 °C and 807 °C (Koranne, Goodwin, & Marcelin, 1994; Pieck, de Val, Granados, Banares, & Fierro, 2002). In this work the observed reduction peaks shift towards high temperature at 654 °C, 698 °C and 805 °C indicated the formation of V₂O₅ crystals (Bineesh, Kim, Jermy, & Park, 2009). However, the temperature of maximum reduction peaks at 789 °C were lower for V-SiW/HZSM-5 catalyst than that of bulk V₂O₅, indicating a significant interaction of crystalline V₂O₅ phase with the support (Klose et al., 2007). The interaction between V and SiW/HZSM-5 originates catalysts from the stabilization of V cations in the original catalyst surface due to the remarkably close atomic radius ratio (V:W = 134 pm: 135 pm). However, V doping could improve the mobility of oxygen in original SiW/HZSM-5 catalyst surface (Lee & Hong, 2015).

The surface acidity of the HZSM-5, SiW, SiW/HZSM-5 catalyst and all metals-doped SiW/HZSM-5 catalysts was determined by NH₃-TPD analysis as shown in Figure 6.5. For SiW/HZSM-5 catalyst, two broad NH₃-TPD peaks appearing at the temperature of 161 °C and 522 °C indicated the presence of weak- and strong-strength acid sites. In the presence of transition metals, the incorporation of Ce did not change the type of acid strength on the surface of SiW/HZSM-5 catalyst. It still had the weak- and strong-strength acid sites, exhibited at 152 °C and 496 °C. However, the introduction of Co, Ni and V changed the types of acid strength significantly. Two broad NH₃-TPD peaks were observed at the temperature of 135 °C and 258 °C for Co-SiW/HZSM-5, indicating the presence of only weak-strength acid sites in their structures. In case of Ni-SiW/HZSM-5 and V-SiW/HZSM-5 catalysts, peaks appearing at 209, 349, 688 °C and 153, 285, 672 °C were observed in their TPD profiles, denoting the presence of weak-, medium- and strong-strength acid sites on their structures. Quantitatively, the amount of acid sites of all metal-doped SiW/HZSM-5 catalysts calculated from the NH₃-TPD desorption peak are summarized in Table 6.2. The incorporation of Co and Ce in the SiW/HZSM-5 catalyst structure led to decreasing total acidity, while the incorporation of Ni and V led to increasing total acidity. This is because the incorporation of V led to a remarkable high surface

area compared to others metal-doped SiW/HZSM-5 catalysts (Atia et al., 2008). However, it could be concluded that the number of acid sites depended not only on their relatively higher catalyst surface but also on the oxidation state number of the surface cation of metal-doped SiW/HZSM-5 catalysts (Chiericato et al., 2014). To confirm the existence of the metal oxide on the surface catalysts, the typical XRF analysis of compound was identified to be the stable form of metal oxide. It was found that the CeO_2 , CoO , NiO and V_2O_5 were observed in all metal-doped SiW/HZSM-5 catalysts. In the presence of V_2O_5 on the surface catalyst, the oxidation state number of V_2O_5 was V^{5+} . It is suggested that V^{5+} as high oxidation state number led to increase the electron acceptor. The increase of electron acceptor might be attributed to the increase acidity of the catalysts. The total acidity of the transition metal-doped SiW/HZSM-5 catalysts was in an order of $\text{V} > \text{Ni} > \text{Ce} > \text{Co}$.

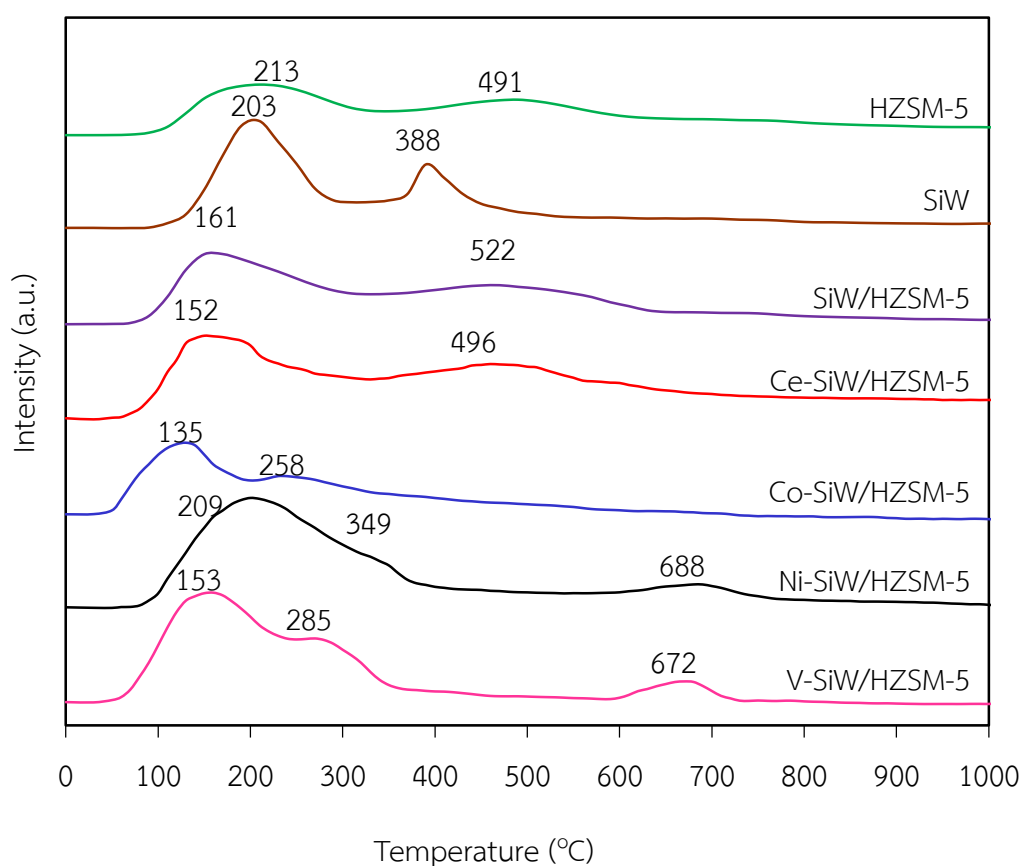


Figure 6.5 NH_3 -TPD profiles for utilized HZSM-5, SiW, 30 wt.% SiW/HZSM-5 and metals-doped SiW/HZSM-5 catalysts with 4 wt.% metals doping.

Table 6.2 NH₃-TPD results for HZSM-5, SiW, 30 wt.% SiW/HZSM-5 and metals-doped SiW/HZSM-5 catalysts with 4 wt.% metals doping.

Catalysts	NH ₃ -TPD peak position (°C)	Acid amount (mmol NH ₃ /g Cat.)	Total acidity (mmol NH ₃ /g Cat.)
HZSM-5	213	0.71 (81-349 °C)	0.96
	491	0.25 (362-640 °C)	
SiW	203	2.88 (108-303 °C)	3.81
	388	0.93 (351-439 °C)	
SiW/HZSM-5	161	0.88 (46-342 °C)	1.31
	522	0.43 (355-669 °C)	
Ce-SiW/HZSM-5	152	0.86 (55-372 °C)	1.27
	496	0.41 (378-631 °C)	
Co-SiW/HZSM-5	135	0.74 (41-200 °C)	1.05
	258	0.31 (202-343 °C)	
Ni-SiW/HZSM-5	209	1.24 (62-447 °C)	1.83
	349	0.29 (302-396 °C)	
	688	0.31 (562-798 °C)	
V-SiW/HZSM-5	153	1.17 (42-239 °C)	2.12
	285	0.53 (239-401 °C)	
	672	0.42 (591-738 °C)	

The oxidative ability of all investigated SiW/HZSM-5 catalysts was also traced by using the O₂-TPD method. As shown in Figure 6.6, types of doped metals played more important role on oxidative ability of such catalysts. Quantitatively, as summarized in Table 6.3, the total O₂ desorption of the metals-doped SiW/HZSM-5 catalysts was in an order of V > Ni > Ce > Co, suggesting that the V-SiW/HZSM-5

catalyst exhibited the highest oxidative ability compared with other metal-doped SiW/HZSM-5 catalysts. This is probably due to the effect of the oxidizing states of doped metal on the catalyst surface. As compared to the original SiW/HZSM-5 catalysts, the doping metals on SiW/HZSM-5 catalysts, the changes in oxidation states of surface cations over metal-doped SiW/HZSM-5 catalysts were occurred. For V-SiW/HZSM-5 catalysts was high oxidation state number (V_2O_5 , V^{5+}) existed on metal oxide catalyst surfaces gave high catalytic oxidation activity for the oxidation of resultant acrylic acid (Shen et al., 2014). According to the obtained H_2 -TPR results, it can be confirmed that the reduction with bulk oxygen of V-SiW/HZSM-5 catalyst surface was attributed to the formation of V_2O_5 crystals (Bineesh et al., 2009). It is well-known that the introduction V in the SiW/HZSM-5 catalyst structure greatly enhanced the oxygen mobility, which was beneficial to the conversion of glycerol to acid products (Lee & Hong, 2015).

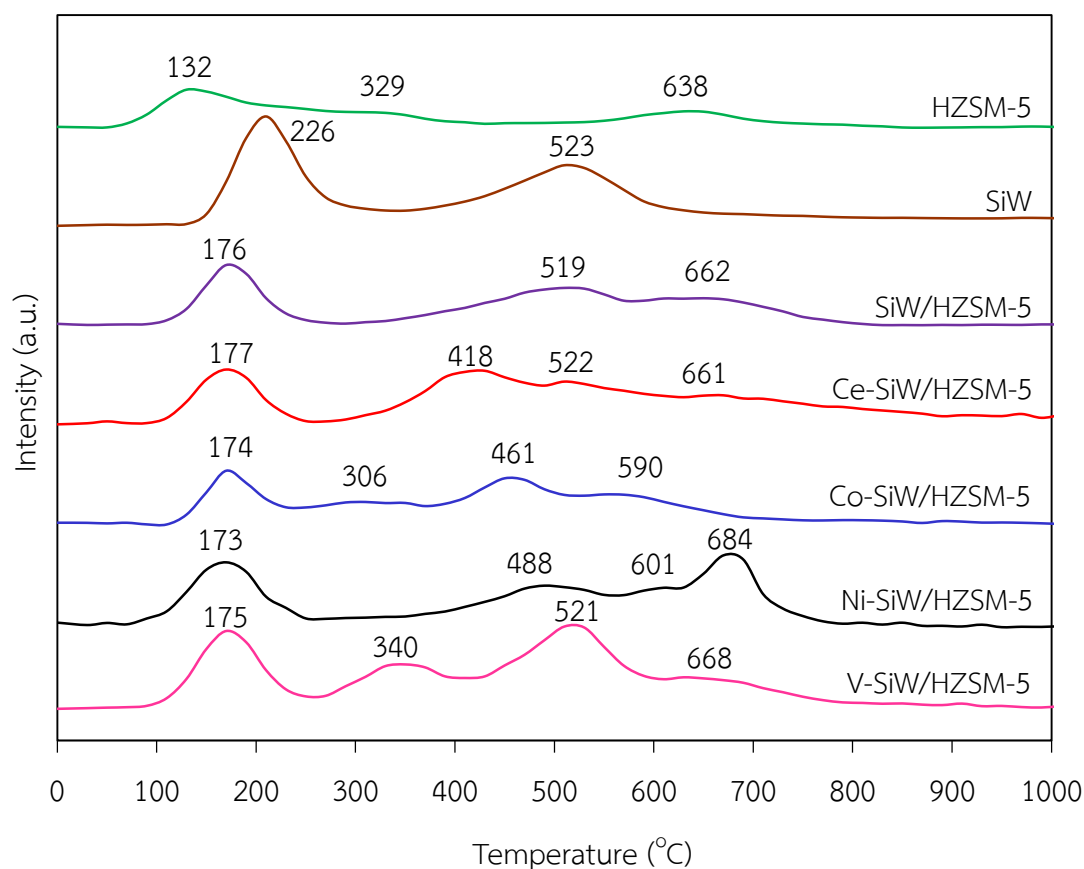


Figure 6.6 O_2 -TPD profiles for utilized HZSM-5, SiW, 30 wt.% SiW/HZSM-5 and metals-doped SiW/HZSM-5 catalysts with 4 wt.% metals doping.

Table 6.3 O₂-TPD results of 30 wt.% SiW/HZSM-5 and metals-doped SiW/HZSM-5 catalysts with 4 wt.% metals doping

Types of catalyst	O ₂ -TPD peak position (°C)	O ₂ desorption (mmol O ₂ /g Cat.)	Total O ₂ desorption (mmol O ₂ /g Cat.)
SiW/HZSM-5	179	0.062 (95-273°C)	0.155
	519	0.058 (317-581 °C)	
	662	0.035 (581-762 °C)	
Ce-SiW/HZSM-5	177	0.065 (94-259°C)	0.146
	418	0.055 (282-493°C)	
	522	0.018 (495-638°C)	
	661	0.008 (638-745°C)	
Co-SiW/HZSM-5	174	0.057 (99-240°C)	0.126
	306	0.010 (240-367°C)	
	461	0.044 (381-516°C)	
	590	0.015 (519-694°C)	
Ni-SiW/HZSM-5	173	0.087 (72-261°C)	0.235
	488	0.052 (365-564°C)	
	601	0.017 (561-630°C)	
	684	0.079 (623-778°C)	
V-SiW/HZSM-5	175	0.089 (85-255°C)	0.261
	340	0.056 (259-402°C)	
	521	0.087 (419-605°C)	
	668	0.028 (610-794°C)	

The activities of SiW/HZSM-5 and metal-doped SiW/HZSM-5 catalysts were tested via the conversion of glycerol at reaction temperature of 90 °C and ambient pressure at identical metal loading of 4 wt.%. As the time proceeded, a similar pattern of glycerol conversion and product yield was observed in the presence of all investigated catalysts. Glycerol conversion increased initially with increasing reaction time and then leveled off at reaction times longer than 120 min (Figure 6.7). With regards to the variation of product yield, the yields of acetic acid, glycolic acid,

formic acid and propionic acid increased slightly with increasing reaction time. The yield of acrylic acid was low during the first 30-120 min of reaction time, while a high yield of acrolein was obtained during the same period. However, at longer reaction times, the yield of acrolein decreased, whilst the yield of acrylic acid increased. This is because acrolein was oxidized to acrylic acid in the presence of supported SiW catalysts (Atia et al., 2008).

Table 6.4 summarizes the glycerol conversion and yield of all desired products at 240 min by the glycerol conversion via the SiW/HZSM-5 and metal-doped SiW/HZSM-5 catalysts. The incorporation of Ce and Co in SiW/HZSM-5 catalysts resulted in the decrease of glycerol conversion of 6.80% and 17.42%, respectively. In addition, there were markedly decreased yields of all desired stable products as well as the value of carbon selectivity. This suggests that both Ce-SiW/HZSM-5 and Co-SiW/HZSM-5 catalysts cannot facilitate the conversion of glycerol to acrylic acid or other desired products but promote the conversion of carbon atoms in glycerol molecules to undesired products (both in gas and liquid phases) such as acetaldehyde, propanal, propionic acid, propane-1,2-diol, propane-1,3-diol, 5-hydroxy-1,3-dioxolane, 5-hydroxyl-2-methyl-1,3-dioxane, benzoic acid as well as CO₂ as our mentioned previously (Thanasilp, Schwank, Meeyoo, Pengpanich, & Hunsom, 2013). In case of Ni and V, doping such metals in the structure of SiW/HZSM-5 catalyst led to an increase in glycerol conversion, yield of all desired stable products and the value of carbon selectivity compared with the original SiW/HZSM-5 catalyst. In summary, the maximum catalytic activity for the conversion of glycerol between the different metals exhibited the trend of V > Ni > Ce > Co. Correlating the properties of metal-doped SiW/HZSM-5 catalysts and their catalytic activity for the glycerol conversion, it seemed to be that the catalytic activity for the glycerol conversion depended on acid strength (low- and medium-strength acid sites) and oxidative ability of the employed catalysts. When V was doped on SiW/HZSM-5 catalyst, V-SiW/HZSM-5 catalyst led to an increased proportion of medium-strength acid sites (Figure 6.5). In the case of V-SiW/HZSM-5 catalyst, it had the highest catalytic activity compared with other catalysts. This might be attributed to the important role of low- and medium-strength acid sites of catalyst that can enhance

the catalytic activity for the glycerol conversion. To confirm this hypothesis, the experiment was then carried out with SiW/HZSM-5 catalysts in the presence of different V loadings.

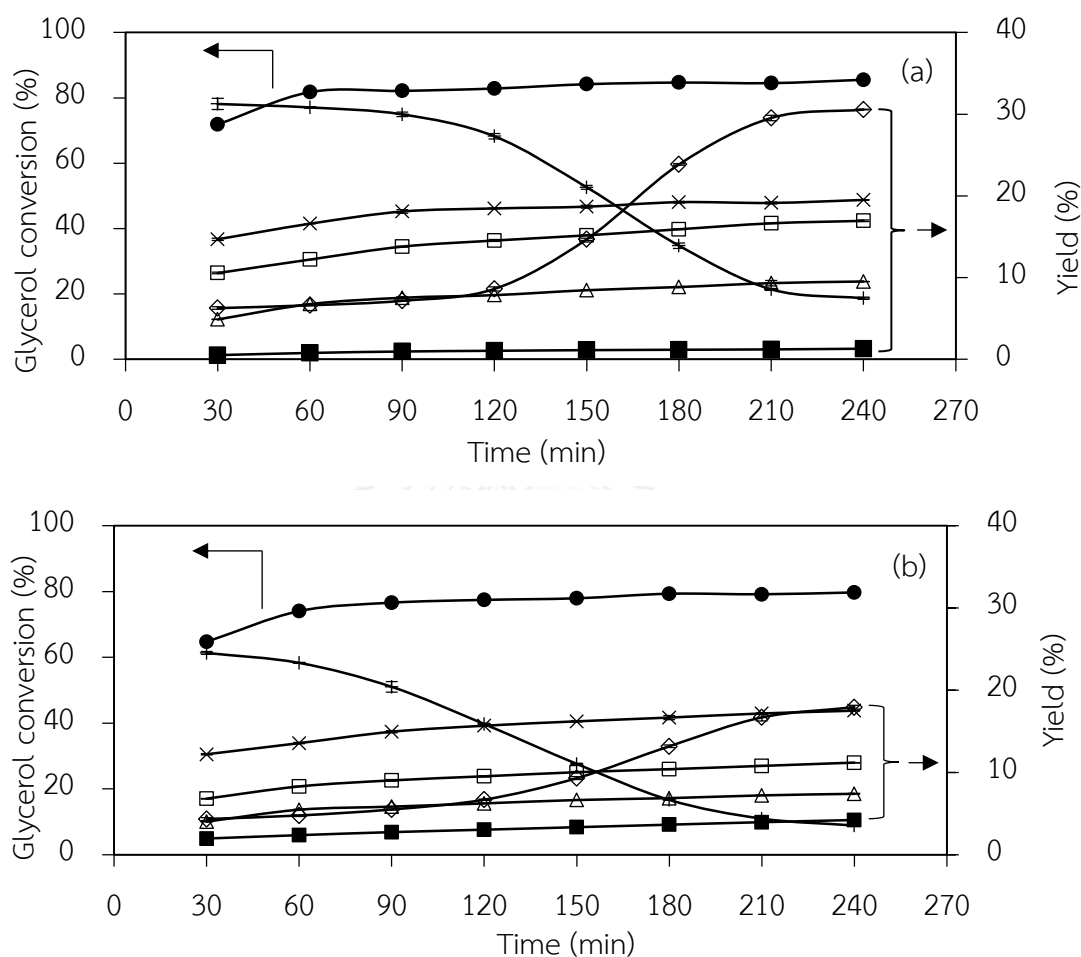


Figure 6.7 Variation of (●) glycerol conversion and yields of (□) glycolic acid, (△) formic acid, (×) acetic acid, (+) acrolein, (◇) acrylic acid and (■) propionic acid as a function of time over (a) SiW/HZSM-5, (b) Ce-SiW/HZSM-5 (c) Co-SiW/HZSM-5, (d) Ni-SiW/HZSM-5 and (e) V-SiW/HZSM-5 with 4 wt.% metal loading at 90 °C.

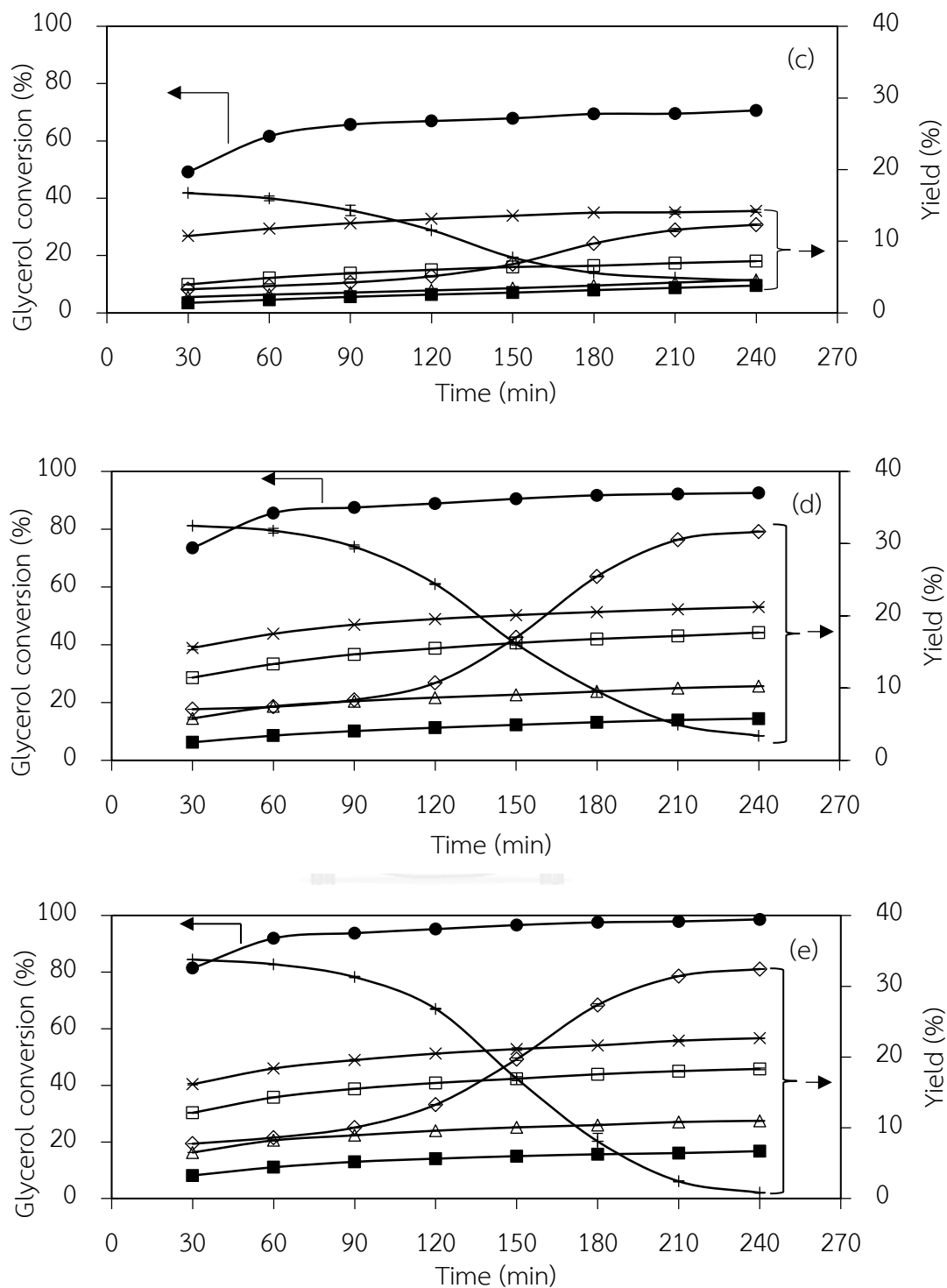


Figure 6.7 (Cont.) Variation of (●) glycerol conversion and yields of (□) glycolic acid, (△) formic acid, (×) acetic acid, (+) acrolein, (◇) acrylic acid and (■) propionic acid as a function of time over (a) SiW/HZSM-5, (b) Ce-SiW/HZSM-5 (c) Co-SiW/HZSM-5, (d) Ni-SiW/HZSM-5 and (e) V-SiW/HZSM-5 with 4 wt.% metal loading at 90 °C.

Table 6.4 Effect of metals on the performance of glycerol conversion over 30 wt.% SiW/HZSM-5 catalyst, temperature of 90 °C at 240 min.

Catalysts	Glycerol conversion (%)	Product yield (%)					Carbon selectivity (%)	
		Glycolic acid	Formic acid	Acetic acid	Acrolein	Acrylic acid	Propionic acid	
SiW/HZSM-5	85.54±0.40	16.95±0.47	9.53±0.67	19.51±0.39	7.47±0.22	30.57±0.21	4.54±0.11	85.33±0.34
Ce-SiW/HZSM-5	79.72±0.08	11.20±0.02	7.41±0.05	17.51±0.04	3.55±0.03	17.93±0.23	4.22±0.01	61.82±0.21
Co-SiW/HZSM-5	70.64±0.62	7.22±0.02	4.61±0.01	14.23±0.20	4.51±0.02	12.30±0.10	3.82±0.01	46.69±0.08
Ni-SiW/HZSM-5	92.54±0.04	17.68±0.02	10.25±0.05	21.22±0.06	3.39±0.02	31.67±0.05	5.77±0.02	89.95±0.01
V-SiW/HZSM-5	98.64±0.03	18.32±0.11	10.99±0.07	22.66±0.04	0.81±0.04	32.44±0.02	6.70±0.00	91.92±0.20

6.2 Effect of transition metal loadings

From section 6.1, it was found that V was the best transition metal for doping SiW/HZSM-5 catalyst. In this part, the V loading in the range of 2-8 wt.% (V2-V8), on the glycerol conversion and product yields was investigated.

The XRD patterns of V-SiW/HZSM-5 catalysts with different V loadings in the range of 2-8 wt.% are exhibited in Figure 6.8. All V-doped catalysts showed the main characteristic peaks of SiW/HZSM-5 catalyst, but with a decreasing intensity as the increasing V loading. No characteristic peaks of doped-metal or their oxides were apparently observed. EDX analysis confirmed the existence of V metal in the structure of V-SiW/HZSM-5 catalysts at 1.58%, 3.38%, 5.50% and 7.38%, close to the nominal quantity of 2 wt.%, 4 wt.%, 6 wt.% and 8 wt.%, respectively (Figure 6.9). Also by the XRF analysis to confirm the existence of the V oxide on the surface catalysts, it was found that the V_2O_5 were observed in all V-SiW/HZSM-5 catalysts with different loading.

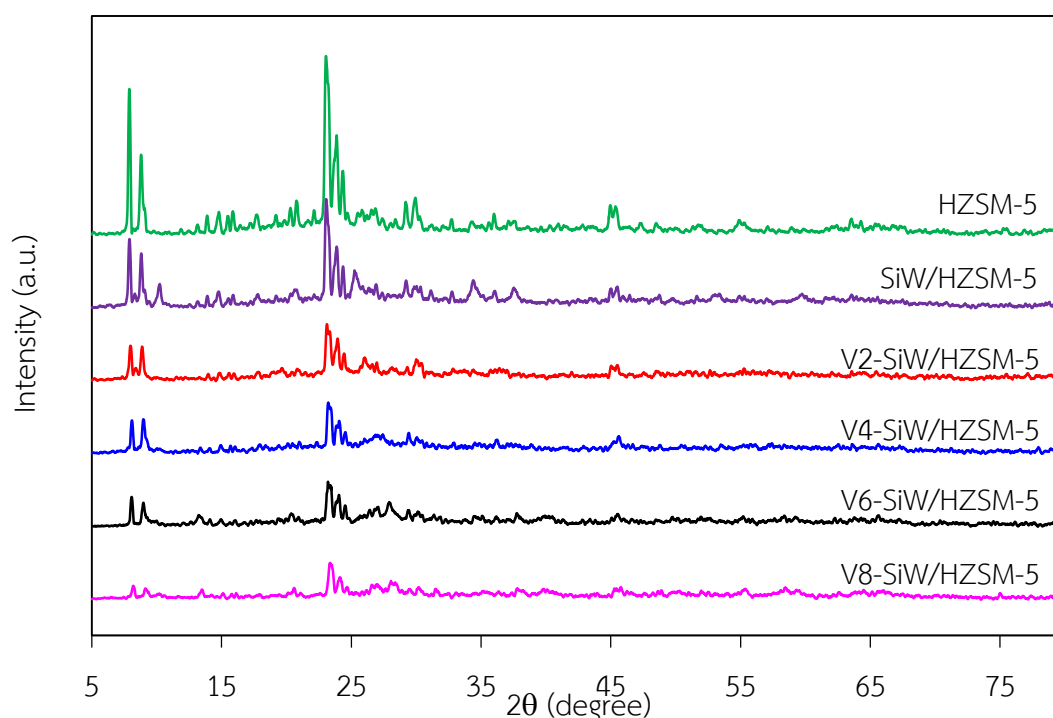


Figure 6.8 XRD patterns of HZSM-5, SiW and V-SiW/HZSM-5 catalysts with different V loadings.

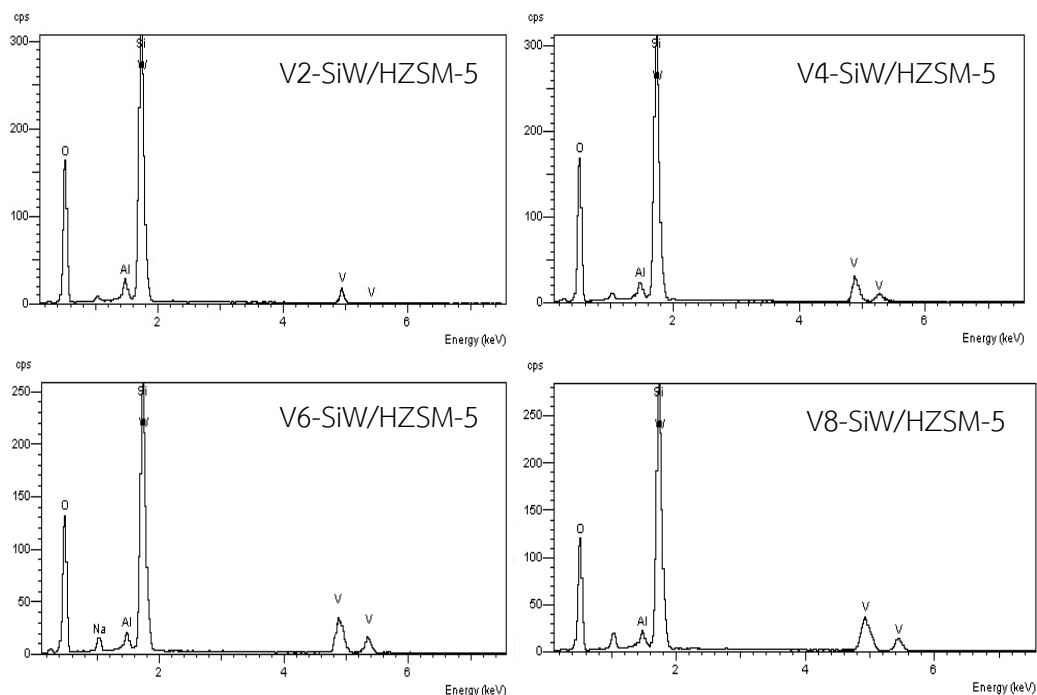


Figure 6.9 EDX analysis of V-SiW/HZSM-5 catalysts at different V loadings.

Regarding the textural properties and surface chemistry of V-SiW/HZSM-5 catalysts at different V loadings, the BET surface area and pore volume diminished with increasing V loading. This might be due to the agglomeration of V on the SiW/HZSM-5 catalyst surface in the presence of high V content, resulting in a slight decrease of pore volume as well as pore diameter, which led to a decline in the BET surface area (Lili et al., 2008). In addition, it also resulted in changes in the amount of effective acid sites (Table 6.5) and the oxidative ability as listed in Table 6.7.

The FT-IR spectra of all V-SiW/HZSM-5 catalysts with different V loadings in the range of 2-8 wt.% are exhibited in Figure 6.10. A similar pattern of FT-IR spectra was obtained for all V-SiW/HZSM-5 catalysts. The typical infrared adsorption peaks of all V-SiW/HZSM-5 catalysts appearing in the range of 1,000 to 1,250 cm^{-1} were identified to be the characteristic of HZSM-5. And the FT-IR spectra of all catalysts showed adsorption peaks ranging from 700 to 1,000 cm^{-1} , which were assigned to SiW anions of Keggin structure (Stangar et al., 2000). According to the obtained FT-IR results, it can be confirmed that the SiW supported on HZSM-5 retained their Keggin structures under our present doping metal on SiW/HZSM-5 catalysts.

Figure 6.11 showed the H₂-TPR results of V-SiW/HZSM-5 catalysts with V loadings in the range of 2-8 wt.%. With the V loading changing from 2 wt.% to 8 wt.%, V-SiW/HZSM-5 showed five peaks H₂-TPR profile. The H₂-TPR profile of SiW/HZSM-5 exhibited at 510 °C, 653 °C and 787 °C, which can be assigned to the interaction between SiW and their support. The H₂-TPR profile of all V-SiW/HZSM-5 catalysts at different V loadings showed the characteristic reduction peaks of SiW, which exhibited that the reduction temperature of SiW slightly changed when doping V on the SiW/HZSM-5 catalyst. The intensity of peak near 300 °C increased with the increase in V content, indicating that reduction with oxygen of V₂O₅ on the catalyst surface increased with V content. In general the H₂-TPR profile of bulk V₂O₅ exhibited the reduction peak at 655 °C, 686 °C and 807 °C (Koranne et al., 1994; Pieck et al., 2002). The H₂-TPR profiles of bulk V₂O₅ of V2-SiW/HZSM-5 (652, 709 and 783 °C), V4-SiW/HZSM-5 (654, 698 and 789 °C), V6-SiW/HZSM-5 (653, 705 and 792 °C) and V8-SiW/HZSM-5 (654, 702 and 794 °C) catalyst shifted to high temperature as compared to the general H₂-TPR profile of bulk V₂O₅, which indicated the formation of V₂O₅ crystals. Therefore, it may be concluded that V-SiW/HZSM-5 catalysts at different V loadings with higher V contents must have both V₂O₅ on the catalyst surface and bulk V₂O₅ which is consistent.

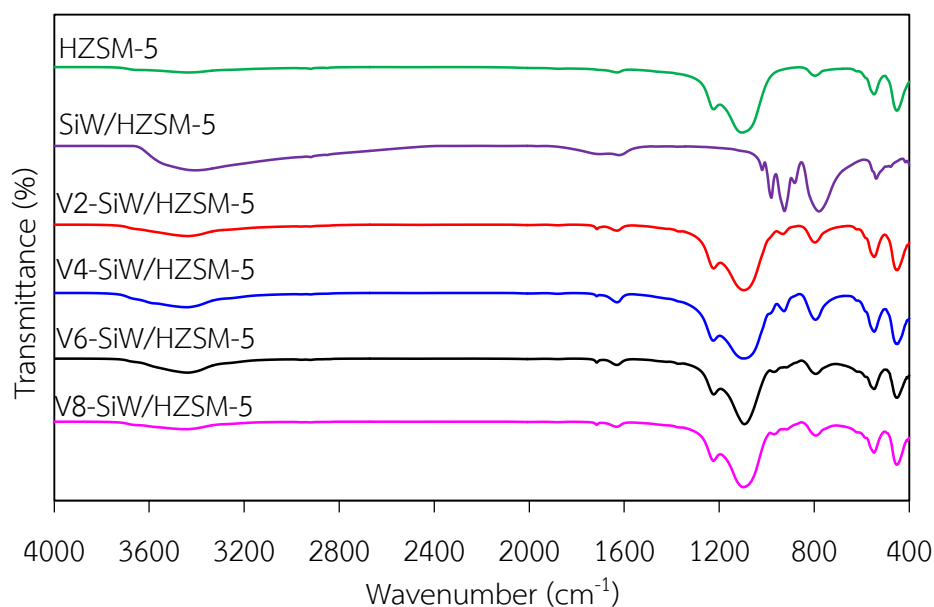


Figure 6.10 FT-IR spectra of HZSM-5, SiW and V-SiW/HZSM-5 catalysts at different V loadings.

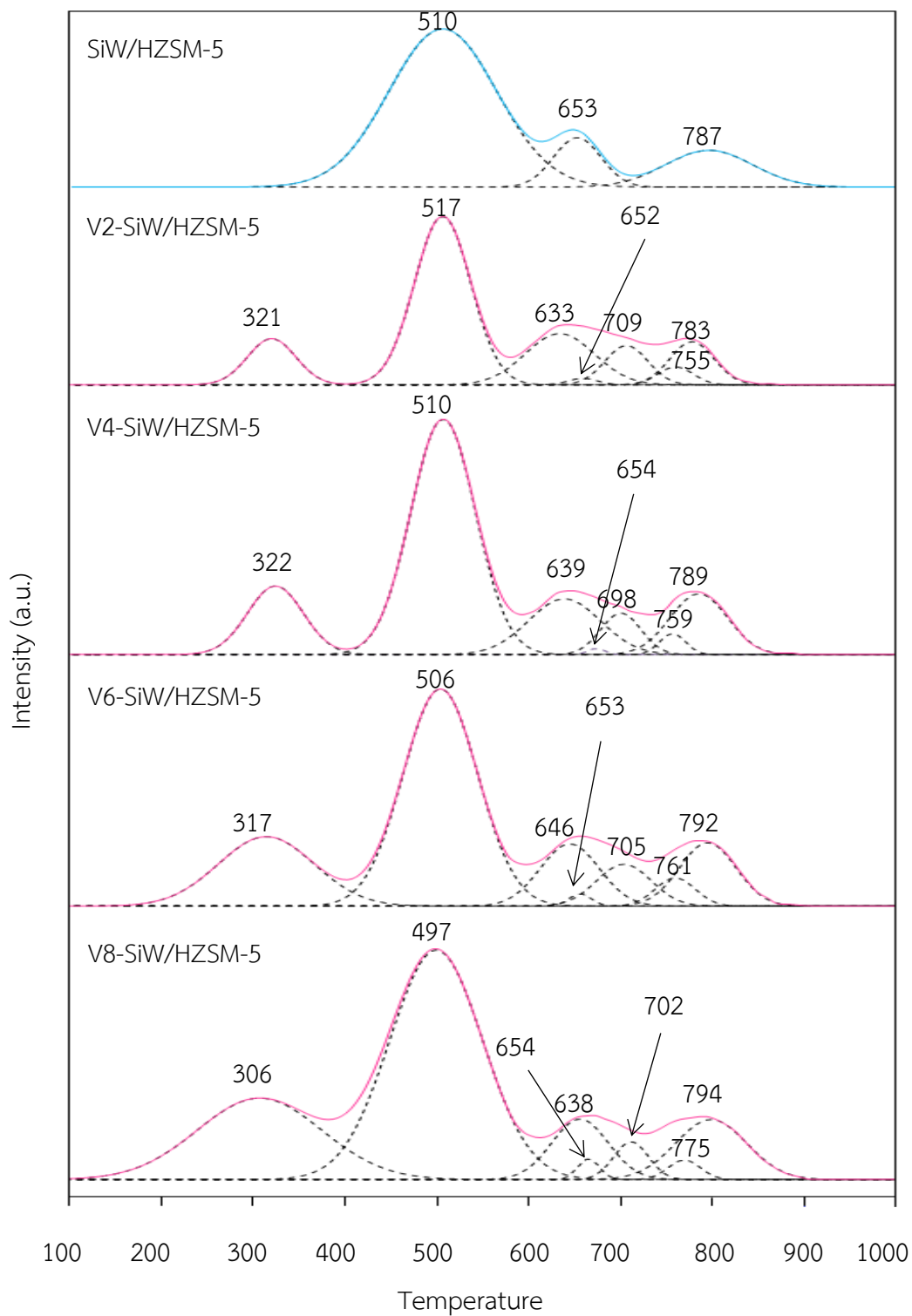


Figure 6.11 H₂-TPR profiles for utilized 30 wt.% SiW/HZSM-5 and V-SiW/HZSM-5 catalysts at different V loadings

Table 6.5 Textural properties and surface chemistry of V-SiW/HZSM-5 catalysts at different V loadings.

Catalysts	Textural properties			Surface chemistry	
	BET surface area (m ² /g)	Pore volume (cm ³ /g)	Average pore diameter (Å)	Acid amount (mmol NH ₃ /g Cat.)	Total acidity (mmol NH ₃ /g Cat.)
HZSM-5	289	0.173	4.32	0.71 (81-349 °C) 0.25 (362-640 °C)	0.97
SiW/HZSM-5	233	0.153	2.62	0.88 (78-321 °C) 0.43 (355-669 °C)	1.31
V2-SiW/HZSM-5	229	0.147	2.60	0.99 (61-224 °C) 0.32 (244-366 °C) 0.28 (542-696 °C)	1.59
V4-SiW/HZSM-5	225	0.138	2.65	1.17 (42-239 °C) 0.53 (239-401 °C) 0.42 (591-738 °C)	2.12
V6-SiW/HZSM-5	222	0.145	2.58	1.50 (44-255 °C) 0.56 (255-395 °C) 0.47 (624-750 °C)	2.53
V8-SiW/HZSM-5	216	0.144	2.72	1.67 (58-240 °C) 0.72 (240-401 °C) 0.52 (639-779 °C)	2.91

Table 6.6 O₂-TPD results for SiW/HZSM-5 and V-SiW/HZSM-5 catalysts at different V loadings.

Types of catalyst	O ₂ -TPD peak position (°C)	O ₂ desorption (mmol O ₂ /g Cat.)	Total O ₂ desorption (mmol O ₂ /g Cat.)
SiW/HZSM-5	179	0.062 (95-273°C)	0.155
	519	0.058 (317-581 °C)	
	662	0.035 (581-762 °C)	
V2-SiW/HZSM-5	176	0.091 (103-242°C)	0.234
	361	0.054 (265-398°C)	
	525	0.066 (420-578°C)	
	659	0.023 (580-755°C)	
V4-SiW/HZSM-5	175	0.089 (85-255°C)	0.261
	340	0.056 (259-402°C)	
	521	0.087 (419-605°C)	
	668	0.028 (610-794°C)	
V6-SiW/HZSM-5	176	0.093 (75-244°C)	0.275
	352	0.067 (261-419°C)	
	522	0.089 (438-576°C)	
	670	0.027 (603-764°C)	
V8-SiW/HZSM-5	171	0.093 (62-238°C)	0.283
	347	0.067 (244-423°C)	
	521	0.093 (442-599°C)	
	674	0.029 (625-765°C)	

With regard to the effect of different V loadings in the range of 2-8 wt.% on the activity of V-SiW/HZSM-5 catalysts, a similar trends of glycerol conversion and product yield along the reaction time were observed as a function of V loadings (Figure 6.12). Glycerol conversion increased considerably during the early period of reaction time and leveled off at reaction times longer than 120 min. The yields of acetic acid, glycolic acid and formic acid increased slightly with increasing reaction

time. A high yield of acrolein was obtained during the first 30-120 min and then decreased considerably due to the oxidation to acrylic acid. At 240 min reaction time, the presence of V at 2 wt.% loading (V2-SiW/HZSM-5) can enhance the glycerol conversion from 85.54% to 92.86%, or around 1.08-fold, and can reduce the transformation of glycerol to undesired products from 14.6% to less than 12.6% (Table 6.7), compared to that in the absence of V. In addition, it can facilitate a higher generation of glycolic acid, formic acid, acetic acid, acrolein, acrylic acid and propionic acid by 1.01, 1.04, 1.06, 0.60, 1.02 and 3.22-fold, respectively. The presence of V at 4 wt.% loading provided slightly lower glycerol conversion (98.64%) compared with that at 6 wt.% V (99.67%). Also, it provided a lower yield of glycolic acid, formic acid, acetic acid, acrolein, acrylic acid and propionic acid of around 1.06, 1.09, 1.04, 0.31, 1.12 and 1.05-fold, respectively. Further raising the V loading to 8 wt.% resulted in the decrease of either glycerol conversion (95.56%) or yield of desired products and also increased the glycerol conversion to undesired species, monitored by the carbon selectivity. This is due to the fact the presence of high V loading can block the pores and lowered the available surface area, leading to a decline in the activity of the catalyst. A similar result was also reported for the gas phase conversion of glycerol to acrylic acid over Mo/V and W/V oxide catalysts (Lili et al., 2008). This suggested that the yield of acrylic acid and acetic acid increased with decreasing of V content.

The acid strength of V-SiW/HZSM-5 catalysts was in the order of V8 > V6 > V4 > V2-SiW/HZSM-5 catalysts. It can be explained as that with the raising V loading in the catalyst, the total acidity and acid strength were increased, while the BET surface area of catalysts was decreased. The catalytic activity for glycerol conversion ranged in the order of V6 > V4 > V8 > V2-SiW/HZSM-5 catalysts. Although V6-SiW/HZSM-5 catalyst had lower acid strength than V8-SiW/HZSM-5 catalyst, they gave higher glycerol conversion under the same operating conditions. This could be due to the fact that the activity of supported SiW catalysts depended on the incorporation effect of BET surface area, the acidity and oxidative ability. In addition, V6-SiW/HZSM-5 catalyst can reduce the glycerol conversion to unwanted species from 10.4% to 1.4%. This is because the catalysts with too high acidity and oxidative ability

facilitated the glycerol conversion to unwanted compounds, which can observe explicitly by a low carbon selectivity at V loading of 8 wt.% as shown in Table 6.7. V2-SiW/HZSM-5 catalyst had the lowest glycerol conversion compared with other utilized catalysts due to their low acid strength and oxidative ability. Among the catalysts investigated, the V6-SiW/HZSM-5 catalyst gave the highest product yield of acrylic acid of around 36.23%, thanks to their high BET surface area, mild acidity and appropriate oxidative ability.

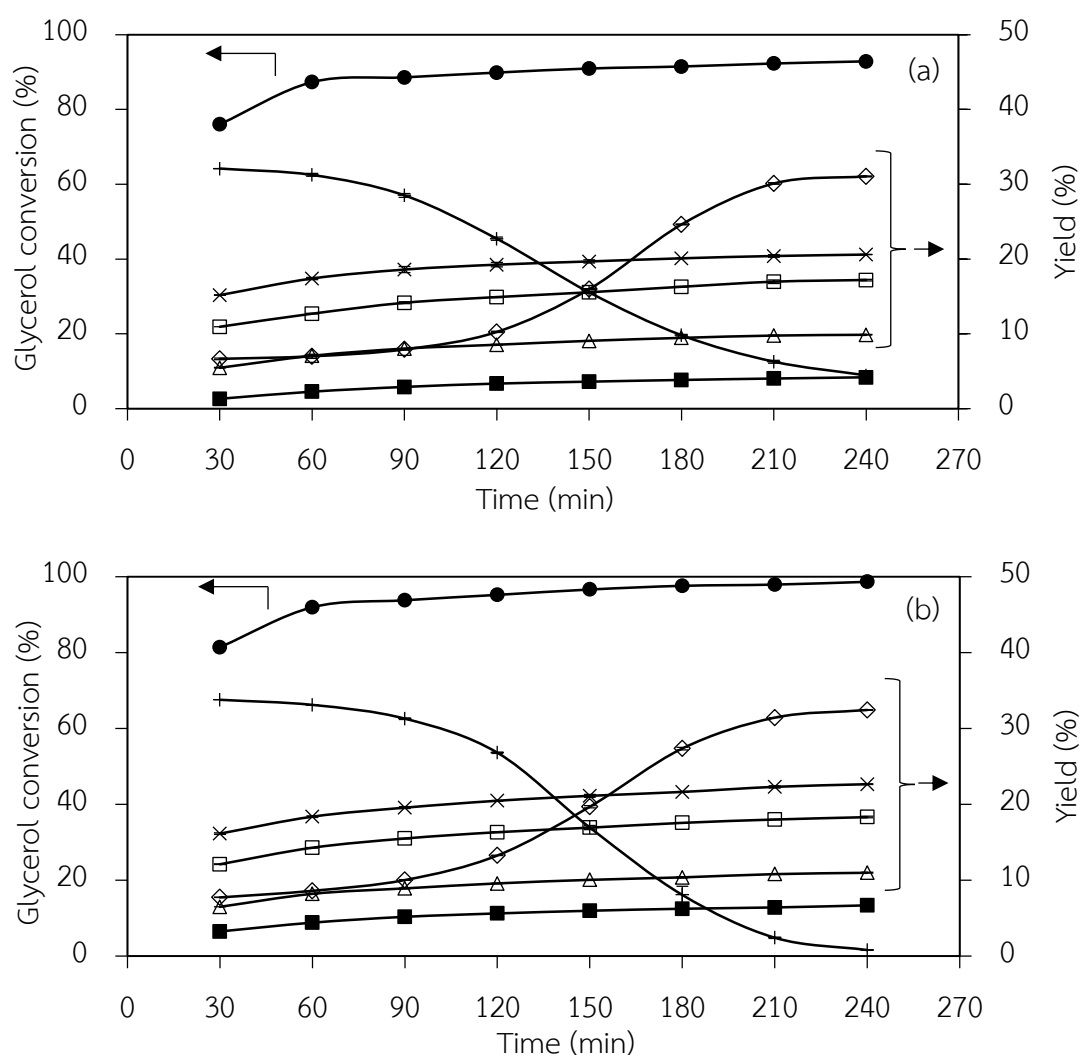


Figure 6.12 Variation of (●) glycerol conversion and yields of (□) glycolic acid, (Δ) formic acid, (X) acetic acid, (+) acrolein, (◇) acrylic acid and (■) propionic acid as a function of time over (a) V2-SiW/HZSM-5, (b) V4-SiW/HZSM-5 (c) V6-SiW/HZSM-5 and (d) V8-SiW/HZSM-5 catalysts at 90 °C.

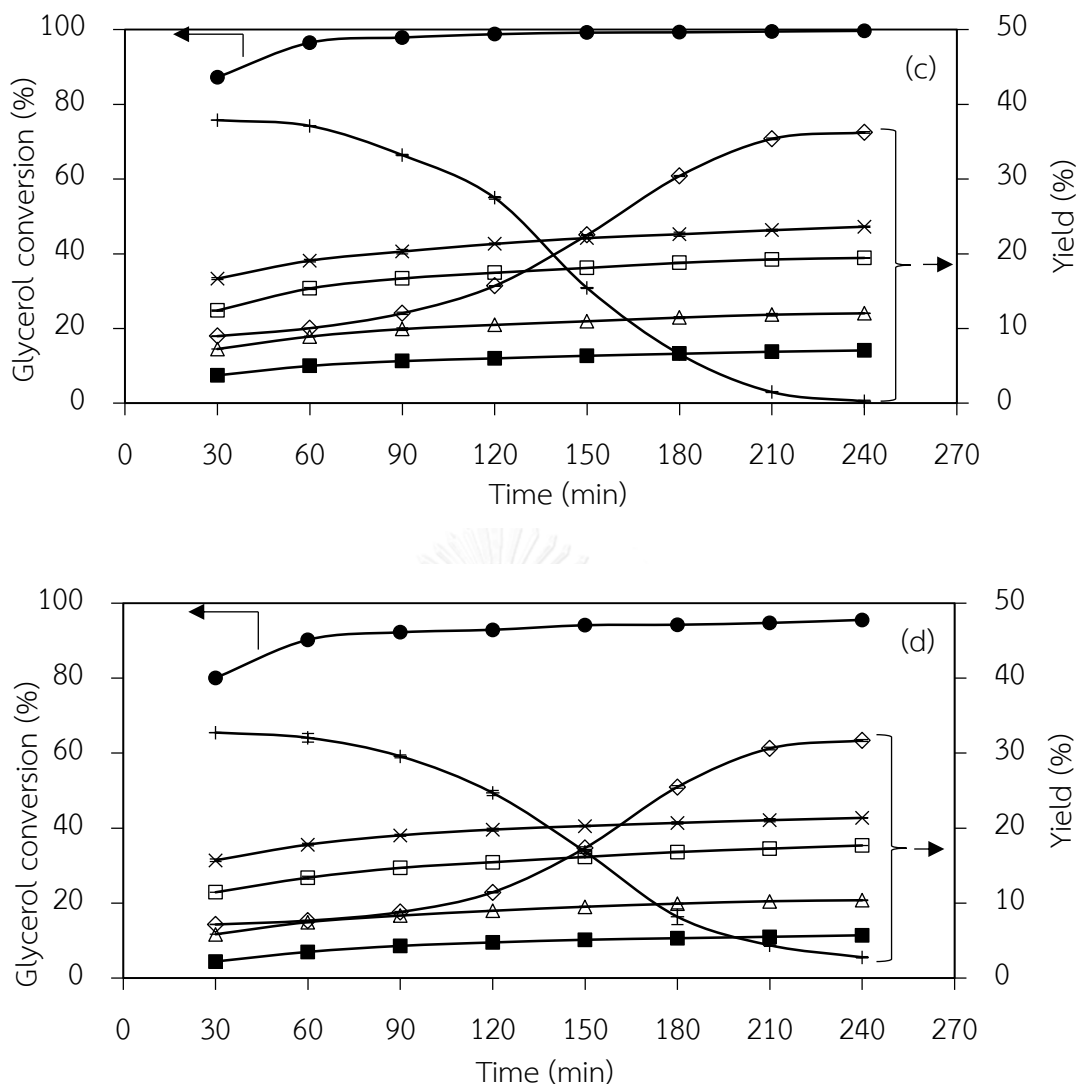


Figure 6.12 (Cont.) Variation of (●) glycerol conversion and yields of (□) glycolic acid, (△) formic acid, (×) acetic acid, (+) acrolein, (◇) acrylic acid and (■) propionic acid as a function of time over (a) V2-SiW/HZSM-5, (b) V4-SiW/HZSM-5 c) V6-SiW/HZSM-5 and (d) V8-SiW/HZSM-5 catalysts at 90 °C.

Table 6.7 Effect of V loading over SiW/HZSM-5 catalysts on the performance of glycerol conversion at SiW loading of 30 wt.%, temperature of 90 °C at 240 min.

V loading (%)	Glycerol conversion (%)	Product yield (%)						Carbon selectivity (%)
		Glycolic acid	Formic acid	Acetic acid	Acrolein	Acrylic acid	Propionic acid	
0	85.54±0.40	16.95±0.47	9.53±0.67	19.51±0.39	7.47±0.22	30.57±0.21	4.54±0.11	85.33±0.34
2	92.86±0.24	17.20±0.00	9.88±0.03	20.60±0.03	4.45±0.05	31.06±0.06	4.19±0.02	87.37±0.14
4	98.64±0.03	18.32±0.11	10.99±0.07	22.66±0.04	0.81±0.04	32.44±0.02	6.70±0.00	91.92±0.20
6	99.67±0.01	19.45±0.04	12.03±0.03	23.62±0.07	0.25±0.01	36.23±0.10	7.06±0.05	98.60±0.28
8	95.56±0.18	17.68±0.08	10.38±0.11	21.36±0.03	2.76±0.08	31.69±0.13	5.70±0.04	89.58±0.02

6.3 Kinetic studies of V-SiW/HZSM-5 catalyst

The kinetics study of glycerol conversion was carried out via the best metal-doped SiW/HZSM-5 catalysts with V loading of 6 wt.% (V6-SiW/HZSM-5) at different temperatures in the range of 60-90 °C. The glycerol and H₂O₂ concentrations were varied from 1.37-5.50 mol/L and 1.37-6.85 mol/L based on individual volumes, respectively. As expected, the conversion of glycerol increased with increasing reaction temperature (Figure 6.13). The data used to determine the kinetics of glycerol conversion was taken from the linear section of glycerol conversion at the conversion less than 40%.

The variation of glycerol conversion rate in the presence of different concentrations of glycerol and H₂O₂ were plotted in Figure 6.14-6.17 and Figure 6.18-6.21, respectively. It can be seen that the concentration of glycerol affected importantly on the reaction rate (Figure 6.14-6.17), while the concentration of H₂O₂ affected very slightly (Figure 6.18-6.21). It can be seen that the rate of glycerol conversion was influenced importantly by glycerol concentration (Figure 6.14-6.17), increasing the glycerol concentration resulted to the increase of reaction rate. However, it was affected unimportantly by H₂O₂ concentration (Figure 6.18-6.21).

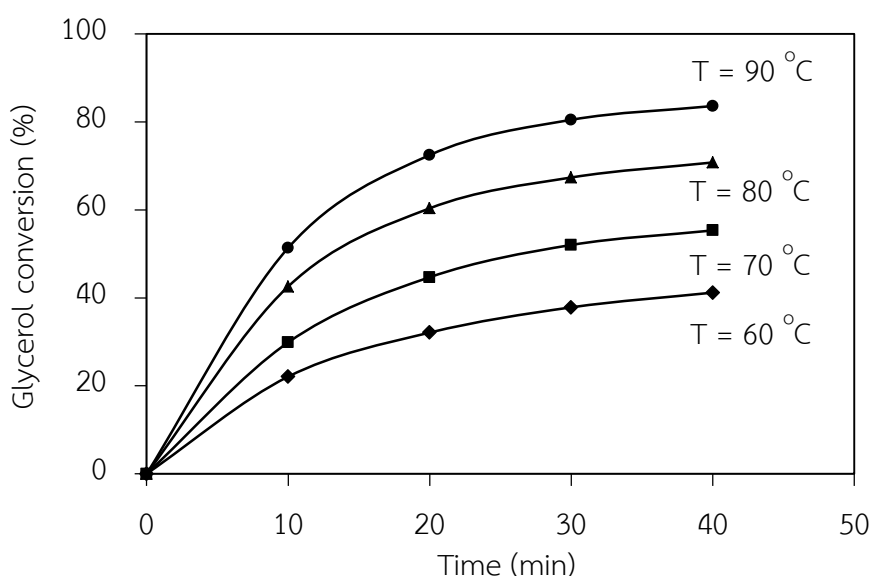


Figure 6.13 Variation of glycerol conversion rate as a function of time at 4 wt.% catalyst loading in the presence of 2.74 mol/L H₂O₂ with the glycerol concentrations of 2.75 mol/L at (◆) 60 °C, (■) 70 °C, (▲) 80 °C and (●) 90 °C.

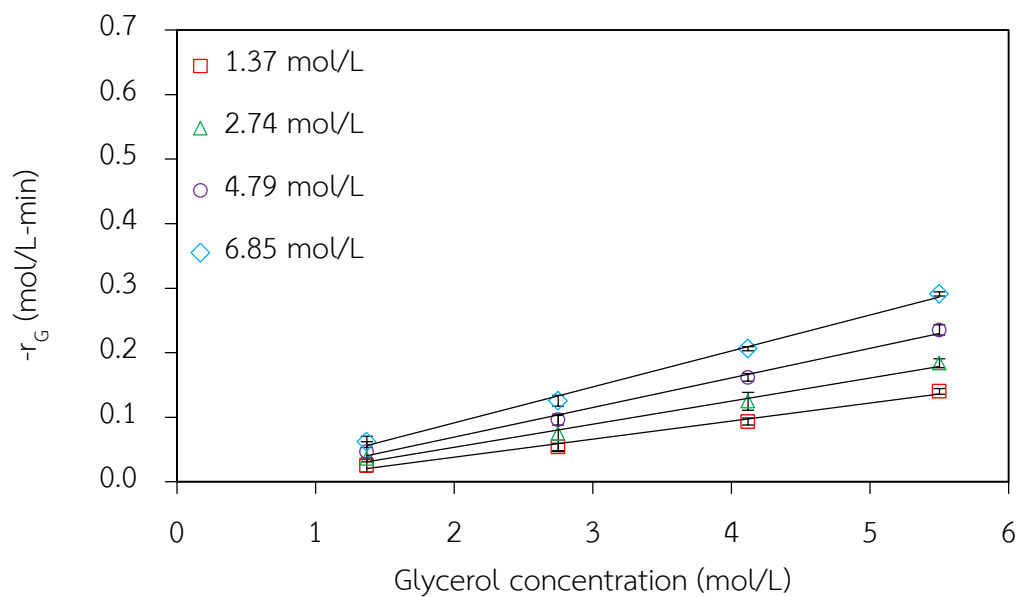


Figure 6.14 Variation of rate of glycerol conversion as a function of glycerol concentrations in the presence of H_2O_2 at 60 °C.

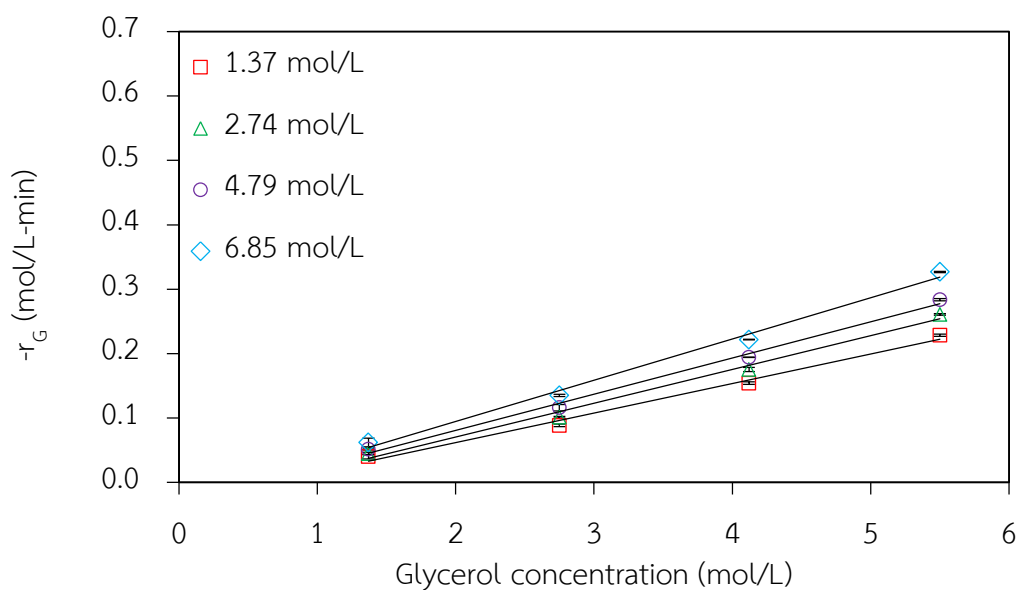


Figure 6.15 Variation of rate of glycerol conversion as a function of glycerol concentrations in the presence of H_2O_2 at 70 °C.

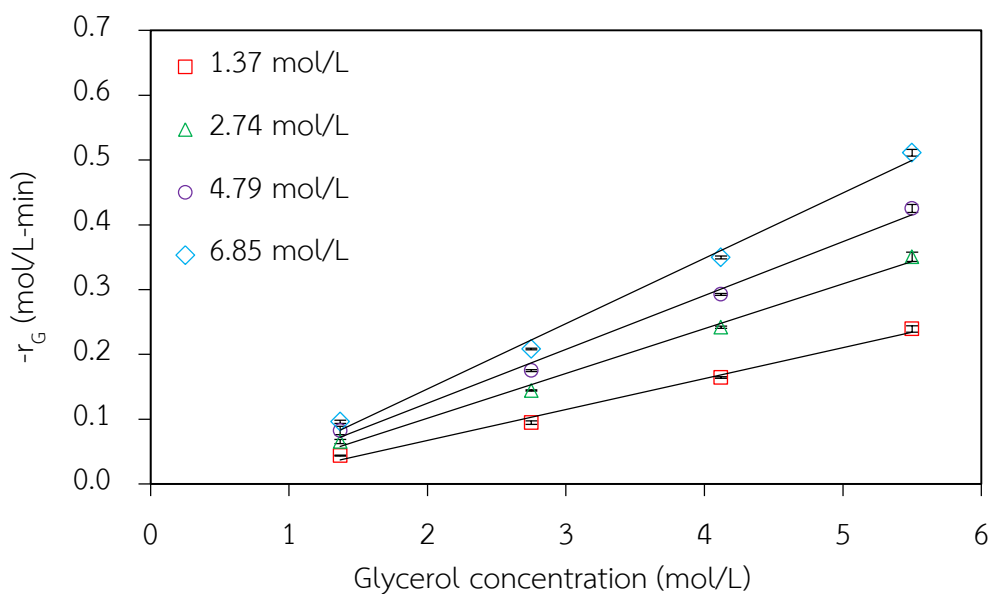


Figure 6.16 Variation of rate of glycerol conversion as a function of glycerol concentrations in the presence of H_2O_2 at 80 °C.

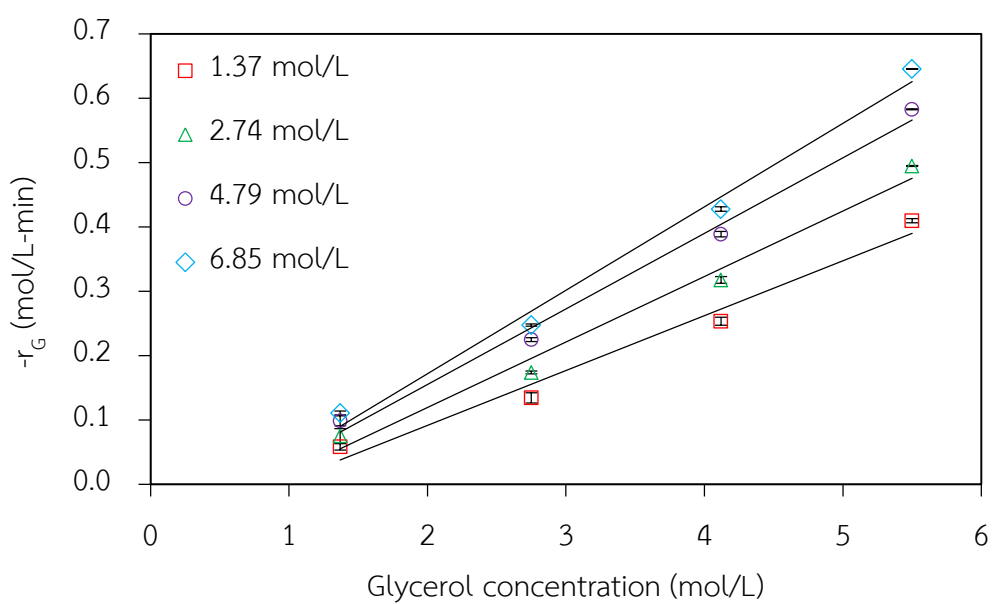


Figure 6.17 Variation of rate of glycerol conversion as a function of glycerol concentrations in the presence of H_2O_2 at 90 °C.

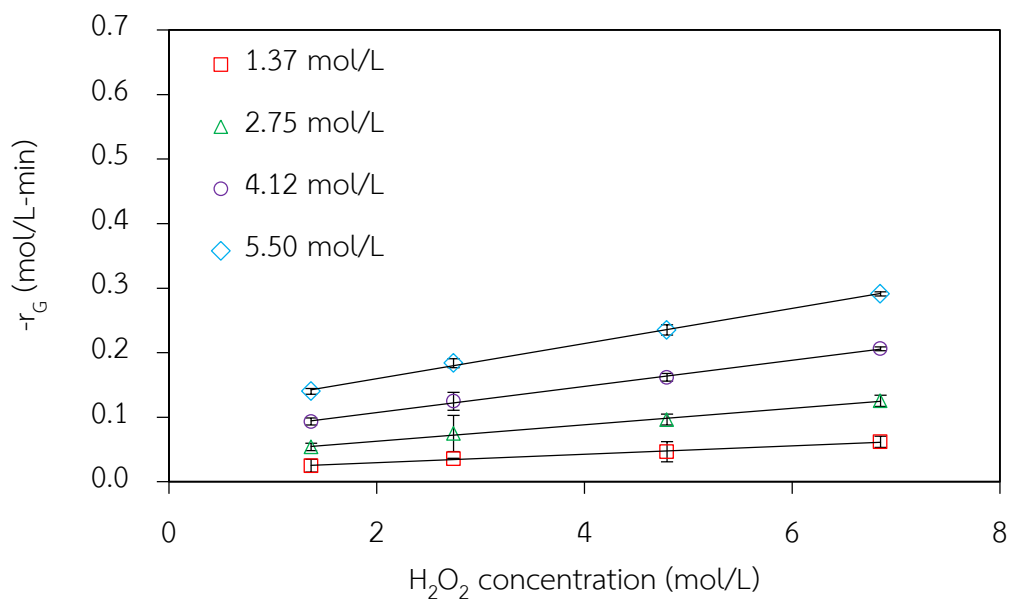


Figure 6.18 Variation of rate of glycerol conversion as a function of H₂O₂ concentrations in the presence of glycerol concentration at 60 °C.

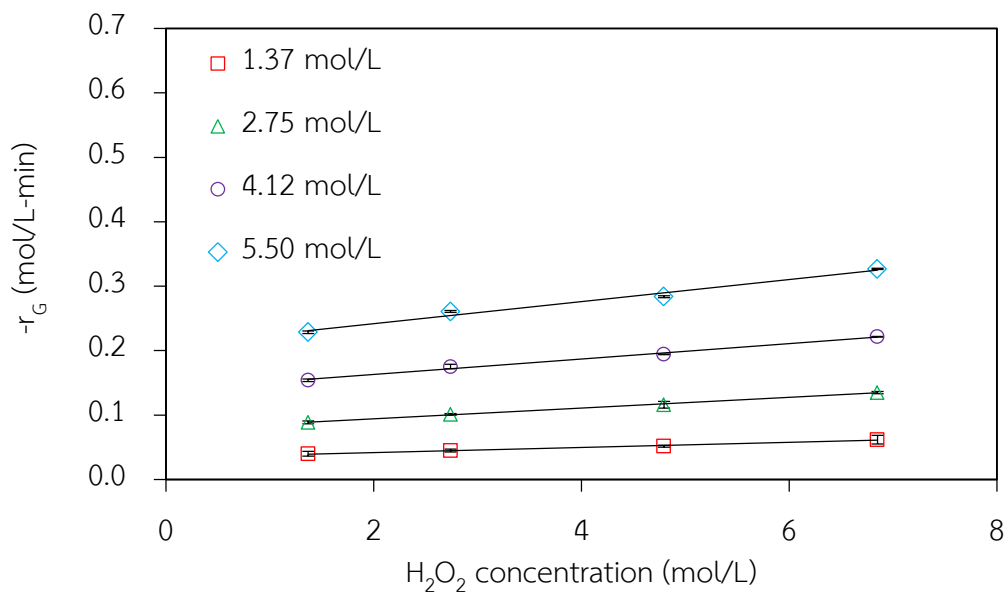


Figure 6.19 Variation of rate of glycerol conversion as a function of H₂O₂ concentrations in the presence of glycerol concentration at 70 °C.

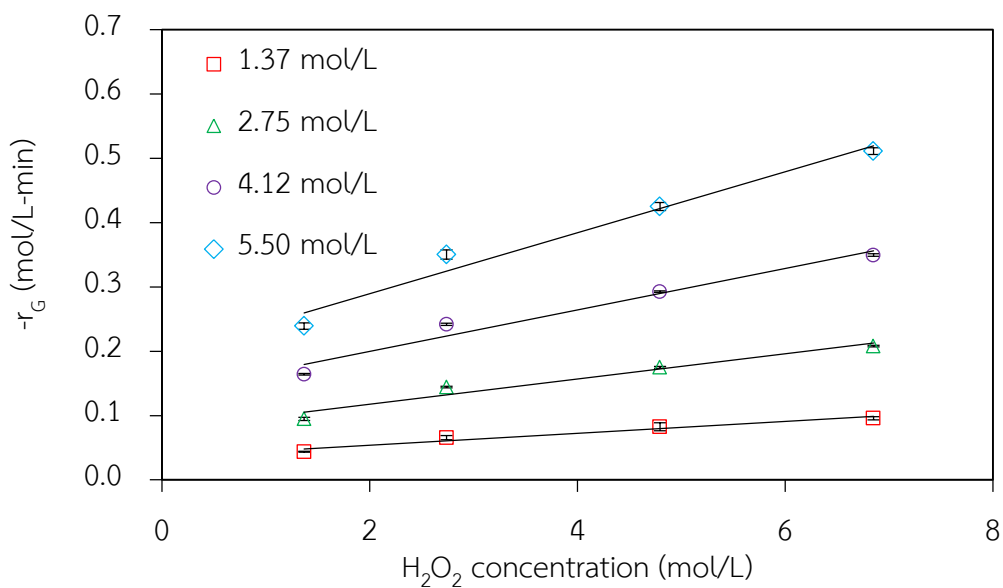


Figure 6.20 Variation of rate of glycerol conversion as a function of H₂O₂ concentrations in the presence of glycerol concentration at 80 °C.

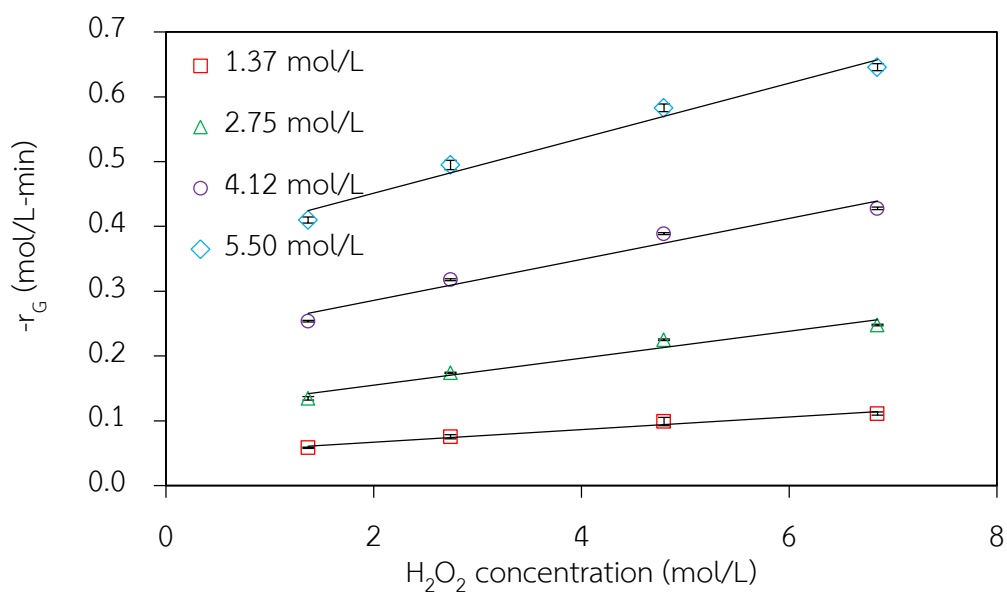


Figure 6.21 Variation of rate of glycerol conversion as a function of H₂O₂ concentrations in the presence of glycerol concentration at 90 °C.

6.3.1 Power law model

The power law model with the rate expression of conversion of glycerol was investigated in Eq.(6.1).

$$r_G = -k[G]^a[H_2O_2]^b \quad (6.1)$$

where	r_G	is the rate of glycerol conversion (mol/L.min)
	k	is the rate constant (min^{-1})
	$[G]$	is the concentration of glycerol (mol/L)
	$[H_2O_2]$	is the concentration of H_2O_2 (mol/L)
	a	is the reaction order of glycerol concentrations
	b	is the reaction order of H_2O_2 concentrations

Rearrangement of Eq.(6.1) gives the linear equation as expressed by Eq.(6.2). By using the matrix operation, the estimated parameters are shown in Table 6.8. The reaction orders of glycerol (a) and H_2O_2 (b) were 1.2 (ca.1) and 0.4 (ca.0), respectively. This demonstrates that the rate of glycerol conversion via V-SiW/HZSM-5 catalyst depended upon the concentration of glycerol concentration according to the pseudo-first order kinetic rate and about zero order with respect to the H_2O_2 concentration.

$$\ln(-r_G) = \ln(k) + a\ln([G]) + b\ln([H_2O_2]) \quad (6.2)$$

Table 6.8 Estimated parameters of the rate expression of glycerol conversion by power law model.

Temperature (°C)	Order of glycerol (a)	Order of H_2O_2 (b)	Rate constant, $k \times 10^{-2}$ (min^{-1})	R^2
60	1.17	0.50	1.48	0.9945
70	1.23	0.24	2.45	0.9956
80	1.20	0.47	2.63	0.9899
90	1.32	0.35	3.48	0.9934
Average	1.23 ± 0.06	0.39 ± 0.12		

Figure 6.22 shows the comparison rate of glycerol conversion obtained from the experiments and the power law model. It is worth noting that R^2 was greater than 0.98, suggesting a good relation between the experimental results and the power law model. In addition, this demonstrates that the parameters a and b

determined from the power law model were appropriated to predict the rate of glycerol conversion over V6-SiW/HZSM-5 catalyst.

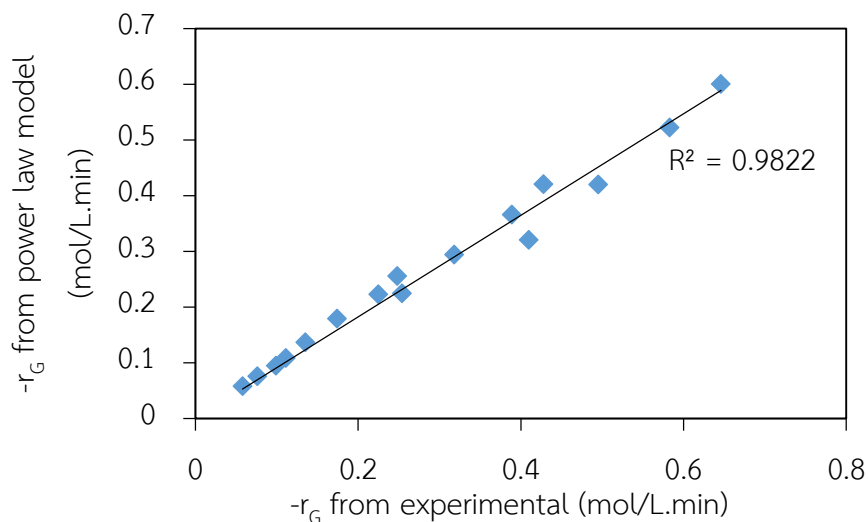


Figure 6.22 The rate of glycerol conversion from the experiments compared with the rate of glycerol conversion from power law model at 90 °C.

According to the Arrhenius's equation, a plot of kinetic rate versus temperature (Figure 6.23) provides the apparent activation energy of 26.63 kJ/mol, which is close to the activation energy reported for the glycerol oxidation over supported gold catalyst at particular oxygen pressures up to 10 bar and at temperatures from 25 to 100 °C (Demirel et al., 2007).

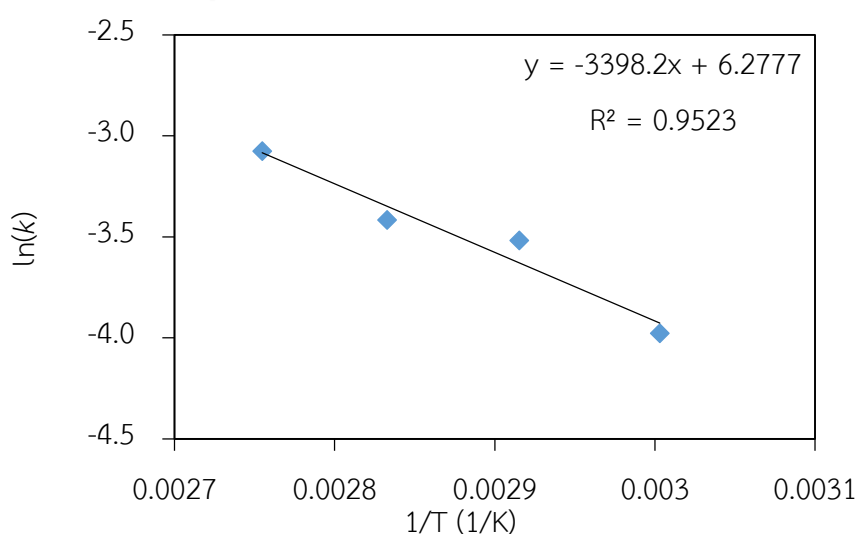


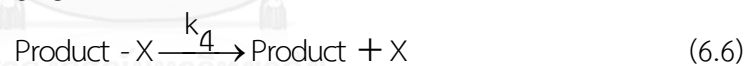
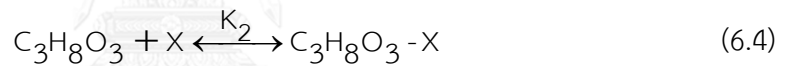
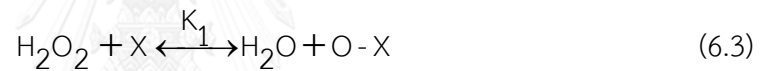
Figure 6.23 Arrhenius plot of k constants for liquid phase conversion of glycerol over V-SiW/HZSM-5 catalyst at 6 wt.% V loading.

6.3.2 Surface reaction kinetic models (Richard, 1996)

Reaction using a heterogeneous catalyst is complicated due to the adsorption and the reaction on the surface of catalyst. Therefore, the rate equations derived from a surface reaction kinetic model can describe more details of the reaction mechanism than the rate equations from a power law model. In this work, a surface reaction model was used (the rate equations derived from the surface reaction kinetic model are shown in the Appendix).

6.3.2.1 Langmuir-Hinshelwood model (Model LH1)

For this model, the hypotheses of the reaction mechanism of glycerol conversion assumes that a monoatomically adsorbed oxygen species on the active site from dissociation of H_2O_2 reacts with the glycerol adsorbed on the active site in non-dissociative form. It is worth noting that desorption of reaction products is irreversible. The reaction mechanisms are shown below.



where X is active site on heterogeneous catalyst

G is glycerol molecule

K_1 is equilibrium rate constant (adsorption-desorption) of Eq.(6.3)

K_2 is equilibrium rate constant (adsorption-desorption) of Eq.(6.4)

k_3 is the reaction rate constant of Eq.(6.5)

k_4 is the reaction rate constant of Eq.(6.6)

If the step of a monoatomic adsorption of oxygen from dissociation of H_2O_2 on the active site or Eq.(6.3) is the rate-determining step of the reaction, the reaction rate can be expressed as:

$$-r_G = \frac{k_1[\text{H}_2\text{O}_2]}{(1 + K_2[\text{G}])} \quad (6.7)$$

If the step of non-dissociative adsorption of glycerol on the active site or Eq.(6.4) is the rate-determining step of the reaction, the reaction rate can be expressed as:

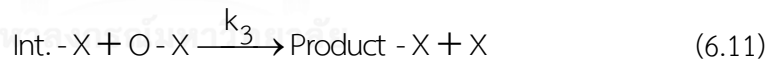
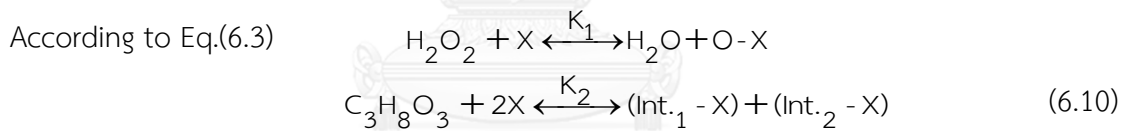
$$-r_G = \frac{k_2[G]}{(1 + K_1[H_2O_2])} \quad (6.8)$$

If the surface reaction step or Eq.(6.5) is the rate-determining step of the reaction, the reaction rate can be expressed as:

$$-r_G = \frac{k_3 K_1 K_2 [H_2O_2][G]}{(1 + K_1[H_2O_2] + K_2[G])^2} \quad (6.9)$$

6.3.2.2 Langmuir-Hinshelwood model (Model LH2)

For this model, the reaction mechanism of glycerol conversion assumes that a monoatomically adsorbed oxygen species from dissociation of H_2O_2 reacts with a dissociatively adsorbed glycerol on the active site (Int.-X). It is worth noting that desorption of reaction products is irreversible. The reaction mechanisms are shown below.



where K_1 is equilibrium rate constant (adsorption-desorption) of Eq.(6.3)
 K_2 is equilibrium rate constant (adsorption-desorption) of Eq.(6.10)
 k_3 is the reaction rate constant of Eq.(6.11)
 k_4 is the reaction rate constant of Eq.(6.6)
 Int. is the intermediate of a dissociative adsorption of glycerol

If the step of a monoatomic adsorption of oxygen from dissociation of H_2O_2 on the active site or Eq.(6.3) is the rate-determining step of the reaction, the reaction rate can be expressed as:

$$-r_G = \frac{k_1[H_2O_2]}{(1 + 2K_2^{1/2}[G]^{1/2})} \quad (6.12)$$

If the step of dissociative adsorption glycerol on the active site (Int.-X) or Eq.(6.10) is the rate-determining step of the reaction, the reaction rate can be expressed as:

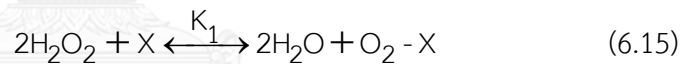
$$-r_G = \frac{k_2[G]}{(1 + K_1[H_2O_2])^2} \quad (6.13)$$

If the surface reaction step or Eq.(6.11) is the rate-determining step of the reaction, the reaction rate can be expressed as:

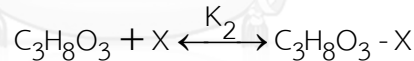
$$-r_G = \frac{k_3 K_1 K_2^{1/2} [H_2O_2] [G]^{1/2}}{(1 + K_1[H_2O_2] + 2K_2^{1/2}[G]^{1/2})^2} \quad (6.14)$$

6.3.2.3 Langmuir-Hinshelwood model (Model LH3)

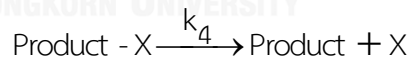
For this model, the reaction mechanism of glycerol conversion assumes that an adsorbed O_2 molecule on the active site from dissociation of H_2O_2 reacts with the glycerol adsorbed on the active site in non-dissociative form. The reaction mechanisms are shown below.



According to Eq.(6.4)



Followed by Eq.(6.6)



where K_1 is equilibrium rate constant (adsorption-desorption) of Eq.(6.15)

K_2 is equilibrium rate constant (adsorption-desorption) of Eq.(6.4)

k_3 is the reaction rate constant of Eq.(6.16)

k_4 is the reaction rate constant of Eq.(6.6)

If the step of adsorption of O_2 molecule on the active site from dissociation of H_2O_2 or Eq.(6.15) is the rate-determining step of the reaction, the reaction rate can be expressed as:

$$-r_G = \frac{k_1[H_2O_2]^2}{(1 + K_2[G])} \quad (6.17)$$

If the step of non-dissociative adsorption glycerol on the active site or Eq.(6.4) is the rate-determining step of the reaction, the reaction rate can be expressed as:

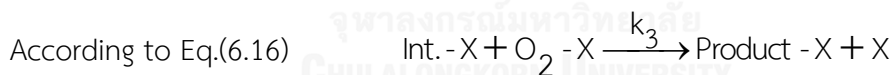
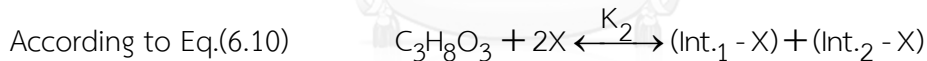
$$-r_G = \frac{k_2[G]}{(1+K_1[H_2O_2])^2} \quad (6.18)$$

If the surface reaction step or Eq.(6.16) is the rate-determining step of the reaction, the reaction rate can be expressed as:

$$-r_G = \frac{k_3 K_1 K_2 [H_2O_2]^2 [G]}{(1 + K_1 [H_2O_2])^2 + K_2 [G]^2} \quad (6.19)$$

6.3.2.4 Langmuir-Hinshelwood model (Model LH4)

For this model, the reaction mechanism of glycerol conversion assumes that an adsorbed O₂ molecule on the active site from decomposition of H₂O₂ reacts with dissociatively adsorbed glycerol on the active site (Intermediate-X). However, desorption of the reaction product is an irreversible reaction. The reaction mechanisms are shown below.



where K_1 is equilibrium rate constant (adsorption-desorption) of Eq.(6.15)

K_2 is equilibrium rate constant (adsorption-desorption) of Eq.(6.10)

k_3 is the reaction rate constant of Eq.(6.16)

k_4 is the reaction rate constant of Eq.(6.6)

Int. is the intermediate of a dissociative adsorption of glycerol

If the step of an adsorption of O₂ molecule on the active site from dissociation of H₂O₂ or Eq.(6.15) is the rate-determining step of the reaction, the reaction rate can be expressed as:

$$-r_G = \frac{k_1[H_2O_2]^2}{(1 + 2K_2^{1/2}[G]^{1/2})} \quad (6.20)$$

If the step of dissociative adsorption glycerol on the active site) or Eq.(6.10) is the rate-determining step of the reaction, the reaction rate can be expressed as:

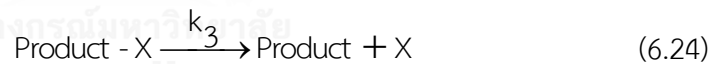
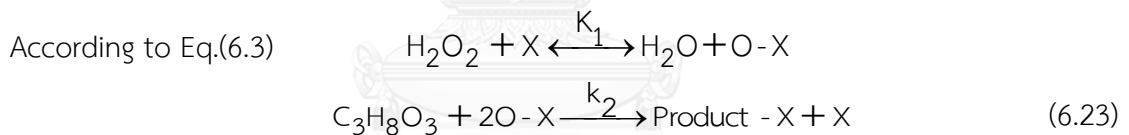
$$-r_G = \frac{k_2[G]}{(1 + K_1[H_2O_2]^2)^2} \quad (6.21)$$

If the surface reaction step or Eq.(6.20) is the rate-determining step of the reaction, the reaction rate can be expressed as:

$$-r_G = \frac{k_3K_1K_2^{1/2}[H_2O_2]^2[G]^{1/2}}{(1 + K_1[H_2O_2]^2 + 2K_2^{1/2}[G]^{1/2})^2} \quad (6.22)$$

6.3.2.5 Eley-Rideal model (Model ER1)

For this model, the reaction mechanism of glycerol conversion assumes that a monoatomically adsorbed oxygen species from dissociation of H_2O_2 reacts with glycerol solution. However, desorption of the reaction product is an irreversible reaction. The reaction mechanisms are shown below.



where K_1 is equilibrium rate constant (adsorption-desorption) of Eq.(6.15)

k_2 is the reaction rate constant of Eq.(6.23)

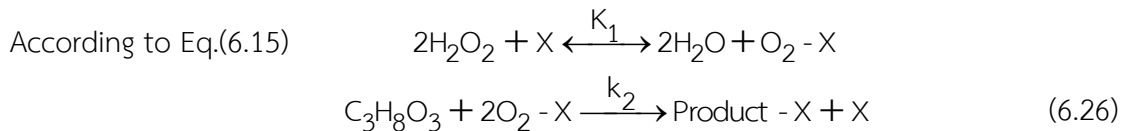
k_3 is the reaction rate constant of Eq.(6.24)

If the surface reaction step or Eq.(6.23) is the rate-determining step of the reaction, the reaction rate can be expressed as:

$$-r_G = \frac{k_2K_1^2[H_2O_2]^2[G]}{(1 + K_1[H_2O_2])^2} \quad (6.25)$$

6.3.2.6 Eley-Rideal model (Model ER2)

For this model, the reaction mechanism of glycerol conversion assumes that an adsorbed O_2 molecule on the active site from decomposition of H_2O_2 directly reacts with glycerol solution. However, desorption of the reaction product is an irreversible reaction. The reaction mechanisms are shown below.



where K_1 is equilibrium rate constant (adsorption-desorption) of Eq.(6.15)

k_2 is the reaction rate constant of Eq.(6.26)

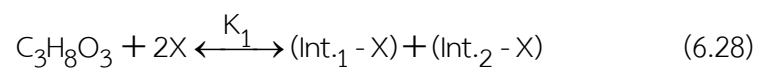
k_3 is the reaction rate constant of Eq.(6.24)

If the surface reaction step or Eq.(6.26) is the rate-determining step of the reaction, the reaction rate can be expressed as:

$$-r_G = \frac{k_2 K_1^2 [H_2O_2]^4 [G]}{(1 + K_1 [H_2O_2])^2} \quad (6.27)$$

6.3.2.7 Eley-Rideal model (Model ER3)

For this model, the reaction mechanism of glycerol conversion assumes that dissociatively adsorbed glycerol on the active site (Intermediate-X) directly reacts with H_2O_2 solution. However, desorption of the reaction product is an irreversible reaction. The reaction mechanisms are shown below.



where K_1 is equilibrium rate constant (adsorption-desorption) of Eq.(6.28)

k_2 is the reaction rate constant of Eq.(6.29)

k_3 is the reaction rate constant of Eq.(6.24)

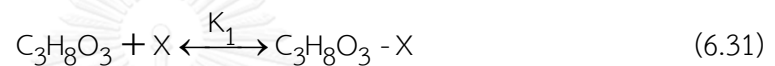
Int. is the intermediate of a dissociative adsorption of glycerol

If the surface reaction step or Eq.(6.29) is the rate-determining step of the reaction, the reaction rate can be expressed as:

$$-r_G = \frac{k_2 K_1 [H_2O_2][G]}{\left(1 + 2K_1^{1/2}[G]^{1/2}\right)^2} \quad (6.30)$$

6.3.2.8 Eley-Rideal model (Model ER4)

For this model, the reaction mechanism of glycerol conversion assumes that a non-dissociatively adsorbed glycerol on the active site directly reacts with H_2O_2 . However, desorption of the reaction product is an irreversible reaction. The reaction mechanisms are shown below.



where K_1 is equilibrium rate constant (adsorption-desorption) of Eq.(6.31)

k_2 is the reaction rate constant of Eq.(6.32)

k_3 is the reaction rate constant of Eq.(6.24)

If the surface reaction step or Eq.(6.32) is the rate-determining step of the reaction, the reaction rate can be expressed as:

$$-r_G = \frac{k_2 K_1^2 [H_2O_2][G]^2}{(1 + K_1[G])^2} \quad (6.33)$$

The reaction rate equations and their linearized form of all six models of surface reaction kinetic are summarized in Table 6.9. The parameters in the rate equations in Table 6.10 to 6.13 can be obtained by performing multi-linear regression model.

Table 6.9 Surface reaction kinetic models used to fit the glycerol conversion reaction.

Model	Reaction mechanism	Rate expression	Linearized
LH1	$\text{H}_2\text{O}_2 + \text{X} \xrightleftharpoons{K_1} \text{H}_2\text{O} + \text{O} - \text{X}$	$-r_G = \frac{k_1[\text{H}_2\text{O}_2]}{(1 + K_2[\text{G}])}$	$\frac{1}{k_1} + \frac{K_2[\text{G}]}{k_1} = \frac{[\text{H}_2\text{O}_2]}{-r_G} \quad (\text{LH1-1})$
	$\text{C}_3\text{H}_8\text{O}_3 + \text{X} \xrightleftharpoons{K_2} \text{C}_3\text{H}_8\text{O}_3 - \text{X}$	$-r_G = \frac{k_2[\text{G}]}{(1 + K_1[\text{H}_2\text{O}_2])}$	$\frac{1}{k_2} + \frac{K_1[\text{H}_2\text{O}_2]}{k_2} = \frac{[\text{G}]}{-r_G} \quad (\text{LH1-2})$
	$\text{C}_3\text{H}_8\text{O}_3 - \text{X} + \text{O} - \text{X} \xrightarrow{k_3} \text{Product} - \text{X} + \text{X}$	$-r_G = \frac{k_3 K_1 K_2 [\text{H}_2\text{O}_2][\text{G}]}{(1 + K_1[\text{H}_2\text{O}_2] + K_2[\text{G}])^2}$	$\frac{1}{\sqrt{K_3 K_1 K_2}} + \frac{K_1[\text{H}_2\text{O}_2]}{\sqrt{K_3 K_1 K_2}} + \frac{K_2[\text{G}]}{\sqrt{K_3 K_1 K_2}} = \frac{[\text{H}_2\text{O}_2]^{1/2} [\text{G}]^{1/2}}{-r_G} \quad (\text{LH1-3})$
	$\text{Product} - \text{X} \xrightarrow{k_4} \text{Product} + \text{X}$		
LH2	$\text{H}_2\text{O}_2 + \text{X} \xrightleftharpoons{K_1} \text{H}_2\text{O} + \text{O} - \text{X}$	$-r_G = \frac{k_1[\text{H}_2\text{O}_2]}{(1 + 2K_2^{1/2}[\text{G}]^{1/2})}$	$\frac{1}{k_1} + \frac{2K_2^{1/2}[\text{G}]^{1/2}}{k_1} = \frac{[\text{H}_2\text{O}_2]}{-r_G} \quad (\text{LH2-1})$
	$\text{C}_3\text{H}_8\text{O}_3 + 2\text{X} \xrightleftharpoons{K_2} (\text{Int}_1 - \text{X}) + (\text{Int}_2 - \text{X})$	$-r_G = \frac{k_2[\text{G}]}{(1 + K_1[\text{H}_2\text{O}_2])^2}$	$\frac{1}{\sqrt{K_2}} + \frac{K_1[\text{H}_2\text{O}_2]}{\sqrt{K_2}} = \frac{[\text{G}]^{1/2}}{-r_G} \quad (\text{LH2-2})$
	$\text{Int}_1 - \text{X} + \text{O} - \text{X} \xrightarrow{k_3} \text{Product} - \text{X} + \text{X}$	$-r_G = \frac{k_3 K_1 K_2^{1/2} [\text{H}_2\text{O}_2][\text{G}]^{1/2}}{(1 + K_1[\text{H}_2\text{O}_2] + 2K_2^{1/2}[\text{G}]^{1/2})^2}$	$\frac{1}{\sqrt{K_3 K_1 K_2^{1/2}}} + \frac{K_1[\text{H}_2\text{O}_2]}{\sqrt{K_3 K_1 K_2^{1/2}}} + \frac{2K_2^{1/2}[\text{G}]^{1/2}}{\sqrt{K_3 K_1 K_2^{1/2}}} = \frac{[\text{H}_2\text{O}_2]^{1/2} [\text{G}]^{1/4}}{-r_G} \quad (\text{LH2-3})$
	$\text{Product} - \text{X} \xrightarrow{k_4} \text{Product} + \text{X}$		

Table 6.9 (Cont.) Surface reaction kinetic models used to fit the glycerol conversion

Model	Reaction mechanism	Rate expression	Linearized
LH3	$2\text{H}_2\text{O}_2 + \text{X} \xrightleftharpoons{K_1} 2\text{H}_2\text{O} + \text{O}_2 - \text{X}$	$-r_G = \frac{k_1[\text{H}_2\text{O}_2]^2}{(1 + K_2[\text{G}])}$	$\frac{1}{k_1} + \frac{K_2[\text{G}]}{k_1} = \frac{[\text{H}_2\text{O}_2]^2}{-r_G} \quad (\text{LH3-1})$
	$\text{C}_3\text{H}_8\text{O}_3 + \text{X} \xrightleftharpoons{K_2} \text{C}_3\text{H}_8\text{O}_3 - \text{X}$	$-r_G = \frac{k_2[\text{G}]}{(1 + K_1[\text{H}_2\text{O}_2]^2)}$	$\frac{1}{k_2} + \frac{K_1[\text{H}_2\text{O}_2]^2}{k_2} = \frac{[\text{G}]}{-r_G} \quad (\text{LH3-2})$
	$\text{C}_3\text{H}_8\text{O}_3 - \text{X} + \text{O}_2 - \text{X} \xrightarrow{k_3} \text{Product} - \text{X} + \text{X}$ Product - X $\xrightarrow{k_4}$ Product + X	$-r_G = \frac{k_3 K_1 K_2 [\text{H}_2\text{O}_2]^2 [\text{G}]}{(1 + K_1[\text{H}_2\text{O}_2]^2 + K_2[\text{G}])^2}$	$\frac{1}{\sqrt{k_3 K_1 K_2}} + \frac{K_1[\text{H}_2\text{O}_2]^2}{\sqrt{k_3 K_1 K_2}} + \frac{K_2[\text{G}]}{\sqrt{k_3 K_1 K_2}} = \frac{[\text{H}_2\text{O}_2][\text{G}]^{1/2}}{-r_G^{1/2}} \quad (\text{LH3-3})$
LH4	$2\text{H}_2\text{O}_2 + \text{X} \xrightleftharpoons{K_1} 2\text{H}_2\text{O} + \text{O}_2 - \text{X}$	$-r_G = \frac{k_1[\text{H}_2\text{O}_2]^2}{(1 + 2K_2^{1/2}[\text{G}]^{1/2})}$	$\frac{1}{k_1} + \frac{2K_2^{1/2}[\text{G}]^{1/2}}{k_1} = \frac{[\text{H}_2\text{O}_2]^2}{-r_G} \quad (\text{LH4-1})$
	$\text{C}_3\text{H}_8\text{O}_3 + 2\text{X} \xrightleftharpoons{K_2} (\text{Int.}_1 - \text{X}) + (\text{Int.}_2 - \text{X})$	$-r_G = \frac{k_2[\text{G}]}{(1 + K_1[\text{H}_2\text{O}_2]^2)^2}$	$\frac{1}{\sqrt{k_2}} + \frac{K_1[\text{H}_2\text{O}_2]^2}{\sqrt{k_2}} = \frac{[\text{G}]^{1/2}}{-r_G^{1/2}} \quad (\text{LH4-2})$
	$\text{Int.} - \text{X} + \text{O}_2 - \text{X} \xrightarrow{k_3} \text{Product} - \text{X} + \text{X}$ Product - X $\xrightarrow{k_4}$ Product + X	$-r_G = \frac{k_3 K_1^{1/2} K_2 [\text{H}_2\text{O}_2]^2 [\text{G}]^{1/2}}{(1 + K_1[\text{H}_2\text{O}_2]^2 + 2K_2^{1/2}[\text{G}]^{1/2})^2}$	$\frac{1}{\sqrt{k_3 K_1 K_2^{1/2}}} + \frac{K_1[\text{H}_2\text{O}_2]^2}{\sqrt{k_3 K_1 K_2^{1/2}}} + \frac{2K_2^{1/2}[\text{G}]^{1/2}}{\sqrt{k_3 K_1 K_2^{1/2}}} = \frac{[\text{H}_2\text{O}_2]^{1/2} [\text{G}]^{1/4}}{-r_G^{1/2}} \quad (\text{LH4-3})$

Table 6.9 (Cont.) Surface reaction kinetic models used to fit the glycerol conversion

Model	Reaction mechanism	Rate expression	Linearized
ER1	$\text{H}_2\text{O}_2 + \text{X} \xrightleftharpoons{K_1} \text{H}_2\text{O} + \text{O} \cdot \text{X}$ $\text{C}_3\text{H}_8\text{O}_3 + 2\text{O} \cdot \text{X} \xrightarrow{k_2} \text{Product} \cdot \text{X} + \text{X}$ $\text{Product} \cdot \text{X} \xrightarrow{k_3} \text{Product} + \text{X}$	$-r_G = \frac{k_2 K_1^2 [\text{H}_2\text{O}_2]^2 [\text{G}]}{(1 + K_1 [\text{H}_2\text{O}_2])^2}$	$\frac{1}{\sqrt{k_2 K_1^2}} + \frac{K_1 [\text{H}_2\text{O}_2]}{\sqrt{k_2 K_1^2}} = \frac{[\text{H}_2\text{O}_2] [\text{G}]^{1/2}}{-r_G^{1/2}} \quad (\text{ER1})$
ER2	$2\text{H}_2\text{O}_2 + \text{X} \xrightleftharpoons{K_1} 2\text{H}_2\text{O} + \text{O}_2 \cdot \text{X}$ $\text{C}_3\text{H}_8\text{O}_3 + 2\text{O}_2 \cdot \text{X} \xrightarrow{k_2} \text{Product} \cdot \text{X} + \text{X}$ $\text{Product} \cdot \text{X} \xrightarrow{k_3} \text{Product} + \text{X}$	$-r_G = \frac{k_2 K_1^2 [\text{H}_2\text{O}_2]^4 [\text{G}]}{(1 + K_1 [\text{H}_2\text{O}_2])^2}$	$\frac{1}{\sqrt{k_2 K_1^2}} + \frac{K_1 [\text{H}_2\text{O}_2]^2}{\sqrt{k_2 K_1^2}} = \frac{[\text{H}_2\text{O}_2]^2 [\text{G}]^{1/2}}{-r_G^{1/2}} \quad (\text{ER2})$

Table 6.9 (Cont.) Surface reaction kinetic models used to fit the glycerol conversion

Model	Reaction mechanism	Rate expression	Linearized
ER3	$\begin{aligned} &C_3H_8O_3 + 2X \xrightarrow{K_1} (Int_1 - X) + (Int_2 - X) \\ &H_2O_2 + 2(Int_1 - X) \xrightleftharpoons{k_2} Product - X + X \\ &Product - X \xrightarrow{k_3} Product + X \end{aligned}$	$-r_G = \frac{k_2 K_1 [H_2O_2][G]}{(1 + 2K_1^{1/2}[G]^{1/2})^2}$	$\frac{1}{\sqrt{k_2 K_1}} + \frac{2K_1^{1/2}[G]^{1/2}}{\sqrt{k_2 K_1}} = \frac{[H_2O_2]^{1/2}[G]^{1/2}}{-r_G} \quad (ER3)$
ER4	$\begin{aligned} &C_3H_8O_3 + X \xrightarrow{K_1} C_3H_8O_3 - X \\ &H_2O_2 + 2(C_3H_8O_3 - X) \xrightleftharpoons{k_2} Product - X + X \\ &Product - X \xrightarrow{k_3} Product + X \end{aligned}$	$-r_G = \frac{k_2 K_1^2 [H_2O_2][G]^2}{(1 + K_1[G])^2}$	$\frac{1}{\sqrt{k_2 K_1^2}} + \frac{K_1[G]}{\sqrt{k_2 K_1^2}} = \frac{[H_2O_2]^{1/2}[G]}{-r_G} \quad (ER4)$

Table 6.10 Rate parameters on kinetic rate expression from surface reaction kinetic

Model	k_1	$k_2 \times 10^{-1}$	k_3	$K_1 \times 10^{-1}$	$K_2 \times 10^{-2}$	R^2
LH1-1	a	b	b	b	a	a
LH1-2	b	a	b	a	b	a
LH1-3	b	b	2.53	1.39	6.18	0.9017
LH2-1	a	b	b	b	a	a
LH2-2	b	a	b	a	b	a
LH2-3	b	b	a	a	a	a
LH3-1	a	b	b	b	a	a
LH3-2	b	a	b	a	b	a
LH3-3	b	b	1.37	2.09	24.28	0.9183
LH4-1	a	b	b	b	a	a
LH4-2	b	a	b	a	b	a
LH4-3	b	b	a	a	a	a
ER1	b	0.52	b	15.32	b	0.9796
ER2	b	1.57	b	5.35	b	0.9925
ER3	b	7.34	b	0.54	b	0.8867
ER4	b	1.81	b	2.31	b	0.6075

Note: Units are varied from model to model. The units must then be determined from the rate equation with rate expressed in $\text{mol/L} \cdot \text{min}$ and all concentration in mol/L

^a Negative value

^b No this parameter in the model

Table 6.11 Rate parameters on kinetic rate expression from surface reaction kinetic models tested in fitting the glycerol conversion reaction at 70 °C.

Model	k_1	$k_2 \times 10^{-1}$	k_3	$K_1 \times 10^{-1}$	$K_2 \times 10^{-2}$	R^2
LH1-1	a	b	b	b	a	a
LH1-2	b	a	b	a	b	a
LH1-3	b	b	3.36	1.27	2.85	0.9410
LH2-1	a	b	b	b	a	a
LH2-2	b	a	b	a	b	a
LH2-3	b	b	a	a	a	a
LH3-1	a	b	b	b	a	a
LH3-2	b	a	b	a	b	a
LH3-3	b	b	1.67	1.39	6.97	0.9379
LH4-1	a	b	b	b	a	a
LH4-2	b	a	b	a	b	a
LH4-3	b	b	a	a	a	a
ER1	b	0.64	b	10.66	b	0.9794
ER2	b	2.16	b	4.37	b	0.9918
ER3	b	5.47	b	3.91	b	0.9206
ER4	b	2.60	b	2.06	b	0.3977

Note: Units are varied from model to model. The units must then be determined from the rate equation with rate expressed in $\text{mol/L} \cdot \text{min}$ and all concentration in mol/L

^a Negative value

^b No this parameter in the model

Table 6.12 Rate parameters on kinetic rate expression from surface reaction kinetic models tested in fitting the glycerol conversion reaction at 80 °C.

Model	k_1	$k_2 \times 10^{-1}$	k_3	$K_1 \times 10^{-1}$	$K_2 \times 10^{-2}$	R^2
LH1-1	a	b	b	b	a	a
LH1-2	b	a	b	a	b	a
LH1-3	b	b	4.10	1.03	1.16	0.9226
LH2-1	a	b	b	b	a	a
LH2-2	b	a	b	a	b	a
LH2-3	b	b	a	a	a	a
LH3-1	a	b	b	b	a	a
LH3-2	b	a	b	a	b	a
LH3-3	b	b	2.15	1.17	3.18	0.9409
LH4-1	a	b	b	b	a	a
LH4-2	b	a	b	a	b	a
LH4-3	b	b	a	a	a	a
ER1	b	0.86	b	8.97	b	0.9806
ER2	b	2.93	b	3.50	b	0.9917
ER3	b	8.96	b	0.94	b	0.8930
ER4	b	3.43	b	2.18	b	0.5703

Note: Units are varied from model to model. The units must then be determined from the rate equation with rate expressed in mol/L•min and all concentration in mol/L

^a Negative value

^b No this parameter in the model

Table 6.13 Rate parameters on kinetic rate expression from surface reaction kinetic models tested in fitting the glycerol conversion reaction at 90 °C.

Model	k_1	$k_2 \times 10^{-1}$	k_3	$K_1 \times 10^{-1}$	$K_2 \times 10^{-2}$	R^2
LH1-1	a	b	b	b	a	a
LH1-2	b	a	b	a	b	a
LH1-3	b	b	4.90	0.93	0.67	0.9118
LH2-1	a	b	b	b	a	a
LH2-2	b	a	b	a	b	a
LH2-3	b	b	a	a	a	a
LH3-1	a	b	b	b	a	a
LH3-2	b	a	b	a	b	a
LH3-3	b	b	2.82	0.75	2.34	0.9396
LH4-1	a	b	b	b	a	a
LH4-2	b	a	b	a	b	a
LH4-3	b	b	a	a	a	a
ER1	b	0.86	b	8.97	b	0.9659
ER2	b	2.93	b	3.50	b	0.9872
ER3	b	8.54	b	2.20	b	0.8373
ER4	b	6.13	b	1.69	b	0.3999

Note: Units are varied from model to model. The units must then be determined from the rate equation with rate expressed in mol/L•min and all concentration in mol/L

^a Negative value

^b No this parameter in the model

From parameters listed in Table 6.10 to 6.13, one cannot find the value of parameters from the regression models in case of using the adsorption step of reactant as a rate-determining step, i.e. LH1-1, LH1-2, LH2-1, LH2-2, LH3-1, LH3-2, LH4-1 and LH4-2 models because negative values were obtained and the parameters did not correspond to the power law model. By using the surface reaction step as a rate-determining step, LH1-3, LH3-3, ER1, ER2, ER3 and ER4 models, positive values of kinetic parameters were observed. Considering R^2 from all six models (LH1-3, LH3-3, ER1, ER2, ER3 and ER4 models), it is worth noting that the values of R^2 in and ER2 model were ranged from 0.98 to 0.99 which are highly acceptable. It is easy to choose ER2 model to be the best model for predicting rate of reaction and mechanism of glycerol conversion on V-SiW/HZSM-5 catalyst in our study. For this model, assuming the reaction between adsorbed oxygen molecule on the active site, obtained from H_2O_2 dissociation, and glycerol molecule provided the best fit with the experimental results. However, desorption of the reaction product is an irreversible reaction. The surface reaction step as a rate-determining step was investigated.

The values of kinetic parameter, i.e. k (rate constant) and K_i (equilibrium constant) on the kinetic rate expression versus temperature are expressed by the Arrhenius and the Van't Hoff equation, respectively as shown in Eq.(6.27) and (6.28).

$$k = k_0 \exp\left\{\frac{-E_R}{RT}\right\} \quad (6.27)$$

And

$$K_i = K_{i,0} \exp\left\{\frac{-\Delta H_{ad,i}}{RT}\right\} \quad (6.28)$$

where

E_R	the activation energy (kJ/mol)
$\Delta H_{ad,i}$	the heat of adsorption (kJ/mol)
k_0	the frequency factor
$K_{i,0}$	the adsorption coefficient (Gotz & Lanny, 1996)

The activation energy can be found from Arrhenius plot (Figure 6.23) based on this surface reaction mechanism of glycerol conversion over this catalyst as being 28.57 kJ/mol. The parameter of heat of oxygen adsorption can be found from the Van't Hoff plot (Figure 6.24) as being 18.45 kJ/mol. Although the reaction mechanism on the surface reaction over the catalyst from the rate expression is consistent with experimental results, errors are probably high because there are several factors involved (Richard, 1996). Therefore, the reaction mechanism proposed in this research is the only mechanism consistent with the experimental data.

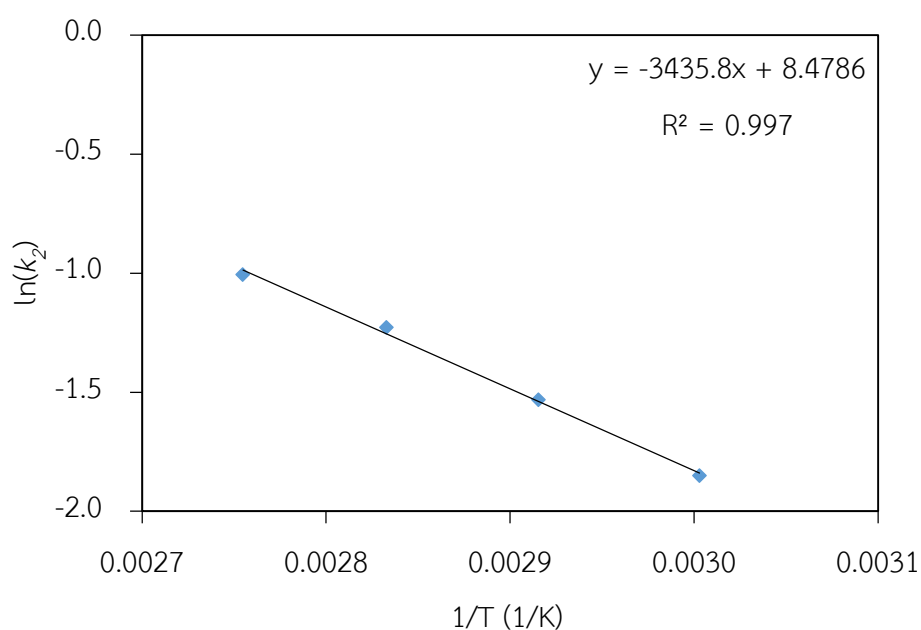


Figure 6.24 Relation of $\ln(k_2)$ vs. $1/T$ (Arrhenius Plot) from the surface reaction kinetic Eley-Rideal model (model ER2).

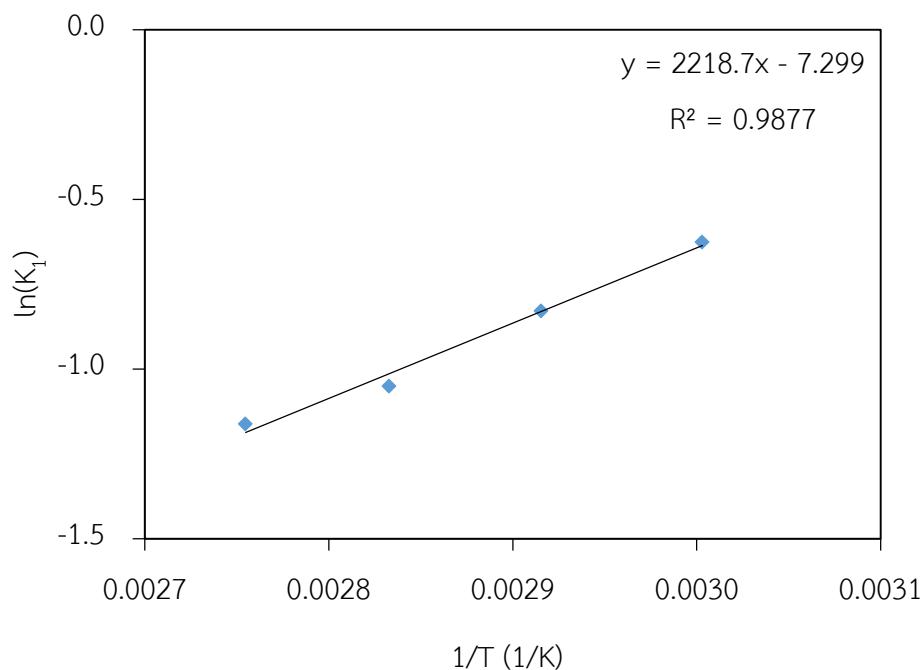


Figure 6.25 Relation of $\ln(K_1)$ vs. $1/T$ (Van't Hoff's Plot) from the surface reaction kinetic Eley-Rideal model (model ER2).

6.4 Reusability test

To test the stability of the metal-doped SiW/HZSM-5 catalyst, the V-SiW/HZSM-5 catalyst at V loading of 6 wt.%, one of which showed the best catalytic performance, has been chosen to reusing for several cycles of reaction. As demonstrated in Figure 6.25, both glycerol conversion and yield of acrylic acid decreased as the increasing cycle of catalyst used. This might be attributed to the change of surface properties of acid catalyst after utilization. Also, the carbon balance decreased drastically from 93.48% to 28.48% after six cycles used, indicating the conversion of glycerol to undesired/non-measurable products. As demonstrated in Table 6.14, the textural properties of used catalysts changed significantly. The average pore diameter increased almost 1.80-fold, while the BET surface and pore volume decreased 1.28- and 1.41-fold, respectively. This indicates the pore widening and coalescence of neighboring pores in the presence of long reaction time. The surface acidity of the used V6-SiW/HZSM-5 catalyst was determined by NH_3 -TPD analysis as shown in Figure 6.26. The NH_3 -TPD peaks of used V6-SiW/HZSM-5 catalyst

shifted to low temperature at weak- and medium- strength acid sites and slightly loss some intensity around 1.34-fold (Figure 6.26), indicating the loss of acid quantity during the reaction. This demonstrates that the V6-SiW/HZSM-5 catalyst prepared by the proposed method tended to be less efficient for reuse. Thus, further work should be carried out to achieve the reusability of such solid acid catalyst and the results will be reported in the future.

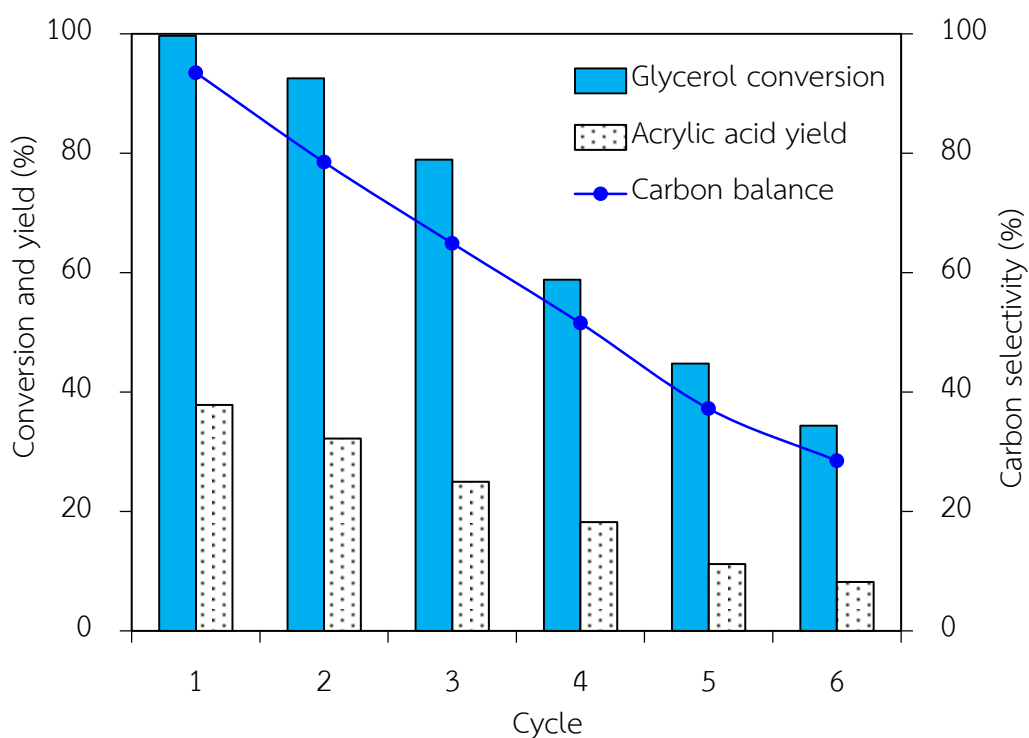


Figure 6.26 Catalytic performance of V6-SiW/HZSM-5 catalyst used in consecutive one-pot conversion of glycerol to acrylic acid.

Table 6.14 Textural properties and surface chemistry of V6-SiW/HZSM-5 catalyst and after use in glycerol conversion for 6 catalytic cycles.

Catalyst	Textural properties			Surface chemistry	
	BET surface area (m ² /g)	Pore volume (cm ³ /g)	Average pore diameter (Å)	Acid amount (mmol NH ₃ /g Cat.)	Total acidity (mmol NH ₃ /g Cat.)
V6-SiW/HZSM-5	222	0.145	2.58	1.54 (44-255 °C) 0.99 (255-395 °C)	2.53
V6-SiW/HZSM-5 ^a (used catalyst)	164	0.103	4.65	1.25 (37-218 °C) 0.63 (225-379 °C)	1.88

^a After utilization for 6 times

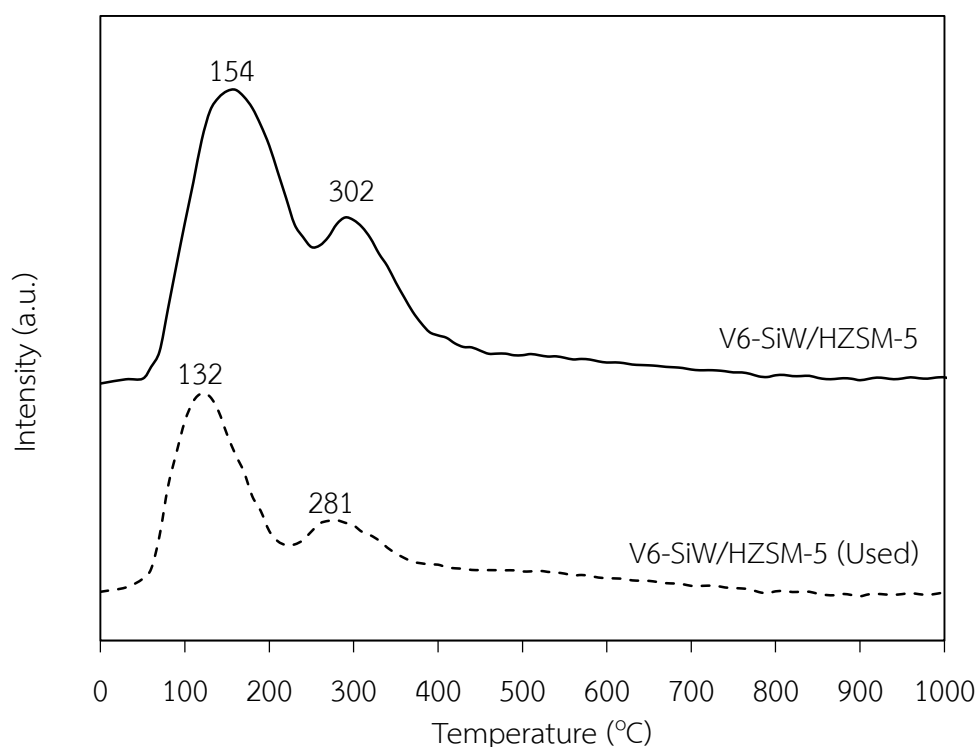


Figure 6.27 NH₃-TPD profiles of fresh V6-SiW/HZSM-5 catalysts and after use in glycerol conversion for 6 catalytic cycles

CHAPTER VII

CONCLUSIONS AND RECOMMENDATIONS

This work was carried out to determine the optimum conditions for conversion of glycerol to acrylic acid. The experiment of glycerol conversion was divided into three parts.

The first part studied the conversion of glycerol to acrylic acid by using Al_2O_3 -supported POM catalysts. The use of Al_2O_3 -supported POM catalysts in a one-pot process for glycerol conversion to acrylic acid was successfully performed in liquid phase. The glycerol conversion and product yield acrylic acid yield were examined in the 2.74 mol/L H_2O_2 over 30 wt.% SiW/ Al_2O_3 catalyst with 4 wt.% catalyst loading at 90 °C. The optimum conditions to provide the highest glycerol conversion of around 83.78% and the yield of glycolic acid, formic acid, acetic acid, acrolein and acrylic acid of 15.34%, 7.90%, 18.83%, 5.44% and 25.11%, respectively. At the end of this part, a reaction pathway of glycerol conversion in the presence of Al_2O_3 -supported POM catalysts was proposed.

In the part of the conversion of glycerol to acrylic acid by using SiW/HZSM-5 catalyst, the optimum condition was found at 90 °C by the addition of 2.74 mol/L H_2O_2 in the presence of SiW/HZSM-5 catalyst with 30 wt.% SiW loading. At this condition was found the glycerol conversion of around 85.54% and the yield of glycolic acid, formic acid, acetic acid, acrolein and acrylic acid of about 16.89%, 9.53%, 19.51%, 7.47% and 30.57%, respectively. The rate of glycerol conversion can be explained by a pseudo-first order reaction with respect to glycerol concentration. According to the Arrhenius's equation, plot of kinetic rate versus temperature provides the apparent activation energy of 29.58 kJ/mol.

For the last part, the doping of vanadium (V) on the surface SiW/HZSM-5 can promote the conversion of glycerol up to 99.67% and providing the yield of glycolic acid, formic acid, acetic acid, acrolein, acrylic acid and propionic acid of 18.45%, 12.03%, 23.62%, 0.25%, 36.23% and 7.06%, respectively. The rate of glycerol conversion over the V-SiW/HZSM-5 catalyst with 6 wt.% V loading can be explained by a pseudo-first order reaction and also the Arrhenius's equation provides the

apparent activation energy of 26.63 kJ/mol. For the surface reaction kinetic models of the best catalyst, considering R^2 from all six models, it is worth noting that the value of R^2 in and ER2 model ranged from 0.98 to 0.99 which are highly acceptable. It is easy to choose ER2 model to be the best model for predicting rate of reaction and mechanism of glycerol conversion on V-SiW/HZSM-5 catalyst in our study. The stability of V-SiW/HZSM-5 catalyst at 6 wt.% V loading had no significant to reusing for several cycles of reaction.

Recommendations

To achieve a higher yield of acrylic acid, the catalytic test in the gas phase was suggested for further study.

To improve the stability of the catalysts, we suggest that encapsulation method for catalyst preparation was an interesting way to achieve a high performance of the POM catalysts.

In addition, we suggest a further study on the benefit or commercialization of other by-products from the conversion of glycerol such as glycolic acid, formic acid, propionic acid, 1,2-propanediol and 1,3-propanediol.

REFERENCES

- Ai, M. (1981). Characteristics of heteropoly compounds as catalysts for selective oxidation. *Journal of Catalysis*, 71, 88-98.
- Ali, M. A., Brisdon, B., & Thomas, W. J. (2003). Alternative routes for catalyst preparation: use of ultrasound and microwave irradiation for the preparation of vanadium phosphorus oxide catalyst and their activity for hydrocarbon oxidation. *Applied Catalysis A: General*, 252, 1-8.
- Ancillotti, F., & Fattore, V. (1998). Oxygenate fuels: Market expansion and catalytic aspect of synthesis. *Fuel Processing Technology*, 57(3), 163-194.
- ASAIM. (2014, 01 14). Glycerol market analysis. from http://www.asaimsea.com/download_doc.php.
- Atia, H., Armbruster, U., & Martin, A. (2008). Dehydration of glycerol in gas phase using heteropolyacid catalysts as active compounds. *Journal of Catalysis*, 258(1), 71-82. doi: 10.1016/j.jcat.2008.05.027
- Atia, H., Armbruster, U., & Martin, A. (2011). Influence of alkaline metal on performance of supported silicotungstic acid catalysts in glycerol dehydration towards acrolein. *Applied Catalysis A: General*, 393(1-2), 331-339. doi: 10.1016/j.apcata.2010.12.015
- Babou, F., Coudurier, G., & Viedrine, J. C. (1995). Acidic Properties of Sulfated Zirconia: An Infrared Spectroscopic Study. *Journal of Catalysis*, 152, 341-349.
- Bardin, B. B., Bordawekar, S. V., Neurock, M., & Davis, R. J. (1998). Acidity of Keggin type heteropoly compounds evaluated by catalytic probe reactions, sorption microcalorimetry, and density functional quantum chemical calculations. *The Journal of Physical Chemistry B*, 102, 10817-10825.
- Barros, I. C. L., Braga, V. S., Pinto, D. S., de Macedo, J. L., Filho, G. N. R., & Dias, J. A. (2008). Effects of niobium addition on ZSM-5 studied by thermal and spectroscopy methods. *Microporous and Mesoporous Materials*, 109, 485-493.
- Bineesh, K. V., Kim, S.-Y., Jermy, B. R., & Park, D.-W. (2009). Synthesis, characterization and catalytic performance of vanadia-doped delaminated zirconia-pillared

- montmorillonite clay for the selective catalytic oxidation of hydrogen sulfide. *Journal of Molecular Catalysis A: Chemical*, 308(1-2), 150-158. doi: 10.1016/j.molcata.2009.04.002
- Bordoloi, A., Vinu, A., & Halligudi, S. B. (2007). Oxyfunctionalisation of adamantane using inorganic-organic hybrid materials based on isopoly and heteropoly anions: Kinetics and mechanistic studies. *Applied Catalysis A: General*, 33(1), 143-152.
- Chai, S., Wang, H., Liang, Y., & Xu, B. (2007). Sustainable production of acrolein: Gas-phase dehydration of glycerol over Nb₂O₅ catalyst. *Journal of Catalysis*, 250(2), 342-349. doi: 10.1016/j.jcat.2007.06.016
- Chen, L., Li, L., & Li, G. (2008). Synthesis of CuO nanorods and their catalytic activity in the thermal decomposition of ammonium perchlorate. *Journal of Alloys and Compounds*, 464, 532-536.
- Chieragato, A., Basile, F., Concepción, P., Guidetti, S., Liosi, G., Soriano, M. D., . . . Nieto, J. M. L. (2012). Glycerol oxidehydration into acrolein and acrylic acid over W-V-Nb-O bronzes with hexagonal structure. *Catalysis Today*, 197(1), 58-65. doi: 10.1016/j.cattod.2012.06.024
- Chieragato, A., Soriano, M. D., Basile, F., Liosi, G., Zamora, S., Concepción, P., . . . López Nieto, J. M. (2014). One-pot glycerol oxidehydration to acrylic acid on multifunctional catalysts: Focus on the influence of the reaction parameters in respect to the catalytic performance. *Applied Catalysis B: Environmental*, 150-151, 37-46. doi: 10.1016/j.apcatb.2013.11.045
- Chino, N., & Okubo, T. (2005). Nitridation Mechanism of Mesoporous Silica: SBA-15. *Microporous and Mesoporous Materials*, 87(1), 15-22.
- Damyanova, S., Fierro, J. L. G., Sobrados, I., & Sanz, J. (1999). Surface behavior of supported 12-heteropoly acid as revealed by nuclear magnetic resonance, X-ray photoelectron spectroscopy, and Fourier transform infrared techniques. *Langmuir*, 15, 469-476.
- Damyanova, S., Perez, C. A., Schmal, M., & Bueno, J. M. C. (2002). Characterization of ceria-coated alumina carrier. *Applied Catalysis A: General*, 234 271-282.

- Delak, K. M., Farrar, T. C., & Sahai, N. (2005). ^{29}Si NMR sensitivity enhancement methods for the quantitative study of organosilicate hydrolysis and condensation. *Journal of Non-Crystalline Solids*, 351(27-29), 2244-2250. doi: 10.1016/j.jnoncrysol.2005.05.013
- Deleplanque, J., Dubois, J. L., Devaux, J. F., & Ueda, W. (2010). Production of acrolein and acrylic acid through dehydration and oxydehydration of glycerol with mixed oxide catalysts. *Catalysis Today*, 157(1-4), 351-358. doi: 10.1016/j.cattod.2010.04.012
- Deltcheff, C. R., Fournier, M., Franck, R., & Thouvenot, R. (1983). Vibration Investigations of Polyoxometalates. 2. Evidence for Anion-Anion Interaction in Molybdenum (VI) and Tungsten(VI) Compounds Related to the Keggin Structure. *Inorganic Chemistry Communications*, 22, 207-216.
- Demirel, S., Lucas, M., Warna, J., Salmi, T., Murzin, D., & Claus, P. (2007). Reaction kinetics and modeling of the gold catalysed glycerol oxidation. *Topics in Catalysis*, 44, 299-305.
- Dharmadi, Y., Murarka, A., & Gonzalez, R. (2006). Anaerobic fermentation of glycerol by *Escherichia coli*: a new platform for metabolic engineering. *Biotechnology and Bioengineering*, 94(5), 821-829.
- Digitallibrary. (2014). Manufacture of acrylic acid by partial oxidation. Retrieved 01 22 <http://digitallibrary.srmuniv.ac.in/dspace/bitstream/123456789/1846/1/4001.pdf>.
- EMO. (2014, 01 15). Biodiesel Market. from <http://www.emerging-markets.com/biodiesel/>.
- Fang, K., Ren, J., & Sun, Y. (2005). Effect of nickel precursors on the performance of Ni/AlMCM-41 catalysts for n-dodecane hydroconversion. *Journal of Molecular Catalysis A: Chemical*, 229, 51-58.
- Fornasiero, P., Balducci, G., Di Monte, R., Kašpar, J., Sergo, V., Gubitosa, G., . . . Graziani, M. (1996). Modification of the redox behaviour of CeO_2 induced by structural doping with ZrO_2 . *Journal of Catalysis*, 164, 173-183.

- Gotz, V., & Lanny, D. S. (1996). Ignition and extinction in the catalytic oxidation of hydrocarbons over platinum. *AIChE Journal*, 42, 1077-1087. . *AIChE Journal*, 42, 1077-1087.
- Guidechem.com. (2014). Retrieved 07 24, from <http://www.guidechem.com/product/>
- Hill, C. L., & Prosser-McCartha, C. M. (1995). Homogeneous catalysis by transition metal oxygen anion clusters. *Coordination Chemistry Reviews*, 143, 407-455.
- Hudlicky, M. (1990). *Oxidation in organic Chemistry*. ACS Monograph-Washington DC.
- HyperPhysics. (2014). Standard electrode potential table. Retrieved 05 20 <http://hyperphysics.phy-astr.gsu.edu/hbase/tables/electpot.html>.
- Icis.com. (2014). Retrieved 07 24, from <http://www.icis.com/about/price-reports/>
- ISTC. (2006). Feasibility report, small scale biodiesel production. *Waste Management and Research Center*.
- Jin, H., Yi, X., Sun, X., Qiu, B., Fang, W., Weng, W., & Wan, H. (2010). Influence of H₄SiW₁₂O₄₀ loading on hydrocracking activity of non-sulfide Ni-H₄SiW₁₂O₄₀/SiO₂ catalysts. *Fuel*, 89(8), 1953-1960. doi: 10.1016/j.fuel.2009.11.031
- João, R. M. A., Fávaro, L. C. L., & Quirino, B. F. (2012). Biodiesel biorefinery: opportunities and challenges for microbial production of fuels and chemicals from glycerol waste. *Biotechnology for Biofuels*, 5, 48-54. doi: 10.1186/1754-6834-5-48
- Kang, S. H., Ryu, J. H., Kim, J. H., Prasad, P. S. S., Bae, J. W., Cheon, J. Y., & Jun, K. W. (2011). ZSM-5 supported cobalt catalyst for the direct production of gasoline range hydrocarbons by Fischer-Tropsch synthesis. *Catalysis Letter*, 141, 1464-1471.
- Kanjina, W., & Trakarnpruk, W. (2009). Heteropolyoxometalate catalysts for oxidation of alcohols with H₂O₂ under green condition. *SILPAKORN UNIVERSITY SCIENCE AND TECHNOLOGY JOURNAL*, 3(1), 7-12.
- Kim, H.-J., Shul, Y.-G., & Han, H. (2006). Synthesis of heteropolyacid (H₃PW₁₂O₄₀)/SiO₂ nanoparticles and their catalytic properties. *Applied Catalysis A: General*, 299, 46-51.

- Kim, Y. T., Jung, K.-D., & Park, E. D. (2010). Gas-phase dehydration of glycerol over ZSM-5 catalysts. *Microporous and Mesoporous Materials*, 131(1-3), 28-36. doi: 10.1016/j.micromeso.2009.11.037
- Kim, Y. T., Jung, K.-D., & Park, E. D. (2011). Comparative study for gas-phase dehydration of glycerol over H-zeolites. *Applied Catalysis A: General*, 393, 275-287.
- Klose, F., Wolff, T., Lorenz, H., Seidel-Morgenstern, A., Suchorski, Y., M., P., & Weiss, H. (2007). Active Species on γ -Alumina Supported Vanadia Catalysts: Nature and Reducibility. *Journal of Catalysis*, 247, 176-193.
- Knothe, G., Gerpen, J. V., & Krahl, J. (2005). *The Biodiesel Handbook* (G. Knothe, J. V. Gerpen & J. Krahl Eds. Vol. 46). Champaign, Illinois: AOCS Press.
- Koranne, M. M., Goodwin, J. G. J., & Marcelin, G. (1994). Characterization of Silica-and Alumina-Supported Vanadia Catalysts Using Temperature Programmed Reduction. *Journal of Catalysis*, 148(1), 369-377.
- Kozhevnikov, I. V. (1995). Homogeneous catalysis by transition metal oxygen anion clusters. *Catalysis Reviews: Science and Engineering*, 37, 311-455.
- Kozhevnikov, I. V. (1998). Catalysis by heteropoly acids and multicomponent and multicomponent polyoxometalates in liquid-phase reactions. *Chemical Reviews*, 98, 171-198.
- Lee, S. M., & Hong, S. C. (2015). Promotional effect of vanadium on the selective catalytic oxidation of NH_3 to N_2 over Ce/V/TiO₂ catalyst. *Applied Catalysis B: Environmental*, 163, 30-39. doi: 10.1016/j.apcatb.2014.07.043
- Lee, S. M., Kim, S. S., & Hong, S. C. (2012). Systematic mechanism study of the high temperature SCR of NO_x by NH_3 over W/TiO₂ catalyst. *Chemical Engineering Science*, 79, 177-185.
- Lercher, J. A., & Jentys, A. (2007). *Introduction to Zeolite Science and Practise 3rd revised Edition* In (J. Cejka, H. V. Bekkum, A. Corma & F. Schuth Eds.). Amsterdam: Elsevier.
- Leung, D. Y. C., Wu, X., & Leung, M. K. H. (2010). A review on biodiesel production using catalyzed transesterification. *Applied Energy*, 87, 1083-1095.

- Li, G., Ding, Y., Wang, J., Wang, X., & Suo, J. (2007). New progress of Keggin and Wells-Dawson type polyoxometalates catalyze acid and oxidative reactions. *Journal of Molecular Catalysis A: Chemical*, 262, 67-76.
- Lili, N., Yunjie, D., Weimiao, C., Leifeng, G., Ronghe, L., Yuan, L., & Qin, X. (2008). Glycerol dehydration to acrolein over activated carbon-supported silicotungstic acids. *Chinese Journal of Catalysis*, 29(3), 212-214
- Liu, S. X., Wang, C. M., Zhai, H. J., Li, D. H., & Wang, E. B. (2004). Synthesis and crystal structures of novel Keggin and Dawson polyoxometalates containing amantadine. *Chinese Chemical Letters*, 15(2), 216-219.
- Luo, M.-F., & Zheng, X.-M. (1999). Redox behaviour and catalytic properties of Ce_{0.5}Zr_{0.5}O₂-supported palladium catalysts. *Applied Catalysis A: General*, 189, 15-21.
- Ma, F., & Hanna, M. A. (1999). Biodiesel production: a review. *Bioresour Technol*, 70, 1-15.
- Maglinao, R. L., & He, B. B. (2011). Catalytic thermochemical conversion of glycerol to simple and polyhydric alcohols using Raney nickel catalyst. *Industrial & Engineering Chemistry Research*, 50, 6028-6033.
- Marchal-Rochand, C., & Millet, J. M. M. (2001). Phosphomolybdic heteropolycompounds as oxidation catalysts. Effect of transition metals as counter-ions. *Journal of Chemistry*, 4, 321-329.
- Mauro, C., & Silvia, G. (2014). Hybrid Materials Based on the Embedding of Organically Modified Transition Metal Oxoclusters or Polyoxometalates into Polymers for Functional Applications: A Review. *Materials*, 7(5), 3956-3989.
- May, N., & Peter, C. B. (2012). A comprehensive comparison of transition-metal and actinyl polyoxometalates *Chemical Society Reviews*, 41, 7354-7367.
- Moffat. (2001). *Metal-Oxygen Clusters-The Surface and Catalytic Properties of Heteropoly Oxometalates*. New York: Kluwer Academic/Plenum Publisher.
- Mori, H., Mizuno, N., & Misono, M. (1991). Factors controlling the selectivity of the oxidation of acetaldehyde over heteropoly compounds. *Journal of Catalysis*, 131(1), 133-142.

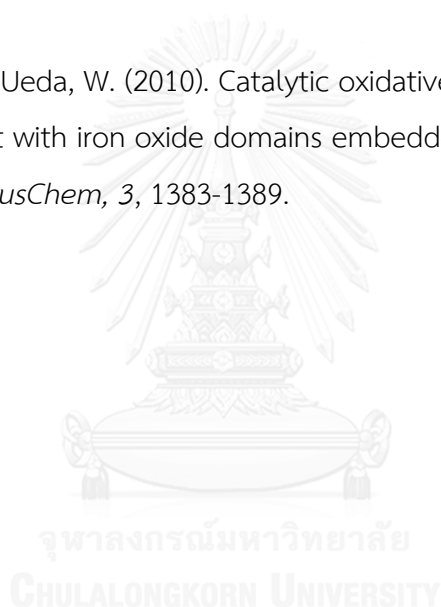
- MRC. (2014). Market price of acrylic acid. Retrieved 01 22
<http://mcgroup.co.uk/researches/acrylic-acid-aa>.
- Muhammad, H. H., Nicholas, F. D., Dazhi, Z., Peter, M., Thomas, E. D., Stuart, H. T., . . . Graham, J. H. (2012). Rubidium- and caesium-doped silicotungstic acid catalysts supported on alumina for the catalytic dehydration of glycerol to acrolein. *Journal of Catalysis*, *286*, 206-213. doi: 10.1016/j.jcat.2011.11.004
- Murugan, B., & Ramaswamy, A. V. (2008). Chemical States and Redox Properties of Mn/CeO₂-TiO₂ Nanocomposites Prepared by Solution Combustion Route. *The Journal of Physical Chemistry C*, *112*, 20429-20442.
- Nexant'sGlobal. (2014). Acrylic acid consumption. Retrieved 01 22
http://www.chemsystems.com/about/cs/news/items/PERP%200809_3_Acrylic%20Acid.cfm.
- Okuhara, T., Mizuno, N., & Misono, M. (1996). Catalytic chemistry of heteropoly compounds. *Advances in Catalysis*, *41*, 113-252.
- Othman, A. I. (2007). Preparation and characterization of copper nanoparticles encapsulated inside ZSM-5 zeolite and NO adsorption. *Materials Science and Engineering: A*, *459*, 294-302.
- Ott, L., Bicker, M., & Vogel, H. (2006). Catalytic dehydration of glycerol in sub- and supercritical water: a new chemical process for acrolein production. *Green Chemistry*, *8*, 214-220.
- Padiyan, D. P., Ethilton, S. J., & Paulraj, K. (2000). Protonic conductivity and photoconductivity studies on H₃PW₁₂O₄₀-21H₂O single crystals. *Crystal Research and Technology*, *35*(1), 87-94.
- Pawelec, B., Damyanova, S., Mariscal, R., Fierro, J. L. G., Sobrados, I., Sanz, J., & Petrov, L. (2004). HDS of dibenzothiophene over polyphosphates supported on mesoporous silica. *Journal of Catalysis*, *223*, 86-97.
- Pieck, C. L., de Val, S., Granados, M. L., Banares, M. A., & Fierro, J. L. G. (2002). Bulk and Surface Structures of V₂O₅/ZrO₂ Systems and Their Relevance for o-Xylene Oxidation. *Langmuir*, *18*, 2642-2648.
- Popa, A., Sasca, V., Kis, E. E., Neducin, R. M., Bokorov, M. T., & Halasz, J. (2005). Structure and texture of some keggin type hetero-polyacids supported on

- silica and titania. *Journal of Optoelectronics and Advanced Materials*, 7(6), 3169-3179.
- Pope, M. T. (1983). *Heteropoly and Isopoly Oxometalates*. New York: Springer-Verlag, Berlin.
- Rao, K. T. V., Rao, P. S. N., Nagaraju, P., Prasad, P. S. S., & Lingaiah, N. (2009). Room temperature selective oxidation of toluene over vanadium substituted polyoxometalate catalysts. *Journal of Molecular Catalysis A: Chemical*, 303(1-2), 84-89. doi: 10.1016/j.molcata.2009.01.006
- Richard, I. M. (1996). *Principles of adsorption and reaction on solid surfaces*. New York, U.S.A: John Wiley & Sons.
- Rodrigues, E. G., Pereira, M. F. R., Delgado, J. J., Chen, X., & Órfão, J. J. M. (2011). Enhancement of the selectivity to dihydroxyacetone in glycerol oxidation using gold nanoparticles supported on carbon nanotubes. *Catalysis Communications*, 16(1), 64-69.
- Sbioinformatics.com. (2014). Acrylic acid: Various commercial processes. Retrieved 01 22 http://www.sbioinformatics.com/design_thesis/Acrylic_Acid/Acrylic2520acid_Methods-2520of-2520Production.pdf.
- Shen, L., Yin, H., Wang, A., Feng, Y., Shen, Y., Wu, Z., & Jiang, T. (2012). Liquid phase dehydration of glycerol to acrolein catalyzed by silicotungstic, phosphotungstic, and phosphomolybdic acids. *Chemical Engineering Journal*, 180, 277-283. doi: 10.1016/j.cej.2011.11.058
- Shen, L., Yin, H., Wang, A., Lu, X., & Zhang, C. (2014). Gas phase oxidehydration of glycerol to acrylic acid over Mo/V and W/V oxide catalysts. *Chemical Engineering Journal*, 244, 168-177. doi: 10.1016/j.cej.2014.01.051
- Song, I. K., & Barteau, M. A. (2002). Bulk redox properties of heteropolyacids determined from surface properties of nanostructured heteropolyacid monolayers. *Journal of Molecular Catalysis A: Chemical*, 182-183, 185-193.
- Soriano, M. D., Concepción, P., Nieto, J. M. L., Cavani, F., S., G., & Trevisanut, C. (2011). Tungsten-Vanadium mixed oxides for the oxidehydration of glycerol into acrylic acid. *Green Chemistry*, 13, 2954-2962.

- Staiti, P., Freni, S., & Hocevar, S. (1999). Synthesis and characterization of proton-conducting materials containing dodecatungstophosphoric and dodecatungstosilic acid supported on silica. *Journal of Power Sources* 79, 250-255.
- Stangar, U. L., Groselj, N., Orel, B., & Colomban, P. (2000). Structure of and interactions between P/SiWA Keggin nanocrystals dispersed in an organically modified electrolyte membrane. *Chemistry of Materials*, 12(12), 3745–3753.
- Subramanian, K. A., Singal, S. K., Saxena, M., & Singhal, S. (2005). Utilization of liquid biofuels in automotive diesel engines: An indian perspective. *Journal of Biomass and Bioenergy*, 29, 65-72.
- Sunder, A., Hanselmann, R., Frey, H., & Mülhaupt, R. (1999). Controlled synthesis of hyperbranched polyglycerols by ring-opening multibranching polymerization. *Macromolecules*, 32, 4240-4246.
- SunGrantBioWeb. (2014). Chemicals from biorefinery carbohydrates of glycerol. Retrieved 01 22 <http://bioweb.sungrant.org/Technical/Bioproducts/Bioproducts+from+Carbohydrates/Glycerol/Glycerol.htm>.
- Sunivo. (2014). Retrieved 2014, 07 15 <http://www.sunivo.com>
- Suppes, G. J., Chiu, C.-W., Sutterlin, W. R., & Ramos, L. R. (2006). Highly Selective Conversion of Glycerol to Propylene Glycol. *The 2006 Annual Meeting*.
- Suprun, W., Lutecki, M., Haber, T., & Papp, H. (2009). Acidic catalysts for the dehydration of glycerol: Activity and deactivation. *Journal of Molecular Catalysis A: Chemical*, 309(1-2), 71-78. doi: 10.1016/j.molcata.2009.04.017
- Tatibouët, J. M., Montalescot, C., & Brückman, K. (1996). A new method to prepare silica supported heteropolyanion catalysts formation on the silica surface of calcium and magnesium salts of phosphomolybdic acid, H₃PMo₁₂O₄₀. *Applied Catalysis A: General*, 138(1), L1-L6.
- Thanasilp, S., Schwank, J. W., Meeyoo, V., Pengpanich, S., & Hunsom, M. (2013). Preparation of supported POM catalysts for liquid phase oxydehydration of glycerol to acrylic acid. *Journal of Molecular Catalysis A: Chemical*, 380, 49-56.

- Thouvenot, R., Rocchiccioli-Deltcheff, C., & Fournier, M. (1991). ^{31}P NMR MAS Spin-lattice relaxation as a dispersion probe: an easy access to active-site concentration in silica-supported dodecamolybdophosphoric acid. *Journal of the Chemical Society, Chemical Communications*, 19 1352–1354.
- Tichý, J. (1997). Oxidation of acrolein to acrylic acid over vanadium-molybdenum oxide catalysts. *Applied Catalysis A: General*, 157(1-2), 363-385.
- Tsukuda, E., Sato, S., Takahashi, R., & Sodesawa, T. (2007). Production of acrolein from glycerol over silica-supported heteropoly acids. *Catalysis Communications*, 8(9), 1349-1353. doi: 10.1016/j.catcom.2006.12.006
- Uchida, S., Inumaru, K., & Misono, M. (2000). States and dynamic behavior of protons and water molecules in H₃PW₁₂O₄₀ pseudoliquid phase analyzed by solid-state MAS NMR. *Journal of Physical Chemistry B*, 104, 8108–8115.
- Vafaeian, Y., Haghighi, M., & Aghamohammadi, S. (2013). Ultrasound assisted dispersion of different amount of Ni over ZSM-5 used as nanostructured catalyst for hydrogen production via CO₂ reforming of methane. *Energy Conversion and Management*, 76, 1093-1103.
- Wang, F., Dubois, J.-L., & Ueda, W. (2009). Catalytic dehydration of glycerol over vanadium phosphate oxides in the presence of molecular oxygen. *Journal of Catalysis*, 268(2), 260-267. doi: 10.1016/j.jcat.2009.09.024
- Wang, F., Dubois, J.-L., & Ueda, W. (2010). Catalytic performance of vanadium pyrophosphate oxides (VPO) in the oxidative dehydration of glycerol. *Applied Catalysis A: General*, 376(1-2), 25-32. doi: 10.1016/j.apcata.2009.11.031
- Wang, J., Yan, L., Li, G., Wang, X., Ding, Y., & Suo, J. (2005). Mono-substituted Keggin-polyoxometalate complexes as effective and recyclable catalyst for the oxidation of alcohols with hydrogen peroxide in biphasic system. *Tetrahedron Letters*, 46(41), 7023-7027. doi: 10.1016/j.tetlet.2005.08.040
- Wang, S., Yin, Q., Guo, J., Ru, B., & Zhu, L. (2013). Improved Fischer–Tropsch synthesis for gasoline over Ru, Ni promoted Co/HZSM-5 catalysts. *Fuel*, 108, 597-603. doi: 10.1016/j.fuel.2013.02.021

- Watanabe, M., Iida, T., Aizawa, Y., Aida, T. M., & Inomata, H. (2007). Acrolein synthesis from glycerol in hot-compressed water. *Bioresour Technol*, *98*(6), 1285-1290. doi: 10.1016/j.biortech.2006.05.007
- Witsuthammakul, A., & Sooknoi, T. (2012). Direct conversion of glycerol to acrylic acid via integrated dehydration–oxidation bed system. *Applied Catalysis A: General*, *413-414*, 109-116.
- Xiaoli, C., Bouasavanh, S., Hang, W., Hongwei, Z., Xiaohong, W., & Mingxi, H. (2013). Polyoxometalate-based ionic liquid as thermoregulated and environmentally friendly catalyst for starch oxidation. *Applied Catalysis B: Environmental*, *138-139*, 161-166.
- Xu, J., Dubois, J.-L., & Ueda, W. (2010). Catalytic oxidative dehydration of glycerol over a catalyst with iron oxide domains embedded in an iron orthovanadate phase. *ChemSusChem*, *3*, 1383-1389.





APPENDICES

จุฬาลงกรณ์มหาวิทยาลัย
CHULALONGKORN UNIVERSITY

APPENDIX A
EXAMPLE OF CALCULATION

A.1 Calculation of the preparation of supported POM catalysts by using incipient wetness impregnation method

Example: SiW/HZSM-5 catalyst with 30 wt.% SiW loading

$$\begin{aligned} \text{Mass of SiW (g)} &= \frac{\text{Mass of HZSM-5(g)} \times 30 \text{ of SiW loading(\%)}}{100 (\%) - 30 \text{ of SiW loading(\%)}} \\ &= \frac{(5 \times 30)}{(100 - 30)} \\ &= 2.1428 \text{ g} \end{aligned}$$

A.2 Calculation of the preparation of metal-doped SiW/HZSM-5 catalysts by using sequential incipient wetness impregnation method

Example: V-SiW/HZSM-5 catalyst with 6 wt.% V loading

$$\begin{aligned} \text{Mass of V (g)} &= \frac{\text{Mass of SiW/HZSM-5(g)} \times 6 \text{ of V loading(\%)}}{100\% - 6 \text{ of V loading(\%)}} \\ &= \frac{(5 \times 6)}{(100 - 6)} \\ &= 0.3191 \text{ g} \end{aligned}$$

Molecular weight of NaVO_3 = 121.93 g/mol

Molecular weight of V = 50.94 g/mol

So, Mass of V = 0.3191 g

$$\begin{aligned} \text{Mass of NaVO}_3, \text{ g} &= \frac{(\text{MW of NaVO}_3) \times (\text{Mass of V at 6\% of V loading})}{(\text{MW of V})} \\ &= \frac{121.93 \times 0.3191}{50.94} \\ &= 0.7638 \text{ g} \end{aligned}$$

$$\begin{aligned} \text{Stock solution of NaVO}_3 \text{ (\%w/v)} &= \frac{\text{Mass of NaVO}_3 \text{ (g)}}{\text{Volume of solution (ml)}} \times 100 \\ &= \frac{5}{50} \times 100 \\ &= 10 \text{ \%w/v} \end{aligned}$$

$$\begin{aligned} \text{Amount of NaVO}_3 \text{ (ml)} &= \text{Content of NaVO}_3 \text{ (\%w/v)} \times \text{Mass of NaVO}_3 \text{ (g)} \\ &= 10 \times 0.7638 \\ &= 7.6380 \text{ ml} \end{aligned}$$

A.2 Calculation of mobile phase of HPLC

Concentration of H ₂ SO ₄	= 98 wt.%
Density of H ₂ SO ₄	= 1.84 g/cm ³
Molecular weight of H ₂ SO ₄	= 98.08 g/mol

$$\begin{aligned} \text{Molar concentration (mol/L)} &= \frac{10 \times \text{Density (g/cm}^3) \times \text{wt.\% concentration}}{\text{Molecular weight (g/mol)}} \\ &= \frac{10 \times 1.84 \times 98}{98.08} \\ &= 18.38 \text{ mol/L} \end{aligned}$$

Example: 0.05 mM H₂SO₄ in 4000 ml HPLC water

$$\begin{aligned} \text{Volume of H}_2\text{SO}_4 \text{ (ml)} &= \frac{\text{Mobile phase concentration (mol/L)} \times \text{Volume of H}_2\text{O}_2 \text{ (ml)}}{\text{Concentration of H}_2\text{SO}_4 \text{ (mol/L)}} \\ &= \frac{(5 \times 10^{-3}) \times 4000}{18.38} \\ &= 1.0881 \text{ ml} \end{aligned}$$

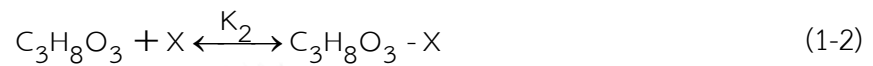
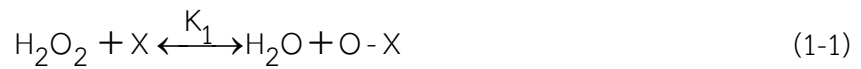
APPENDIX B

KINETIC DERIVATION FROM THE SURFACE REACTION KINETIC MODEL

B.1 Model LH1

Langmuir-Hinshelwood model (dissociative adsorption of H_2O_2 reacts with non-dissociative adsorption of glycerol)

Reaction mechanism



where X is active site on heterogeneous catalyst

G is glycerol molecule

K_1 is equilibrium rate constant (adsorption-desorption) of Eq.(1-1) = (k_1/k_1')

K_2 is equilibrium rate constant (adsorption-desorption) of Eq.(1-2) = (k_2/k_2')

k_3 is the reaction rate constant of Eq.(1-3)

k_4 is the reaction rate constant of Eq.(1-4)

B.1.1 Model LH1-1

If Eq.(1-1) is the rate-determining step of the reaction (the step of H_2O_2 adsorption on the active site). The reaction rate can be expressed as:

$$-r_G = k_1 [H_2O_2] (X) \quad (1-5)$$

At equilibrium, from Eq.(1-2), we get:

$$k_2 [C_3H_8O_3] (X) = k_2' (C_3H_8O_3 - X) \quad (1-6)$$

From Eq.(1-3) and (1-4) we get:

$$k_3 (C_3H_8O_3 - X) (O - X) = 0 \quad (1-7)$$

$$k_4 (\text{Product} - X) = 0 \quad (1-8)$$

Active site balance:

$$1 = (X) + (C_3H_8O_3 - X) + (O - X) + (\text{Product} - X) \quad (1-9)$$

Rearranging Eq.(1-6) to (1-8), we get:

$$(C_3H_8O_3 - X) = K_2[C_3H_8O_3](X) \quad (1-10)$$

$$(O - X) = 0 \quad (1-11)$$

$$(\text{Product} - X) = 0 \quad (1-12)$$

Substitute (O-X), (C₃H₈O₃ - X) and (Product - X) in Eq.(1-9), we get:

$$(X) = \frac{1}{1 + K_2[C_3H_8O_3]} \quad (1-13)$$

Substitute (X) in Eq.(1-5), we get:

$$-r_G = \frac{k_1[H_2O_2]}{1 + K_2[G]} \quad (1-14)$$

B.1.2 Model LH1-2

If Eq.(1-2) is the rate-determining step of the reaction (the step of glycerol adsorption on the active site). The reaction rate can be expressed as:

$$-r_G = k_2[C_3H_8O_3](X) \quad (1-15)$$

At equilibrium, from Eq.(1-1), we get:

$$k_1[H_2O_2](X) = k_1'(O - X) \quad (1-16)$$

From Eq.(1-3) and (1-4), we get Eq.(1-7) and (1-8):

$$k_3(C_3H_8O_3 - X)(O - X) = 0$$

$$k_4(\text{Product} - X) = 0$$

For the active site balance, from Eq.(1-9):

$$1 = (X) + (O - X) + (C_3H_8O_3 - X) + (\text{Product} - X)$$

Rearranging Eq.(1-16), (1-7) and (1-8), we get:

$$(O - X) = K_1[H_2O_2](X) \quad (1-17)$$

$$(C_3H_8O_3 - X) = 0$$

$$(\text{Product} - X) = 0$$

Substitute (O-X), (C₃H₈O₃ - X) and (Product - X) in Eq.(1-9), we get:

$$(X) = \frac{1}{1 + K_1[H_2O_2]} \quad (1-18)$$

Substitute (X) in Eq.(1-16):

$$-r_G = \frac{k_2[G]}{1 + K_1[H_2O_2]} \quad (1-19)$$

B.1.3 Model LH1-3

If Eq.(1-3) is the rate-determining step of the reaction (the step of surface reaction). The reaction rate can be expressed as:

$$-r_G = k_3(C_3H_8O_3 - X)(O - X) \quad (1-20)$$

At equilibrium, from Eq.(1-1) and (1-2), we get Eq.(1-16) and (1-6):

$$k_1[H_2O_2](X) = k'_1(O - X)$$

$$k_2[C_3H_8O_3](X) = k'_2(C_3H_8O_3 - X)$$

From Eq.(1-4), we get Eq.(1-8):

$$k_4(\text{Product} - X) = 0$$

For the active site balance, from Eq.(1-9):

$$1 = (X) + (O - X) + (C_3H_8O_3 - X) + (\text{Product} - X)$$

Rearranging Eq.(1-16), (1.6) and (1-8), we get:

$$(O - X) = K_1[H_2O_2](X)$$

$$(C_3H_8O_3 - X) = K_2[C_3H_8O_3](X)$$

$$(\text{Product} - X) = 0$$

Substitute (O-X), (C₃H₈O₃ - X) and (Product - X) in Eq.(1-9), we get:

$$(X) = \frac{1}{1 + K_1[H_2O_2] + K_2[C_3H_8O_3]} \quad (1-21)$$

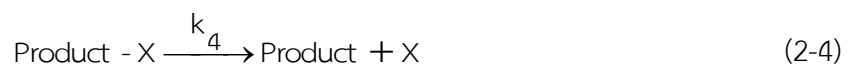
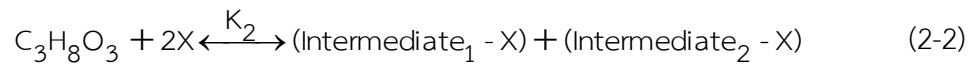
Substitute (X) in Eq.(1-9):

$$-r_G = \frac{k_3 K_1 K_2 [H_2O_2][G]}{(1 + K_1[H_2O_2] + K_2[G])^2} \quad (1-22)$$

B.2 Model LH2

Langmuir-Hinshelwood model (dissociative adsorption of H_2O_2 reacts with dissociative adsorption of glycerol)

Reaction mechanism



where K_1 is equilibrium rate constant (adsorption-desorption) of Eq.(2-1) = (k_1/k'_1)

K_2 is equilibrium rate constant (adsorption-desorption) of Eq.(2-2) = (k_2/k'_2)

k_3 is the reaction rate constant of Eq.(2-3)

k_4 is the reaction rate constant of Eq.(2-4)

B.2.1 Model LH2-1

If Eq.(2-1) is the rate-determining step of the reaction (the step of H_2O_2 adsorption on the active site). The reaction rate can be expressed as:

$$-r_G = k_1[H_2O_2](X) \quad (2-5)$$

At equilibrium, from Eq.(2-2) to (2-4), we get:

$$k_2[C_3H_8O_3](X)^2 = k'_2(\text{Intermediate}_1 - X)(\text{Intermediate}_2 - X) \quad (2-6)$$

From Eq.(2-3) and (2-4), we get:

$$k_3(\text{Intermediate} - X)(O - X) = 0 \quad (2-7)$$

$$k_4(\text{Product} - X) = 0 \quad (2-8)$$

Active site balance:

$$1 = (X) + (O - X) + (\text{Intermediate}_1 - X) + (\text{Intermediate}_2 - X) + (\text{Product} - X) \quad (2-9)$$

Rearranging Eq.(2-6) to (2-8), we get:

$$(\text{Intermediate}_1 - X)(\text{Intermediate}_2 - X) = K_2[\text{C}_3\text{H}_8\text{O}_3](X)^2 \quad (2-10)$$

$$(O - X) = 0 \quad (2-11)$$

$$(\text{Product} - X) = 0 \quad (2-12)$$

Assume $(\text{Intermediate}_1 - X) = (\text{Intermediate}_2 - X) = (\text{Intermediate} - X)$, we can rewrite Eq.(2-10) as:

$$(\text{Intermediate} - X) = K_2^{1/2}[\text{C}_3\text{H}_8\text{O}_3]^{1/2}(X) \quad (2-13)$$

Substitute $(O - X)$, $(\text{Intermediate}_1 - X)$, $(\text{Intermediate}_2 - X)$ and $(\text{Product} - X)$ in Eq.(2-9):

$$(X) = \frac{1}{1 + K_2^{1/2}[\text{C}_3\text{H}_8\text{O}_3]^{1/2} + K_2^{1/2}[\text{C}_3\text{H}_8\text{O}_3]^{1/2}} \quad (2-14)$$

Substitute (X) in Eq.(2-5):

$$-r_G = \frac{k_1[\text{H}_2\text{O}_2]}{1 + 2K_2^{1/2}[\text{G}]^{1/2}} \quad (2-15)$$

B.2.2 Model LH2-2

If Eq.(2-2) is the rate-determining step of the reaction (the step of glycerol adsorption on the active site). The reaction rate can be expressed as:

$$-r_G = k_1[\text{G}](X)^2 \quad (2-16)$$

At equilibrium, from Eq.(2-1), we get:

$$k_1[\text{H}_2\text{O}_2](X) = k_1'(O - X) \quad (2-17)$$

From Eq.(2-3) and (2-4), we get Eq.(2.7) and (2-8):

$$k_3(\text{C}_3\text{H}_8\text{O}_3 - X)(O - X) = 0$$

$$k_4(\text{Product} - X) = 0$$

For the active site balance, from Eq.(2-9):

$$1 = (X) + (O - X) + (\text{Intermediate}_1 - X) + (\text{Intermediate}_2 - X) + (\text{Product} - X)$$

Rearranging Eq.(2-17), Eq.(2-7) and (2-8), we get:

$$(O - X) = K_1 [H_2O_2](X) \quad (2-18)$$

$$(C_3H_8O_3 - X) = 0$$

$$(Product - X) = 0$$

Assume $(Intermediate_1 - X) = (Intermediate_2 - X) = (Intermediate - X)$, from Eq.(2-13):

$$(Intermediate - X) = K_2^{1/2} [C_3H_8O_3]^{1/2} (X)$$

Substitute $(O - X)$, $(Intermediate_1 - X)$, $(Intermediate_2 - X)$ and $(Product - X)$ in Eq.(2-9):

$$(X) = \frac{1}{1 + K_1 [C_3H_8O_3]^{1/2}} \quad (2-19)$$

Substitute (X) in Eq.(2-8):

$$-r_G = \frac{k_2 [G]}{(1 + K_1 [H_2O_2])^2} \quad (2-20)$$

B.2.3 Model LH2-3

If Eq.(2-3) is the rate-determining step of the reaction (the step of surface reaction). The reaction rate can be expressed as:

$$-r_G = k_3 (C_3H_8O_3 - X)(O - X) \quad (2-21)$$

At equilibrium, from Eq.(2-1) and (2-2), we get Eq.(2-17) and (2-6):

$$k_1 [H_2O_2](X) = k_1' (O - X)$$

$$k_2 [C_3H_8O_3](X)^2 = k_2' (Intermediate_1 - X)(Intermediate_2 - X)$$

From Eq.(2-4), we get Eq.(2-8):

$$k_4 (Product - X) = 0$$

For the active site balance, from Eq.(2-9):

$$1 = (X) + (O - X) + (Intermediate_1 - X) + (Intermediate_2 - X) + (Product - X)$$

Rearranging Eq.(2-17), (2-6) and (2-8), we get:

$$(O - X) = K_1 [H_2O_2](X)$$

$$(Intermediate_1 - X)(Intermediate_2 - X) = K_2 [C_3H_8O_3](X)^2$$

$$(Product - X) = 0$$

Assume $(\text{Intermediate}_1 - X) = (\text{Intermediate}_2 - X) = (\text{Intermediate} - X)$, from Eq.(2-13):

$$(\text{Intermediate} - X) = K_2^{1/2} [\text{C}_3\text{H}_8\text{O}_3]^{1/2} (X)$$

Substitute $(O - X)$, $(\text{Intermediate}_1 - X)$, $(\text{Intermediate}_2 - X)$ and $(\text{Product} - X)$ in Eq.(2-9):

$$(X) = \frac{1}{\left(1 + K_1[\text{H}_2\text{O}_2] + 2K_2^{1/2}[\text{C}_3\text{H}_8\text{O}_3]^{1/2}\right)} \quad (2-22)$$

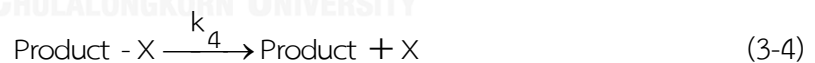
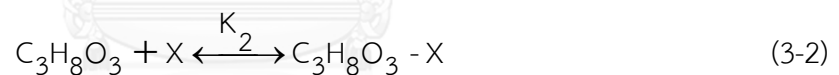
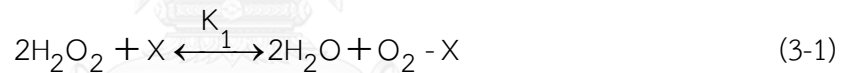
Substitute (X) in Eq.(2-21):

$$-r_G = \frac{k_3 K_1 K_2^{1/2} [\text{H}_2\text{O}_2] [\text{G}]^{1/2}}{\left(1 + K_1[\text{H}_2\text{O}_2] + 2K_2^{1/2}[\text{G}]^{1/2}\right)^2} \quad (2.23)$$

B.3 Model LH3

Langmuir-Hinshelwood model (non-dissociative adsorption of H_2O_2 reacts with non-dissociative adsorption of glycerol)

Reaction mechanism



where K_1 is equilibrium rate constant (adsorption-desorption) of Eq.(3-1) = (k_1/k_1')

K_2 is equilibrium rate constant (adsorption-desorption) of Eq.(3-2) = (k_2/k_2')

k_3 is the reaction rate constant of Eq.(3-3)

k_4 is the reaction rate constant of Eq.(3-4)

B.3.1 Model LH3-1

If Eq.(3-1) is the rate-determining step of the reaction (the step of H_2O_2 adsorption on the active site). The reaction rate can be expressed as:

$$-r_G = k_1 [H_2O_2](X) \quad (3-5)$$

At equilibrium, from Eq.(3-2), we get:

$$k_2 [C_3H_8O_3](X) = k'_2 (C_3H_8O_3 - X) \quad (3-6)$$

From Eq.(3-3) and (3-4), we get:

$$k_3 (C_3H_8O_3 - X)(O_2 - X) = 0 \quad (3-7)$$

$$k_4 (Product - X) = 0 \quad (3-8)$$

Active site balance:

$$1 = (X) + (O_2 - X) + (C_3H_8O_3 - X) + (Product - X) \quad (3-9)$$

Rearranging Eq.(3-6) to (3-8), we get:

$$(C_3H_8O_3 - X) = K_2 [C_3H_8O_3](X) \quad (3-10)$$

$$(O_2 - X) = 0 \quad (3-11)$$

$$(Product - X) = 0 \quad (3-12)$$

Substitute $(O - X)$, $(C_3H_8O_3 - X)$ and $(Product - X)$ in Eq.(3-9):

$$(X) = \frac{1}{1 + K_2 [C_3H_8O_3]} \quad (3-13)$$

Substitute (X) in Eq.(3-5):

$$-r_G = \frac{k_1 [H_2O_2]^2}{1 + K_2 [G]} \quad (3-14)$$

B.3.2 Model LH3-2

If Eq.(3-2) is the rate-determining step of the reaction (the step of glycerol adsorption on the active site). The reaction rate can be expressed as:

$$-r_G = k_2 [C_3H_8O_3](X) \quad (3-15)$$

At equilibrium, from Eq.(3-1), we get:

$$k_1 [H_2O_2]^2 (X) = k'_1 (O_2 - X) \quad (3-16)$$

From Eq.(3-3) and (3-4), we get Eq.(3-7) and (3-8):

$$\begin{aligned}k_3(C_3H_8O_3 - X)(O_2 - X) &= 0 \\k_4(\text{Product} - X) &= 0\end{aligned}$$

For the active site balance, from Eq.(3-9):

$$1 = (X) + (O_2 - X) + (C_3H_8O_3 - X) + (\text{Product} - X)$$

Rearranging Eq.(3-16), (3-7) and (3-8), we get:

$$\begin{aligned}(O_2 - X) &= K_1[H_2O_2]^2(X) & (3-17) \\(C_3H_8O_3 - X) &= 0 \\(\text{Product} - X) &= 0\end{aligned}$$

Substitute $(O_2 - X)$, $(C_3H_8O_3 - X)$ and $(\text{Product} - X)$ in Eq.(3-9):

$$(X) = \frac{1}{1 + K_1[H_2O_2]^2} \quad (3-18)$$

Substitute (X) in Eq.(3-15):

$$-r_G = \frac{k_2[G]}{1 + K_1[H_2O_2]^2} \quad (3-19)$$

B.3.3 Model LH3-3

If Eq.(3-2) is the rate-determining step of the reaction (the step of surface reaction). The reaction rate can be expressed as:

$$-r_G = k_2(C_3H_8O_3 - X)(O_2 - X) \quad (3-20)$$

At equilibrium, followed by Eq.(3-16) and (3-6):

$$\begin{aligned}k_1[H_2O_2]^2(X) &= k_1'(O_2 - X) \\k_2[C_3H_8O_3](X) &= k_2'(C_3H_8O_3 - X)\end{aligned}$$

From Eq.(3-8), we get Eq.(3-8):

$$k_4(\text{Product} - X) = 0$$

For the active site balance, from Eq.(3-9):

$$1 = (X) + (O_2 - X) + (C_3H_8O_3 - X) + (\text{Product} - X)$$

Rearranging Eq.(3-16), (3-6) and (3-8), we get:

$$\begin{aligned}(O_2 - X) &= K_1 [H_2O_2]^2 (X) \\ (C_3H_8O_3 - X) &= K_2 [C_3H_8O_3] (X)\end{aligned}$$

$$(\text{Product} - X) = 0$$

Substitute $(O_2 - X)$, $(C_3H_8O_3 - X)$ and $(\text{Product} - X)$ in Eq.(3-9):

$$(X) = \frac{1}{1 + K_1 [H_2O_2]^2 + K_2 [C_3H_8O_3]} \quad (3-21)$$

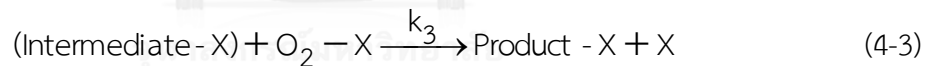
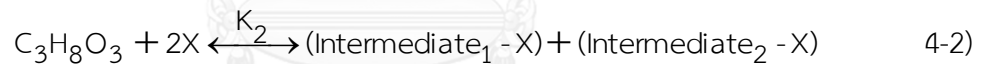
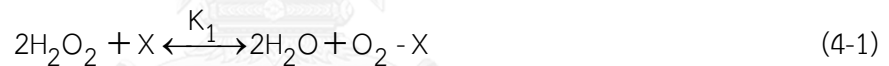
Substitute (X) in Eq.(27):

$$-r_G = \frac{k_3 K_1 K_2 [G] [H_2O_2]^2 [G]}{\left(1 + K_1 [H_2O_2]^2 + K_2 [G]\right)^2} \quad (3-22)$$

B.4 Model LH4

Langmuir-Hinshelwood model (non-dissociative adsorption of H_2O_2 reacts with dissociative adsorption of glycerol)

Reaction mechanism



where K_1 is equilibrium rate constant (adsorption-desorption) of Eq.(4-1) = (k_1/k_{-1})

K_2 is equilibrium rate constant (adsorption-desorption) of Eq.(4-2) = (k_2/k_{-2})

k_3 is the reaction rate constant of Eq.(4-3)

k_4 is the reaction rate constant of Eq.(4-4)

B.4.1 Model LH4-1

If Eq.(4-1) is the rate-determining step of the reaction (the step of H_2O_2 adsorption on the active site). The reaction rate can be expressed as:

$$-r_G = k_1 [H_2O_2]^2 (X) \quad (4-5)$$

At equilibrium, from Eq.(4-2), we get:

$$k_2[C_3H_8O_3](X)^2 = k'_2(\text{Intermediate}_1 - X)(\text{Intermediate}_2 - X) \quad (4-6)$$

From Eq.(4-3) and (4-4), we get:

$$k_3(C_3H_8O_3 - X)(O_2 - X) = 0 \quad (4-7)$$

$$k_4(\text{Product} - X) = 0 \quad (4-8)$$

Active site balance

$$1 = (X) + (O_2 - X) + (\text{Intermediate}_1 - X) + (\text{Intermediate}_2 - X) + (\text{Product} - X) \quad (4-9)$$

Rearranging Eq.(4-6) to (4-8), we get

$$(\text{Intermediate}_1 - X)(\text{Intermediate}_2 - X) = K_2[C_3H_8O_3](X)^2 \quad (4-10)$$

$$(\text{Product} - X) = 0 \quad (4-11)$$

$$(O_2 - X) = 0 \quad (4-12)$$

Assume $(\text{Intermediate}_1 - X) = (\text{Intermediate}_2 - X) = (\text{Intermediate} - X)$, we can rewrite

Eq.(4-10) as:

$$(\text{Intermediate} - X) = K_2^{1/2}[C_3H_8O_3]^{1/2}(X) \quad (4-13)$$

Substitute $(O_2 - X)$, $(\text{Intermediate}_1 - X)$, $(\text{Intermediate}_2 - X)$ and $(\text{Product} - X)$ in Eq.(4-9):

$$(X) = \frac{1}{1 + 2K_2^{1/2}[C_3H_8O_3]^{1/2}} \quad (4-14)$$

Substitute (X) in Eq.(4-5)

$$-r_G = \frac{k_1[H_2O_2]^2}{1 + 2K_2^{1/2}[G]^{1/2}} \quad (4-15)$$

B.4.2 Model LH4-2

If Eq.(4-2) is the rate-determining step of the reaction (the step of glycerol adsorption on the active site). The reaction rate can be expressed as:

$$-r_G = k_1[C_3H_8O_3](X)^2 \quad (4-16)$$

At equilibrium, from Eq.(4-1), we get:

$$k_1[H_2O_2]^2(X) = k'_1(O_2 - X) \quad (4-17)$$

From Eq.(4-3) and (4-4), we get Eq.(4-7) and (4-8):

$$k_3(C_3H_8O_3 - X)(O_2 - X) = 0$$

$$k_4(\text{Product} - X) = 0$$

For the active site balance, from Eq.(4-9):

$$1 = (X) + (O_2 - X) + (\text{Intermediate}_1 - X) + (\text{Intermediate}_2 - X) + (\text{Product} - X)$$

Rearranging Eq.(4-17), (4-7) and (4-8), we get:

$$(O_2 - X) = K_1 [H_2O_2]^2 (X) \quad (4-18)$$

$$(\text{Product} - X) = 0$$

$$(C_3H_8O_3 - X) = 0$$

Assume $(\text{Intermediate}_1 - X) = (\text{Intermediate}_2 - X) = (\text{Intermediate} - X)$, from Eq.(4-13):

$$(C_3H_8O_3 - X) = K_2^{1/2} [C_3H_8O_3]^{1/2} (X)$$

Substitute $(O_2 - X)$, $(\text{Intermediate}_1 - X)$, $(\text{Intermediate}_2 - X)$ and $(\text{Product} - X)$ in Eq.(4-9):

$$(X) = \frac{1}{1 + K_1 [H_2O_2]^2} \quad (4-19)$$

Substitute (X) in Eq.(4-16):

$$-r_G = \frac{k_2 [G]}{(1 + K_1 [H_2O_2]^2)^2} \quad (4-20)$$

B.4.3 Model LH4-3

If Eq.(4-3) is the rate-determining step of the reaction (the step of surface reaction). The reaction rate can be expressed as:

$$-r_G = k_3(C_3H_8O_3 - X)(O_2 - X) \quad (4-21)$$

At equilibrium, from Eq.(4-1) and (4-2), we get Eq.(4-17) and (4-6):

$$k_1 [H_2O_2]^2 (X) = k_1' (O_2 - X)$$

$$k_2 [C_3H_8O_3] (X)^2 = k_2' (\text{Intermediate}_1 - X)(\text{Intermediate}_2 - X)$$

From Eq.(4-4), we get Eq.(4-8):

$$k_4(\text{Product} - X) = 0$$

For the active site balance, from Eq.(4-9):

$$1 = (X) + (O_2 - X) + (\text{Intermediate}_1 - X) + (\text{Intermediate}_2 - X) + (\text{Product} - X)$$

Rearranging Eq.(4-17), (4-6) and (4-8), we get:

$$(O_2 - X) = K_1 [H_2O_2]^2 (X)$$

$$(\text{Intermediate}_1 - X)(\text{Intermediate}_2 - X) = K_2 [C_3H_8O_3] (X)^2$$

$$(\text{Product} - X) = 0$$

Assume $(\text{Intermediate}_1 - X) = (\text{Intermediate}_2 - X) = (\text{Intermediate} - X)$, from Eq.(4-13):

$$(\text{Intermediate} - X) = K_2^{1/2} [C_3H_8O_3]^{1/2} (X)$$

Substitute $(O_2 - X)$, $(\text{Intermediate}_1 - X)$, $(\text{Intermediate}_2 - X)$ and $(\text{Product} - X)$ in Eq.(4-9):

$$(X) = \frac{1}{(1 + K_1 [H_2O_2]^2 + 2K_2^{1/2} [C_3H_8O_3]^{1/2})} \quad (4-22)$$

Substitute (X) in Eq.(4-21):

$$-r_G = \frac{k_3 K_1 K_2^{1/2} [H_2O_2]^2 [G]^{1/2}}{(1 + K_1 [H_2O_2]^2 + 2K_2^{1/2} [G]^{1/2})^2} \quad (4-23)$$

B.5 Model ER1

Eley-Rideal model (dissociative adsorption of H_2O_2 reacts with glycerol solution)

Reaction mechanism



where K_1 is equilibrium rate constant (adsorption-desorption) of Eq.(5-1) = (k_1/k_1')

k_2 is the reaction rate constant of Eq.(5-2)

k_3 is the reaction rate constant of Eq.(5-3)

If Eq.(5-2) is the rate-determining step of the reaction (the step of surface reaction). The reaction rate can be expressed as:

$$-r_G = k_2 [C_3H_8O_3] (O - X)^2 \quad (5-4)$$

At equilibrium, from Eq.(5-1), we get:

$$k_1[\text{H}_2\text{O}_2](\text{X}) = k_1'(\text{O} - \text{X}) \quad (5-5)$$

From Eq.(5-3), we get:

$$k_3(\text{Product} - \text{X}) = 0 \quad (5-6)$$

Active site balance:

$$1 = (\text{X}) + (\text{O} - \text{X}) + (\text{Product} - \text{X}) \quad (5-7)$$

Rearranging Eq.(5-5) and (5-6), we get:

$$(\text{O} - \text{X}) = K_1[\text{H}_2\text{O}_2](\text{X}) \quad (5-8)$$

$$(\text{Product} - \text{X}) = 0 \quad (5-9)$$

Substitute (O-X) and (Product - X) in Eq.(5-7):

$$(\text{X}) = \frac{1}{(1 + K_1[\text{H}_2\text{O}_2])} \quad (5-10)$$

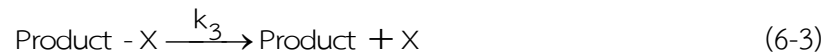
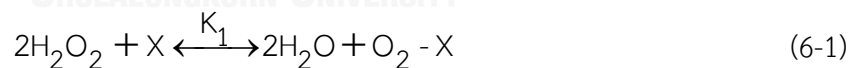
Substitute (X) in Eq.(5-4):

$$-r_G = \frac{k_2 K_1^2 [\text{H}_2\text{O}_2]^2 [\text{G}]}{(1 + K_1[\text{H}_2\text{O}_2])^2} \quad (5-11)$$

B.6 Model ER2

Eley-Rideal model (non-dissociative adsorption of H_2O_2 reacts with glycerol solution)

Reaction mechanism



where K_1 is equilibrium rate constant (adsorption-desorption) of Eq.(6-1) = (k_1/k_1')

k_2 is the reaction rate constant of Eq.(6-2)

k_3 is the reaction rate constant of Eq.(6-3)

If Eq.(6-2) is the rate-determining step of the reaction (the step of surface reaction). The reaction rate can be expressed as:

$$-r_G = k_2 [C_3H_8O_3] (O_2 - X)^2 \quad (6-4)$$

At equilibrium, from Eq.(6-1), we get:

$$k_1 [H_2O_2]^2 (X) = k_1' (O - X) \quad (6-5)$$

From Eq.(6-3), we get:

$$k_3 (\text{Product} - X) = k_3' [\text{Product}] (X) \quad (6-6)$$

Active site balance:

$$1 = (X) + (O_2 - X) + (\text{Product} - X) \quad (6-7)$$

Rearranging Eq.(6-5) and (6-6), we get:

$$(O_2 - X) = K_1 [H_2O_2]^2 (X) \quad (6-8)$$

$$(\text{Product} - X) = 0 \quad (6-9)$$

Substitute $(O_2 - X)$ and $(\text{Product} - X)$ in Eq.(6-7):

$$(X) = \frac{1}{(1 + K_1 [H_2O_2]^2)} \quad (6-10)$$

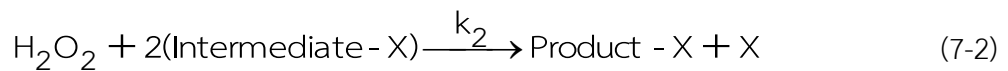
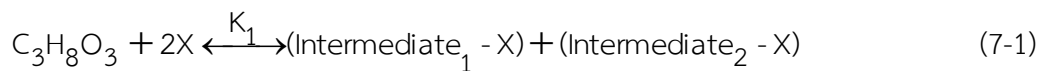
Substitute (X) in Eq.(6-4):

$$-r_G = \frac{k_2 K_1^2 [H_2O_2]^4 [G]}{(1 + K_1 [H_2O_2]^2)^2} \quad (6-11)$$

B.7 Model ER3

Eley-Rideal model (dissociative adsorption glycerol reacts with H_2O_2)

Reaction mechanism



where K_1 is equilibrium rate constant (adsorption-desorption) of Eq.(7-1) = (k_1/k_1')

k_2 is the reaction rate constant of Eq.(7-2)

k_3 is the reaction rate constant of Eq.(7-3)

If Eq.(7-2) is the rate-determining step of the reaction (the step of surface reaction). The reaction rate can be expressed as:

$$-r_G = k_2[H_2O_2](\text{Intermediate} - X)^2 \quad (7-4)$$

At equilibrium, from Eq.(7-1), we get:

$$k_1[C_3H_8O_3](X)^2 = k'_1(\text{Intermediate}_1 - X)(\text{Intermediate}_2 - X) \quad (7-5)$$

From Eq.(7-3), we get:

$$k_3(\text{Product} - X) = 0 \quad (7-6)$$

Active site balance:

$$1 = (X) + (\text{Intermediate}_1 - X) + (\text{Intermediate}_2 - X) + (\text{Product} - X) \quad (7-7)$$

Rearranging Eq.(7-5) and (7-6), we get:

$$K_1[C_3H_8O_3](X)^2 = (\text{Intermediate}_1 - X)(\text{Intermediate}_2 - X) \quad (7-8)$$

$$(\text{Product} - X) = 0 \quad (7-9)$$

Assume $(\text{Intermediate}_1 - X) = (\text{Intermediate}_2 - X) = (\text{Intermediate} - X)$, we can rewrite Eq.(7-8):

$$(\text{Intermediate} - X) = K_1^{1/2}[C_3H_8O_3]^{1/2}(X)$$

Substitute $(\text{Intermediate}_1 - X)$, $(\text{Intermediate}_2 - X)$ and $(\text{Product} - X)$ in Eq.(7-7):

$$(X) = \frac{1}{\left(1 + K_1^{1/2}[C_3H_8O_3]^{1/2} + K_1^{1/2}[C_3H_8O_3]^{1/2}\right)} \quad (7-10)$$

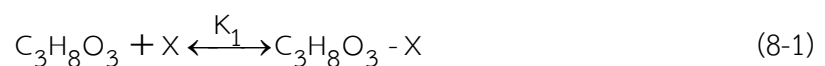
Substitute (X) in Eq.(7-4):

$$-r_G = \frac{k_2 K_1 [H_2O_2] [G]}{\left(1 + 2K_1^{1/2}[G]^{1/2}\right)^2} \quad (7-11)$$

B.8 Model ER4

Eley-Rideal model (non-dissociative adsorption glycerol reacts with H_2O_2)

Reaction mechanism



where K_1 is equilibrium rate constant (adsorption-desorption) of Eq.(8-1) = (k_1/k'_1)

k_2 is the reaction rate constant of Eq.(8-2)

k_3 is the reaction rate constant of Eq.(8-3)

If Eq.(8-2) is the rate-determining step of the reaction (the step of surface reaction). The reaction rate can be expressed as:

$$-r_G = k_2[H_2O_2](C_3H_8O_3 - X)^2 \quad (8-4)$$

At equilibrium, from Eq.(8-1), we get:

$$k_1[C_3H_8O_3](X) = k'_1(C_3H_8O_3 - X) \quad (8-5)$$

From Eq.(8-3), we get:

$$k_3(\text{Product} - X) = k'_3[\text{Product}](X) \quad (8-6)$$

Active site balance:

$$1 = (X) + (C_3H_8O_3 - X) + (\text{Product} - X) \quad (8-7)$$

Rearranging Eq.(8-5) and (8-6), we get:

$$(C_3H_8O_3 - X) = K_1[C_3H_8O_3](X) \quad (8-8)$$

$$(\text{Product} - X) = 0 \quad (8-9)$$

Substitute $C_3H_8O_3$ and $(\text{Product} - X)$ in Eq.(8-7):

$$(X) = \frac{1}{(1 + K_1[C_3H_8O_3])} \quad (8-10)$$

Substitute (X) in Eq.(8-4):

$$-r_G = \frac{k_2 K_1^2 [H_2O_2] [G]^2}{(1 + K_1 [G])^2} \quad (8-11)$$

APPENDIX C
LIST OF COMPOUNDS GENERATED FROM GLYCEROL CONVERSION VIA
V6-SiW/HZSM-5 CATALYST

Table C.1 List of compounds generated from glycerol conversion over supported POM catalyst with H₂O₂ under mild condition.(Guidechem.com, 2014)

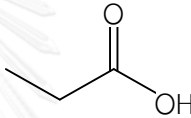
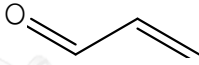
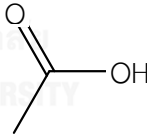
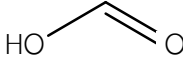
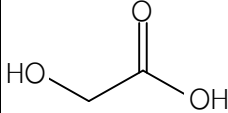
IUPAC name (Molecular formula)	Other names	Chemical structure	Prices (\$/lb) (%Purity) (Guidechem.com, 2014; Icis.com, 2014; Sunivo, 2014)
Propanoic acid C ₃ H ₆ O ₂	Propionic acid or Ethanecarboxylic acid		0.98 (99%) ^a 10.25 (>99.5%) ^b [79-09-4]
Prop-2-enal (C ₃ H ₄ O)	Acrolein or Ethylene Aldehyde		393.57 (>95%) ^c [107-02-8]
Acetic acid (C ₂ H ₄ O ₂)	Ethanoic acid		0.35 ^d [64-19-7]
Formic acid (CH ₂ O ₂)	Methanoic Acid		0.22 (85%) ^a [64-18-6]
2-Hydroxyethanoic acid (C ₂ H ₄ O ₃)	glycolic acid or hydroxyacetic acid		129.00 (99%) ^b [79-14-1]

Table C.1 List of compounds generated from glycerol conversion over supported POM catalyst with H₂O₂ under mild condition.

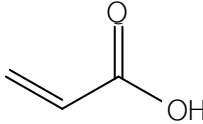
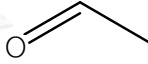
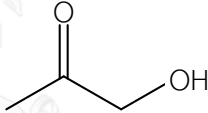
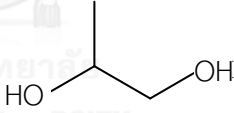
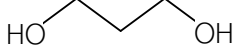
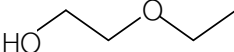
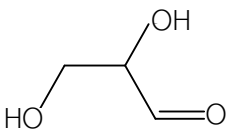
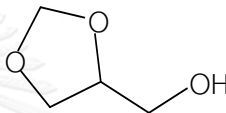
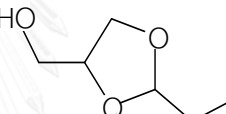
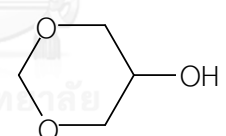
IUPAC name (Molecular formula)	Other names	Chemical structure	Prices (\$/lb) (%Purity) (Guidechem.com, 2014, Icis.com, 2014 and Sunivo, 2014)
Prop-2-enoic acid (C ₃ H ₄ O ₂)	Acrylic acid or Acroleic acid		1.09-1.12 (99.5%) ^a [79-10-7]
Ethanal (C ₂ H ₄ O)	Acetaldehyde		222.85 (>99%) ^b [75-07-0]
1-hydroxy-2-propanone (C ₃ H ₆ O ₂)	Hydroxyacetone		N/A [116-09-6]
Propane-1,2-diol (C ₃ H ₈ O ₂)	1,2-Propanediol or Propylene glycol		0.52 (99.5%) ^a 4.77 (>99.5%) ^c [57-55-6]
Propane-1,3-diol (C ₃ H ₈ O ₂)	Trimethylene glycol or 1,3-Dihydroxypropane		0.72 (99%) ^a [504-63-2]
2-ethoxyethanol (C ₄ H ₁₀ O ₂)	Oxitol or Ethyl Cellosolve		6.80 (99.9%) ^b [110-80-5]

Table C.1 (Cont.) List of compounds generated from glycerol conversion over supported POM catalyst with H₂O₂ under mild condition.

IUPAC name (Molecular formula)	Other names	Chemical structure	Prices (\$/lb) (%Purity) (Guidechem.com, 2014, Icis.com, 2014 and Sunivo, 2014)
2,3-dihydroxypropanal (C ₃ H ₆ O ₃)	2,3-dihydroxypropanal		N/A [6998-60-3]
(3-dioxolan-4-yl)methanol (C ₄ H ₈ O ₃)	4-(Hydroxymethyl)-1,3-dioxolane		N/A [5464-28-8]
(2-ethyl-1,3-dioxolane-4-yl)methanol (C ₆ H ₁₂ O ₃)	2-ethyl-1,3-dioxolane-4-methanol		N/A N/A
1,3-dioxan-5-ol (C ₄ H ₈ O ₃)	5-Hydroxy-1,3-dioxane		N/A [4740-78-7]

Note: ^a Industrial grade

^b Reagent grade

^c Natural grade

^d No report

APPENDIX D

COMPARISON RATE OF GLYCEROL CONVERSION FROM EXPERIMENTAL RESULTS
AND POWER LAW MODEL

D.1 The comparison rate of glycerol conversion from the experiments and the power law model over 30 wt.% SiW/HZSM-5 catalyst at different temperature in the range of 70-90 °C

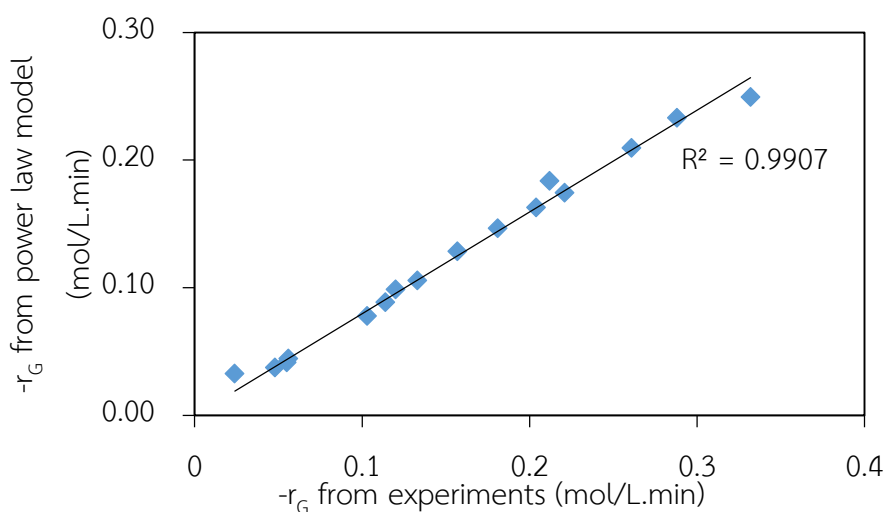


Figure D.1 The rate of glycerol conversion from the experiments compared with the rate of glycerol conversion from power law model at 70 °C.

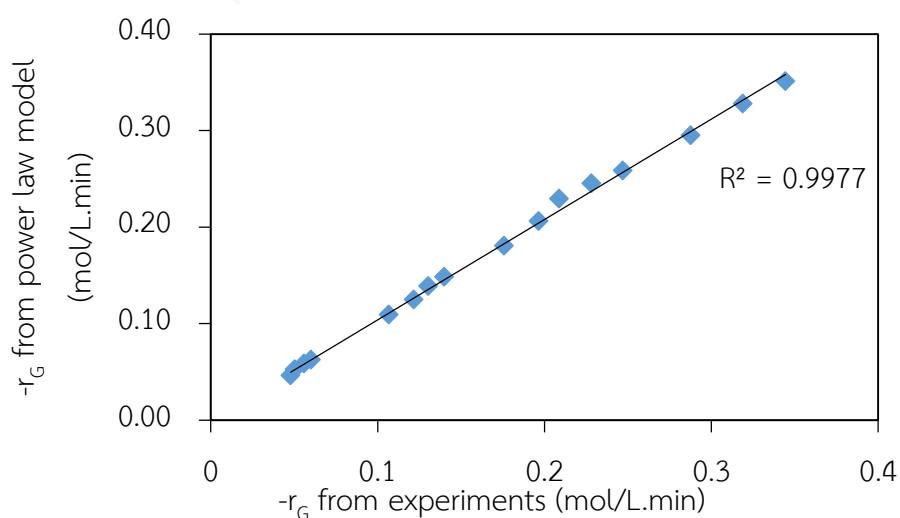


Figure D.2 The rate of glycerol conversion from the experiments compared with the rate of glycerol conversion from power law model at 80 °C.

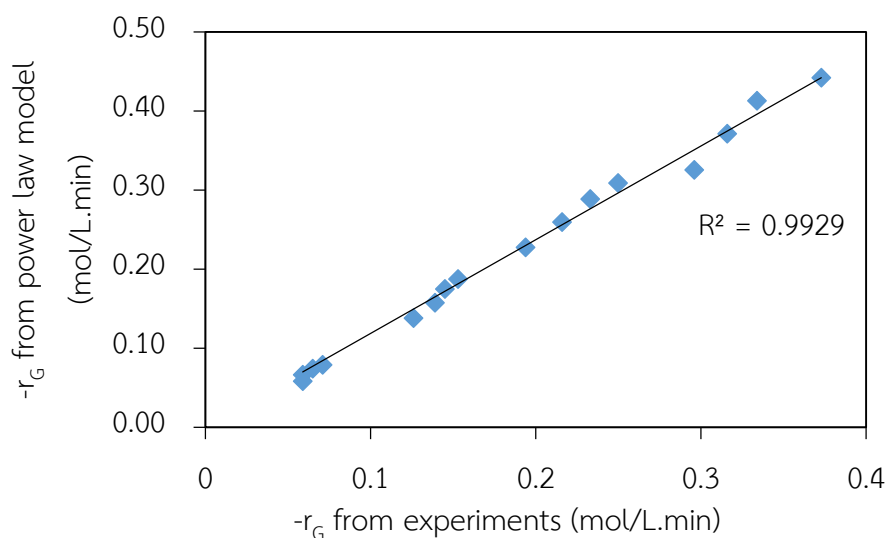


Figure D.3 The rate of glycerol conversion from the experiments compared with the rate of glycerol conversion from power law model at 90 °C.

D.2 The comparison rate of glycerol conversion from the experiments and the power law model over V6-SiW/HZSM-5 catalyst at different temperature in the range of 60-90 °C

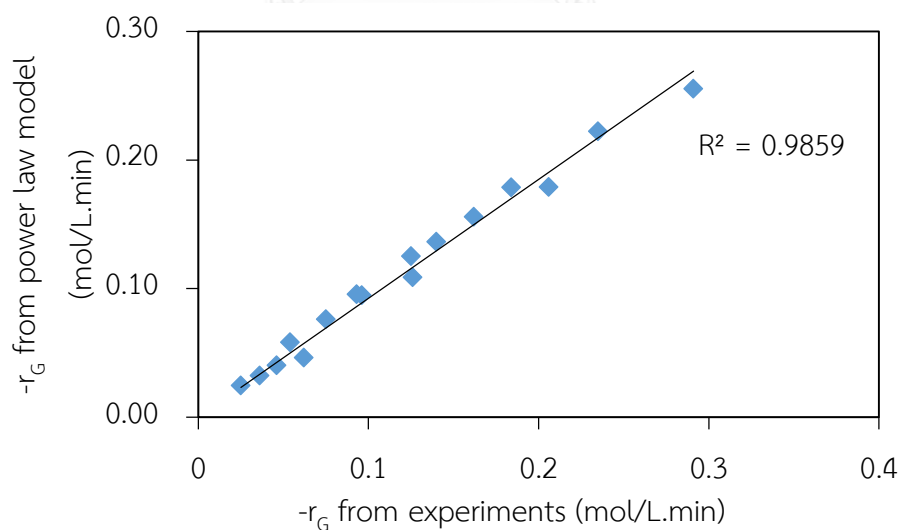


Figure D.4 The rate of glycerol conversion from the experiments compared with the rate of glycerol conversion from power law model at 60 °C.

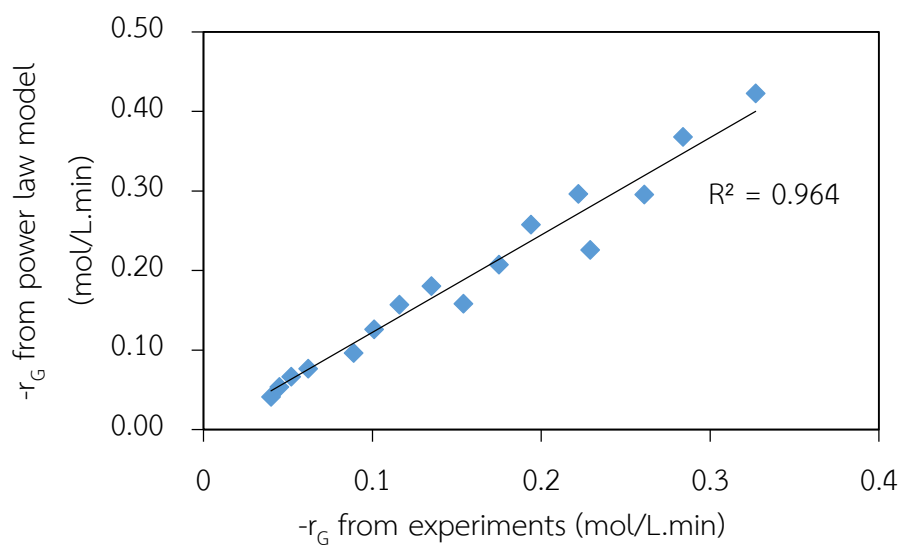


Figure D.5 The rate of glycerol conversion from the experiments compared with the rate of glycerol conversion from power law model at 70 °C.

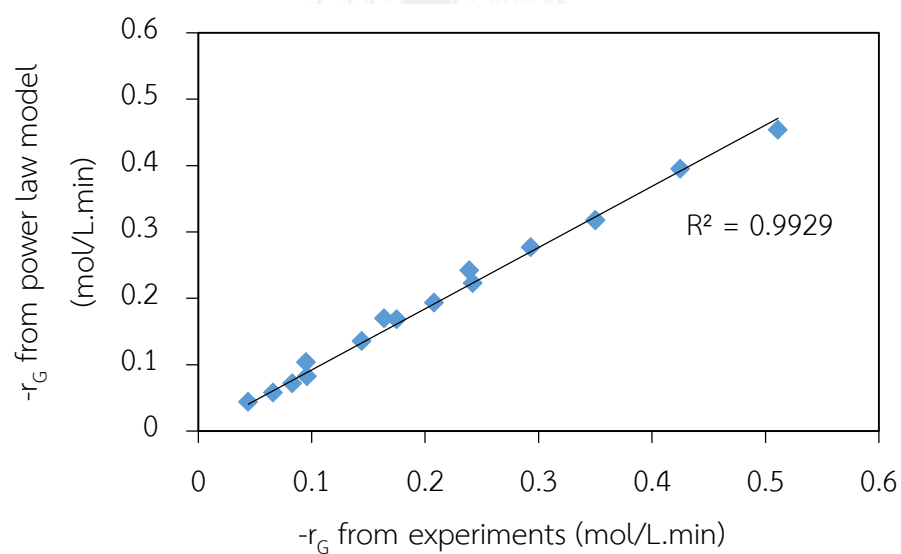


Figure D.6 The rate of glycerol conversion from the experiments compared with the rate of glycerol conversion from power law model at 80 °C.

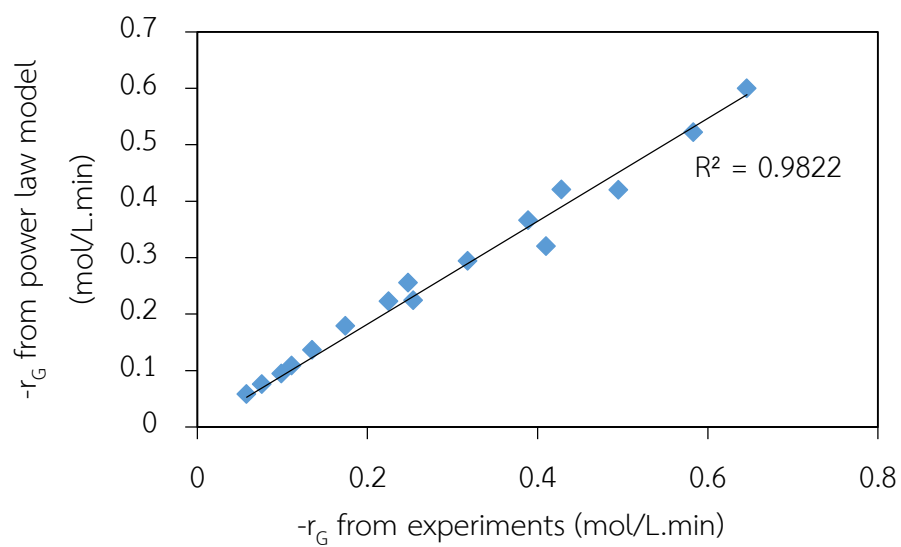


Figure D.7 The rate of glycerol conversion from the experiment compared to the rate of glycerol conversion from power law model at 90 °C.



VITA

The author who is responsible for this dissertation is Miss Sarawalee Thanasilp. She was born on October 8th, 1984 in Nakornpathom, Thailand. She learned the Bachelor of Science in Chemistry, Chulalongkorn University. In 2010, she also earned the Master of Science in Fuel Technology, Chulalongkorn University. She has received the Royal Golden Jubilee Scholarship from Thailand Research Fund for her Ph.D.

